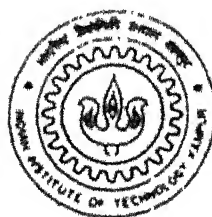# ITERATIVE DE-BLURRING IN MAGNETIC RESONANCE IMAGING

by

V.S.N. KALI PRASAD

DEPARTMENT OF MATHEMATICS

INDIAN INSTITUTE OF TECHNOLOGY KANPUR

January, 2000

ITERATIVE DE-BLURRING IN MAGNETIC RESONANCE IMAGING

A Thesis Submitted
in Partial Fulfillment of the Requirements
for the Degree of

DOCTOR OF PHILOSOPHY

by

V.S.N. KALI PRASAD

to the

DEPARTMENT OF MATHEMATICS

INDIAN INSTITUTE OF TECHNOLOGY KANPUR

January, 2000

Dedicated
To
My Gurujis

Hanumath Kali Vara Prasad Babuji
And
Prof. R.K.S. Rathore

CERTIFICATE

It is certified that the work contained in the thesis entitled, **"ITERATIVE DE-BLURRING IN MAGNETIC RESONANCE IMAGING"**, by V.S.N. Kali Prasad, has been carried out under my supervision and that this work has not been submitted elsewhere for a degree.

R.K.S. Rathore

Professor

Department of Mathematics

I.I.T. Kanpur

January, 2000

ACKNOWLEDGEMENTS

Thanks are due to my colleague S.B. Rao for his moral support and kindly help during the course of this work.

I owe a lot to my friends   Hari, Bhavna, S.V. Rao, Sailaja, TSR, Dasji, Keshav , KCS, Alok Srivastava, Rajan, Balaji and Mohit for making my stay at I.I.T. Kanpur a memorable one.

Special thanks are due to my cousins, Padmaja, Radhika and Ratna who gave me emotional support at critical hours and reddened me with a balanced perspective of life. My eternal gratitude to them.

And finally, I wish to express my gratitude to my parents for their permission to pursue my Ph.D. program despite of the precarious financial conditions of the family. My family silently suffered due to my crazy dream of Ph. D. degree and offered whatever cooperation they could. My sisters Raja Laxmi , Kali Matha provided all the encouragement and help that was required to continue my program. My sincere thanks to all of them.

-KaliPrasad

CONTENTS

LIST OF FIGURES

LIST OF TABLES

LIST OF GRAPHS

CHAPTER 0 : INTRODUCTION

Magnetic resonance imaging (MRI) is regarded as today's most powerful non-invasive diagnostic tool in medicine. Many areas of science, engineering and technology have contributed to its growth and are continuing to do so. This thesis is an offshoot of the collaboration between the Indian Institute of Technology, Kanpur and the Sanjay Gandhi Post Graduate Institute of Medical Sciences, Lucknow, started by the enthusiastic efforts of Professor R.K.S. Rathore, Department of Mathematics, I.I.T. Kanpur and Professor R.K. Gupta, Department of Radiology, SGPGIMS.

One of the achievements of the collaboration has been the observation of Professor Rathore that the MRI images look blurred to him, and to de-blur which he proposed an effective iterative technique currently being used at the SGPGIMS. The technique has been demonstrated at several radiological meetings, including the 5th National Symposium on Magnetic Resonance, IIP Dehradun, a brain storming session at SGPGIMS, and a National Workshop on MRI Imaging with Emphasis on Neuro-Sciences at SGPGIMS, attended by leading MRI experts of the country and abroad.

The thesis, in brief, is a study of this technique from a classical point of view, in which the models of the blurring explored are taken to be the celebrated Fejér sums σ_n, the generalized Jackson operators $L_{n,p}$, and the variation diminishing integrals V_n of De la Vallée-Poussin. The operators σ_n, $L_{n,p}$, and V_n are linear positive operators, well known in the theory of approximation of functions. Of these, the last two produce blurrings of the respective orders $\omega_2(f;1/n)$ and $\omega_2(f;1/\sqrt{n})$, which are precise. However, for the Fejér sums σ_n, no such general comprehensive order is yet known (they blur Lip α functions with order $1/n^\alpha$, $0 < \alpha < 1$, and Lip 1 functions with order $(\ln n)/n$). These three distinct behaviors have been the chief reason motivating their inclusion in this study. In the thesis we obtain theoretical direct and inverse results about the related sequences of de-blurrings and also consider their application on actual MRI images, with the numerical simulations showing their effectiveness.

This introductory chapter describes some of the basics of MRI, the de-blurring technique of R.K.S. Rathore, an overview of the main theme of approximation theory that degree of approximation depends on the smoothness of the approximated function, followed by a summary of contents of the rest of the chapters of the thesis.

0.1 BASICS OF MRI

For the basics of Nuclear Magnetic Resonance (NMR) imaging, a number of excellent texts, e.g., T. Farrar and E. Becker (1971), P.T. Callaghan (1991), P. Mansfield and P. Morris (1982), C.L. Partain, R.R. Price, J.A. Patton, M.V. Kulkarni and E.V. James Jr. (1988) are available. [References are arranged alphabetically by authors names (year of publication) at the end of the thesis]

A schematic diagram of an NMR imaging system is shown in Fig. 0.1.
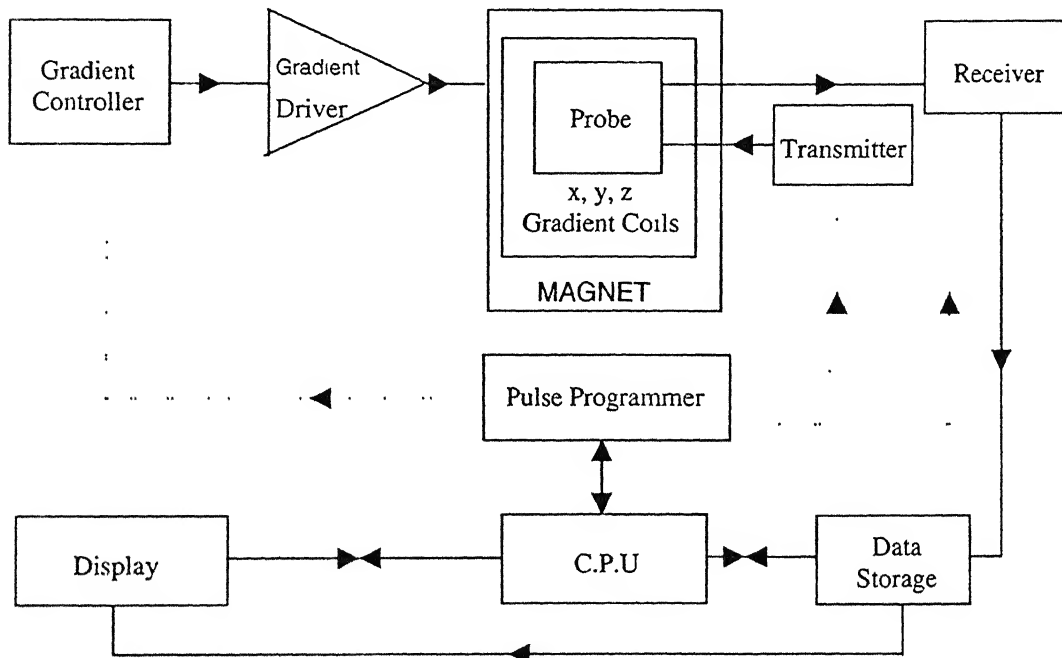
Fig. 0.1: Schematic diagram of a general NMR imaging system

The patient lies in the probe area. The pulse sequence chosen determines the action of gradient controller, transmitter and the receiver coils. The receiver gets signals in the audible range which are amplified and digitized for data measurement and storage purposes. The signal amplification, measurement and its digitization are some of the possible sources of system blurring of interest to us. The CPU, which computes the reconstructions, may also be instructed to apply additional filters, depending upon the noise characteristics of the pathological region under consideration and the number of acquisitions of the data for a particular experiment to improve upon the signal statistics. The reconstructed images could be displayed, stored and put on a transparency. The physics of MRI and related mathematical equations follow next.

BULK MAGNETIZATION VECTOR

Following R.R. Price, W.H. Stephens and C.L. Partain (1988), when an external static magnetic field $\mathbf{B}_0$ is applied, the alignment of the randomly oriented magnetic moments of individual nuclei creates a macroscopic magnetization $\mathbf{M}$ pointing along the axis of the external field as shown in the Fig. 0.2.
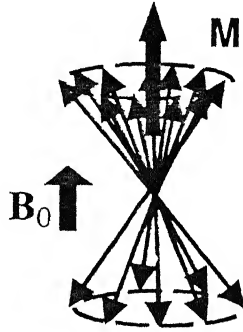
Fig. 0.2 Alignment of the individual magnetic moment vectors creates a macroscopic magnetization $\mathbf{M}$ pointing along the axis of the external static magnetic field $\mathbf{B}_0$

PRECESSIONAL FREQUENCY

In the presence of an applied magnetic filed $\mathbf{B}_0$, the magnetic momentum vectors experience a torque and precess about the axis of the magnetic field with a rate given by the Larmor's relationship

$$ f = \frac{\omega}{2\pi} = \frac{\gamma\, \mathbf{B}_0}{2\pi}, $$

where f is the *resonance frequency*, ω is the *angular frequency* and γ is *gyromagnetic ratio*. The gyromagnetic ratio is equal to the ratio of the magnitude of the magnetic moment of the nucleus to the magnitude of its spin angular momentum.

RADIO-FREQUENCY MAGNETIC FIELD

Magnetic resonance absorption can be detected only if transverse magnetization is created, since it is the transverse component M_{xy} of $\mathbf{M}$, that is time dependent and thus according to Faraday's law of induction, can induce a voltage in the receiver coil.

Referring to Fig. 0.3, when the radio frequency magnetic field B_1 is turned on, it appears perpendicular both to M and to the angular momentum of M, with the result being that M will try to precess around B_1 with the effect that M tips away from its original orientation. When this happens M acquires a component that is perpendicular to B_0 causing it also try to precess around B_0. With B_1 constantly changing at an arbitrary frequency M just wobbles about it original orientation. However if the frequency of B_1 field is equal to the Larmor frequency of the field B_0, due to resonance the effect of much smaller B_1 is cumulative, causing the angle of the tip to continue to become larger and larger. If the duration of the B_1 field is such that the net magnetization is rotated by an angle 90^0, it will become transverse. The angle of rotation θ, the RF flip angle, is given by $\theta = \gamma B_1 \tau$, where B_1 is the amplitude of the RF field and τ is its duration. Hence, RF angle can be controlled via the amplitude or the duration of the B_1 field.
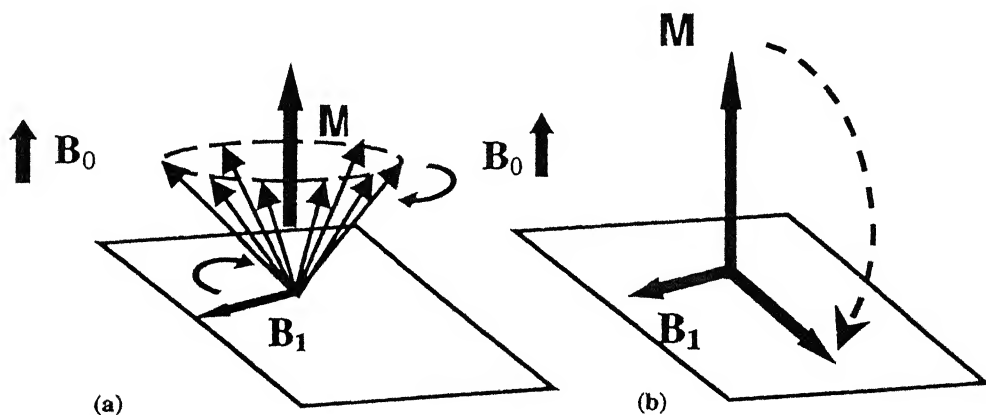
Fig. 0.3 (a) Radio frequency filed B_1 rotating synchronously with the precessing spins.
(b) A 90° flip to magnetization M brings the entire magnetization in the xy plane

FREE INDUCTION DECAY (FID):

When the rf-field B_1 is removed the magnetization is subjected to the effect of the static field only and hence precesses about it. Now by placing a conductive coil around the sample, with the axis lying on the xy-plane, it will induce an electric signal in the coil. This is the only measurable quantity in an MR experiment and is known as Free Induction Decay (FID).

THE BLOCH EQUATIONS

F. Bloch (1946) explained the motion of the macroscopic magnetization in the presence of an applied magnetic field in terms of phenomenological differential equations. The classical equation of motion (see, e g., A. Abragam (1961), and T.C. Farrar and E. Becker (1971)) of a magnetic moment in a magnetic field **B** *states* that the *rate of change of angular momentum of the spinning nucleus*, p, *depends upon the torque*, $\mu \times \mathbf{B}$, *exerted on the magnetic moment by the applied field* as:

$$\frac{d\mathbf{p}}{dt} = \mu \times \mathbf{B}.$$

Using the fact that $\mu = \gamma\, \mathbf{p}$,

$$\frac{d\mu}{dt} = \gamma \frac{d\mathbf{p}}{dt} = \gamma\, \mu \times \mathbf{B}.$$

For the macroscopic magnetization $\mathbf{M} = \Sigma\,\mu_i$, above relationship will be

$$\frac{d\mathbf{M}}{dt} = \gamma\, \mathbf{M} \times \mathbf{B}.$$

In general **B** consists of both the static applied field $\mathbf{B}_0$, and the magnetic vector of the radio frequency (rf) field $\mathbf{B}_1$. The rf-field can be thought of as a field rotating in the xy-plane at angular frequency ω. During the RF pulse, the magnetic field is

$$\mathbf{B}(t) = B_1(t)\cos \omega t\, \mathbf{i} - B_1(t)\sin \omega t\, \mathbf{j} + B\mathbf{k},$$

where $B = B_0 + h$, h being the contribution of the gradients. Thus Bloch equations become

$$\frac{dM_x}{dt} = \gamma M_y B - \gamma M_z B_1(t)\sin \omega t,$$

$$\frac{dM_y}{dt} = \gamma M_z B_1 \cos \omega t - \gamma M_x B,$$

and
$$\frac{dM_z}{dt} = \gamma M_x B_1 \sin \omega t - \gamma M_y B_1 \cos \omega t.$$

With the initial condition $\begin{pmatrix} M_x(0) & M_y(0) & M_z(0) \end{pmatrix}^T$, the solution of the above system of equations is given by:

$$M_x(t) = M_x(0)\left\{ \frac{b^2}{a^2+b^2}\cos \omega t + \frac{a^2}{a^2+b^2}\cos ct \cos \omega t + \frac{a}{\sqrt{a^2+b^2}}\sin ct \sin \omega t \right\}$$

$$+ M_y(0)\left\{\frac{a^2}{\sqrt{a^2+b^2}}\sin\omega t\cos\omega t - \cos ct\sin\omega t\right\}$$

$$+ M_z(0)\left\{\frac{ab}{a^2+b^2}\cos\omega t - \frac{ab}{a^2+b^2}\cos ct\cos\omega t - \frac{b}{\sqrt{a^2+b^2}}\sin ct\sin\omega t\right\},$$

$$M_y(t) = M_x(0)\left\{\frac{b^2}{a^2+b^2}\sin\omega t + \frac{a^2}{a^2+b^2}\cos ct\sin\omega t - \frac{a}{\sqrt{a^2+b^2}}\sin ct\cos\omega t\right\}$$

$$+ M_y(0)\left\{\frac{a^2}{\sqrt{a^2+b^2}}\sin ct\sin\omega t + \cos ct\cos\omega t\right\}$$

$$+ M_z(0)\left\{\frac{ab}{a^2+b^2}\sin\omega t - \frac{ab}{a^2+b^2}\cos ct\sin\omega t + \frac{b}{\sqrt{a^2+b^2}}\sin ct\cos\omega t\right\},$$

and
$$M_z(t) = M_x(0)\frac{ab}{a^2+b^2}(1-\cos ct) - M_y(0)\frac{b}{\sqrt{a^2+b^2}}\sin ct$$

$$+ M_z(0)\frac{1}{a^2+b^2}(a^2+b^2\cos ct),$$

where $a = \gamma B + \omega$, $b = \gamma B_1$ and $c = \sqrt{a^2+b^2}$.

THE SPIN-LATTICE AND SPIN-SPIN RELAXATION

F. Bloch (1946) assumed that spin-lattice and spin-spin relaxation could be treated as first order processes with characteristic times T_1, *spin-lattice relaxation* or *longitudinal relaxation* time, and T_2, *spin-spin relaxation* or *transverse relaxation* time, respectively. The transverse components M_x and M_y decay back to their equilibrium value zero, while the longitudinal component M_z returns to its equilibrium value M_0.

In the absence of RF field and considering T_1, T_2 relaxation, Bloch equations become

$$\frac{dM_x}{dt} = \gamma M_y B - \frac{M_x}{T_2},$$

$$\frac{dM_y}{dt} = -\gamma M_x B - \frac{M_y}{T_2},$$

$$\frac{dM_z}{dt} = -\frac{M_z - M_0}{T_1}.$$

With the initial condition $\left(M_x(0) \quad M_y(0) \quad M_z(0)\right)^T$, the solution to the above system of equations is given by:

$$M_x(t) = \exp(-t/T_2)\left\{M_x(0)\cos\gamma Bt + M_y(0)\sin\gamma Bt\right\},$$

$$M_y(t) = \exp(-t/T_2)\left\{M_y(0)\cos\gamma Bt - M_x(0)\sin\gamma Bt\right\},$$

and $\qquad M_z(t) = M_0 + (M_z(0) - M_0)\exp(-t/T_1).$

Thus, if $M_T(t)$ denotes the *magnitude* of the transverse component of the magnetic moment vector and $M_L(t)$ denotes the longitudinal component *itself* after a duration of time t of relaxation, and $M_T(0)$, and $M_L(0)$ denote the corresponding values at the start, the T_1 and T_2 relaxation effects are given by

$$M_L(t) = M(1 - e^{-t/T_1}) + M_L(0)e^{-t/T_1},$$

$$M_T(t) = M_T(0)e^{-t/T_2} \quad (true\ T_2\ decay),\ \&$$

$$M_T(t) = M_T(0)e^{-t/T_2^*} \quad (FID\ decay),$$

where $M = M_0$, the equilibrium value, and T_2^* denotes the transverse decay constant in the presence of possible magnetic field inhomogeneities, as compared with T_2, which ought to be a purely atomic constant.

In the case of the standard spin-echo (SE) experiment (see J.P. Jones (1988)), the first starting sequence has the event-wise associated longitudinal and transverse magnetic moment components given by Table 0.1:

Event	Longitudinal Component	Transverse Component
Start	M	0
90°	0	M
TE/2	$M(1 - e^{-TE/2T_1})$	$Me^{-TE/2T_2^*}$
180°	$-M(1 - e^{-TE/2T_1})$	$Me^{-TE/2T_2^*}$
TE/2	$M(1 - 2e^{-TE/2T_1} + e^{-TE/T_1})$	Me^{-TE/T_2}
		$\leftarrow measure$
End	$M(1 - 2e^{-(TR-TE/2)/T_1} + e^{-TR/T_1})$	$Me^{-TE/T_2}e^{-TD/T_2^*}$

Table 0.1:The First Spin-Echo Sequence

The second spin-echo sequence, which is used for acquiring the T_1, T_2 and density weighted SE-images, has the corresponding longitudinal and the transverse components given by the following Table 0.2:

Event	Longitudinal Component	Transverse Component
Start	$M(1 - 2e^{-(TR-TE/2)/T_1} + e^{-TR/T_1})$	≈ 0
90°	0	$M(1 - 2e^{-(TR-TE/2)/T_1} + e^{-TR/T_1})$
TE/2	$M(1 - e^{-TE/2T_1})$	$M(1 - 2e^{(TR-TE/2)/T_1} + e^{-TR/T_1})e^{-TE/T_2^*}$
180°	$-M(1 - e^{-TE/2T_1})$	$M(1 - 2e^{-(TR-TE/2)/T_1} + e^{-TR/T_1})e^{-TE/T_2^*}$
TE/2	$M(1 - 2e^{-TE/2T_1} + e^{-TE/T_1})$	$M(1 - 2e^{-(TR-TE/2)/T_1} + e^{-TR/T_1})e^{-TE/T_2}$
		$\leftarrow$ *measure*
End	$M(1 - 2e^{-(TR-TE/2)/T_1} + e^{-TR/T_1})$	$M(1 - 2e^{-(TR-TE/2)/T_1} + e^{-TR/T_1})e^{-TE/T_2}e^{-TD/T_2^*}$

Table 0.2: The Second Spin-Echo Sequence

TWO AND THREE DIMENSIONAL IMAGING

The basic idea of a spatial labeling by an encoding process was given by P.C. Lauterbur (1973), who also obtained the first MR-images using the projection reconstruction. His technique is known as *frequency encoding*.

The *Fourier magnetic resonance imaging* proposed by A. Kumar, D. Welti, and Richard R. Ernst (1975) uses *both frequency and phase encoding* to obtain the Fourier coefficients of the tissue parameter weighted distribution of the magnetic moment vector **M** in the region R of concern. Thus, using the standard spin echo sequence the data provided by an MRI scanner consists of the mathematical quantity given by

$$\hat{F}(t_y, t) = \int_R S(x, y, z) e^{i\gamma(G_x t x + G_y t_y y + G_z t_z z)} dV,$$

where γ is the gyromagnetic ratio; G_x, G_y, G_z are the respective x, y, and z gradient strengths; t_y, t_z are the y and z phase encoding times and S denotes the effective intensity of the signal at the point (x, y, z). Different choice of t, t_y, and t_z enables us to measure the 3D-Fourier coefficients of the signal intensity function.

In the normal 2D-imaging one simply does not use the z-gradient phase encoding to obtain the 2D-Fourier coefficients of the particular planar slice under consideration. However, the slice selection takes place via a z-gradient on the basis of which the appropriate rf-frequency range is invoked.

TISSUE CONTRAST

In MR-imaging, the contrast between tissues depends upon local values of spin density ρ, relaxation times T_1, T_2 and inter-pulse time intervals - echo time TE, repetition time TR, delay time TD, etc. Using the Bloch equations, signal expression for spin echo (SE) sequence (90^0-TE/2-180^0-TE/2-measure-TD), where TD = TR-TE, can be written as (see, e.g., G. Sebastiani and P. Barone (1991) & Tables 0.1-2),

$$I_{SE} = M_0(1 - 2e^{-(TR-TE/2)/T_1} + e^{-TR/T_1})e^{-TE/T_2},$$

where is M_0 is proportional to the proton density, ρ of water in the tissue.

The following Table 0.3 shows different contrasts in the image which can be achieved by suitably choosing the sequence parameters *TE*, *TR* in the case of spin echo SE-pulse sequence.

Contrast	*TE* -Setting	*TR* -Setting
T_1	*As short as possible (preferably less than 20 ms)*	*Comparable to T_1's of two tissues (towards the shorter T_1 is better)*
T_2	*Comparable to T_2's of the two tissues (towards the longer T_2 is better)*	*Long compared to the T_1's of the two tissues (2000 ms or greater)*
Proton Density	*As short as possible (preferably less than 20 ms)*	*Long compared to the T_1's of the two tissues (2000 ms or greater)*

Table 0.3: Different contrasts obtainable in Spin Echo Imaging by varying TE, TR

THREE MAIN TEST CASE IMAGES

The following three test case images (see Fig. 0.4) are some T_1, T_2 and Proton density weighted images of the same cross-section, obtained by spin echo sequences with appropriate TE, TR values.
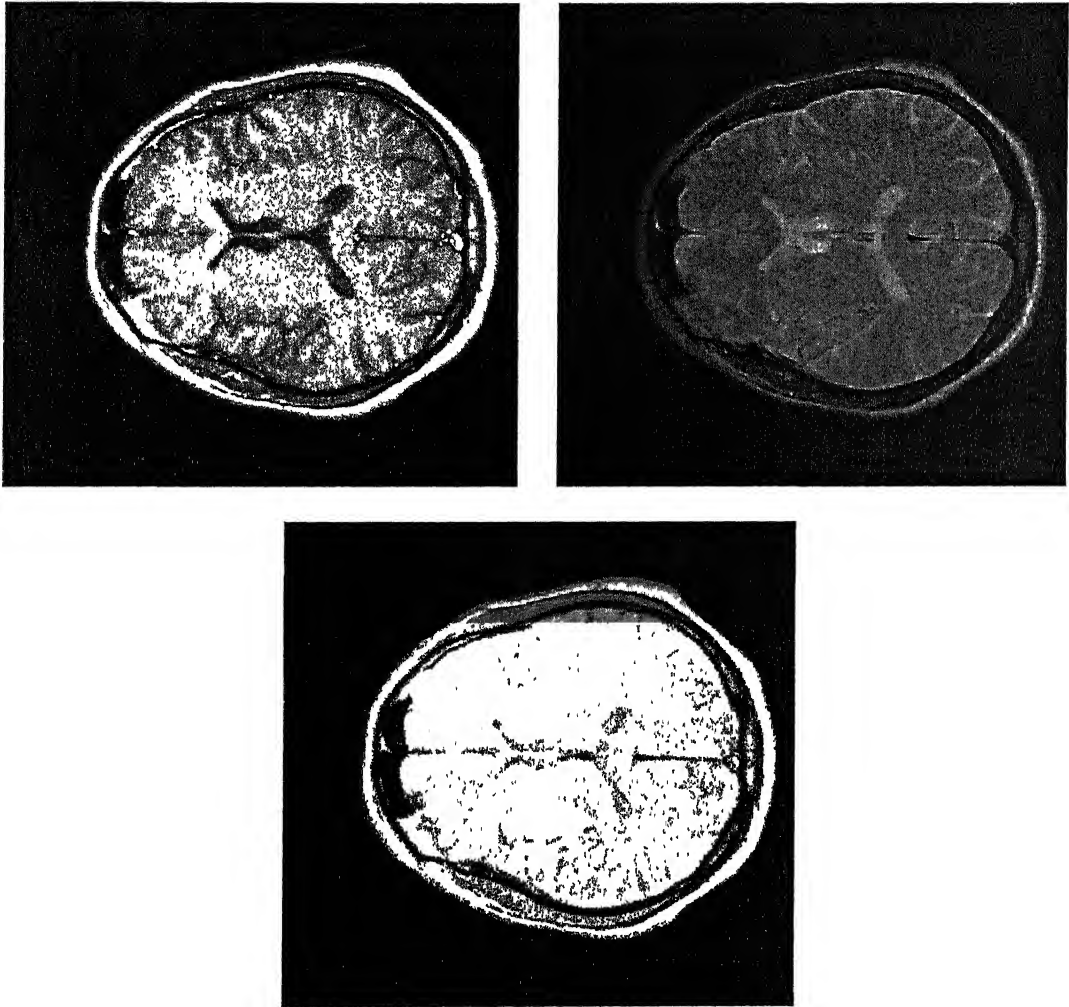
Fig. 0.4: T_1 (TE = 15 ms, TR = 300 ms), T_2 (TE = 80 ms, TR = 2000 ms), and Proton density (TE = 20 ms, TR = 2000 ms) weighted SE-images

In each of the main chapters 1-3, these T_1, T_2, and ρ-weighted images have been used as reference images (or actual function f) for simulations. Subsequently they are blurred ($A_0 f$) by the filters concerned and the performance of the de-blurring ($A_1 f$, $A_2 f$, $A_3 f$,…etc.) has been documented in the chapters by computing different error measures associated with the degree of approximation ($e_j \equiv f - A_j f$, $j \geq 0$). The MRI data for the thesis has been acquired on a 1.5 Tesla machine at SGPGIMS, Lucknow.

0.2 ON THE ITERATIVE DE-BLURRING SCHEME OF R.K.S. RATHORE

The need for filtering in MRI is different from that in digital image processing. In the latter it is to compensate for a degradation that the image itself has suffered, while in the former it is to reduce the data noise associated with the high frequency terms in the K-space. The filtered image, however, looks blurred or unfocussed. Thus assuming that the effect of the noise gets diminished, to achieve a finer diagnosis at SGPGIMS, Lucknow, Professor R.K.S. Rathore proposed a de-blurring based on some good approximation of a localized spatial blurring model suitable for the MRI scanner in use. His spatial de-blurring technique consists of a surprisingly effective iterative inverse filtering procedure, through which the noise contribution continues to remain dissipated, whereas the image structure tries to re-focus and thereby acquire approximately the original sharpness so that the overall visual diagnostic resolution of the cross section gets sufficiently improved.

Following R.K.S. Rathore (1994), let the actual cross section be f and the local blurring operator be denoted by U. The filtered image could then be modeled as $Uf + N$, where N is the residual dissipated noise in the image. Note that, as mentioned earlier, U and N arise due to a variety of factors including the signal amplification. Postulating an approximation A of U, the proposed class of sharpening operators is given by

$$A_m = \sum_{j=1}^{m} (-1)^{j-1} \; {}^mC_j A^{j-1}, m = 1, 2, 3, 4, \ldots$$

If $\|\Delta\| = \|I\text{-}A\| < 1$, $A_m(Uf) - f \rightarrow A^{-1}(U\text{-}A)\,f$, whereas $\|A_m N\| \leq [(1\text{-}\|\Delta\|^m)/(1\text{-}\|\Delta\|)]\|N\|$. Thus the resulting error on the application of A_m for a moderate m would have the order of approximation of the modeling error and the noise could increase by maximum multiplicative bound $(1\text{-}\|\Delta\|)^{-1}$, which would normally be of the order of unity. In the reconstructions shown in this section, A was chosen to be an appropriate blurring model (based on a variant of the Fejér sums) quite suitable for the present SGPGIMS MRI scanner. Note that in general, the order of approximation would be higher for the smoother structures in the cross section [R.K.S. Rathore (1994)].

It may be noted that most of the usual methods e.g., Wiener filtering or inverse filtering by dividing the Fourier data by the Fourier transform of the point spread function (psf) do not give good results in the MRI context. This is because the former itself causes a blurring, while the inverse filtering leads to severe artifacts in the image arising due to meagerness of the higher order frequency content of the psf. The problem is further complicated because of the erratic behavior of the signal amplifier for the meager K-space signal at the higher frequencies, as example in Fig.0.5 shows:

Scanned Image · Second Iterate A_3

Third Iterate A_4 · Inverse Filtered Image
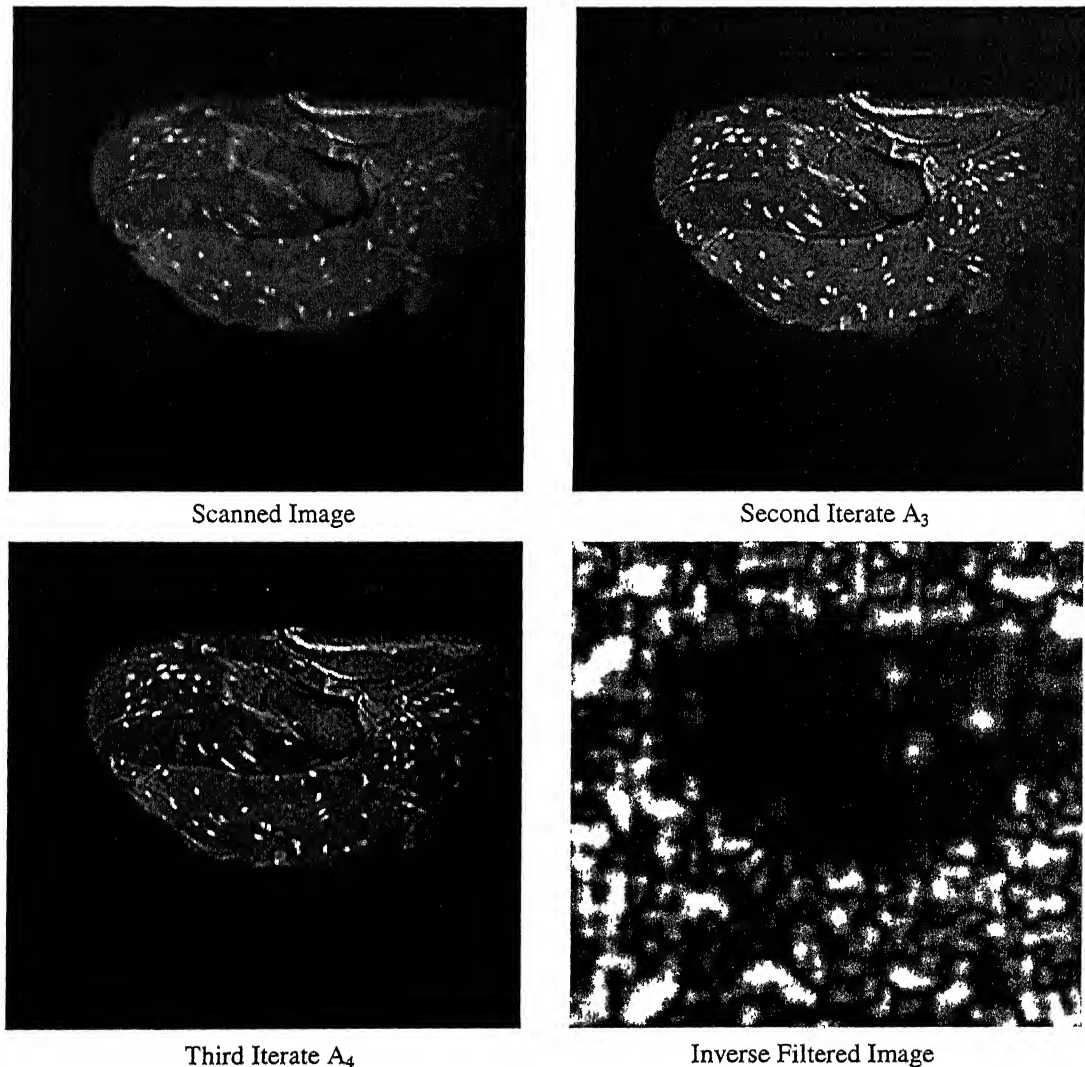
Fig. 0.5: Top left – scanner image (A_1), top right – A_3, bottom left – A_4, bottom right – inverse filtered

In Fig. 0.5, the scanner image A_1 is that of a pig muscle (TE = 80, TR = 2750) laden with of cysticercal cysts. The inverse filtered image consists of pure artifacts, whereas the resolution enhancement in the iterates A_3 and A_4 is visibly obvious allowing a clear counting of the number of cysts from a magnified version.

His technique was clinically tested on data from 250 patients who had MRI for different pathological conditions involving brain and spine. The images obtained with different pulse sequences like conventional spin echo, gradient echo and magnetization transfer, were subjected to the technique to look for resolution enhancement. The enhancement of resolution was independently confirmed by two experienced MR radiologists with more than 10 years of exposure to MR image interpretation. The resolution was considered to be enhanced if the lesion became more conspicuous on applying the technique than without it. Further test of resolution was done on a pig muscle full of cysticercal cysts (a section shown in Fig. 0.5). The number of cysts seen before using the technique and after using the technique were compared with actual counting on *ex vivo* and were more on post processed images compared to preprocessed images and were found equal to the actual number of cysts.
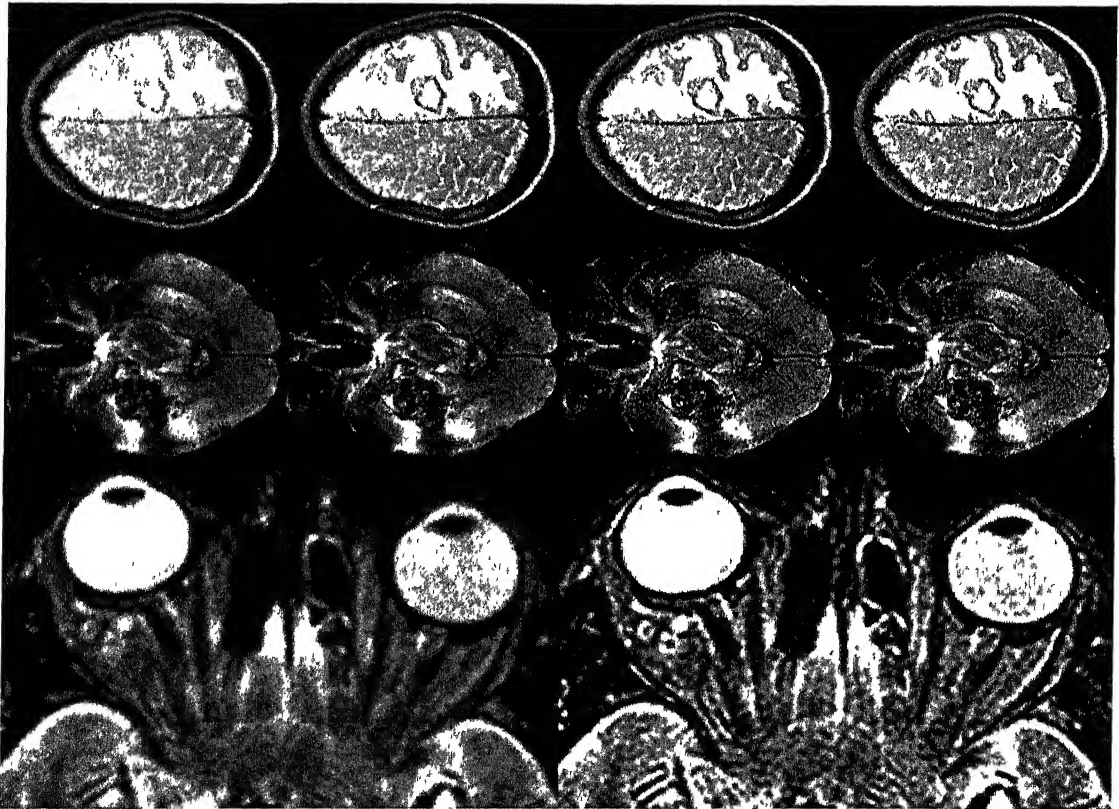
Fig. 0.6: Iterative De-blurring in SE and GE-images

Fig. 0.6 has three rows of images, in each of which the first image A_1 is the unprocessed one. The first two rows subsequently display the first to third iterates A_2, A_3, A_4, while in the last row the second image corresponds to the third iterate A_4.

For the fist routine T_2 weighted, SE-image (TE = 80 ms, TR = 2200 ms), the mean (μ) and standard deviation (σ) statistics were computed for some three ROI's and are displayed in the Table 0.4. It is seen that μ in different regions is not affected much, while the σ increases in the sharpened images with the increase in the index m. This is expected, as a higher resolution implicitly means more discrimination and consequently a higher variability in regions of a cross-section having less smoothness.

IMAGE	REGION 1		REGION 2		REGION 3	
	μ	σ	μ	σ	μ	σ
A_1	169.1	37.9	124.7	15 2	63.5	59.1
A_2	169.1	44 1	125.3	19.8	63.7	61.4
A_3	169.4	46 5	125.3	22.3	64.1	61.8
A_4	169.3	47 8	125 3	23.9	64.1	62 3

Table 0.4: Mean (μ) and S.D. (σ) in Different Regions

Row 2 of Fig. 0.5 corresponds to a T_1 weighted, gradient echo BOLD-image (TE = 46 ms and TR = 93 ms) and equally well shows the progressive sharpness of the resolution in the iterates A_2, A_3, A_4.

Row 3 of Fig. 0.5 corresponding to a standard T_2 weighted SE image (TE = 80 ms, TR = 2200 ms) shows multiple lesions in the lateral rectus of the right eye of a patient. The eccentrically placed scolex is more clearly visible in the post-processed image A_4 compared to the preprocessed A_1. Demonstration of the scolex is essential for the diagnosis of cysticercal cyst, as it is pathognomonic of this condition.

In the numerous reconstructions obtained by his technique, no artifacts or any lesion degradations were found. The sharpness achieved in all cases had been encouraging throughout. A few follow-ups confirmed the diagnoses retrospectively.

The technique, thus, was found to be a very promising tool to remove the blurring in MRI images. The resulting images did not show artefacts or lesion degradation and were sharp. In the clinical practice they have led to several successful diagnoses, which otherwise would have at best been categorized as borderline cases.

0.3 AN OVERVIEW OF APPROXIMATION THEORY

An MRI reconstruction is basically a Fourier reconstruction, which is related with the area of approximation theory dealing with the approximation of 2π-periodic functions by trigonometric polynomials. The main emphasis there is on the approximation of 2π-periodic continuous functions, the class of which is denoted by $C_{2\pi}$.

The discontinuities in the functions responsible for the well-known Gibbs phenomena, etc. need to be treated by a special asymptotic analysis, distributional methods, or by regarding them as points of very rough smoothness. For MRI purposes it seems useful to regard a cross section as a sum of several functions with graded smoothness. Thus, while one analyses a particular region, because of the localization of errors in Fourier reconstructions, one has mainly to keep the smoothness of the region under consideration.

If $\{L_N\}$ is a sequence of bounded linear operators on $C_{2\pi}$, we shall use the writing convention $L_N(f; x) \equiv L_N(f(t); x)$, where "$t$" represents a dummy variable. It is to be understood in the sense of the following working expressions:

$$S_n(f;x) = \frac{1}{2\pi}\int_{-\pi}^{\pi} f(t)\frac{\sin\dfrac{(2n+1)(t-x)}{2}}{\sin\dfrac{t-x}{2}}\,dt = S_n(f(t);x).$$

Several definitions become easy with this usage, e.g., the k-th moment of L_N at x could be defined as: $\mu_{k,N}(x) = L_N((t-x)^k; x)$.

For approximating functions of two variables, which constitute the MRI images, we use $\{L_{M,N}\}$, the derived Cartesian array defined by

$$L_{M,N}(f; x, y) = L_N(L_M(f(t, s); x); y) \equiv L_M(L_N(f(t, s); y); x),$$

where L_M acts on the first argument "t" and L_N on the second argument "s" of $f(t, s)$. For such Cartesian product operators, writing

$$\|f\| = \sup_x \sup_y |f(x, y)|,$$

degree of approximation results for $L_{M,N}$ are immediately obtainable from those about L_M and L_N, for:

$$\left\|L_{MN}f - f\right\| = \left\|L_M(L_N f) - f\right\| = O\left(\varphi(\tfrac{1}{M}) + \varphi(\tfrac{1}{N})\right), \ M, N \to \infty.$$

is equivalent to

$$\left\|L_M f - f\right\| = O\left(\varphi(\tfrac{1}{M})\right), \ M \to \infty, \ \left\|L_N f - f\right\| = O\left(\varphi(\tfrac{1}{N})\right), \ N \to \infty.$$

Similarly, if $w(g ; \tau)$ is a measure of smoothness ($w(g ; \tau) \to 0, \tau \to 0$), for functions g of one variable and for functions $f(x, y)$ of two variables we define

$$w(f ; t, \tau) = \sup_y w(f(., y); \tau) + \sup_x w(f(x, .); t),$$

then with $\tau_N \to 0, \ N \to \infty$, and $\tau_M \to 0, \ M \to \infty$, we have

$$\left\|L_M f - f\right\| = O(w(f ; \tau_M)), M \to \infty, \ \& \ \left\|L_N f - f\right\| = O(w(f ; \tau_N)), N \to \infty$$

are together equivalent to

$$\left\|L_{MN}f - f\right\| = O(w(f ; \tau_N, \tau_M)), M, N \to \infty.$$

In view of this discussion, since the MRI filtering is of the above Cartesian nature, the degree of approximation results in the thesis have been derived for the one dimensional case only. The numerical simulations, however, correspond to 2-D arrays, where a convolution in x-direction is followed up by another in the y-direction. In the case of convolutions the operations being commutative: $L_m L_n = L_n L_m$.

For literature on basic results in approximation theory dealing with the degree of approximation, we refer to the excellent texts of N. Wiener (1932), A. Zygmund (1959), I.P. Natanson (1964), A.F. Timan (1966), P.P. Korovkin (1960), G.G. Lorentz (1966), P.L. Butzer and H. Berens (1967), H.S. Shapiro (1969), R.A. DeVore (1972), and Z. Ditzian and V. Totic (1987), to quote a few. The historical material on the Fourier series is very nicely dealt with in the classic text of H.S. Carslaw (1930).

To summarize, Joseph Fourier in the year 1822 asserted the trigonometric series expression of an arbitrary function. The proper systematization began with the classical approximation theorem of Karl Weierstrass in the year 1885 stating that an arbitrary $C_{2\pi}$ function can be approximated arbitrarily closely by a trigonometric polynomial.

The degree of approximation by trigonometric polynomials started with the celebrated Jackson theorem, which constituted the doctoral dissertation of Dunham Jackson (1912) stating that:

$$E_n(f) \leq A\omega(f; 1/n), \; n = 1, 2, \ldots , f \in C_{2\pi},$$

where A is an absolute constant independent of f and n, $\omega(f; \delta)$ stands for the classical *modulus of continuity* of f, defined by

$$\omega(f; \delta) = \max_{|h| \leq \delta} \|f(x+h)-f(x)\|, \; \delta > 0,$$

and $E_n(f)$ denotes the error in the best approximation of f by trigonometric polynomials of order n. Thus, if $\omega(f; \delta) = O(\delta^{\alpha})$, $E_n(f) = O(n^{-\alpha})$, $0 < \alpha \leq 1$. The estimates of the type of Jackson are referred to in the literature as *Jackson type inequalities*, *direct theorems*, or *a priori* error estimates. The proof of Jackson was constructed with the help of a sequence of linear trigonometric polynomial operators, known as Jackson operators. These correspond to the case $p = 2$ in the sequence of generalized Jackson operators $\{L_{n,p}\}$ considered in Chapter 2 of this thesis.

Sergi N. Bernstein (1912) came out with the converse of the above result of D. Jackson, stating that $E_n(f) = O(n^{-\alpha})$, $0 < \alpha < 1$, in turn implies that $\omega(f; \delta) = O(\delta^{\alpha})$. Bernstein, however, could only prove that $\omega(f; \delta) = O(\delta \ln (1/\delta))$, in the case $\alpha = 1$, i.e., if $E_n(f) = O(n^{-1})$. Results of these types are called *converse*, or *inverse theorems*. S.N. Bernstein pervaded the approximation scene from that time on. The famous Bernstein's inequality,

$$\|T'_n\| \leq n\|T_n\|, n = 0,1,2,\ldots,$$

in which T_n denotes a trigonometric polynomial of order n, and which he introduced and used in his proof became the model of a key inequality in the investigation of converse, or inverse, results on the degree of approximation by best as well as linear approximations. Inequalities of this type are called *Bernstein type inequalities*.

From the above it follows (see I.P. Natanson (1964)) that for $k = 1, 2, \ldots$.

$$E_n(f) \leq (B_k/n^k) \; \omega(f^{(k)}; 1/n), \; n = 1, 2, \ldots , f \in C_{2\pi},$$

and that $E_n(f) = O(n^{-(k+\alpha)})$, $0 < \alpha < 1$, in turn implies that $\omega(f^{(k)}; \delta) = O(\delta^{\alpha})$ and moreover, that $E_n(f) = O(n^{-k})$, in turn, implies that $\omega(f^{(k-1)}; \delta) = O(\delta \ln (1/\delta))$.

The above results are sufficient to conclude that f is infinitely differentiable iff $\lim_{n\to\infty} n^k E_n(f) = 0$, for all k. S.N. Bernstein went further to characterize analytic functions by their degree of approximation satisfying: $\lim_{n\to\infty} (E_n(f))^{1/n} < 1$, and the entire functions by: $\lim_{n\to\infty} (E_n(f))^{1/n} = 0$. These characterizations were obtained with the help of the Fourier series itself.

The precise characteristic of the structural property of f that is responsible for $E_n(f) = O(n^{-1})$, however, could not get resolved until Anthony Zygmund (1945) arrived on the scene and proved that: $E_n(f) = O(n^{-1})$ iff $\omega_2(f; \delta) = O(\delta)$, where

$$\omega_2(f; \delta) = \max_{|h|\le\delta} \|f(x+h)-2f(x)+f(x-h)\|, \delta > 0.$$

The class of functions satisfying the Zygmund's condition is known as the *Zygmund class Z*.

The result of A. Zygmund naturally led to the investigation of the notion of the *modulus of smoothness* of a general order m defined by

$$\omega_k(f; \delta) = \max_{|h|\le\delta} \|\Sigma_{0\le k\le m} (-1)^{m-k} \, {}^mC_k f(x+kh) \|, \delta > 0,$$

and the Jackson's theorem was updated to

$$E_n(f) \le A_k \omega_k(f; 1/n), n = 1, 2, \ldots, f \in C_{2\pi},$$

and the Bernstein's theorem to:

$$E_n(f) = O(n^{-\alpha}), 0 < \alpha < k,$$

implies that

$$\omega_k(f; \delta) = O(\delta^\alpha).$$

The Zygmund's theorem led to:

$$E_n(f) = O(n^{-k}) \ iff \ \omega_{k+1}(f; \delta) = O(\delta^k), k \ge 1,$$

the functions satisfying $\omega_{k+1}(f; \delta) = O(\delta^k)$ being said to belong to the generalized Zygmund's class Z_{k+1}. Thus Z is the same as Z_2.

The Jackson-Bernstein-Zygmund theorems seemed to round up the chapter on the degree of best approximations. However, several mathematicians, mostly related with the Russian school, with A.F. Timan as a chief proponent, were not satisfied with the orders $n^{-\alpha}$ in the inverse theorems. The basic question took the shape of when does

it happen that $E_n(f)$ is precisely of the order $\omega_k(f; 1/n)$, i.e., under what conditions can one assert that there exists a constant B_k such that $\omega_k(f; 1/n) \leq B_k E_n(f)$, so that in view of the Jackson theorem: $E_n(f) \sim \omega_k(f; 1/n)$? In the max-norm case, which is the case we are considering in this thesis, a partial answer was provided by S.M. Lozinskii and N.K. Bari and S.B. Stechkin (for which see A.F. Timan (1966)) by the statement that it happens if f satisfies

$$t^k \int_t^1 [\omega_k(f;u)/u^{k+1}]du = O(\omega_k(f;t)), \ (t \to 0).$$

This condition, however, is only a sufficient condition, and is not necessary for the equivalence $E_n(f) \sim \omega_k(f; 1/n)$ to hold. It is, nevertheless, necessary for the relation:

$$n^{-k} \sum_{v=0}^{n} (v+1)^{k+1} E_v(f) = O(E_n(f)), \ (n \to \infty).$$

The necessary and sufficient condition for $E_n(f) \sim \omega_k(f; 1/n)$, was obtained recently by R.K.S. Rathore (1994). His result states that:

$E_n(f) \sim \omega_k(f; 1/n), \ (n \to \infty)$ iff $\omega_{k+1}(f; \delta) \sim \omega_k(f; \delta), \ (\delta \to 0), \ (k \geq 1)$.

For a corresponding development in the degree of approximation by linear operators we refer to the texts in approximation theory mentioned earlier, and in particular to the work of Z. Ditzian and V. Totic (1987). For the developments in the inverse theorems of a general order $\varphi(1/n)$, as compared with the orders $n^{-\alpha}$ in the above, both in best approximations and in approximations by linear operators, we refer to R.K.S. Rathore (2000) and the bibliography therein.

An order function $\varphi(t)$ in the thesis is supposed to be associated with a growth function $\phi(t)$ subject to the conditions (see R.K.S. Rathore (1994)) that φ and ϕ are positive functions on $(0, c]$, such that for all $h \in (0, 1]$: $q(h) = \sup_{t \in (0,c]} (\phi(th)\varphi(t))/(\phi(t)\varphi(th)) < \infty$, $u(h) = \sup_{t \in (0,c]} \varphi(t)/\varphi(th) < \infty$, $w(h) = \sup \{u(t) : t \in [h, 1]\} < \infty$, and $\lim_{t \to 0} q(t) = 0$.

The growth functions $\phi(t)$ in the thesis are of the type $\phi(t) = t^\mu. (\mu = m,$ or $\mu = 2m$, m being a positive integer: 1, 2, 3, ... For this $\phi(t)$, some examples of appropriate $\varphi(t)$ are t^α, $t^\alpha \log(1/t)$, $t^\alpha/(\log(1/t))^3$, $0 < \alpha < \mu$, any k-th order modulus of smoothness $\omega_k(t)$ $(k < \mu)$ (see G.G. Lorentz (1966)) of any function in L_q $(1 \leq q \leq \infty)$, $C_{2\pi}$ etc.

It may also be remarked that all the above degree of approximation results on the best approximation by trigonometric polynomials have been obtained essentially by a proper use of appropriate sequences of linear operators themselves that provide a so-called "good" trigonometric polynomial approximation (see, e.g., H.S. Shapiro (1969)). Thus the history of degree of best approximations is not really separate from the history of approximation by linear operators. Such results of our interest, about the operators that we have considered in the thesis, are included in the first sections of the respective chapters.

0.4 CONTENTS OF THE THESIS

The rest of the thesis consists of four chapters:

Chapter 1: is a study of the de-blurring when the blurring operator is modeled as the Fejér sum operator σ_n given by

$$\sigma_n(x) = \frac{a_0}{2} + \sum_{k=1}^{n} \left(1 - \tfrac{k}{n}\right)\left(a_n \cos kx + b_n \sin kx\right),$$

where the a_k and b_k denote the Fourier coefficients of the function f and could be expressed in an integral form as:

$$\sigma_n(f;x) = \frac{1}{2n\pi} \int_{-\pi}^{\pi} f(t) \left(\frac{\sin \dfrac{n(t-x)}{2}}{\sin \dfrac{t-x}{2}}\right)^2 dt, \qquad n = 0,1,\ldots,$$

After a brief history of the operators in Section 1.1, we state some basic results required in the proof of our main results about the degree of approximation in the de-blurring by

$$\sigma_{n,m}^{f}(x) = \sigma_{n,m}(f;x) = \sum_{k=1}^{m}(-1)^{k-1}\binom{m}{k}\sigma_n^k(f;x)$$

in Section 1.2.

The main degree of approximation results, presented in Section 1.3, of this chapter utilize the Peetre's K-functional defined by:

$$K_m(t,f) = \inf_{g \in S(R_n^m)} \left(\|f - g\| + t\|g\|_m\right), m \geq 1,$$

where
$$\|f\|_m = \| \sum_1^\infty k^m A_k(f,x) \|_\infty = \left\| H^m f^{(m)} \right\|_\infty,$$

and $\|H^m f^{(m)}\|_\infty$ denotes the norm of the m-th derivative of the conjugate function of f when m is odd and equals the norm of the ordinary m-th derivative of f if m is even. In the latter case, as is well-known, this K-functional is equivalent to the m-th order modulus of smoothness of f. The main results are:

THEOREM (DIRECT)

There exists a constant C_m such that $\| \sigma_{n,m} f - f \| \le C_m K_m(n^{-m}, f)$, $f \in C_{2\pi}$.

THEOREM (INVERSE)

Let the order function $\varphi(t)$ be associated with the growth function $\phi(t) = t^m$. Then:
$$\|\sigma_{n,m} f - f\| = O(\varphi(1/n)) \text{ iff } K_m(t^m, f) = O(\varphi(t)), \text{ and,}$$
$$\|\sigma_{n,m} f - f\| = o(\varphi(1/n) \text{ iff } K_m(t^m, f) = o(\varphi(t)).$$

COROLLARY

Let $0 < \alpha < m$. Then:
$$\|\sigma_{n,m} f - f\| = O(n^{-\alpha}) \text{ iff } K_m(t^m, f) = O(t^\alpha), \text{ and,}$$
$$\|\sigma_{n,m} f - f\| = o(n^{-\alpha}) \text{ iff } K_m(t^m, f) = o(t^\alpha).$$

Finally, Section 1.4 contains results on numerical simulations with the operators $\sigma_{n,m}$. We show by an example that a direct inversion does not provide any meaningful de-blurring with an actual MRI cross-section. Whereas, on the other hand, the iterative de-blurring by the operators $\sigma_{n,m}$ does provide sharpened images. In the next simulation, to obtain the numerical behavior of the error remaining after the de-blurring we take the cross-sections given in the Fig. 0.4 as original cross-sections. These we blur by using Fejér sum blurring and then de-blur by the sequence of de-blurring operators $\sigma_{n,m}$. The resulting images, the error graphs and the error tables have been presented. To assist in understanding the behavior of the error from point to point, we also include a graph of the point-wise errors occurring along the horizontal midline at the 128th pixel of a cross-section. The graph shows that the errors decrease more or less monotonically point wise with the increase in the iteration number. The points where the errors are more may be seen to be the points where cross-section is less smooth.

Chapter 2: studies de-blurring associated with the generalized Jackson operators regarded as a blurring model. The generalized Jackson operators are given by

$$L_{n,p}(f;x) = \frac{1}{A_{n,p}} \int_{-\pi}^{\pi} f(t) \left(\frac{\sin \frac{n(t-x)}{2}}{\sin \frac{t-x}{2}} \right)^{2p} dt = \frac{1}{2} a_0 + \sum \rho_k^{n,p} (a_\lambda \cos kx + b_\lambda \sin kx),$$

for n, p positive integers, with

$$A_{n,p} = \int_{-\pi}^{\pi} \left(\frac{\sin nt/2}{\sin t/2} \right)^{2p} dt, \quad \rho_\lambda^{n,p} = \frac{\mu_k^{n,p}}{\mu_0^{n,p}},$$

where

$$\mu_\lambda^{n,p} = \sum_{j=0}^{p-1} (-1)^j \binom{2p}{j} \binom{np+p-nj-k-1}{2p-1}, \quad n \ge 1, \; k \ge 0.$$

In Section 2.1 we present some known results on these operators primarily due to F. Schurer and F.W. Steutel (1967), R.K.S. Rathore (1974 & 1976), and G.G. Lorentz (1966). This is followed by the inclusion of some lemmas necessary to prove our main results in Section 2.2. The main results on the de-blurring by the operators

$$L_{n,p}^{[m]}(f;x) = \sum_{j=1}^{m} (-1)^{j-1} \binom{m}{m} L_{n,p}^j(f;x), \quad n = 1,2,3, \, .., \, (1 \le m \le p-1),$$

obtained in Section 2.3, are the following :

THEOREM (DIRECT)

For all $f \in C_{2\pi}$ there holds the error estimate:

$$\left\| L_{n,p}^{[m]} f - f \right\| \le A_{m,p} \omega_{2m}(f;n^{-1}), \quad 1 \le m \le p-1, (n \ge 1).$$

where the constant $A_{m,p}$ does not depend on n or f.

THEOREM (INVERSE)

Let the order function $\varphi(t)$ be associated with the growth function $\phi(t) = t^{2m}$, where $1 \le m \le p-1$. Then, for $f \in C_{2\pi}$:

$$\left\| L_{n,p}^{[m]} f - f \right\| = O(\varphi(1/n)) \quad \text{iff} \quad \omega_{2m}(f;t) = O(\varphi(t)), \text{ and,}$$

$$\left\| L_{n,p}^{[m]} f - f \right\| = o(\varphi(1/n)) \quad \text{iff} \quad \omega_{2m}(f;t) = o(\varphi(t)).$$

COROLLARY

Let $0 < \alpha < 2m$, and $1 \le n \le p$ Then for $f \in C_{2\pi}$:

$$\left\| L_{n,p}^{[m]} f - f \right\| = O(n^{-\alpha}) \ \textit{iff} \ \omega_{2m}(f;t) = O(t^\alpha),$$

and, $\left\| L_{n,p}^{[m]} f - f \right\| = o(n^{-\alpha}) \ \textit{iff} \ \omega_{2m}(f;t) = o(t^\alpha).$

These results are followed by Section 2.4 on numerical simulations wherein we consider the cases $p = 2$, $n = 65$; $p = 3$, $n = 45$; *and* $p = 4$, $n = 35$ of the generalized Jackson operators $L_{n,p}$. These make $np-p$, the order of the blurring polynomial kernel or *point spread function* (psf) equal 128, 132 and 136, respectively. A graph of pint-wise errors along the horizontal midline at 128th pixel corresponding to the same cross-section as considered in the previous chapter confirms the more or less monotone decrease of the point-wise errors with increase in iteration number, also in the case of the operators $L_{n,p}$ of this chapter.

Chapter 3: considers De La Vallée-Poussin integrals

$$V_n = V_n(f;x) = \frac{(2n)!!}{2\pi(2n-1)!!} \int_{-\pi}^{\pi} f(t) \cos^{2n} \frac{t-x}{2} \, dt,$$

as the model of the de-blurring and is a study of the rate of convergence of the de-blurring sequence $\{V_n^{[m]}(f;x)\}$ defined as: $V_n^{[m]}(f;x) = \sum_{j=1}^{m} (-1)^{j-1} \binom{m}{j} V_n^j(f;x).$

After presenting some well-known results about these operators in Section 3.1, in Section 3.2 we obtain some basic lemmas of interest in the proofs of our main results. Section 3.3 contains the main results consisting of a direct estimate and an inverse result on the corresponding de-blurring operators. These are:

THEOREM (DIRECT)

For all $f \in C_{2\pi}$ there holds the error estimate:
$$\left\| V_n^{[m]} f - f \right\| \le A_m \omega_{2m}(f;n^{-1/2}), \quad 1 \le m, (n \ge 1).$$

where the constant A_m does not depend on n or f.

THEOREM (INVERSE)

Let $\varphi(t)$ be an order function associated with the growth function $\phi(t) = t^{2m}$. Then, for $f \in C_{2\pi}$:
$$\left\| V_n^{[m]} f - f \right\| = O(\varphi(1/\sqrt{n})) \ \textit{iff} \ \omega_{2m}(f;\delta) = O(\varphi(\delta)), \textit{and,}$$
$$\left\| V_n^{[m]} f - f \right\| = o(\varphi(1/\sqrt{n})) \ \textit{iff} \ \omega_{2m}(f;\delta) = o(\varphi(\delta)).$$

COROLLARY

Let $0 < \alpha < 2m$ *and* $f \in C_{2\pi}$. *Then:* $\left\| V_n^{[m]} f - f \right\| = O(n^{-\alpha/2})$ *iff* $\omega_{2m}(f;\delta) = O(\delta^\alpha)$,

and, $\left\| V_n^{[m]} f - f \right\| = o(n^{-\alpha/2})$ *iff* $\omega_{2m}(f;\delta) = o(\delta^\alpha)$.

The numerical simulations are presented in Section 3.4, where in view of the fact that the Vallée-Poussin integrals induce a considerable blurring, we utilize their filter coefficients corresponding to the case $n = 16 \times 128$ whose square root is approximately 45, which is the n for the Jackson operators considered with the case $p = 3$ in the previous chapter. Numerical simulations show the behavior of the de-blurring errors similar to the case of Jackson operator for $p = 3$ and $n = 45$. As in the previous chapters, a graph of point-wise signed errors, corresponding to the same cross-section as considered in the previous chapters, confirms the more or less monotone decrease of the point wise errors with increase in iteration number in the operators $\{ V_n^{[m]} \}$.

Chapter 4: entitled "Applications to MRI diagnosis" consists of numerical simulations done in order to obtain an insight in to the applicability of the de-blurring in the actual practice where the knowledge of the system blurring operator could be obtained only indirectly. In the first section we analyze the filter coefficients of the operators considered earlier with the purpose of grading the blurrings induced by them. The second section presents numerical studies on cross-filtering in which each of the three operators of previous chapters is used in blurring the images. Each blurred images is subsequently iteratively de-blurred by all of the associated de-blurring operators and the resulting images are cross analyzed. This methodology, with appropriate models of blurrings, could be used as an empirical basis for estimating system blurring on a particular MRI machine. The experiment also indicates that neighboring models perform more or less equally well.

In the third section we examine the behavior of errors in de-blurring on images reconstructed with varying data sizes to see the effect of de-blurring on machine scans at different resolutions. Starting with a 512x512 machine data we generate the associated images of sizes 64x64, 128x128, 256x256 and 512x512. These are images that would be obtained on the machine if the reconstructions of the respective sizes were to be acquired with the data so gathered. These are next blurred by the Fejér

filter associated with an image of size 512x512 by operations in the frequency domain.. This is followed by the iterative de-blurring of the same. The errors in reconstructing the original image from these (on the 512x512 grid using zero padding in the frequency domain) have been calculated. The results show a decrease in the errors with the increase of the data size. The de-blurring errors are also calculated by regarding the corresponding 64x64, 128x128, 256x256 images themselves as original. The results of direct filter inversion (by the same 512x512 Fejér filter) and iterative de-blurrings performed on the 512x512 machine image are also presented.

The fourth section in this chapter examines the use of iterative de-blurring to obtain T_1, T_2 and proton density weighted images from which the calculation of the corresponding T_1, T_2 and density values is expected to give more accurate results. We start with synthetic T_1, T_2 and density maps used as inputs to the synthesis of T_1, T_2 and density weighted spin echo MRI images. These images are blurred using the Fejér sums. Subsequently the tissue parameters have been calculated from the blurred images and the corresponding de-blurred images. The tabulated results display the decrease of the errors in the tissue parameter calculations with the successive de-blurrings.

The chapter concludes by presenting the graphs of the discrete point spread functions (the result of applying an operator on an array of data having the central entry 1 and the rest zero) of the blurring and the de-blurring operators considered in the thesis and by relating their shapes to their numerically observed approximation and de-blurring properties.

CHAPTER 1 : DE-BLURRING BY FEJÉR SUMS

In this chapter we study the degree of approximation in the de-blurring by the Fejér sum filters

$$\sigma_{n,m}^f(x) = \sigma_{n,m}(f;x) = \sum_{k=1}^{m}(-1)^{k-1}\binom{m}{k}\sigma_n^k(f;x).$$

In the first section entitled "Fejér Sums" we collect some material about the operators $\{\sigma_n\}$, the second section contains some basic results needed in the subsequent analysis, and the third section contains our main results on the rate of convergence of the sequence $\{\sigma_{n,m}^f(x)\}$. The final section on the simulation results includes numerical illustrations of the de-blurring achieved on MRI cross-sections.

1.1. FEJÉR SUMS

The complex Fourier coefficients of $f \in C^* \equiv C_{2\pi}$ are defined as:

$$\hat{f}(k) = \frac{1}{2\pi}\int_{-\pi}^{\pi} f(t)e^{-ikt}dt, \qquad k = 0, \pm 1, \ldots,$$

and the real Fourier coefficients are given by:

$$a_k \equiv a_k(f) = \frac{1}{\pi}\int_{-\pi}^{\pi} f(t)\cos kt \; dt, \; b_k \equiv b_k(f) = \frac{1}{\pi}\int_{-\pi}^{\pi} f(t)\sin kt \; dt, \; k = 0, 1, 2, \ldots,$$

with the Fourier series of f as:

$$f \sim \sum_{k=-\infty}^{\infty} \hat{f}(k)e^{ikx} = \frac{a_0(f)}{2} + \sum_{k=1}^{\infty}[a_k(f)\cos kx + b_k(f)\sin kx] = \sum_0^{\infty} A_k(f,x).$$

The partial sums of the Fourier series of f are given by

$$s_n^f(x) = S_n(f;x) = S_n^f(x) = \sum_{k=-n}^{n} \hat{f}(k)e^{ikx} = \frac{a_0(f)}{2} + \sum_{k=1}^{n}(a_k(f)\cos kx + b_k(f)\sin kx).$$

They are expressed as a convolution of f with the Dirichlet kernel as follows:

$$S_n(f;x) = \frac{1}{2\pi} \int\limits_{-\pi}^{\pi} f(t) \frac{\sin \dfrac{(2n+1)(t-x)}{2}}{\sin \dfrac{t-x}{2}} \, dt, \qquad n = 0,1,\ldots,$$

The Fejér sums, or the $(C, 1)$-sums for a function $f \in C_{2\pi}$ are defined by:

$$\sigma_n(x) \equiv \sigma_n^f(x) = \frac{S_0(x) + S_1(x) + \ldots + S_{n-1}(x)}{n} = \frac{a_0}{2} + \sum_{k=1}^{n} \left(1 - \tfrac{k}{n}\right)\left(a_n \cos kx + b_n \sin kx\right),$$

and could be expressed as:

$$\sigma_n(f;x) = \frac{1}{2n\pi} \int\limits_{-\pi}^{\pi} f(t) \left(\frac{\sin \dfrac{n(t-x)}{2}}{\sin \dfrac{t-x}{2}} \right)^2 dt, \qquad n = 0,1,\ldots,$$

The celebrated result of L. Fejér is as follows:

1.1.1. THEOREM (L. FEJÉR (1904))

If $f(x) \in C_{2\pi}$, the sums $\sigma_n(x)$ converge uniformly along the entire axis toward $f(x)$:

$$\lim_{n \to \infty} \sigma_n(x) = f(x).$$

The following well known corollary of the above convergence is due to the fact that $(C, 1)$ is a regular summability method:

1.1.2. COROLLARY

If the Fourier series of a function $f(x) \in C_{2\pi}$ converges at a point x_0 then its sum is equal to $f(x_0)$.

The class $\text{Lip}_M \, \alpha, \, 0 < \alpha \le 1$, defined as:

$$\text{Lip}_M \, \alpha = \{ \, f \in C_{2\pi} : \, |f(x) - f(y)| \le M \, |x - y|^\alpha, x, y \in \mathbb{R}\},$$

where $\mathbb{R}$ denotes the real line.

The order of approximation by Fejér sums for the class Lip $_M \alpha$, $0 < \alpha < 1$ is given by:

1.1.3. THEOREM (S.N. BERNSTEIN (1912))

Let $f \in C_{2\pi}$. Then, for $f \in \text{Lip}_M \alpha$, $0 < \alpha < 1$: $\left| \sigma_n(x) - f(x) \right| \le C_\alpha M / n^\alpha$, $x \in \mathbb{R}$, the

factor C_α depending only on α; and, for $f \in \text{Lip}_M 1$:

$\left| \sigma_n(x) - f(x) \right| \le A M (\ln n)/n$, $x \in \mathbb{R}$, $n > 1$, A being an absolute constant.*

The "ln n" term in the above result is a must, as follows from:

1.1.4. THEOREM (I.P. NATANSON (1964))

Suppose that the function $f(x) \in C_{2\pi}$ has at the point x_0 a finite derivative

$f_+'(x_0)$ on the right and a finite derivative $f_-'(x_0)$ on the left. Then

$$\lim_{n \to \infty} \left\{ \frac{n}{\ln n} \left[\sigma_n(x_0) - f(x_0) \right] \right\} = \frac{f_+'(x_0) - f_-'(x_0)}{\pi}.$$

In fact, much more precisely, there holds:

1.1.5. THEOREM (S.M. NIKOLSKIĬ (1940))

If $\Delta_n(\alpha) = \sup\limits_{f \in Lip_1 \alpha} \{ \max\limits_x \left| \sigma_n(x) - f(x) \right| \}$, then:

$$\lim\nolimits_{n \to \infty} (n / \ln n) \Delta_n(1) = 2/\pi,$$

and,

$$\lim\nolimits_{n \to \infty} n^\alpha \Delta_n(\alpha) = 2(\pi(1-\alpha))^{-1} \Gamma(\alpha) \sin(\alpha \pi / 2), \ (0 < \alpha < 1).$$

We may mention two other direct error estimates (R.A. DeVore (1972), p.35) about the Fejér sums σ_n:

$$\| f - \sigma_n(f) \| \le (1 + \pi) \omega(f, n^{-1/2}), \ f(x) \in C_{2\pi}$$

and

$$\| f - \sigma_n(f) \| \le 2\pi^2 n^{-1/2} \omega(f', n^{-1/2}) + \pi^2 \| f' \| n^{-1}/2, \ f(x) \in C_{2\pi}^{(1)},$$

where $C_{2\pi}^{(m)}$ denotes the space of 2π-periodic, m-times continuously differentiable functions.

1.2. SOME BASIC RESULTS

The conjugate series of f is defined by:

$$\tilde{f} \sim \sum_{1}^{\infty}(-b_k(f)\cos kx + a_k(f)\sin kx)$$

If $f \in C_{2\pi}$ the conjugate series of f is the Fourier series of a function $\tilde{f} \in L_1[-\pi, \pi]$, called the *conjugate function* of f. Let H denote the mapping $f \to \tilde{f}$, i.e., $Hf = \tilde{f}$.

In the analysis of de-blurring by the Fejér sums we shall use the saturation results about the *typical means* of the Fourier series. These typical means of order $\alpha > 0$, which for $0 < \alpha < 2$ constitute positive operators, are defined by (R.A. DeVore (1972), p. 66):

$$R_n^{\alpha}(f,x) = \frac{1}{2} + \sum_{1}^{n}\left(1 - \left(\frac{k}{n+1}\right)^{\alpha}\right)A_k(f,x).$$

The m–th iterate $\sigma_{n,m}$ is related to the typical means of the Fourier series by $\sigma_{n,m} = R_{n-1}^m$, as is easily verifiable by the actions of the two sides on the exponential e^{ikx}, $k = 0, \pm 1, \ldots$. The following saturation result about $\{R_n^{\alpha}\}$ is due to S. Aljancic (1961) (see also G. Sunouchi and C. Watari (1958-59), cf., R.A. DeVore (1972), Th. 3.5, p. 66). In the sequel we use it to obtain our direct and inverse results about $\sigma_{n,m}$.

1.2.1. THEOREM (S. ALJANCIC (1961))

The sequence $\left\{R_n^{\alpha}\right\}$ is saturated with order $n^{-\alpha}$ and saturation class

$$S(R_n^{\alpha}) = \{f : \sum_{k=1}^{\infty}k^{\alpha}A_k(f,x) \in L_{\infty}\},$$

i.e., $\| R_n^{\alpha}f - f \| = o(n^{-\alpha})$ iff f is a constant, and $\| R_n^{\alpha}f - f \| = O(n^{-\alpha})$ iff $f \in S(R_n^{\alpha})$.

The saturation of the sequence of Fejér sums, due to G. Alexits (1941), corresponds to the case $\alpha = 1$ in above. In view of the saturation of $\{R_n^m\}$, the space of zero mean $C_{2\pi}$ functions $f \in S(R_n^m)$ is complete with respect to the norm

$$\|f\|_m = \|f\|_{S,m} = \|\sum_1^\infty k^m A_k(f,x)\|_\infty = \|H^m f^{(m)}\|_\infty.$$

In the sequel, unless otherwise indicated, the norm under consideration is the sup norm defined by

$$\| f \| = \sup_x | f(x)|, \ f \in C_{2\pi}.$$

Certain classes of functions related with our analysis are as follows: $W^{(r)}(\alpha, M, \ldots, M_r)$ denotes the set of functions for which

$$\|f^{(i)}\| \le M_i, 0 \le i \le r,$$

and

$$\omega(f^{(r)}, t) \le M t^\alpha, t > 0;$$
$$W^{(r)}(\alpha, M) = \bigcup_{M_0, \ldots, M_r > 0} \{f \in W^{(r)}(\alpha, M, M_0, \ldots, M_r)\};$$

and

$$W^{(r)}(\alpha) = \bigcup_{M>0} W^{(r)}(\alpha, M).$$

The class $L_\infty^{(r)}(M)$ denotes the set of all functions f with $|f^{(r)}(x)| \le M$ a.e. and $L_\infty^{(r)}$ denotes the union of all $L_\infty^{(r)}(M)$.

The classes $L_\infty^{(r)}$ and $W^{(r-1)}(1)$ are same.

1.2.2. THEOREM (R.A. DEVORE (1972), TH. 1.9, P.16)

The class of $f \in C_{2\pi}$ which satisfy $\sum k^r A_k(f,x) \sim g \in L_\infty$ and $\|g\|_\infty \le M$ is $W^{(r-1)}(1,M)$ when r is even and $\widetilde{W}^{(r-1)}(1,M) = \{f : (f^{(r-1)}\widetilde{)} \in Lip(1,M)\}$ when r is odd.

The following result is used in the sequel to prove the inverse theorems of a general order φ corresponding to the degree of approximation of de-blurring by all the filters considered in the thesis:

1.2.3. Oh-oh-LEMMA (R.K.S. RATHORE (1994))

Let c be a positive number, $K(t)$ a non-decreasing positive function and $\delta(t)$ a positive function on $(0, c]$. Let φ and ϕ be positive functions on $(0, c]$, such that for all $h \in (0, 1]$: $q(h) = \sup_{t \in (0,c]} (\phi(th)\varphi(t))/(\phi(t)\varphi(th)) < \infty$, $u(h) = \sup_{t \in (0,c]} \varphi(t)/\varphi(th) < \infty$, $w(h) = \sup \{u(t) : t \in [h, 1]\} < \infty$, and $\lim_{t \to 0} q(t) = 0$. Let $t_n \in (0,c]$, $n \geq 1$, be such that $0 < \alpha < t_{n+1}/t_n \leq \beta < 1$, where α and β are independent of n. If for some constant M, $K(t_j) \leq M\{\delta(t_n) + \phi(t_j)K(t_n)/\phi(t_n)\}$, for $n \geq 1$ and $n < j$, then as $t \to 0$, (i) $K(t) = O(\varphi(t))$ if $\delta(t) = O(\varphi(t))$, (ii) $K(t) = o(\varphi(t))$ if $\delta(t) = o(\varphi(t))$.

The following two results are also to be used in our subsequent analysis:

1.2.4. LEMMA

If T is a trigonometric polynomial of order n, $\|\tilde{T}_n'\| \leq 2n \|T_n\|$.

Proof: Since $T = \sigma_n^T + \tilde{T}'/n$, the result follows from $\|\sigma_n\| = 1$.

1.2.5. LEMMA

If $f \in C_{2\pi}$, $(f^{(m)}\tilde{)} = (\tilde{f})^{(m)}$.

Proof: From $(\tilde{f})' \sim \sum_{k=1}^{\infty} k(b_k \sin kx + a_k \cos kx)$, $(f'\tilde{)} = (\tilde{f})'$, the result for $m = 1$. Using induction, assuming the result for m, thus

$$(f^{(m+1)}\tilde{)} = ((f^{(m)})'\tilde{)} = ((f^{(m)}\tilde{)})' = ((\tilde{f})^{(m)})' = (\tilde{f})^{(m+1)},$$

completing the proof.

We will also need the well-known S.N. Bernstein's inequality (see e.g., I.P. Natanson (1964), p. 90) mentioned in Chapter 0:

1.2.6. LEMMA (BERNSTEIN'S INEQUALITY)

If T is a trigonometric polynomial of order n, $\|T_n'\| \le n\|T_n\|$.

In this chapter, we shall take $\phi(t) = t^m$, m a positive integer. For this choice of $\phi(t)$, some examples of appropriate $\varphi(t)$ are t^α, $t^\alpha \log(1/t)$, $t^\alpha/(\log(1/t))^3$, $0 < \alpha < m$, any k-th order modulus of smoothness $\omega_k(t)$ $(k < m)$ of any function in L_q $(1 \le q \le \infty)$, $C_{2\pi}$ etc. In the sequel, the statement "$\varphi(t)$ is associated with $\phi(t)$" means that the order function $\varphi(t)$ and the growth function $\phi(t)$ are positive functions on $(0, c]$, for some c such that for all $h \in (0, 1]$: $q(h) = \sup_{t \in (0,c]} (\phi(th)\varphi(t))/(\phi(t)\varphi(th)) < \infty$, $u(h) = \sup_{t \in (0,c]} \varphi(t)/\varphi(th) < \infty$, $w(h) = \sup\{u(t) : t \in [h, 1]\} < \infty$, and $\lim_{t \to 0} q(t) = 0$.

1.3. DEGREE OF DE-BLURRING BY FEJÉR SUMS

The Peetre's K-functionals associated with the typical means of Fourier series of integral order are defined as:

$$K_m(t, f) = \inf_{g \in S(R_n^m)} (\|f - g\| + t\|g\|_m) \equiv \inf_{g \in S(R_n^m)} (\|f - g\| + t\|H^m g^{(m)}\|_m), m \ge 1.$$

where $H : f \to \tilde{f}$ denotes the conjugation operation defined before.

A *Jackson-type* direct error estimate on the degree of approximation by $\{\sigma_{n,m}\}$ can be given using the K-functional K_m as follows:

.3.1. THEOREM (DIRECT)

There exists a constant C_m such that $\|\sigma_{n,m}f - f\| \le C_m K_m(n^{-m}, f)$, $f \in C_{2\pi}$.

Proof: In view of the saturation Theorem 1.2.1, there is a constant B_m such that for any $g \in S(R_n^m)$,

$$(n-1)^m \|R_{n-1}^m g - g\| \le B_m \|g\|_m.$$

Hence, $\sigma_{n,m}$ being bounded, for a constant C_m:

$$\left\|\sigma_{n,m}f - f\right\| \le \left\|R_{n-1}^{m}(f-g)\right\| + \left\|R_{n-1}^{m}g - g\right\| + \left\|g - f\right\| \le C_{m}[\left\|f-g\right\| + (n^{-m})\left\|g\right\|_{m}].$$

The result now follows by taking infimum with respect to $g \in S(R_{n}^{m})$.

1.3.2. COROLLARY

Let $f \in C_{2\pi}$. *If* $K_{m}(t^{m}, f) = O(\varphi(t))$, *then* $\left\|\sigma_{n,m}f - f\right\| = O(\varphi(1/n))$,

and,

if $K_{m}(t^{m}, f) = o(\varphi(t))$, *then* $\left\|\sigma_{n,m}f - f\right\| = o(\varphi(1/n))$.

1.3.3. THEOREM (INVERSE)

Let $\varphi(t)$ *be an order function associated with the growth function* $\phi(t) = t^{m}$. *Then, for* $f \in C_{2\pi}$:

$$\left\|\sigma_{n,m}f - f\right\| = O(\varphi(1/n)) \text{ iff } K_{m}(t^{m}, f) = O(\varphi(t))$$

and

$$\left\|\sigma_{n,m}f - f\right\| = o(\varphi(1/n)) \text{ iff } K_{m}(t^{m}, f) = o(\varphi(t)).$$

Proof: By the Lemmas 1.2.4, 1.2.5, and 1.2.6, there exist constants A and B, independent of f and g such that

$$K_{m}(t^{m}, f) \le K_{m}(t^{m}, f - \sigma_{n,m}f) + K_{m}(t^{m}, \sigma_{n,m}(f - g)) + K_{m}(t^{m}, \sigma_{n,m}g)$$

$$\le \left\|\sigma_{n,m}f - f\right\| + t^{m}[An^{m}\left\|f - g\right\| + B\left\|g\right\|_{m}].$$

Taking supremum over g,

$$K_{m}(t^{m}, f) \le \left\|\sigma_{n,m}f - f\right\| + O((tn)^{m})K_{m}(1/n^{m}, f).$$

Hence, for a constant M independent of f,

$$K_{m}(t^{m}, f) \le M[\left\|\sigma_{n,m}f - f\right\| + (tn)^{m}K(1/n^{m}, f)].$$

By the Oh-oh Lemma 1.2.3, $\left\|\sigma_{n,m}f - f\right\| = O(\varphi(1/n)) \Rightarrow K_{m}(t^{m}, f) = O(\varphi(t))$, and

$$\left\|\sigma_{n,m}f - f\right\| = o(\varphi(1/n)) \Rightarrow K_{m}(t^{m}, f) = o(\varphi(t)).$$

Since the converse is already covered by the Corollary 1.3.2 before, the proof is complete.

As a particular case, taking $\varphi(t) = t^{\alpha}$, we have:

1.3.4. COROLLARY

Let $f \in C_{2\pi}$, and $0 < \alpha < m$. Then:

$$\left\| \sigma_{n,m} f - f \right\| = O(n^{-\alpha}) \text{ iff } K_m(t^m, f) = O(t^\alpha),$$

and,

$$\left\| \sigma_{n,m} f - f \right\| = o(n^{-\alpha}) \text{ iff } K_m(t^m, f) = o(t^\alpha).$$

Note that, as a special case of Theorem 1.2.1, with c denoting a constant, the saturation of $\{\sigma_{n,m}\}$ could be summarized as:

$$\| \sigma_{n,m} f - f \| = O(n^{-m}) \text{ iff } \sum_{k=1}^{\infty} k^m A_k(f,x) \in L_\infty, \quad \& \quad \| \sigma_{n,m} f - f \| = o(n^{-m}) \text{ iff } f \equiv c.$$

Also, in view of the equivalence of K_{2m} and ω_{2m}, mentioned in Chapter 0, some of the above results for even order iterates may be rephrased as corollaries below:

1.3.5. COROLLARY

There exists a constant B_m such that $\| \sigma_{n,2m} f - f \| \leq B_m \omega_{2m}(f; n^{-1})$, $f \in C_{2\pi}$.

1.3.6. COROLLARY

Let $\varphi(t)$ be an order function associated with the growth function $\phi(t) = t^{2m}$. Then, for $f \in C_{2\pi}$:

$$\left\| \sigma_{n,2m} f - f \right\| = O(\varphi(1/n)) \text{ iff } \omega_{2m}(f; t) = O(\varphi(t))$$

and

$$\left\| \sigma_{n,2m} f - f \right\| = o(\varphi(1/n)) \text{ iff } \omega_{2m}(f; t) = o(\varphi(t)).$$

1.3.7. COROLLARY

Let $f \in C_{2\pi}$, and $0 < \alpha < 2m$. Then:

$$\left\| \sigma_{n,2m} f - f \right\| = O(n^{-\alpha}) \text{ iff } \omega_{2m}(f; t) = O(t^\alpha),$$

and,

$$\left\| \sigma_{n,2m} f - f \right\| = o(n^{-\alpha}) \text{ iff } \omega_{2m}(f; t) = o(t^\alpha).$$

1.4. SIMULATION RESULTS

This section contains results on numerical experiments with the de-blurring induced by the Fejér operators σ_n. The operations of blurring, de-blurring and direct inversion are done in both the phase and the frequency encoding directions utilizing the two dimensional Cartesian methodology described in Chapter 0. Here: (i) we compare the iterative de-blurring with a direct inversion, (ii) compute the reconstructions, error tables, and the error graphs for a supposedly known set of weighted MRI cross-sections, and (iii) obtain graphs of the point-wise signed errors along a straight line through the middle of the cross-section, superimposed on a crop of the cross-section.

1.4.1 ITERATIVE DE-BLURRING COMPARED WITH DIRECT INVERSION

In the first experiment we verify the effectiveness of the de-blurring scheme $\sigma_{n,m}$ as compared with the de-blurring based on a direct inversion of the Fejér filter. To start with a model that closely mimics the real life situation, an actual machine image output called "Original" is taken to be the example of a blurred image. The assumed blurring model is taken to be the Fejér filter corresponding to n = 128. The images associated with the original, four of the iterates $\sigma_{n,m}$, named "Iteration 1", "Iteration 2", "Iteration 3", and "Iteration 4" that correspond to m = 2, 3, 4, and 5 in $\sigma_{n,m}$ and the result of the inverse filtering, called "Direct filter inversion" have been displayed in Fig. 1.1.

It is clear from a visual comparison of the images in Fig. 1.1 that the inverse Fejér filter produces severe artifacts, whereas the iterative de-blurrings with $\sigma_{n,m}$ produce much sharper images. The clarity and effectiveness after using the $\sigma_{n,m}$, in the separation of the gray and the white matter, as well as in delineating the fine structure of the entire topography of the regions containing CSF, is amply clear from the figure.
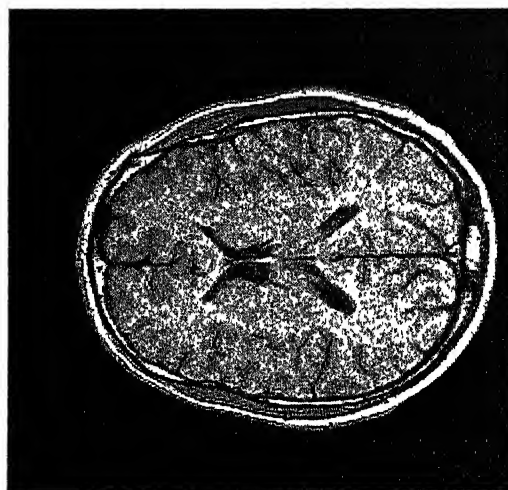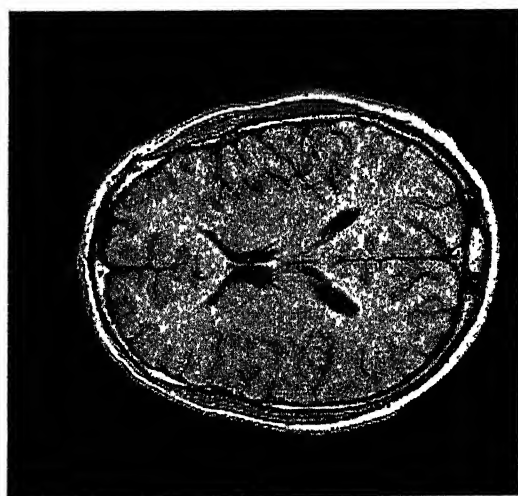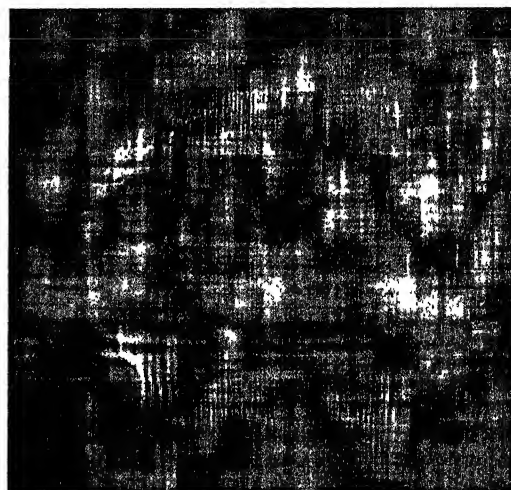
Original
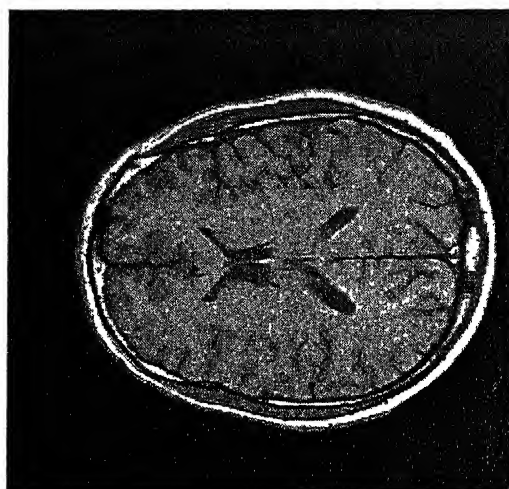
Iteration 1
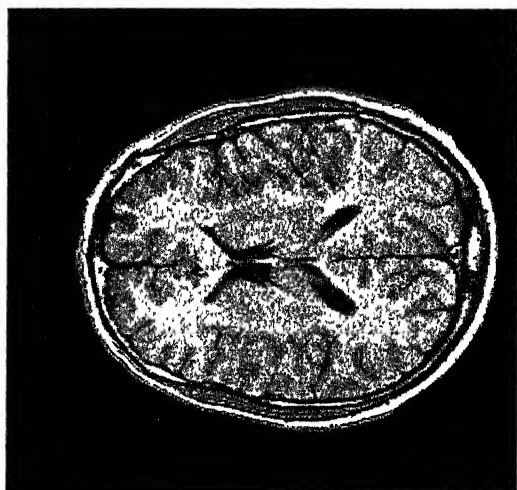
Iteration 2

Iteration 3

Iteration 4

Direct filter inversion

**Fig. 1.1** : De-Blurring by Fejér Sums and Direct Filter Inversion

1.4.2 NUMERICAL ERRORS IN THE ITERATIVE DE-BLURRING BY $\sigma_{n,m}$

The second experiment studies a quantitative behavior of the errors in the iterative de-blurrings with $\sigma_{n,m}$. To start with a model that closely mimics the real life situations, machine outputs associated with images of different tissue contrasts (each of which is called an "Original") are taken to be the examples of actual reference cross-sections. Thus, the cross-sections under consideration are assumed to be the same as the T_1, T_2 and proton density-weighted two dimensional SE images given in Fig. 0.4. The associated gray-levels constitute the functions f for the "Original" cross-sections in Fig. 1.2, Fig. 1.3, and Fig. 1.4, respectively.

These functions f representing the cross sections are blurred by the Fejér filter σ_n, with n = 128, in both the frequency and the phase encoding directions, to obtain the "Blurred" images shown as the second images in each of the figures 1.2-4. The images that result on applying the de-blurring operators $\sigma_{n,m}$ on these blurred images are named "Iteration 1", "Iteration 4", "Iteration 7", and "Iteration 10" and are presented in the second and the third image rows in the figures. These reconstructed images correspond to the values $m = 2, 5, 8$, and 11, respectively in $\sigma_{n,m}f$.

A visual comparison of the "Original" images with the "Blurred" images shows the nature of blur in the latter images due to the Fejér operator σ_n. The progressive return to the sharpness of the original cross-sections through the use of $\sigma_{n,m}$ may be seen from the images corresponding to the iterates "Iteration 1" through "Iteration 10", given in the Figs: 1.2-1.4.

The Tables 1.1-1.3 contain the corresponding numerical values of the associated errors. The same are displayed in the Graphs 1.1-1.3 . The percentage errors have been calculated by using the formula: **%error = 100×‖original–reconstruction‖/‖original‖**, where the norms under consideration are the L_1, L_2, and L_∞ norms computed over the entire set of 256×256 pixels in the images.
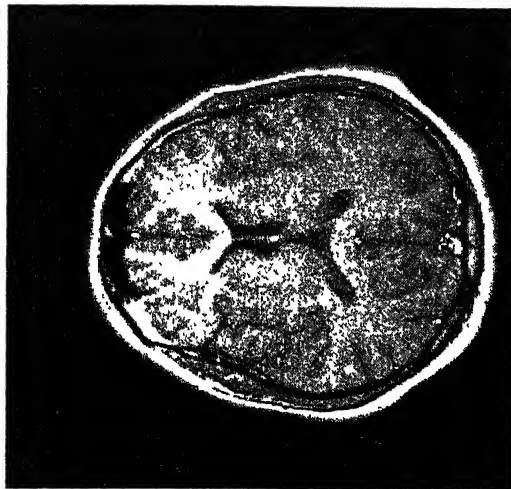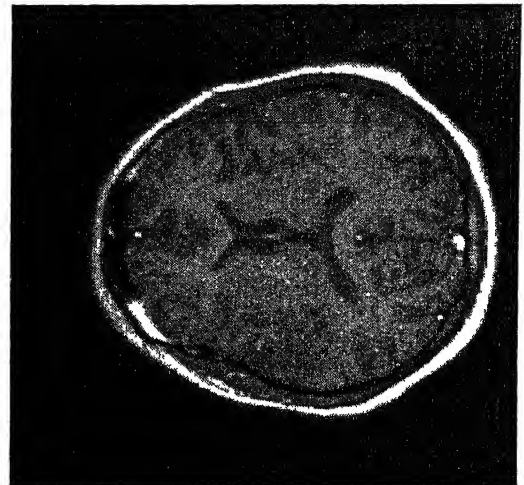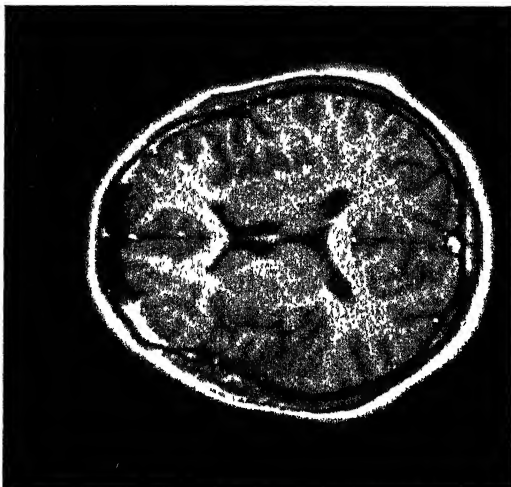
Original

Blurred

Iteration 1

Iteration 4

Iteration 7

Iteration 10

Fig. 1.2 : De-Blurring by Fejér Sums (T_1-Weighted Image)

Original

Blurred

Iteration 1

Iteration 4

Iteration 7

Iteration 10

Fig. 1.3 : De-Blurring by Fejér Sums (T$_2$-Weighted Image)

Original
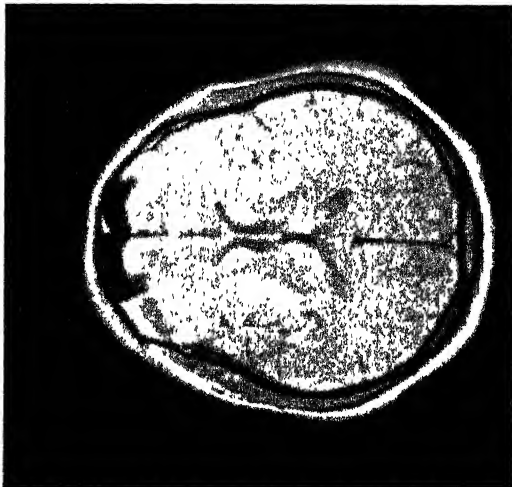
Blurred
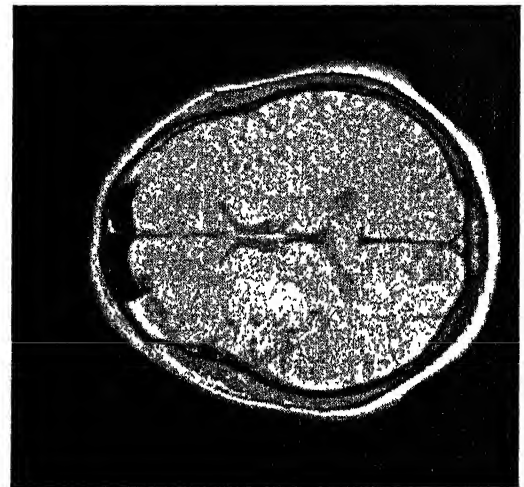
Iteration 1
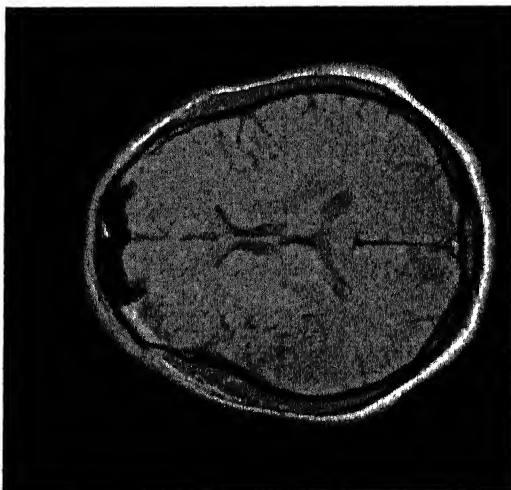
Iteration 4
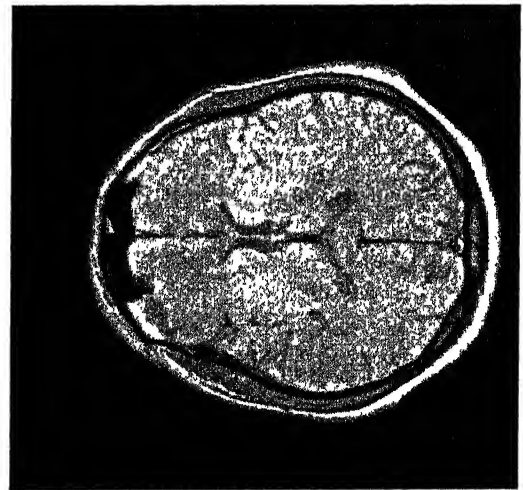
Iteration 7

Iteration 10

Fig. 1.4 : De-Blurring by Fejér Sums (Density-Weighted Image)
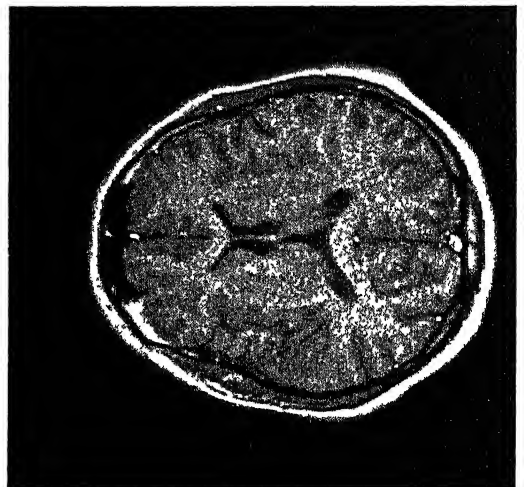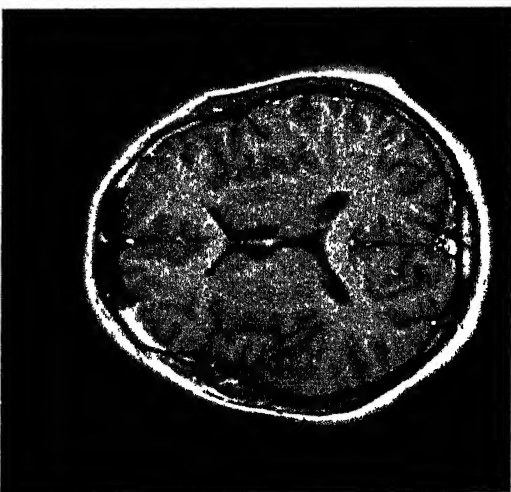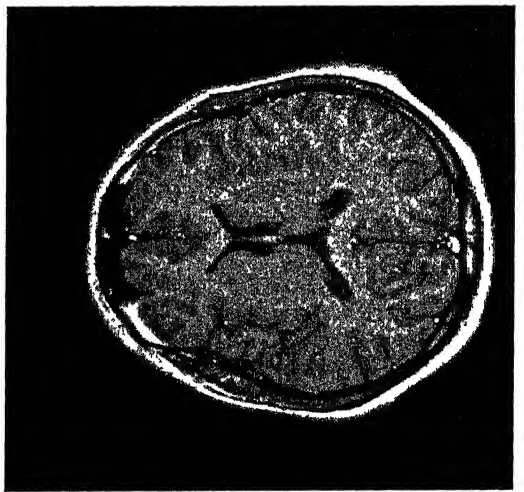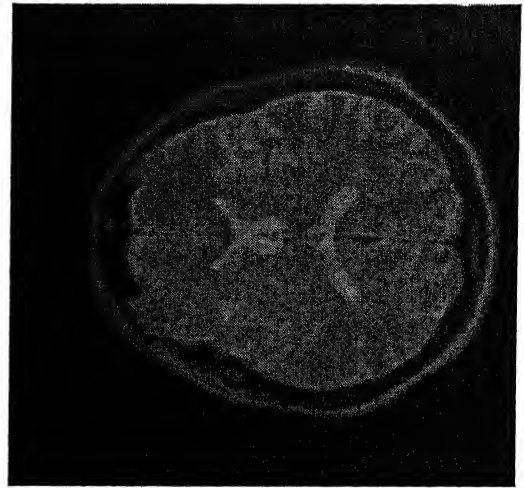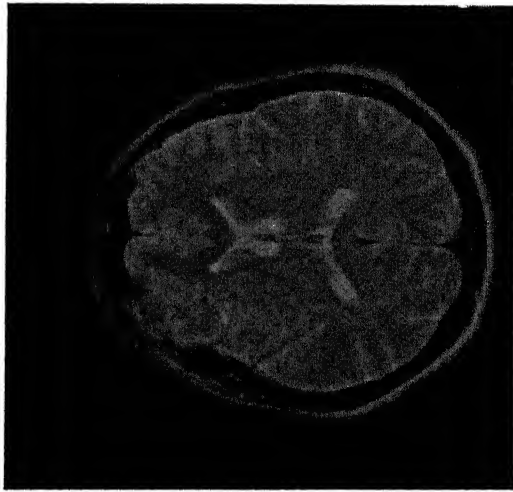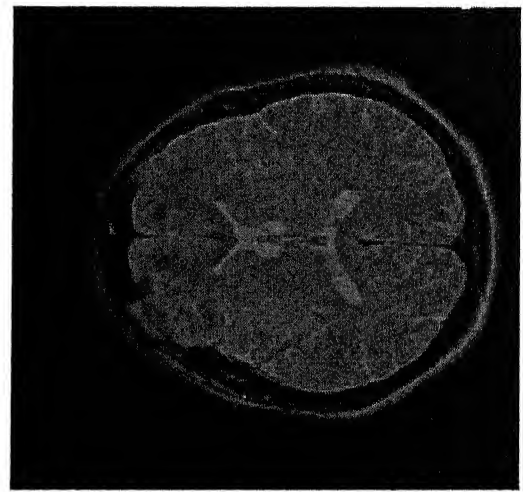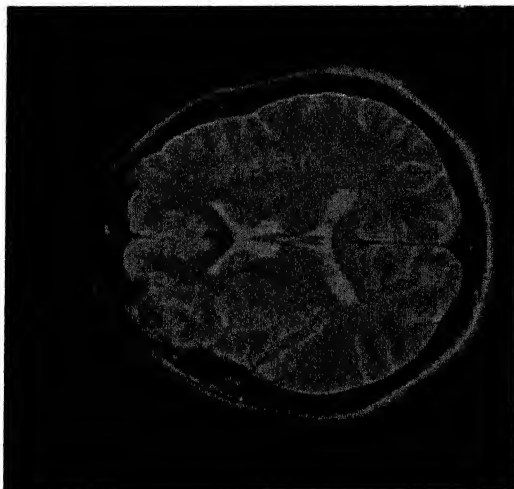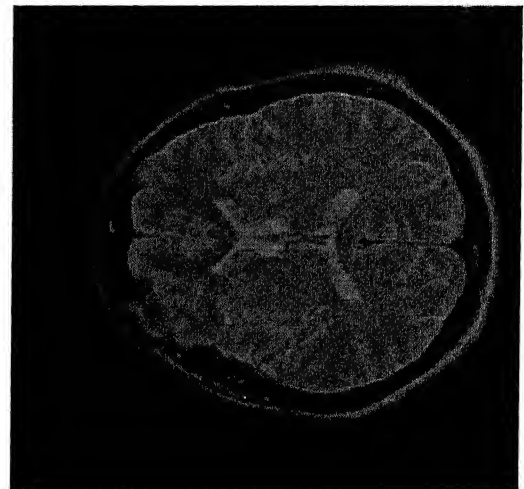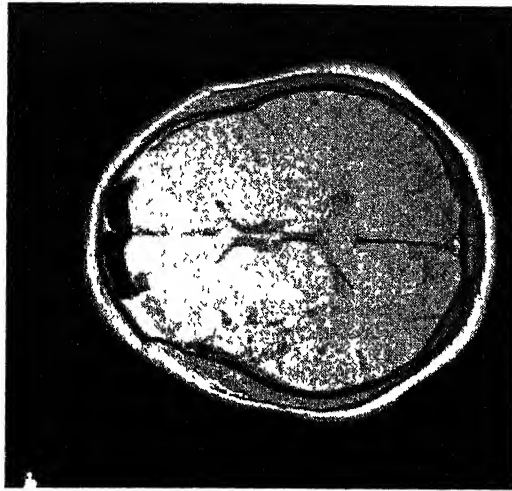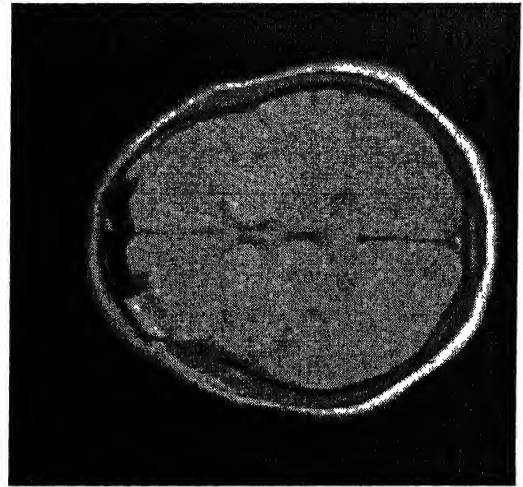
	L_1 Error	L_2 Error	L_∞ Error
blurred	11 261830	14 123094	36 462578
A_1	7.380088	8.570640	21 222672
A_2	6 174041	6.765291	16 828613
A_3	5 501431	5 805688	14 031715
A_4	5 037621	5 180599	12.076420
A_5	4 689713	4 731967	10 619979
A_6	4.416478	4 390537	9.486083
A_7	4.194215	4 119931	8.574721
A_8	4.008613	3 898783	7.824581
A_9	3.849524	3 713710	7.195639
A_{10}	3 711652	3.555907	6.736442

Table 1.1 : %-Errors in De-Blurring by Fejér Sums (T_1-Weighted Image)

	L_1 Error	L_2 Error	L_∞ Error
blurred	9 862069	13.041315	48.783108
A_1	7.433221	9.534259	31.627174
A_2	6.494610	8.031424	24.256310
A_3	5 909182	7.100663	19.793056
A_4	5.488180	6.446733	16.759327
A_5	5.162197	5.959298	14.542024
A_6	4 899826	5.580925	12.840414
A_7	4.682350	5.274752	11.488226
A_8	4 498209	5.019303	10.385134
A_9	4.338958	4.801332	9.466558
A_{10}	4.199403	4.612151	8.688783

Table 1.2 : %-Errors in De-Blurring by Fejér Sums (T_2-Weighted Image)

	L_1 Error	L_2 Error	L_∞ Error
blurred	7.287275	9.150213	32.423275
A_1	4.688092	5.572545	23 089937
A_2	3.913486	4 438324	18.803730
A_3	3.477801	3 828713	15.780841
A_4	3.180496	3.426594	13.955763
A_5	2 958243	3.135305	12.585967
A_6	2.783412	2.912204	11.490121
A_7	2.641571	2.734616	10.578156
A_8	2.523775	2.589091	9.799665
A_9	2.423231	2.467083	9.123506
A_{10}	2.335815	2.362873	8.528898

Table 1.3 : %-Errors in De-Blurring by Fejér Sums (Density-Weighted Image)
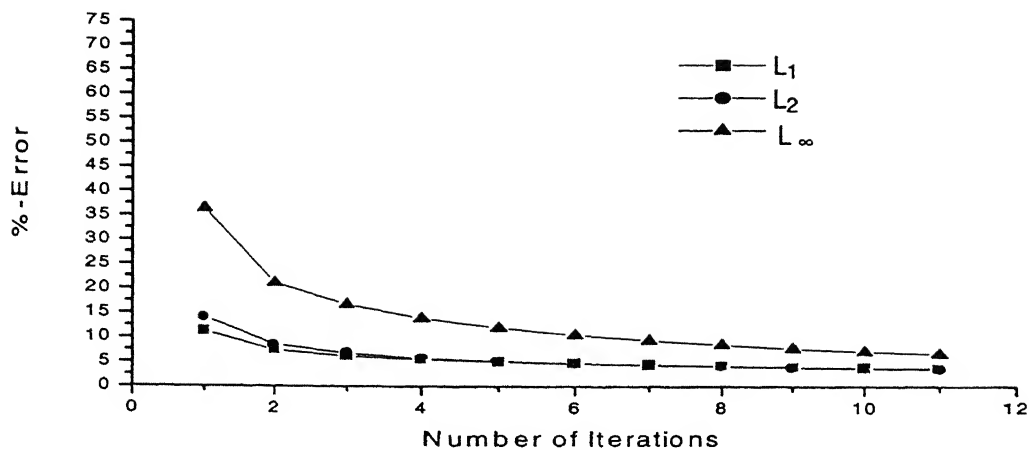
Graph 1.1 : %-Error in De-Blurring by Fejér Sums (T_1-Weighted Image)
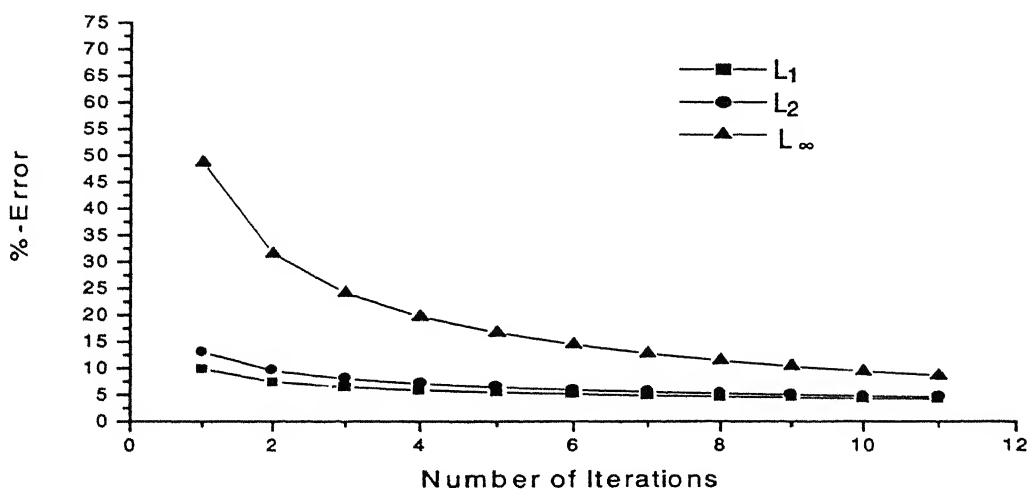
Graph 1.2 : %-Error in De-Blurring by Fejér Sums (T_2-Weighted Image)
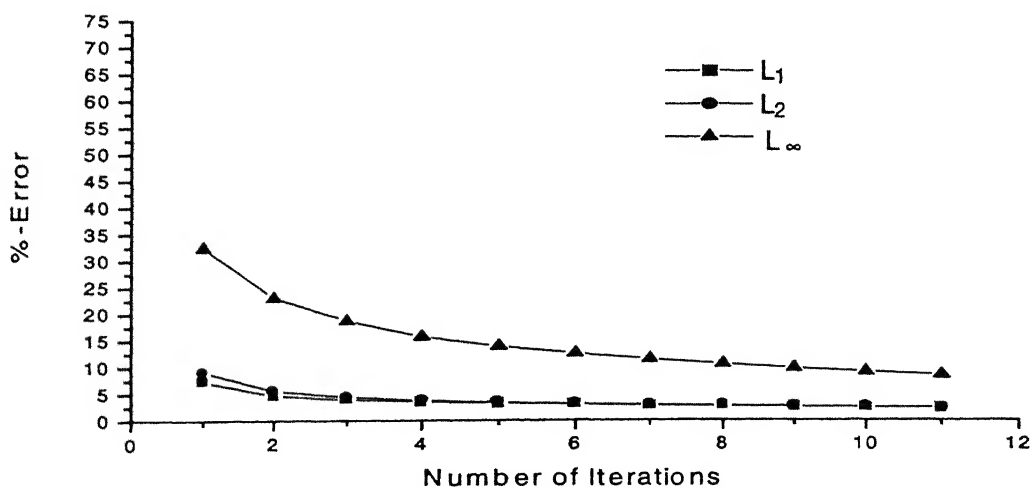
Graph 1.3 : %-Error in De-Blurring by Fejér Sums (Density-Weighted Image)

A look at the Table 1.1 reveals that the %-L_1-errors suddenly drop from 11 26 in the case of blurred image to its about 66% value 7.38 right in the case of the first iterate. The subsequent decrease of the errors is rather slow but monotone. The final error 3.71 in the 10th iterate is about 33% of the initial error. The corresponding percentage drops in L_2-errors starting at the value 14.12, are from 60% to 25%, and for the L_∞-error, starting at 36.46, the decrease is from 58% to 18%.

In the Table 1.2, giving the errors in the case of T_2-weighted image, the respective figures in the L_1-case are: 9.86, 75%, and 43%; in the L_2-case: 13.04, 73%, and 35%; and in the L_∞-case: 48.78, 64%, and 18%.

Similarly, from the Table 1.3, giving the errors in the case of proton density weighted image, these are - in the L_1-case: 7.28, 64%, and 32%; in the L_2-case: 9.15, 61%, and 26%; and in the L_∞-case: 32.42, 71%, and 26%.

The above values are summarized in the following Table 1.4. On the basis of the initial errors it gets reiterated that the density weighted images are the smoothest, followed by the T_2 weighted and the T_1 weighted images, which are approximately of the same smoothness. The large entry 48.78 in the T_2-case is probably due to the exceptional behavior of the L_∞-norm in discrete situations (as a single pixel may alter the norm drastically and also the numerator and denominator functions may possibly attain their maximum values at different pixels). With respect to the L_1 and L_2 norms (which, essentially, are averages), the performance of the de-blurring, on the whole, is similar for the density and the T_1 weighted images, followed by the T_2 weighted images. For the L_∞ norm, however, the gradation of images according to the performance of the de-blurring is T_1, T_2, and density. These gradations, however, are not very pronounced.

|	Drop in the L_1-error from the first to the last iterate			Drop in the L_2-error from the first to the last iterate			Drop in the L_∞-error from the first to the last iterate		
	Initial %-Error	First Iterate	Last Iterate	Initial %-Error	First Iterate	Last Iterate	Initial %-Error	First Iterate	Last Iterate
T_1	11 26	66%	33%	14.12	60%	25%	36 46	58%	18%
T_2	9.86	75%	43%	13.04	73%	35%	48.78	64%	18%
ρ	7.28	64%	32%	9.15	61%	26%	32.42	71%	26%

Table 1.4 : Effectiveness of De-Blurring of T_1, T_2, & Density Weighted Images by Fejér Sums

## 1.4.3 SIGNED ERRORS IN THE ITERATIVE DE-BLURRINGS BY $\sigma_{n,m}$

To get some information on the point-wise behavior of the convergence of the iterative de-blurrings by $\sigma_{n,m}f$, in the following strip graphs(Graph 1.4.(a)-(b)) the point-wise signed errors $f - \sigma_{n,m}f$ in the reconstructions $\sigma_{n,m}f$ of f are shown in the form of strip-graphs for the first T_1-weighted cross-section. These errors were calculated for the horizontal 128th mid-row and for all the 256- pixels on it. The unit for the graphs is single gray level when the original image f is a 256-gray level image.

The signed errors for the blurred image are shown in the first strip-graph. These errors for the de-blurred cases of the first ten iterates occur in the next ten strip-graphs. The last strip-graph is a superposition of all the signed errors of the ten iterates as well as the blurred image. The signed differences have been restricted to the range -15 to 25. Values crossing this range are not shown. For a better view of the image has been compressed in y-direction.

These strip-graphs show a more or less monotone behavior of the point-wise errors with increasing m. The point-wise errors $f - \sigma_{n,m}f$, along the mid line which is shown blackened on the background crop of the image, may be observed to be relatively small for the pixels where the cross-section is relatively more smooth and large where the cross section is less smooth. The patterns of point-wise signed errors for different m's are more or less similar and the magnitudes of the errors keep on reducing as m increases. One may also notice a sudden surge in the magnitude of the point-wise errors if the pixels under consideration fall near the boundary of an anatomical structure. In the case of the first and the last strip-graphs, some values have actually gone outside the frame and so are not visible (due essentially to a limitation of the graphic routine in depicting and joining points associated with abrupt and large changes). Such values are associated with the sharp peaks occurring at the right.
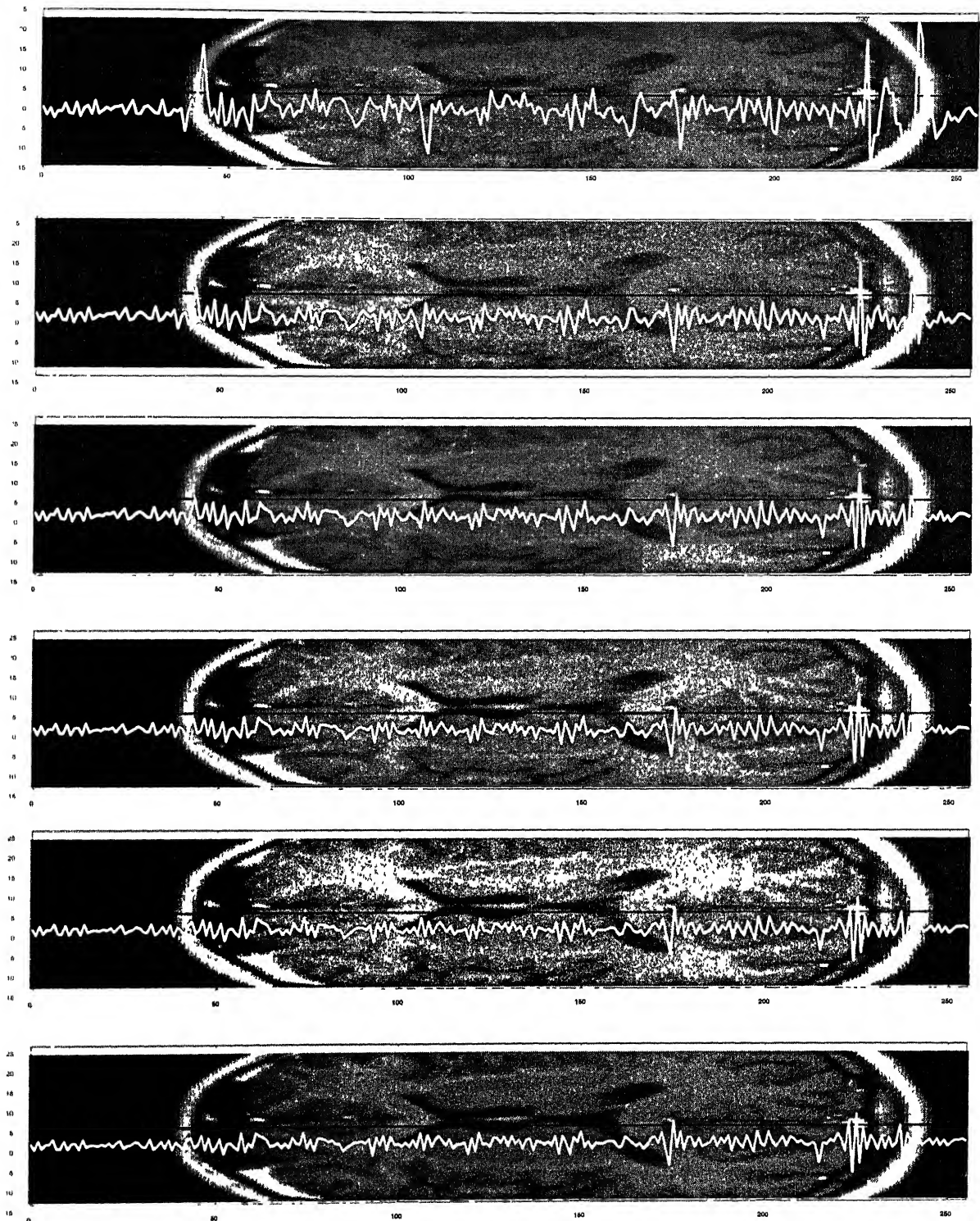
Graph 1.4. (a) : Signed De-Blurring Errors ($f - \sigma_{n,m}f$, $m = 1, 2, 3, 4, 5, 6$)
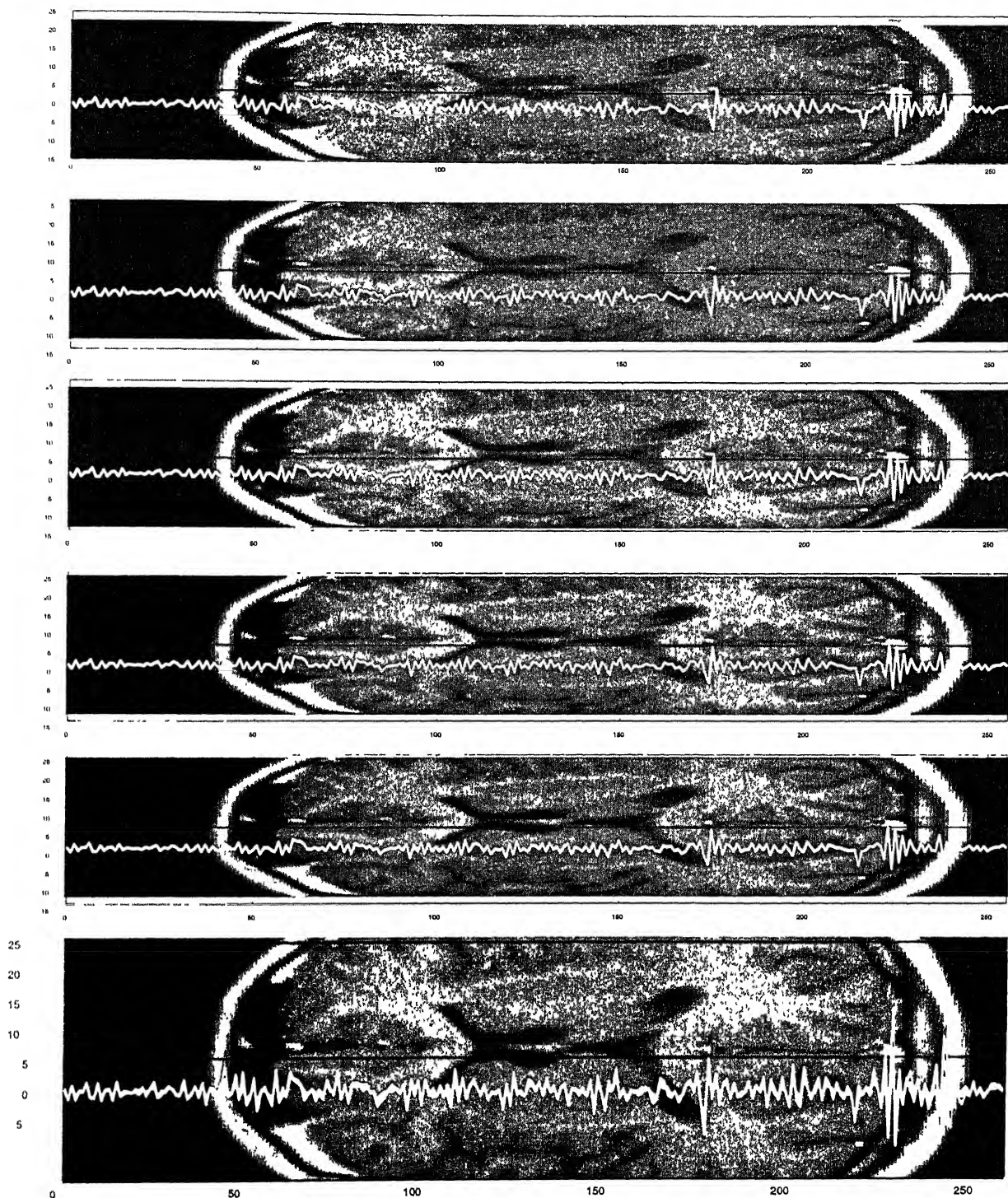
Graph 1.4. (b) : Signed De-Blurring Errors ($f - \sigma_{n,m}f$, $m = 7,8,9,10,11$) & superposition of all 11 above.

CHAPTER 2: DE-BLURRING BY GENERALIZED JACKSON OPERATORS

This chapter is a study of the rate of convergence of the de-blurring achieved by the operators:

$$L_{n,p}^{[m]}(f;x) = \sum_{J=1}^{m} (-1)^{J-1} \binom{m}{m} L_{n,p}^{J}(f;x), \ n = 1,2,3,..., \ (1 \leq m \leq p-1).$$

where the generalized Jackson operators $\{L_{n,p}\}$ are defined as:

$$L_{n,p}(f;x) = \frac{1}{A_{n,p}} \int_{-\pi}^{\pi} f(t) \left(\frac{\sin \dfrac{n(t-x)}{2}}{\sin \dfrac{t-x}{2}} \right)^{2p} dt = \frac{1}{2} a_0 + \sum \rho_k^{n,p} (a_k \cos kx + b_k \sin kx),$$

for n, p positive integers and $x \in \mathbb{R}$, the real line, where

$$A_{n,p} = \int_{-\pi}^{\pi} \left(\frac{\sin nt/2}{\sin t/2} \right)^{2p} dt \ , \ \rho_k^{n,p} = \frac{\mu_k^{n,p}}{\mu_0^{n,p}} \ ,$$

where

$$\mu_k^{n,p} = \sum_{J=0}^{p-1} (-1)^J \binom{2p}{j} \binom{np+p-nj-k-1}{2p-1} , \ n \geq 1, \ k \geq 0,$$

are the coefficients in the expansion

$$\left(\frac{\sin nt/2}{\sin t/2} \right)^{2p} = \mu_0^{(n,p)} + 2 \sum_{k=1}^{np-p} \mu_k^{(n,p)} \cos k .$$

The first section entitled "Generalized Jackson Operators" is an introduction about the operators $\{L_{n,p}\}$, the second section contains some basic results needed in the subsequent analysis, and the third section contains our main results on the rate of

convergence of the sequence $\{L_{n,p}^{[m]}(f;x)\}$. The final section on the simulation results includes numerical illustrations of the de-blurring achieved on MRI cross-sections using $\{L_{n,p}\}$.

2.1. GENERALIZED JACKSON OPERATORS

The Jackson operators U_n defined by

$$U_n(f;x) = \frac{3}{2\pi n(2n^2+1)} \int_{-\pi}^{\pi} f(t) \left(\frac{\sin\frac{n(t-x)}{2}}{\sin\frac{t-x}{2}} \right)^4 dt,$$

were introduced by D. Jackson to prove his celebrated classical Jackson theorem:

$$E_n(f) \le C\omega(f;1/n), f \in C_{2\pi},$$

where $E_n(f)$ denotes the error in the best approximation of f by trigonometric polynomials of order n, and $\omega(f;\delta)$ denotes the modulus of continuity of f of order 1. The generalizations $L_{n,p}$, $p \ge 2$, as defined above, have subsequently been considered by many researchers, including G.P. Safranova (1950), I.M. Petrov (1958, 1960), P.P. Korovkin (1960), I.M. Petrov (1960), Y. Matsuoka (1960), I.P. Natanson (1964), Wang Xing-Hua(1964), F.D. van Niekerk (1965), F. Schurer(1965), G.G. Lorentz (1966), F. Schurer and Steutel (1967), R.K.S. Rathore (1974, 1976) and many others.

G.G. Lorentz (1966) used the modification $I_{n,r}$ of the generalized Jackson operators defined by

$$I_{n,r} = \frac{1}{A_{n,r}} \int_{-\pi}^{\pi} \left(\frac{\sin\frac{nt}{2}}{\sin\frac{t}{2}} \right)^{2p} \sum_{k=1}^{r+1} (-1)^{k-1} \binom{r+1}{k} f(x+kt) dt$$

to prove a higher modulus of smoothness estimate:

$$|f(x) - I_{n,r}(x)| \le M_r \omega_{r+1}(f;\tfrac{1}{n}), \quad n = 1, 2, \ldots, \quad p \ge \tfrac{1}{2}(r+3)$$

R.K.S. Rathore (1974) considered the linear combinations

$$\mathcal{L}_{n,p}^{[m]}(x) = \Delta_{m+1}(L_{n,p})/\Delta_{m+1},$$

where $\Delta_{m+1} = \det((1/i^{j-1})_{i,j=1}^{m+1})$, and $\Delta_{m+1}(L_{n,p})$ is the determinant obtained from Δ_{m+1} by replacing the first column elements a_{i1} by $L_{n,p}(f;x)$, $i = 1, 2, \ldots, m+1$, and proved that: $\|\mathcal{L}_{n,p}^{[m]}(x) - f(x)\| \le C_k \omega_k(f;n^{-1})$, $(k \le m + 1)$, where C_k is an absolute constant independent of f and n.

A proof of the basic convergence of $L_{n,p}(f;x)$ is given in F. Schurer and F.W. Steutel (1967), which also contains most of the results on $L_{n,p}(f;x)$ described below.

2.1.1. THEOREM

The sequence $\{L_{n,p}(f;x)\}$ $(n = 1, 2, \ldots)$ converges to f(x) uniformly on $[-\pi, \pi]$.

The following modulus of continuity estimate for $p = 2$ is due to P.P. Korovkin and was extended for a general p by F. Schurer and F.W. Steutel (1967):

2.1.2. THEOREM

For all $f(x) \in C_{2\pi}$ and all integers $p \ge 3$,
$$\left\| L_{n,p}(f) - f \right\| \le \left(1 + \tfrac{1}{2}\pi\sqrt{2}\right)\omega\left(f;\tfrac{1}{n}\right), \qquad (n = 1, 2, \ldots).$$

Interestingly enough, the least constant associated with $\omega(f; 1/n)$ turns out to be 3/2. For $p = 2$, this result is due to Wang Xing-Hua (1964); for $p = 3, 4$ due to van Niekerk (1965) and for $p \ge 5$ due to F. Schurer and F.W. Steutel (1967).

2.1.3. THEOREM

Let $p = 2, 3, \ldots$. Then the smallest constant C_p such that

$$\left\| L_{n,p} f - f \right\| \le C_p \omega(f;\tfrac{\pi}{2n}), \quad n = 1, 2, \ldots; f \in C_{2\pi},$$

is given by $C_p = 3/2$.

A Voronovskaja-type asymptotic formula for $L_{n,p}(f;x)$ is given by:

2.1.4. THEOREM (F. SCHURER AND F.W. STEUTEL (1967))

If $f \in C_{2\pi}$ has a second derivative at the fixed point $x \in [-\pi, \pi]$, then for $p \geq 2$

$$L_{n,p}(f;x) - f(x) = a_p \frac{f^{(2)}(x)}{n^2} + o\left(\frac{1}{n^2}\right)$$

where:

$$a_p = 2\frac{S(p, p-1)}{S(p,p)} = (2p-1)(p-1)\frac{\sum_{j=0}^{p-1}(-1)^{j+1}\binom{2p}{j}(p-j)^{2p-3}}{\sum_{j=0}^{p-1}(-1)^{j}\binom{2p}{j}(p-j)^{2p-1}}.$$

Here, the functions $S(\nu, \mu)$ arise in the context of the following:

2.1.5. LEMMA (G.M. FICHTENHOLZ (1964))

If ν and μ are positive integers, then

$$S(\nu, \mu) = \int_0^\infty \frac{(\sin x)^{2\nu}}{x^{2\mu}}\,dx = \frac{(-1)^{\nu+\mu}}{2^{2\nu}(2\mu-1)!}\sum_{j=0}^{\nu-1}(-1)^j\binom{2\nu}{j}(2\nu-2j)^{2\mu-1} \quad, \quad (\nu \geq \mu),$$

$$S(\nu, \mu + \tfrac{1}{2}) = \int_0^\infty \frac{(\sin x)^{2\nu}}{x^{2\mu+1}}\,dx = \frac{(-1)^{\nu+\mu+1}}{2^{2\nu-1}(2\mu)!}\sum_{j=0}^{\nu-1}(-1)^j\binom{2\nu}{j}(2\nu-2j)^{2\mu}\log(2\nu-2j),$$

$(\nu > \mu)$.

For the class of functions $Z = \{f \in C_{2\pi}: |f(x+t) - 2f(x) + f(x-t)| \leq 2|t|\}$, which actually is a section of the Zygmund-class,

$$b_{n,p} = np \sup_{f(x) \in Z} |L_{n,p}(f) - f|, \quad (p \geq 2),$$

may be regarded as a measure for the quality of the approximation of the class Z by means of the operators $L_{n,p}$.

For the case $p = 2$ I.M. Petrov (1958) has proved that

$$\lim_{n\to\infty} b_{n,2} = \frac{12\log 2}{\pi} = 2.647\ldots$$

For the quantities b_p defined by

$$b_p = \lim_{n\to\infty} b_{n,p} \quad (p = 2,3,\ldots)$$

the following results are due to F. Schurer and F.W. Steutel (1967).

2.1.6. THEOREM

If for the operators $L_{n,p}$ the quantities $b_{n,p}$ are defined as above, then

$$b_p = 2p\frac{S(p, p-\frac{1}{2})}{S(p, p)}.$$

2.1.7. COROLLARY

$$b_p \sim 2\sqrt{\frac{3p}{\pi}}, \quad (p \to \infty).$$

2.1.8. THEOREM

$$\min_{(p)} b_p = b_2 = \frac{12\log 2}{\pi}.$$

Similarly, for the class $Z_2 = \{f \in C_{2\pi}: |f(x+t) - 2f(x) + f(x-t)| \le t^2\}$ (the notation Z_2 here is different from that of Chapter 0) of functions there holds:

2.1.9. THEOREM (F. SCHURER AND F.W. STEUTEL (1967))

With $c_{n,p}$ is defined by

$$c_{n,p} = n^2 p^2 \sup_{f(x)\in Z_2} \left\| L_{n,p}(f) - f \right\| \qquad (p \ge 2),$$

$$c_p = \lim_{n\to\infty} c_{n,p} = 2p^2\frac{S(p, p-1)}{S(p, p)} = (2p-1)p^2(p-1)\frac{\displaystyle\sum_{j=0}^{p-1}(-1)^{j+1}\binom{2p}{j}(p-j)^{2p-3}}{\displaystyle\sum_{j=0}^{p-1}(-1)^j\binom{2p}{j}(p-j)^{2p-1}}.$$

2.1.10. COROLLARY

$$c_p \sim 3p, \qquad (p \to \infty).$$

The following results on the approximation of derivatives by the derivatives of $L_{n,p}(f; x)$ and a Voronovskaja-type formula in this simultaneous approximation were obtained by R.K.S. Rathore (1976):

2.1.11. THEOREM (R.K.S. RATHORE (1976))

Let p and r be positive integers such that r ≤ 2p-2. Let f be a 2π-periodic integrable

function. If at a point x ∈ ℝ, both the right and the left derivatives $f_+^{(r)}(x)$ and

$f_-^{(r)}(x)$ exist, then

$$\lim_{n \to \infty} L_{n,p}^{(r)}(f;x) = (f_+^{(r)}(x) + f_-^{(r)}(x))/2 .$$

Further, if f is such that the derivative $f^{(r)}(x)$ exists in an open interval containing an

interval [a, b] ⊆ ℝ and is continuous at each x ∈ [a, b], then uniformly in x ∈ [a, b]:

$$\lim_{n \to \infty} L_{n,p}^{(r)}(f;x) = f^{(r)}(x) .$$

2.1.12. THEOREM (R.K.S. RATHORE (1976))

Let p and r be positive integers with r ≤ 2p-4. Let f be a 2π-periodic integrable

function. If at a point x ∈ ℝ, the right and the left derivatives $f_+^{(r+2)}(x)$ and $f_-^{(r+2)}(x)$

exist, then

$$L_{n,p}^{(r)}(f;x) - f^{(r)}(x) = (1 - \mu_1^{(n,p)}/\mu_0^{(n,p)})(f_+^{(r+2)}(x) + f_-^{(r+2)}(x))/2 + o(1/n^2), \ n \to \infty .$$

Further, if f is such that the derivative $f^{(2r+2)}(x)$ exists in an open interval containing

an interval [a, b] ⊆ ℝ and is continuous at each x ∈ [a,b], then uniformly in x ∈ [a,b]:

$$L_{n,p}^{(r)}(f;x) - f^{(r)}(x) = (1 - \mu_1^{(n,p)}/\mu_0^{(n,p)})f^{(r+2)}(x) + o(1/n^2), \ n \to \infty .$$

It was also pointed out in R.K.S. Rathore (1976) that by the technique of linear combinations of the operators obtained in R.K.S. Rathore (1974), the convergence to the value $f^{(r)}(x)$ can be substantially accelerated for sufficiently smooth functions.

2.2. SOME BASIC RESULTS

In this section we collect some basic results needed to prove our results on the degree of approximation in the de-blurring by the operators

$$L_{n,p}^{[m]} = \sum_{J=1}^{m} (-1)^{J-1} \binom{m}{j} L_{n,p}^J .$$

2.2.1. LEMMA (R.K.S. RATHORE (1974))

Let m be a positive number and $2p > m+1$; then

$$L_{n,p}\left(|t|^m;0\right) \equiv L_{n,p}\left(|t-x|^m;x\right) \le C_{m,p} n^{-m},$$

where $C_{m,p}$ is a constant independent of n, and $L_{n\ p}\left(|t|^{2p};0\right) \le C n^{-(2p-1)}$, $n \to \infty$.

2.2.2. LEMMA

$$L^j_{n,p}\left(\sin^{2k}\frac{t-x}{2};x\right) = O(n^{-2k}), \ n\to\infty, \ j = 1, 2, 3, \ldots, (k < p).$$

Proof: For $j = 1$, the result follows from the previous Lemma 2.2.1. For $j \ge 2$, by induction, assuming the result up to $(j-1)$-th iterates of $L_{n,p}$, we have

$$L^j_{n,p}\left(\sin^{2m}\frac{t-x}{2};x\right) = L^{j-1}_{n,p}\left(L_{n,p}\left(\sin^{2m}\frac{t-s+s-x}{2};s\right);x\right)$$

$$= L^{j-1}_{n,p}\left(L_{n,p}\left((\sin\frac{t-s}{2}\cos\frac{s-x}{2}+\cos\frac{t-s}{2}\sin\frac{s-x}{2})^{2m};s\right);x\right)$$

$$\le L^{j-1}_{n,p}\left(L_{n,p}\left((2\sin^2\frac{t-s}{2}+2\sin^2\frac{s-x}{2})^m;s\right);x\right)$$

$$\le 2^m\sum_{k=0}^{m}\binom{m}{k}L^{j-1}_{n,p}\left((\sin^{2k}\frac{s-x}{2})L_{n,p}((\sin^{2(m-k)}\frac{t-s}{2};s);x\right)$$

$$\le 2^m\sum_{k=0}^{m}\binom{m}{k}L^{j-1}_{n,p}\left((\sin^{2k}\frac{s-x}{2});x\right)L_{n,p}\left((\sin^{2(m-k)}\frac{t-x}{2};x\right)$$

$$\le 2^m\sum_{k=0}^{m}\binom{m}{k}L^{j-1}_{n,p}\left((\sin^{2k}\frac{t-x}{2});x\right)L_{n,p}\left((\sin^{2(m-k)}\frac{t-x}{2};x\right)$$

$$\le 2^m\sum_{k=0}^{m}\binom{m}{k}O(n^{-2k})O(n^{-2(m-k)}) = O(n^{-2m})$$

as the variables t and s are just the dummy variables, completing the proof.

2.2.3. LEMMA (G. FREUD (1967))

$$\|f^{(k-1)}\| \le 2\pi\|f^{(k)}\|, f\in C^{(k)}_{2\pi}, k \ge 2.$$

2.2.4. LEMMA

There exist trigonometric polynomials T_k, such that for $f \in C^{(2m)}_{2\pi}$,

$$|f(t)-f(x)-\sum_{k=1}^{2m-1}[f^{(k)}(x)/k!]T_k(t-x)| \le A\|f^{(2m)}\|\sin^{2m}(t-x)/2$$

where A is a constant independent of f.

Proof: For the functions $\Omega^{(k)}$ given by

$$\Omega^{(k)}(t, x) = -\Delta^{(k)}(t, x)/\Delta^{(0)}(x, x),$$

where $\Delta^{(k)}(t, x)$, $k = 0, 1, \ldots, m+1$, are the determinants of $(m+1)$-th order defined by

$\Delta^{(k)}(t, x) = |(a_{ij}^k)_{i,j=1}^{m+1}|$, where with $[j/2]$ denoting the largest integer not greater than $j/2$,

$$a_{1j}^{(k)} = \begin{cases} 1, & j = 1 \\ \sin[j/2]t, & j \text{ is even}, \\ \cos[j/2]t, & j \text{ is odd} \end{cases}$$

$$a_{k+1j}^{(k)} = \begin{cases} 1, & j = 1 \\ \sin[j/2]x, & j \text{ is even}, \quad k \neq 0, \\ \cos[j/2]x, & j \text{ is odd} \end{cases}$$

and

$$a_{ij}^{(k)} = \frac{d^{i-1}}{dx^{i-1}} a_{k+1j}^{(k)}, 1 \neq i \neq k+1,$$

R.K.S. Rathore (1974) showed that $\Omega^{(k)}(t, x) = (t\text{-}x)^k + O(|t\text{-}x|^{m+1})$, and moreover that

$$f(t) - f(x) = \sum_{k=1}^{r} [f^{(k)}(x)/k!]\Omega^{(k)} + h_x(t)(t-x)^r, (r \leq m),$$

where, with $h_x(x) = 0$, $h_x(t)$ is bounded and is continuous at $t = x$. From this by using L'Hospital's rule we find that: $|h_x(t)| \leq C[|f'(x)| + |f''(x)| + \ldots + |f^{(r-1)}(x)| + \|f^{(r)}\|]$, for some constant C, not depending on f or x.

Replacing m in above by $2m$, and taking $T_k(t) = \Omega^{(k)}(t, 0)$, in view of the G. Freud's inequality: $\|f^{(k)}\| \leq (2\pi)^{2m-k} \|f^{(2m)}\|$, $f \in C_{2\pi}^{(k)}$, $2m > k \geq 2$, and elementary fact that for $0 \leq |t - x| \leq \pi$, $\sin^2(t - x)/2 \geq \pi^{-2}(t - x)^2$, the result follows.

2.2.5. LEMMA

If T is a trigonometric polynomial, $\left\|L_{n,p}^{[m]}T - T\right\| = O(n^{-2m}), n \to \infty$.

Proof: If $f_k(x)$ is one of the functions $\cos kx$, or $\sin kx$, in view of $1 - \rho_k^{n,p} = O(n^{-2})$, which follows from the asymptotic formula of F. Schurer and F.W. Steutel (1967),

$$L_{n,p}^{[m]}f_k - f_k = -(1 - \rho_k^{n,p})^m f_k = O(n^{-2m}), n \to \infty.$$

Since any trigonometric polynomial is a combination of these functions and the operator maps 1 into 1, the result follows.

The modulus ω_m of smoothness of order m occurring in the sequel is defined by:

$$\omega_m(f;\delta) = \max_{|h|\le\delta}\left\|\sum_{k=0}^{m}(-1)^k\binom{m}{k}f(x+kh)\right\|,$$

the norm being the sup-norm with respect to the variable x.

The following general result using $\omega_m(f,\delta)$, was proved by G. Freud (1959) for the case $m = 2$ and was conjectured by him for arbitrary integer m. In full generality it was subsequently proved by G.I. Sunouchi (1964):

2.2.6. LEMMA (G.I. SUNOUCHI (1964))

Let B be a linear operator $C_{2\pi} \to C_{2\pi}$, $B^{(m)}$ the restriction of B to the space $C_{2\pi}^{(m)}$ of 2π-periodic functions having a continuous 2π-periodic m-th derivative. Then, for an arbitrary $f \in C_{2\pi}$ and an arbitrary integer v, we have for all x,

$$\|B(f)\|_{C_{2\pi}} = \max | B(f;x) |\le K_m\left(\|B\|+v^m\|B^{(m)}\|\right)\omega_m(f;v^{-1}),$$

where the norms of the linear operators B, respectively, $B^{(m)}$ are defined as

$$\|B\| = \sup_{|f|_{C_{2\pi}}\le 1}\|B(f)\|_{C_{2\pi}},\ \|B^{(m)}\| = \sup_{f\in C_{2\pi}^{(m)},\|f^{(m)}\|\le 1}\|B^{(m)}(f)\|_{C_{2\pi}}.$$

We will also use the following version of Jackson-Bernstein theorem (a consequence of Theorem 5.1, in R.K.S. Rathore (2000)):

2.2.7. THEOREM

Let $E_n(f)$ denote the error in approximating $f \in C_{2\pi}$ by the trigonometric polynomial of order n of best approximation. Then:

$$E_n(f) = O(\varphi(1/n))\ \ \textit{iff}\ \ \omega_{2m}(f;t) = O(\varphi(t)),$$

and

$$E_n(f) = o(\varphi(1/n))\ \ \textit{iff}\ \ \omega_{2m}(f;t) = o(\varphi(t)).$$

In this theorem, and in the rest of this chapter, $\varphi(t)$ denotes an order function associated with the growth function $\phi(t) = t^{2m}$, as in the Oh-oh-Lemma 1.2.3.

2.3. DEGREE OF DE-BLURRING BY GENERALIZED JACKSON OPERATORS

Based on the results of the previous section, a direct theorem on the degree of approximation of f by the de-blurring operation $L_{n,p}^{[m]} f$ is as follows:

2.3.1. THEOREM

For all $f \in C_{2\pi}$, there holds the error estimate:

$$\left\| L_{n,p}^{[m]} f - f \right\| \le A_{m,p} \omega_{2m}(f; n^{-1}), \quad 1 \le m \le p-1, \ (n \ge 1).$$

where the constant $A_{m,p}$ does not depend on n or f.

Proof: Operating on the estimate

$$\left| f(t) - f(x) - \sum_{k=1}^{2m-1} [f^{(k)}(x)/k!] T_k(t-x) \right| \le A \left\| f^{(2m)} \right\| \sin^{2m}(t-x)/2,$$

obtained in the previous section, we have

$$\left| L_{n,p}^{[m]}(f;x) - f(x) \right| \le \sum_{k=1}^{m-1} \frac{\left\| f^{(2k)}(x) \right\|}{(2k)!} A_{k,m} n^{-2m} + A(2^m - 1) \left\| f^{(2m)} \right\| O(n^{-2m}).$$

In view of G. Freud's inequalities $\left\| f^{(k-1)} \right\| \le 2\pi \left\| f^{(k)} \right\|$, $k > 1$, $f \in C_{2\pi}^{(k)}$, therefore

$$\left\| L_{n,p}^{[m]} f - f \right\| \le B n^{-2m} \left\| f^{(2m)} \right\|, \quad 1 \le m \le p-1, \quad f \in C_{2\pi}^{(2m)},$$

where B is an absolute constant, independent of f and n.

Using G.I. Sunouchi's result, as $\left\| L_{n,p}^{j} \right\| = 1$, $(j \ge 1)$, we have

$$\left\| L_{n,p}^{[m]} f - f \right\| \le K_{2m} \left(\left\| L_{n,p}^{[m]} - I \right\| + v^{2m} \left\| \left(L_{n,p}^{[m]} - I \right)^{(2m)} \right\| \right) \omega_{2m}(f; v^{-1})$$

$$\le K_{2m} \left(2^m + v^{2m} B n^{-2m} \right) \omega_{2m}(f; v^{-1})$$

Taking $v = n$, the theorem follows.

Note that since the approximations $L_{n,p}^{[m]} f$ are trigonometric polynomials of order $np-p$, their above order of approximation is the same as that of the trigonometric polynomials of best approximation given by the classical Jackson theorem: $E_n(f) \leq C_k \omega_{2m}(f;1/n)$.

The estimate of Theorem 2.3.1 and the Theorem 2.2.7 of the previous section now implies the following:

2.3.2. THEOREM (INVERSE)

If $f \in C_{2\pi}$, $1 \leq m \leq p-1$ and $\varphi(t)$ is an order function associated with the growth function $\phi(t) = t^{2m}$, then:

$$\left\| L_{n,p}^{[m]} f - f \right\| = O(\varphi(1/n)) \text{ iff } \omega_{2m}(f;t) = O(\varphi(t))$$

and,

$$\left\| L_{n,p}^{[m]} f - f \right\| = o(\varphi(1/n)) \text{ iff } \omega_{2m}(f;t) = o(\varphi(t)).$$

Proof: The 'if part' of the result is a consequence of Theorem 2.3.1 and the 'only if part' that of Theorem 2.2.7.

A self contained proof of the 'only if part' of the above theorem could be based on the Bernstein's inequality $\| T_n' \| \leq n \| T_n \|$ for a Trigonometric polynomial of order n, along the lines of the last theorem (Theorem 3.3.2) in the next chapter.

Taking $\varphi(t) = t^\alpha$, in Theorem 2.3.2, we have the following:

2.3.3. COROLLARY

Let $0 < \alpha < 2m \leq 2p-2$, and $f \in C_{2\pi}$. Then:

$$\left\| L_{n,p}^{[m]} f - f \right\| = O(n^{-\alpha}) \text{ iff } \omega_{2m}(f;t) = O(t^\alpha),$$

and,

$$\left\| L_{n,p}^{[m]} f - f \right\| = o(n^{-\alpha}) \text{ iff } \omega_{2m}(f;t) = o(t^\alpha).$$
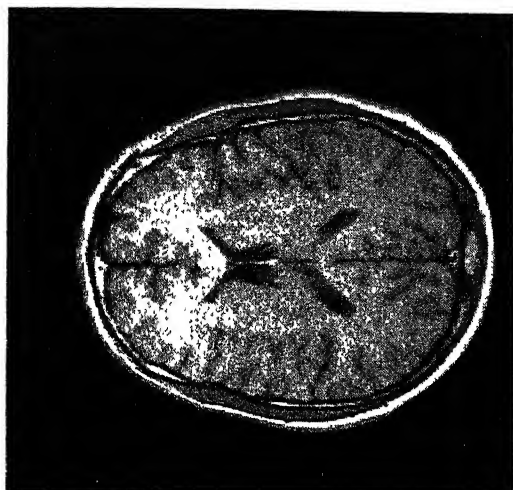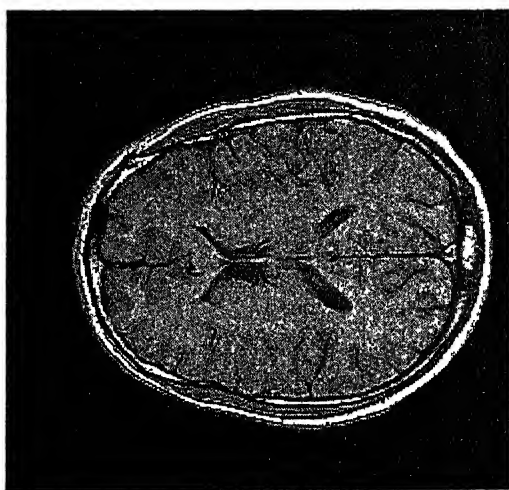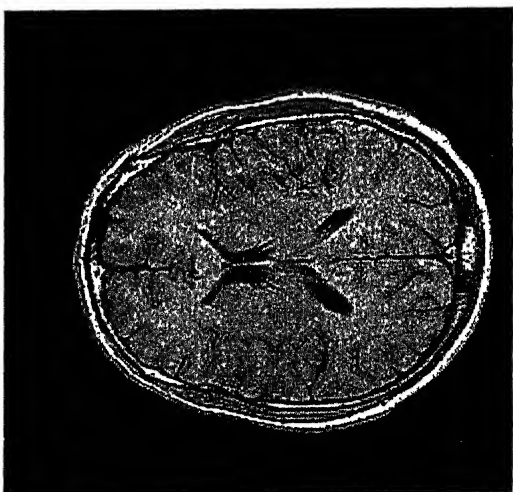
Original
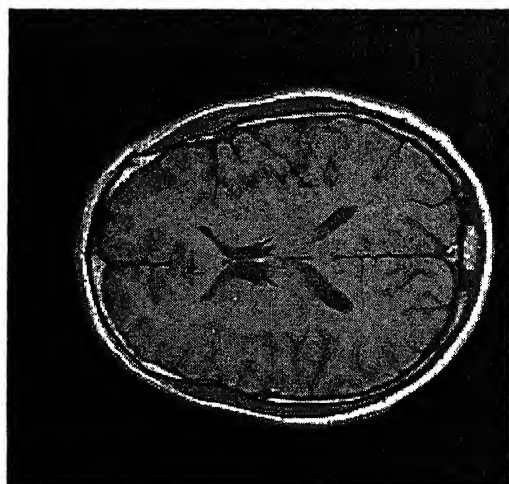
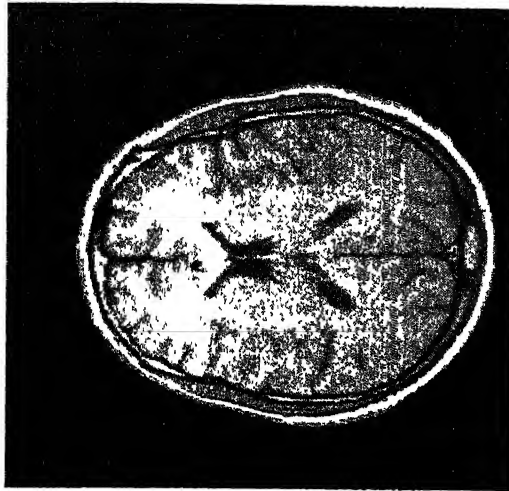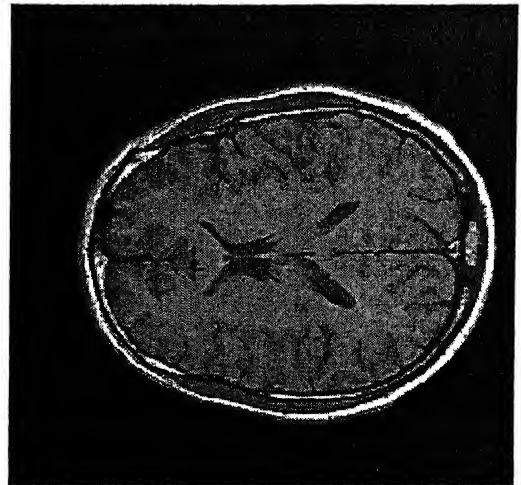
Iteration 1
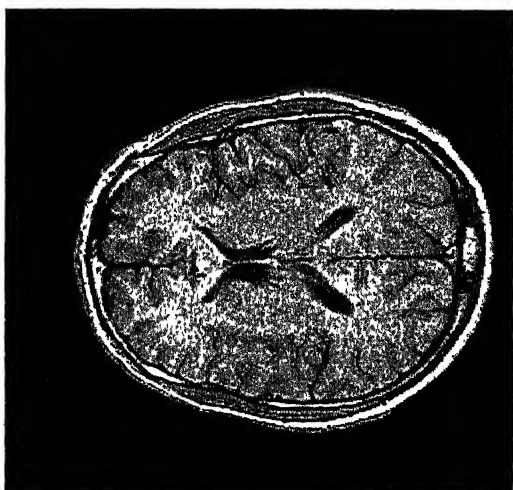
Iteration 2

Iteration 3

Iteration 4

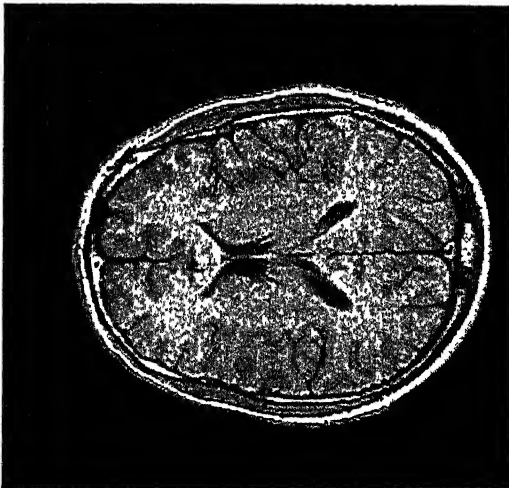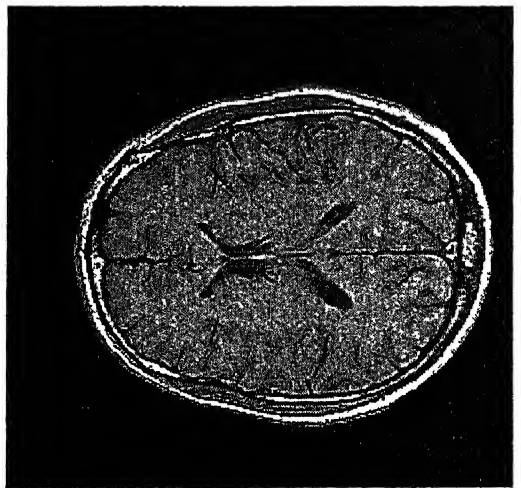
Direct Filter Inversion

Fig. 2.1 : Deblurring by Generalized Jackson operator (p=2) and direct filter inversion
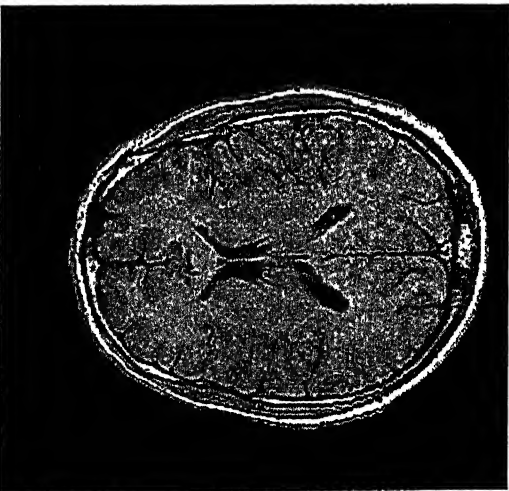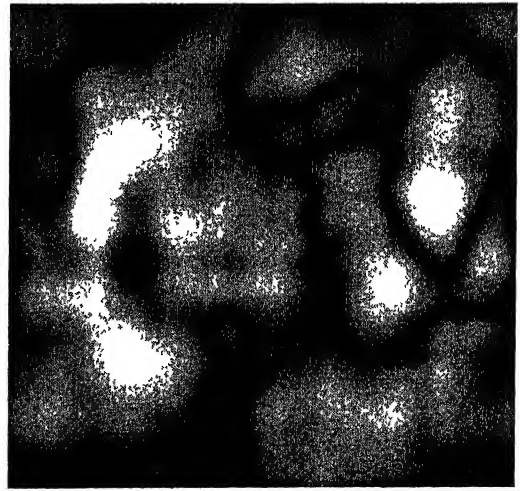
Original
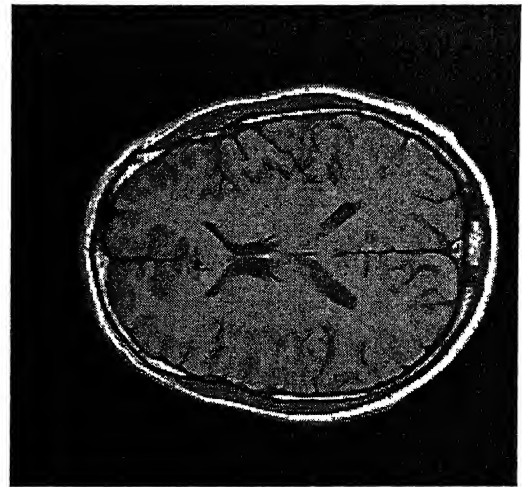

Iteration 1

Iteration 2

Iteration 3

Iteration 4

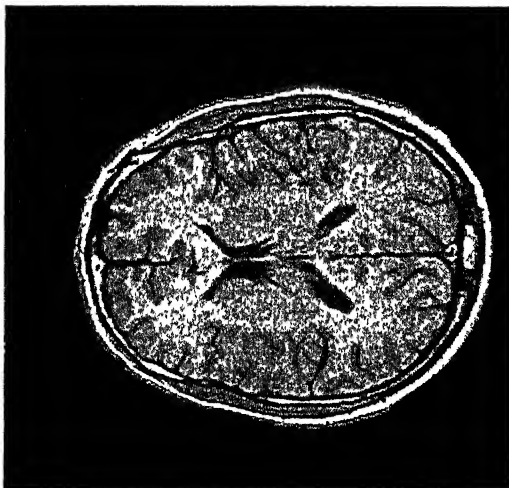
Direct Filter Inversion

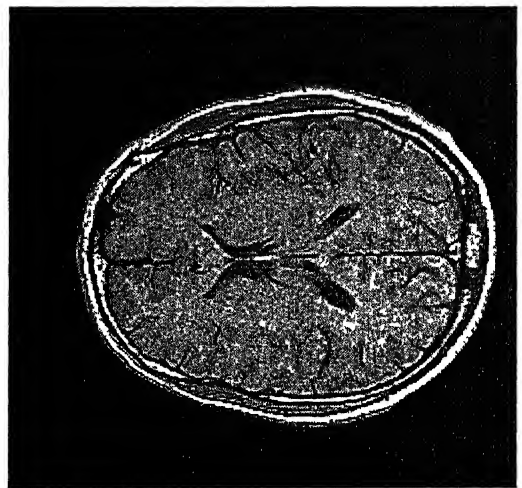**Fig. 2.2** : Deblurring by Generalized Jackson operator (p=3) and direct filter inversion
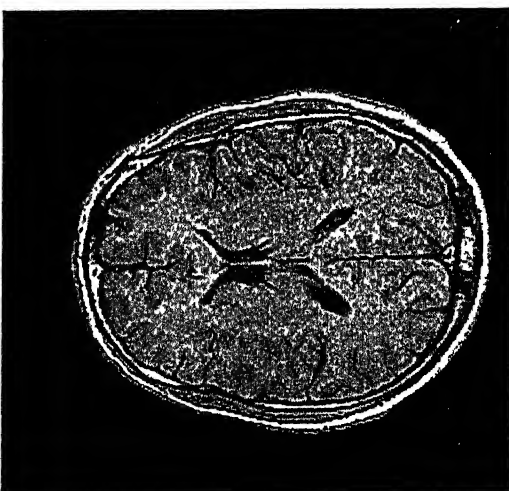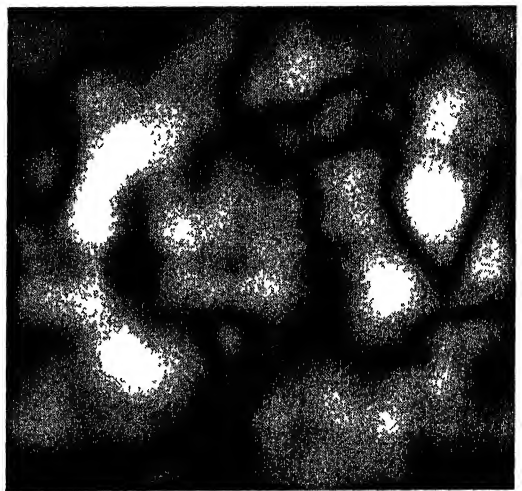
Original

Iteration 1

Iteration 2

Iteration 3

Iteration 4

Direct filter Inversion

Fig. 2.3 : Deblurring by Generalized Jackson operator (p=4) and direct filter inversion

2.4.2 NUMERICAL ERRORS IN THE ITERATIVE DE-BLURRINGS BY $L_{n,p}^{[m]}$

The second experiment studies the quantitative behavior of the errors in the iterative de-blurrings with $L_{n,p}^{[m]}$. The setup is essentially the same as that of Chapter 1. The same originals as before are taken to be the examples of actual reference cross-sections, which were the T_1, T_2 and proton density-weighted SE images given in Fig. 0.4. The associated gray-levels constitute the functions f for the "Original" cross-sections in Figs. 2.6-2.8.

These functions f representing the cross sections are blurred by the Generalized Jackson filters $L_{n,p}$ (p = 2, 3, 4, with respective n = 65, 45, 35), in both the frequency and the phase encoding directions, to obtain the "Blurred" images shown as the second images in the Figs. 2.6-2.8. The images that result on applying the de-blurring operators $L_{n,p}^{[m]}$ on these blurred images are named "Iteration 1", "Iteration 4", "Iteration 7", and "Iteration 10" and are presented in the second and the third image rows in the figures. These reconstructed images $L_{n,p}^{[m]}$ correspond to the values $m = 2, 5, 8$, and 11, respectively.

A visual comparison of the "Original" images with the "Blurred" images shows the nature of blur in the latter images due to the generalized Jackson operators $L_{n,p}$. The progressive return to the sharpness of the original cross-sections through the use of $L_{n,p}^{[m]}$ may be seen from the images corresponding to the iterates "Iteration 1" through "Iteration 10", given in the Figs: 2.6-2.8.
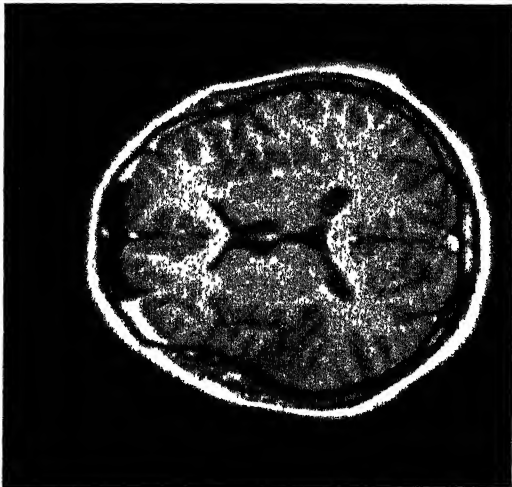
The Tables 2.5-2.7. contain the corresponding numerical values of the associated errors. The same are displayed in the Graphs 2.4-2.6 . The %-errors have been calculated by using the formula: error = 100×||original−reconstruction||/||original||, where the norms under consideration are the L_1, L_2, and L_∞ norms computed over the entire set of 256×256 pixels in the images.
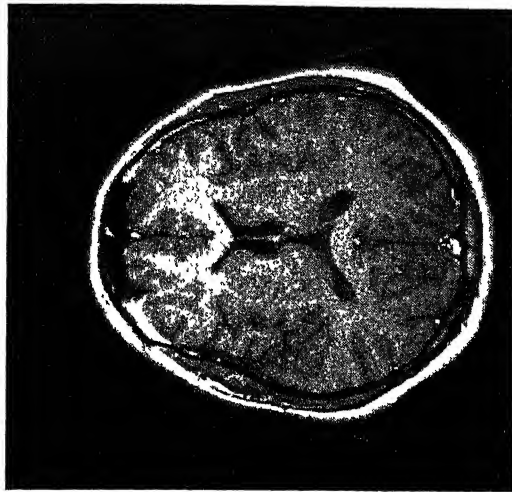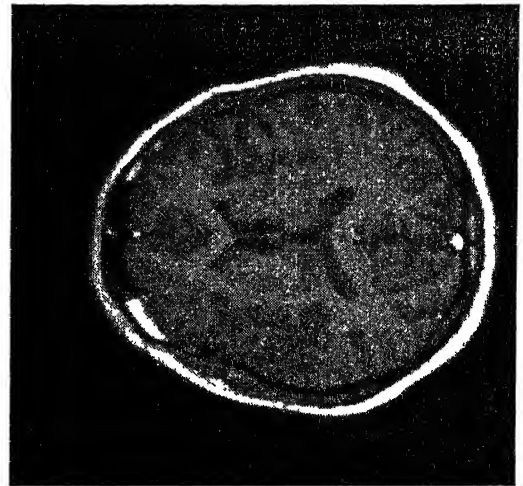
Original

Blurred

Iteration 1

Iteration 4

Iteration 7

Iteration 10

Fig. 2.4 : De-Blurring by Generalized Jackson operator (p=2) (T_1 weighted image)
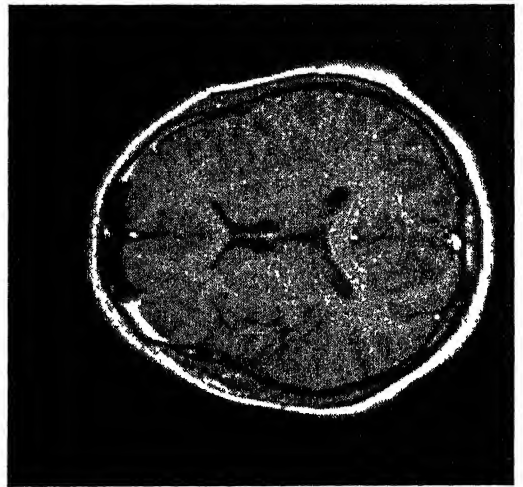
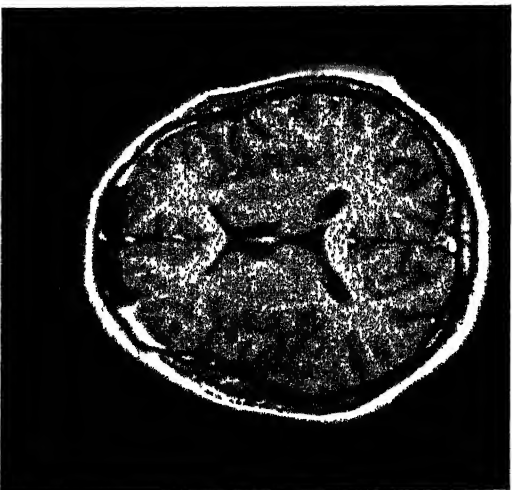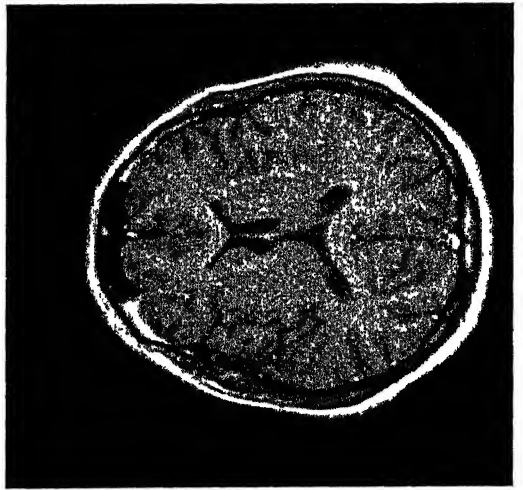Original

Blurred
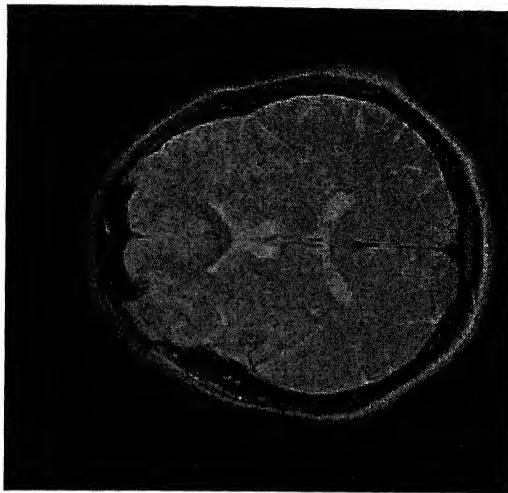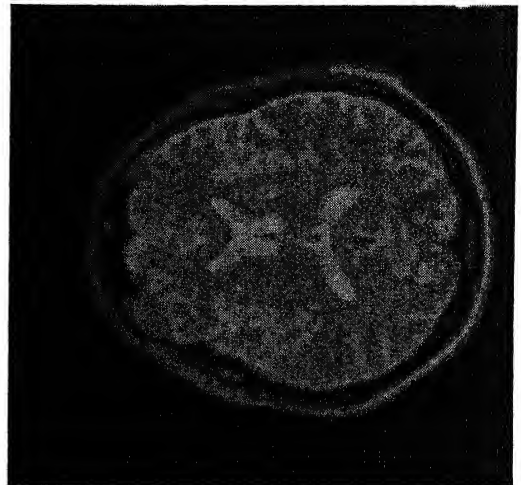
Iteration 1

Iteration 4

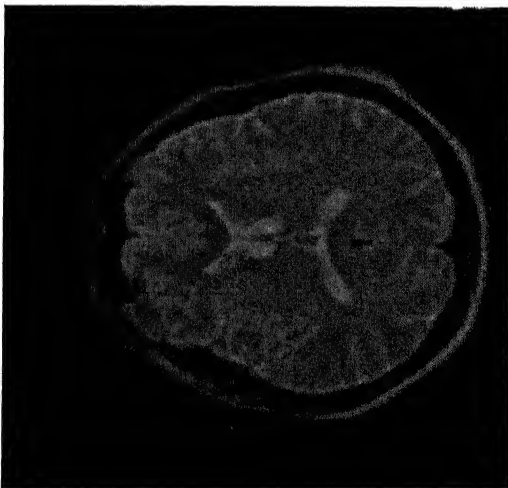Iteration 7

Iteration 10

Fig. 2.5 : De-Blurring by Generalized Jackson operator (p=2) (T$_2$ weighted image)

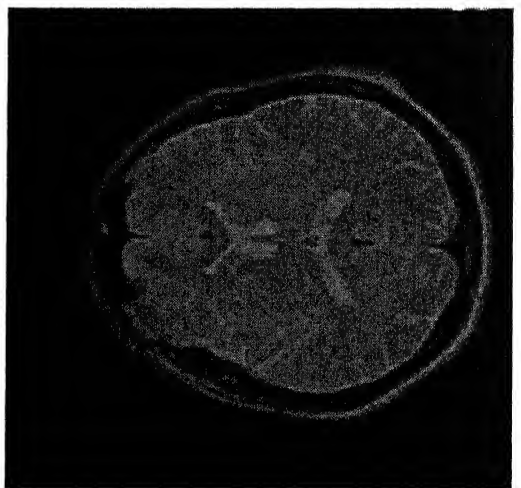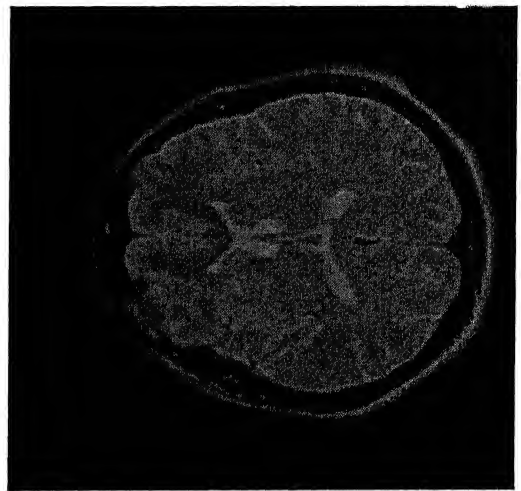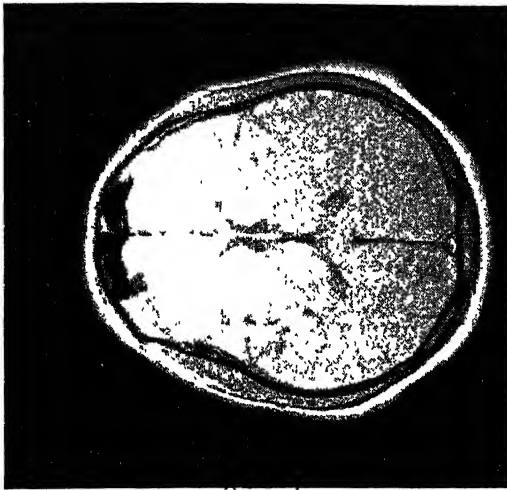Original

Blurred

Iteration 1

Iteration 4

Iteration 7

Iteration 10

Fig. 2.6 : De-Blurring by Generalized Jackson operator (p=2) (Density weighted image)

	L_1 Error	L_2 Error	L_∞ Error
blurred	11.826023	15 174283	39.176308
A_1	9.655653	11 779855	28.377062
A_2	8.924964	10 542892	25 624622
A_3	8 486915	9.811369	23.834412
A_4	8.168295	9 295283	22.535946
A_5	7.918212	8.899959	21 526028
A_6	7 714353	8.582493	20 702404
A_7	7.542678	8.319170	20 007799
A_8	7.395671	8.095625	19.407467
A_9	7.266559	7.902443	18 878998
A_{10}	7 152111	7.733020	18.407181

Table 2.1 : %-Error in De-Blurring by Generalized Jackson operator (p=2)
(T_1 weighted Image)

	L_1 Error	L_2 Error	L_∞ Error
blurred	10.898792	15.052915	57.442039
A_1	9.570345	13 023810	45.283543
A_2	9.032103	12 105190	39.900150
A_3	8.706363	11 514212	36.862049
A_4	8.460309	11.075411	34.657135
A_5	8.258093	10.721021	32.933746
A_6	8.087586	10.421531	31.522835
A_7	7.940648	10.161642	30.331257
A_8	7.812851	9.932296	29.302383
A_9	7.700998	9.728980	28.399206
A_{10}	7.602109	9.548022	27.596172

Table 2.2 . %-Error in De-Blurring by Generalized Jackson operator (p=2)
(T_2 weighted Image)

	L_1 Error	L_2 Error	L_∞ Error
blurred	7.587895	9.755048	37.955128
A_1	6.166692	7.612876	32.114063
A_2	5.685149	6.856499	30.864574
A_3	5.397155	6.411814	29.555965
A_4	5.191302	6.096819	28.291136
A_5	5.031132	5.853706	27.114025
A_6	4.900396	5.656725	26.034811
A_7	4.789762	5.492030	25.050058
A_8	4.694689	5.351151	24.151577
A_9	4.611548	5.228565	23.330147
A_{10}	4.537868	5.120420	22.576988

Table 2.3 : %-Error in De-Blurring by Generalized Jackson operator (p=2)
(Density weighted Image)
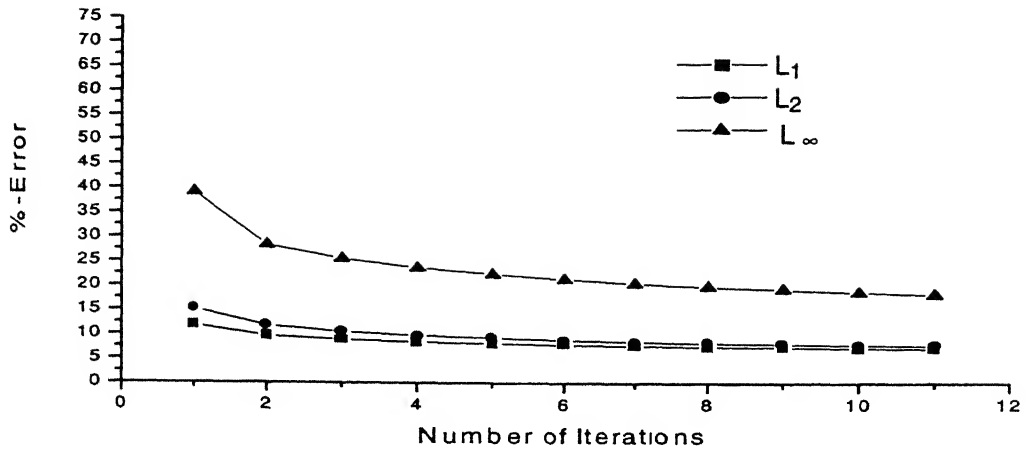
Graph 2.1 : %-Error in De-Blurring by Generalized Jackson operator (p=2) (T_1 weighted image)
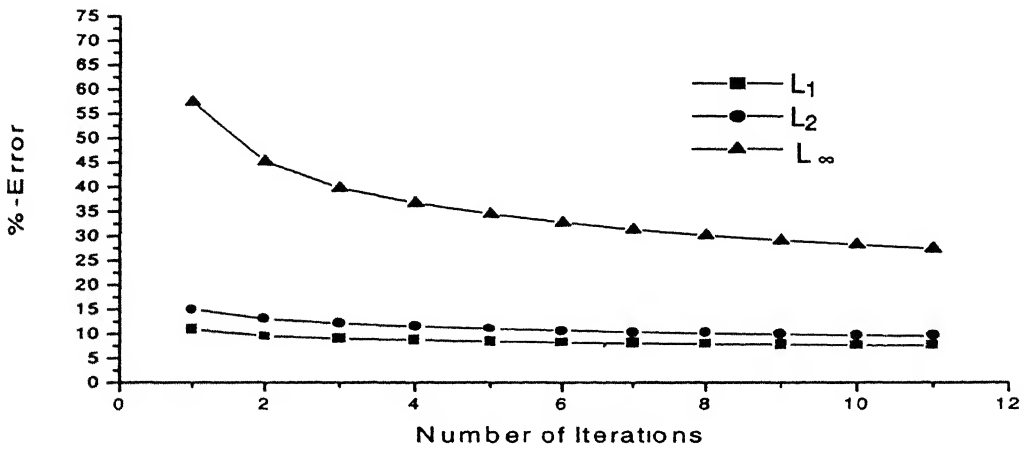
Graph 2.2 : %-Error in De-Blurring by Generalized Jackson operator (p=2) (T_2 weighted image)
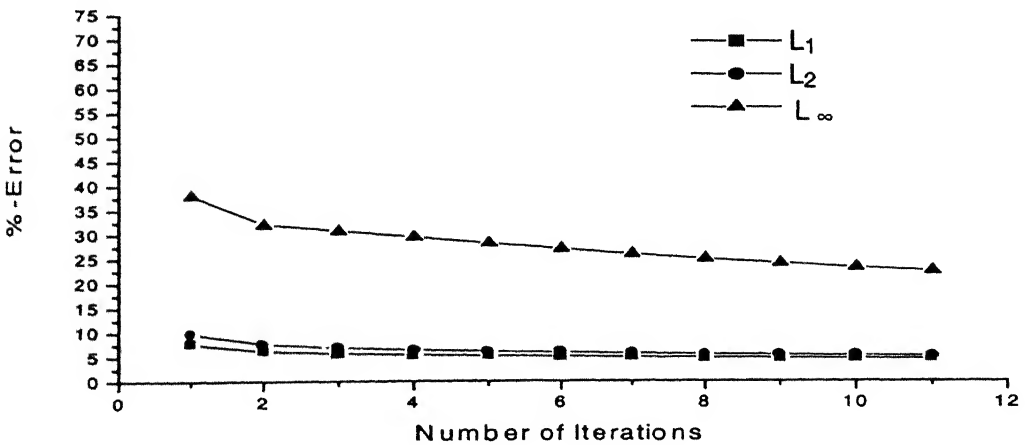
Graph 2.3 : %-Error in De-Blurring by Generalized Jackson operator (p=2) (Density weighted image)

Original

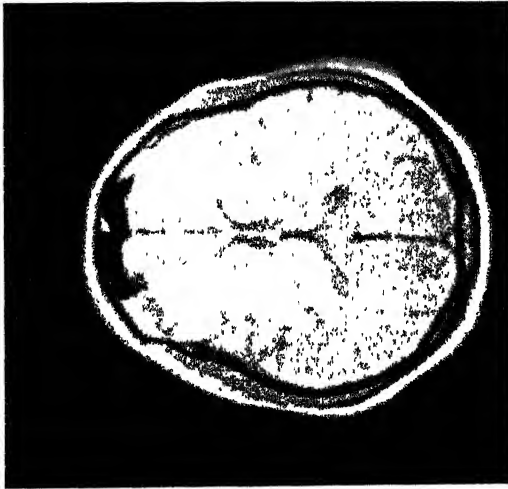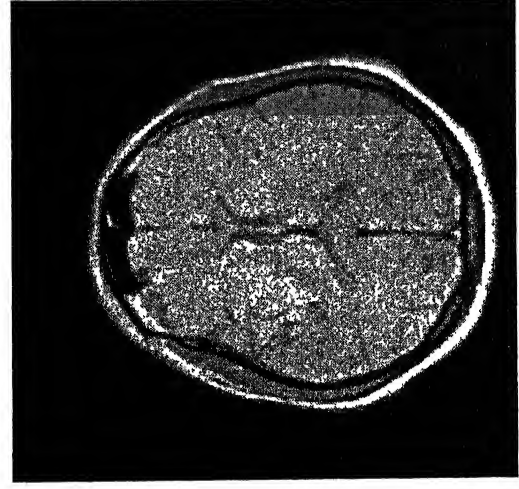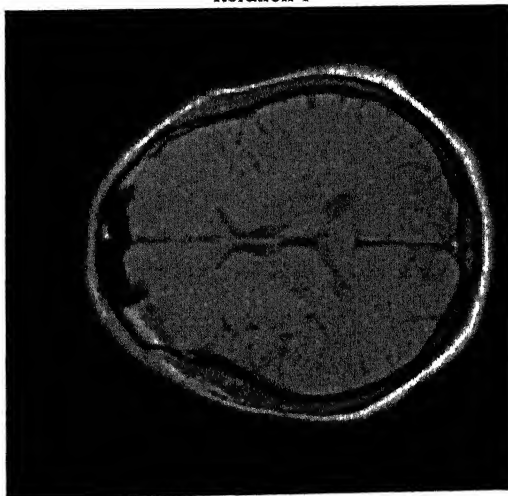Blurred

Iteration 1

Iteration 4

Iteration 7

Iteration 10

Fig. 2.7 : De-Blurring by Generalized Jackson operator (p=3) (T$_1$ weighted image)

Original

Blurred

Iteration 1

Iteration 4

Iteration 7

Iteration 10

Fig. 2.8 : De-Blurring by Generalized Jackson operator (p=3) (T$_2$ weighted image)

Original

Blurred

Iteration 1

Iteration 4

Iteration 7

Iteration 10

Fig. 2.9 : De-Blurring by Generalized Jackson operator (p=3) (Density weighted image)

	L_1 Error	L_2 Error	L_∞ Error
Blurred	13.303324	17.429298	45.340599
A_1	10.916542	13.792450	34 178101
A_2	10.167757	12 509728	29 566097
A_3	9.755668	11.791772	27 978689
A_4	9.472075	11.299795	26 830168
A_5	9.255418	10.926807	25 945477
A_6	9.079027	10 627378	25 233311
A_7	8.929787	10.377771	24.641037
A_8	8.801180	10.164518	24 136005
A_9	8.688785	9.978837	23.696793
A_{10}	8.588157	9 814838	23.308788

Table 2.4 . %-Error in De-Blurring by Generalized Jackson operator (p=3)
(T_1 weighted Image)

	L_1 Error	L_2 Error	L_∞ Error
blurred	11.878249	16.498714	64.058960
A_1	10.547678	14.551584	53.267841
A_2	10.041962	13.712990	47.590000
A_3	9.730365	13.189909	43 934147
A_4	9.513884	12.812903	41.970104
A_5	9.354856	12.520995	40.485146
A_6	9.229193	12.284058	39.281612
A_7	9.123915	12.084971	38.271519
A_8	9.030957	11.913160	37.402035
A_9	8.946622	11.759972	36.639194
A_{10}	8.869592	11.621891	35.959953

Table 2.5 : %-Error in De-Blurring by Generalized Jackson operator (p=3)
(T_2 weighted Image)

|	L_1 Error	L_2 Error	L_∞ Error
blurred	8.557381	11.186337	41.888958
A_1	6.994592	8.855388	35.729176
A_2	6.498222	8.060233	33.982243
A_3	6.221765	7.623755	33.660534
A_4	6.032843	7.328251	33.222908
A_5	5.889729	7.105361	32.732426
A_6	5.773912	6.926474	32.224869
A_7	5.677165	6.777238	31.719654
A_8	5.594154	6.649395	31.227001
A_9	5.521667	6 537702	30 751942
A_{10}	5.457621	6.438704	30.296625

Table 2.6 : %-Error in De-Blurring by Generalized Jackson operator (p=3)
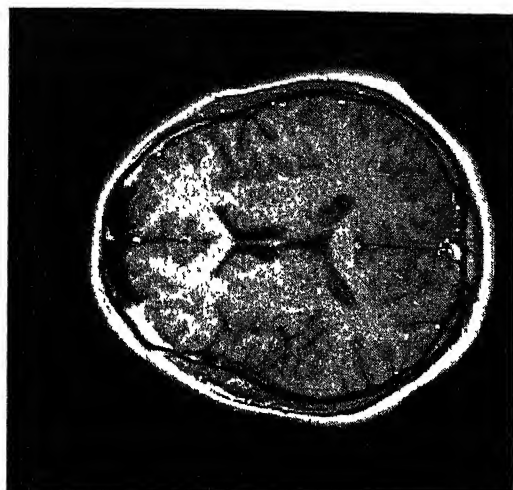(Density weighted Image)
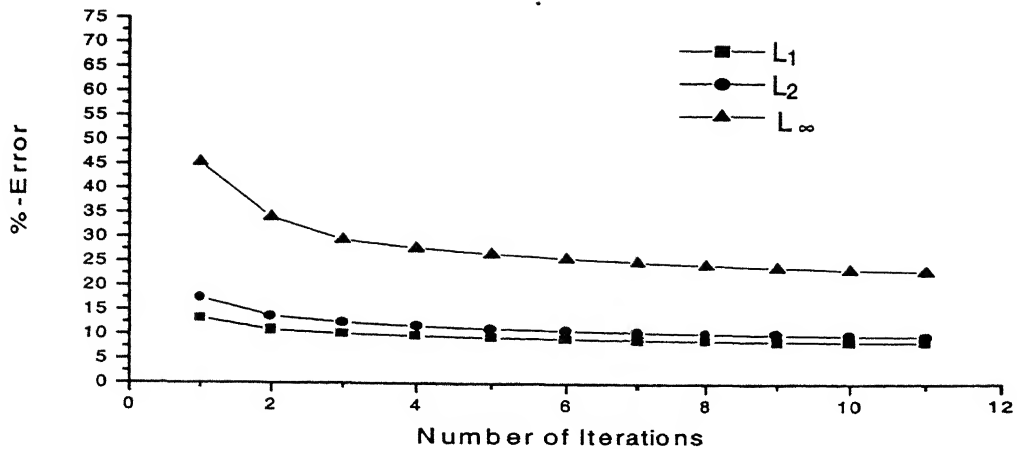
Graph 2.4 : %-Error in De-Blurring by Generalized Jackson operator (p=3) (T_1 weighted image)
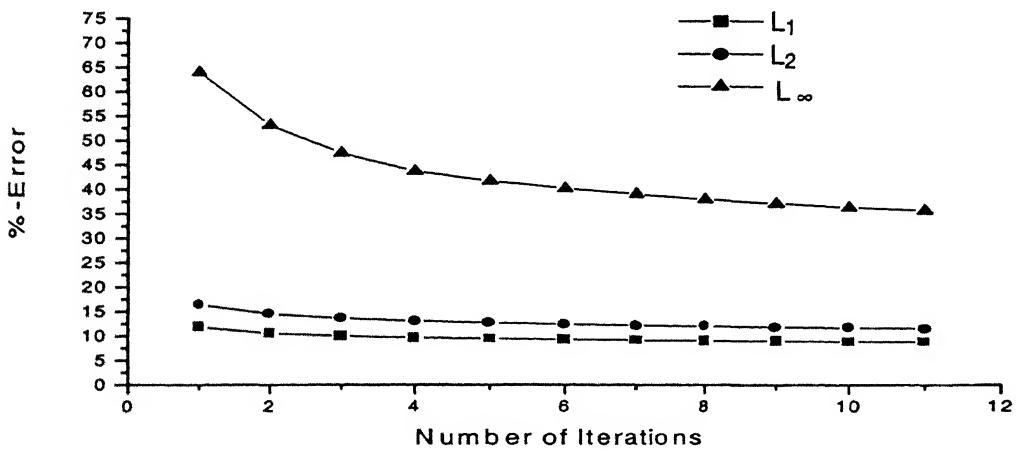
Graph 2.5 : %-Error in De-Blurring by Generalized Jackson operator (p=3) (T_2 weighted image)
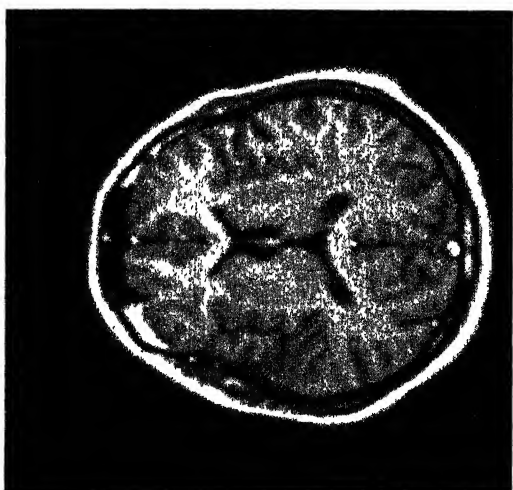

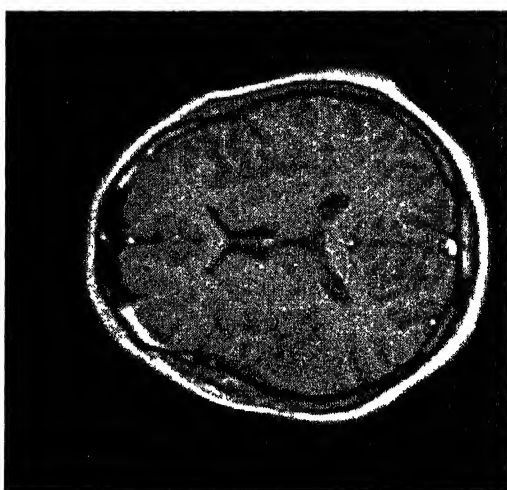**Graph 2.6** : %-Error in De-Blurring by Generalized Jackson operator (p=3) (Density weighted image)
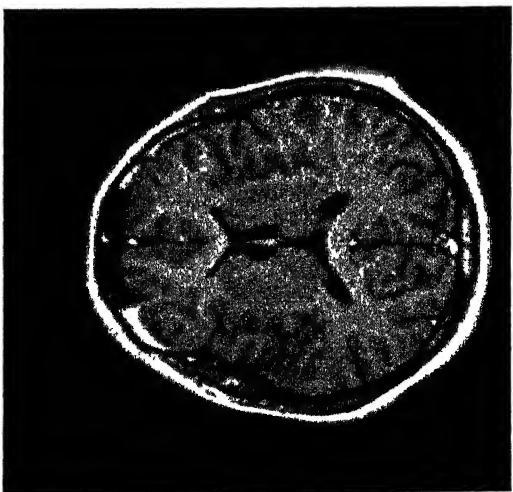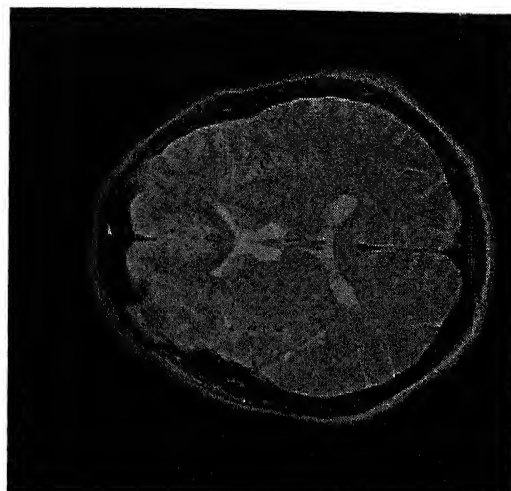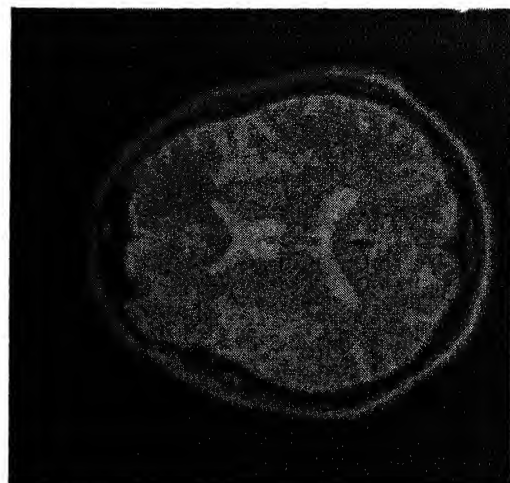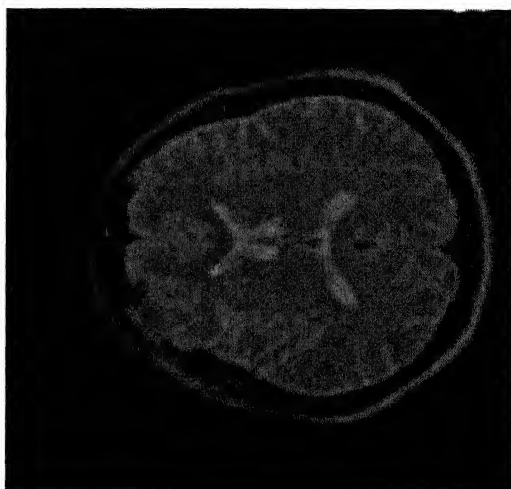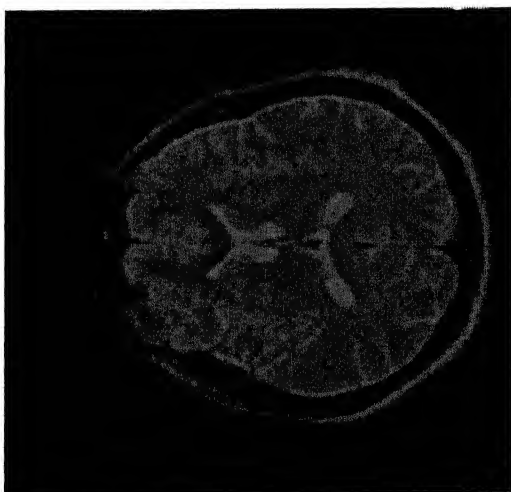
Original

Blurred
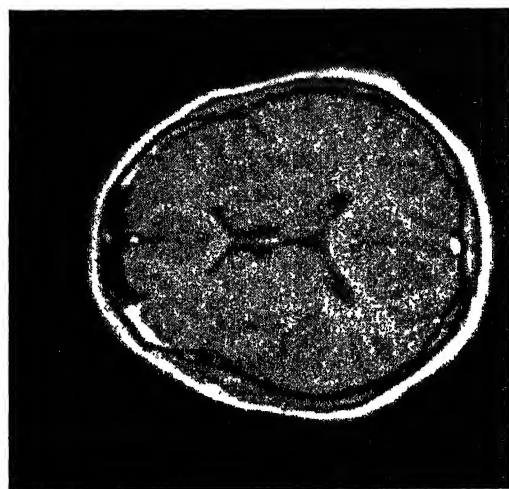
Iteration 1
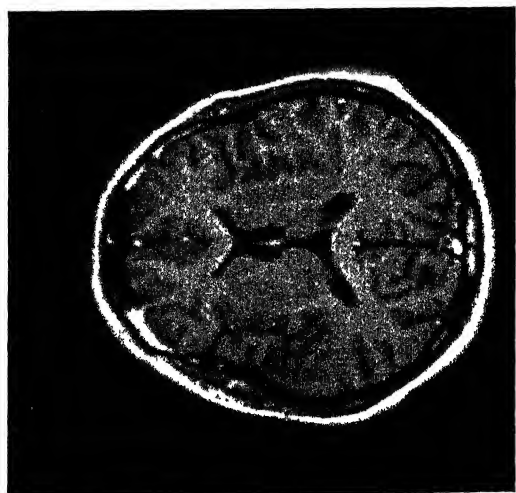
Iteration 4
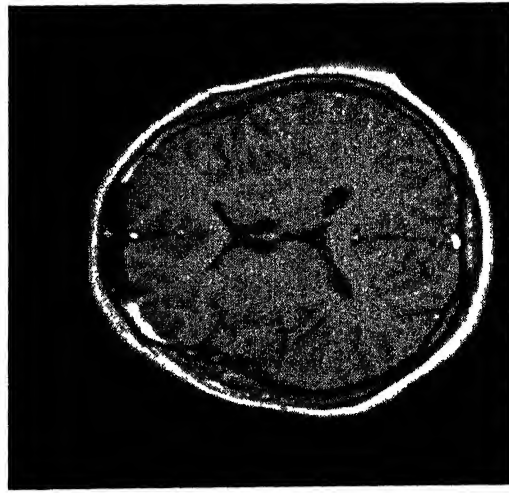
Iteration 7

Iteration 10

Fig. 2.10 : De-Blurring by Generalized Jackson operator (p=4) (T_1 weighted image)
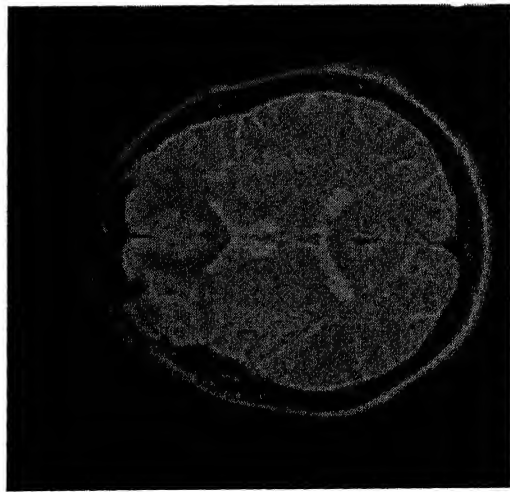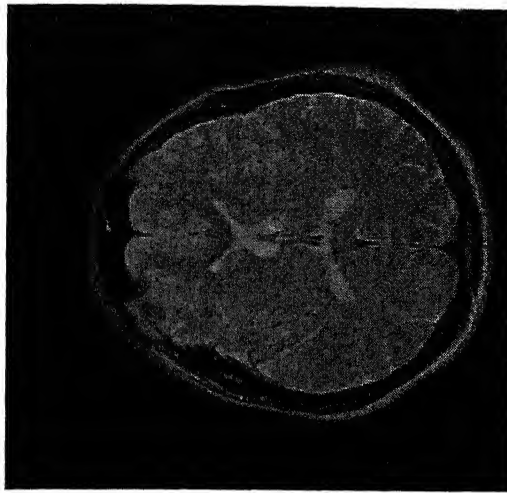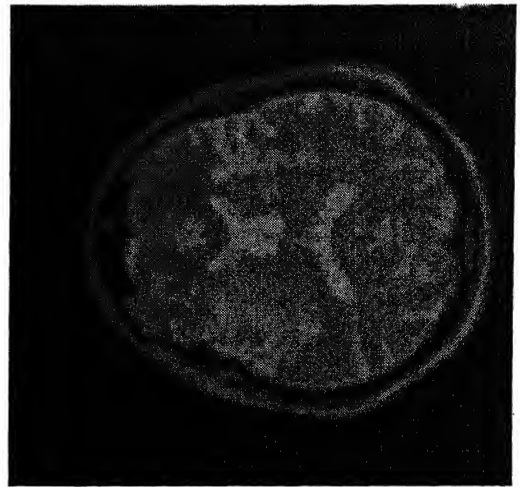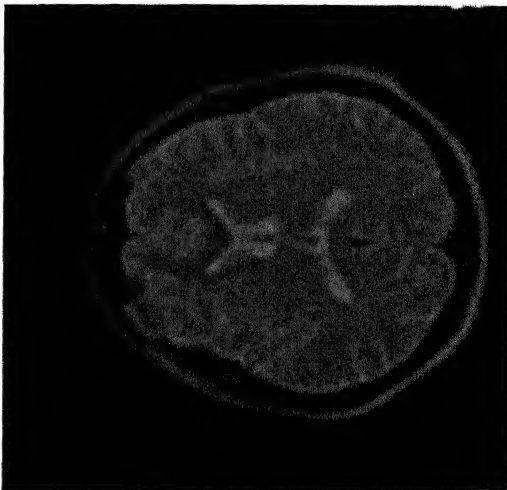
Original
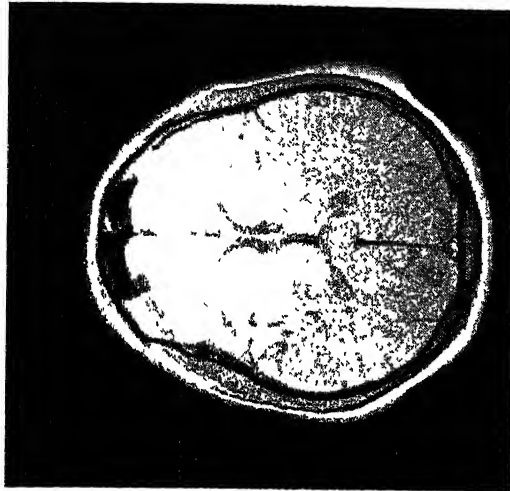

Blurred
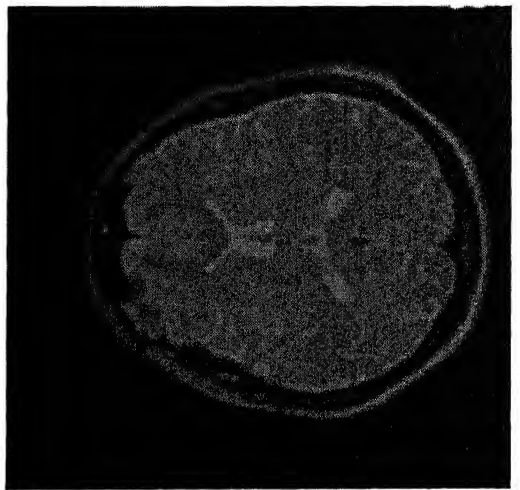
Iteration 1
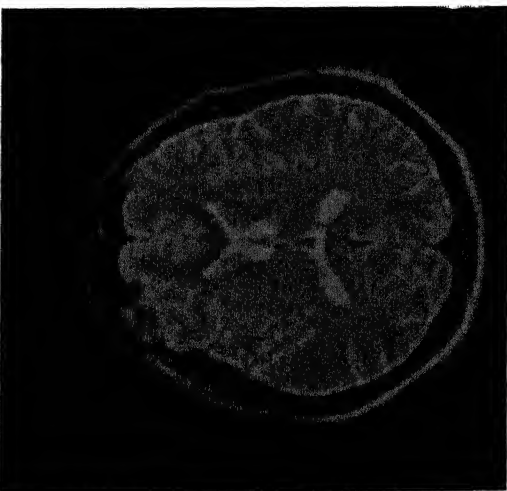
Iteration 4
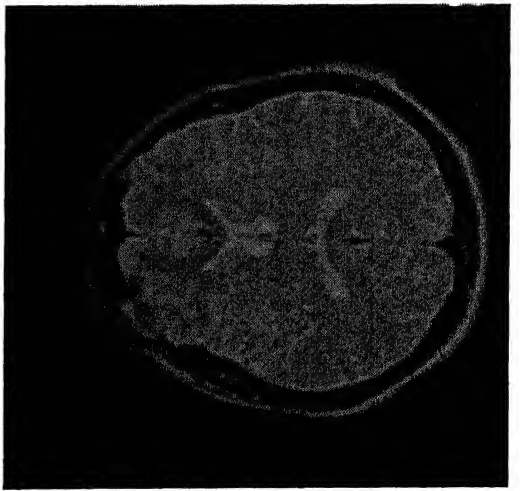
Iteration 7

Iteration 10

Fig. 2.11 : De-Blurring by Generalized Jackson operator (p=4) (T_2 weighted image)
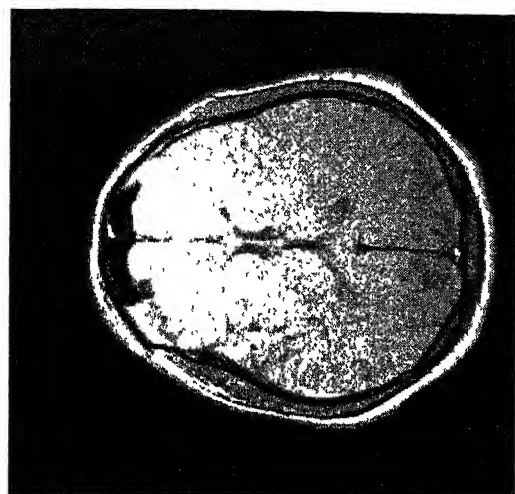
Original
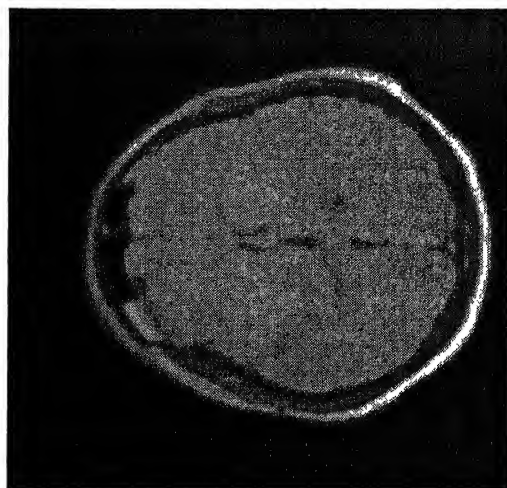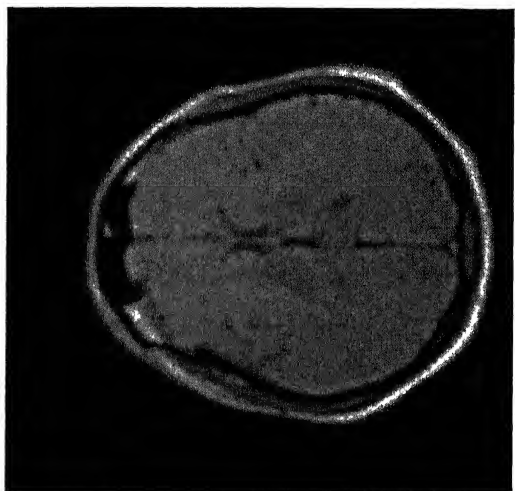
Blurred

Iteration 1

Iteration 4
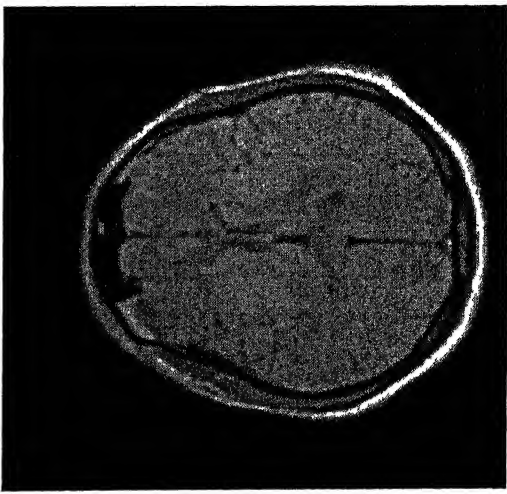
Iteration 7

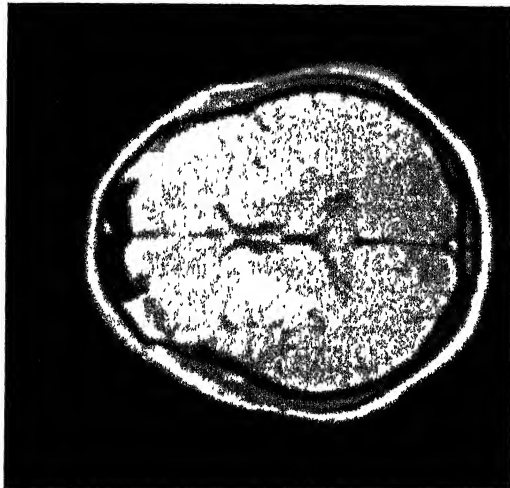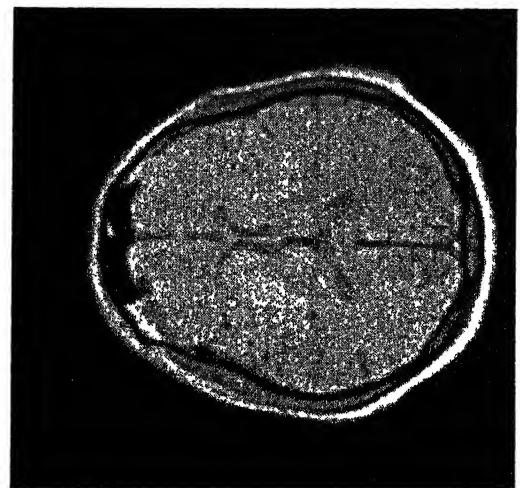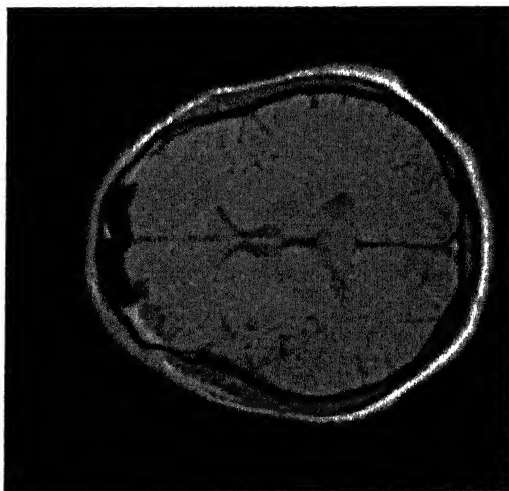Iteration 10

Fig. 2.12 : De-Blurring by Generalized Jackson operator (p=4) (Density weighted image)

	L_1 Error	L_2 Error	L_∞ Error
blurred	14.356292	19.006977	49.467300
A_1	11.755407	15.125175	38.051437
A_2	10.925048	13.751358	33.262249
A_3	10 504880	13 007795	30 409939
A_4	10 226680	12 514482	29.230158
A_5	10.018459	12.148420	28 390139
A_6	9 853121	11.858305	27.713596
A_7	9.716592	11 618515	27.152107
A_8	9.598671	11.414445	26 675184
A_9	9.495715	11 237056	26.262535
A_{10}	9.404180	11.080329	25.900021

Table 2.7 : %-Error in De-Blurring by Generalized Jackson operator (p=4)
(T_1 weighted Image)

	L_1 Error	L_2 Error	L_∞ Error
blurred	12.518543	17.406057	67.959724
A_1	11.127961	15 453486	58.020721
A_2	10.629580	14.633122	52.682335
A_3	10.334711	14 132834	49.198338
A_4	10.122963	13.775389	46.677059
A_5	9.959428	13.498801	44.732990
A_6	9 828265	13.274008	43.509285
A_7	9.721177	13.086461	42.582291
A_8	9.633188	12.926210	41 790131
A_9	9.558999	12.786831	41.099354
A_{10}	9.494246	12.663932	40 487347

Table 2.8 : %-Error in De-Blurring by Generalized Jackson operator (p=4)
(T_2 weighted Image)

	L_1 Error	L_2 Error	L_∞ Error
blurred	9.244117	12 198750	44.153336
A_1	7.545388	9.684868	38.582577
A_2	7.002904	8.820059	35.470993
A_3	6.717432	8.360008	34.856041
A_4	6.527386	8.059769	34.813709
A_5	6.386542	7.839794	34.681816
A_6	6.275219	7.666822	34.494614
A_7	6.183958	7.524434	34.274326
A_8	6.106483	7.403521	34.035374
A_9	6.038725	7.298472	33.787163
A_{10}	5.978663	7.205680	33.535870

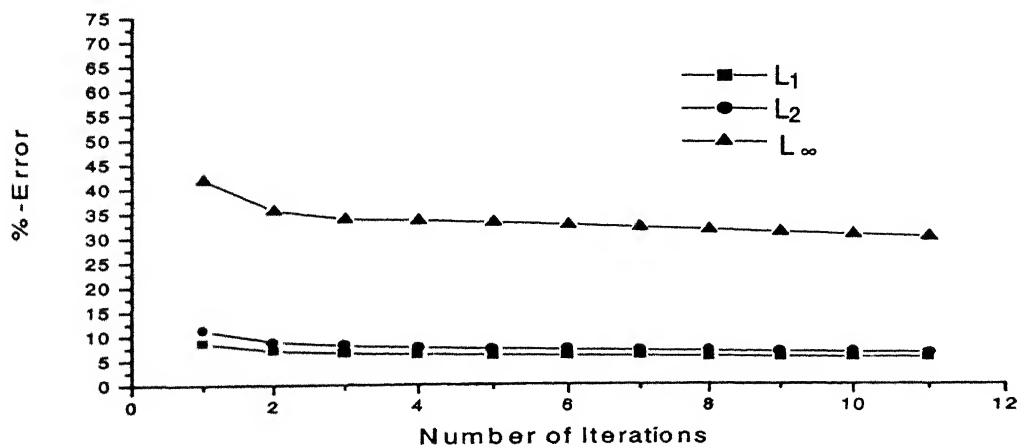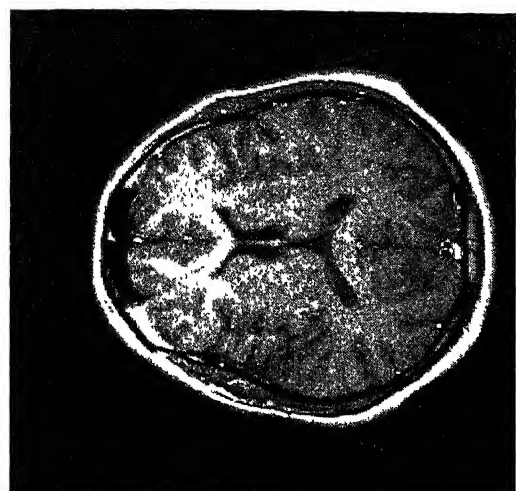**Table 2.9** : %-Error in De-Blurring by Generalized Jackson operator (p=4)
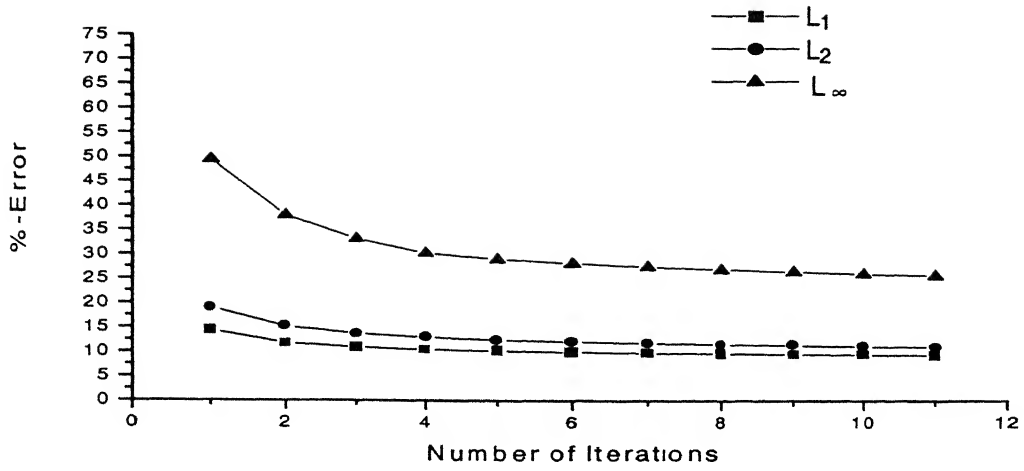
Graph 2.7 : %-Error in De-Blurring by Generalized Jackson operator (p=4) (T_1 weighted image)
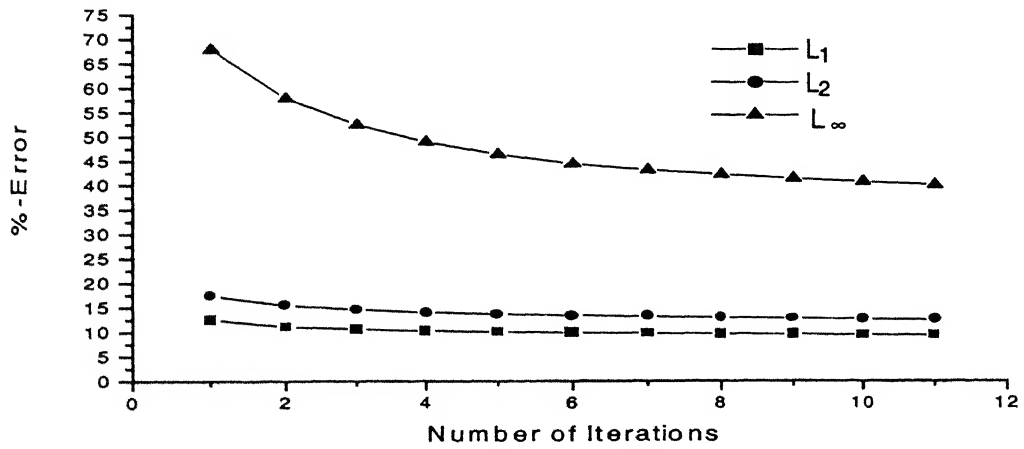
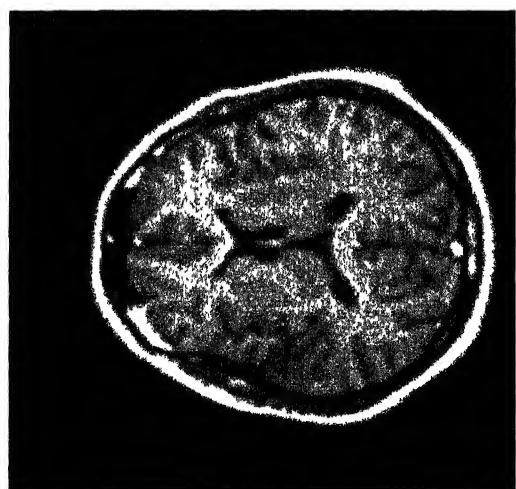**Graph 2.8** : %-Error in De-Blurring by Generalized Jackson operator (p=4) (T_2 weighted image)
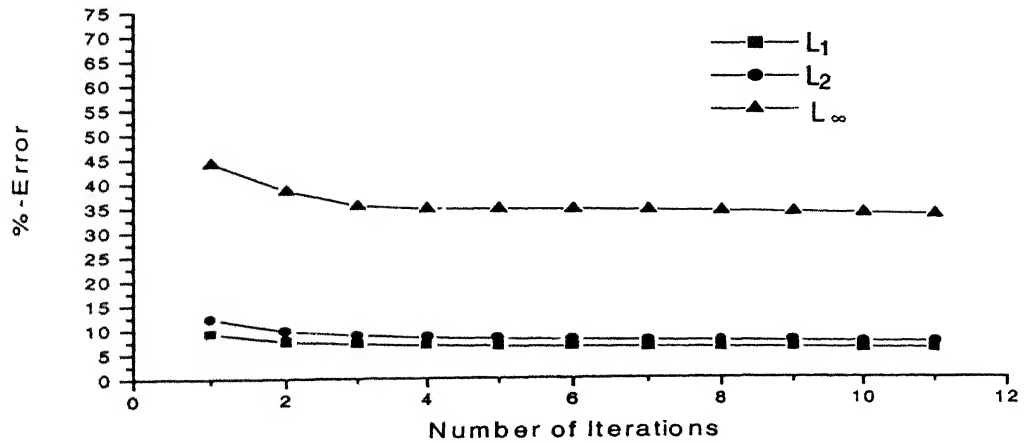
Graph 2.9 : %-Error in De-Blurring by Generalized Jackson operator (p=4) (Density weighted image)

A look at Table 2.1 reveals that the %-L_1-errors drop from 11.82 in the case of blurred image to its about 81% value 9.65 in the case of the first iterate. The subsequent decrease of the errors is rather slow but monotone. The final error 7.15 in the 10th iterate is about 60% of the initial error. The corresponding percentage drops in L_2-errors starting at the value 15.17, are from 77% to 50.9%, and for the L_∞-error, starting at 39.17, the decrease is from 72% to 46%.

In Table 2.2, of T_2-weighted image, the respective figures in the L_1-case are: 10.89, 87%, and 69%; in the L_2-case: 15.05, 86%, and 63%; and in the L_∞-case: 57.44, 78%, and 48%.

In Table 2.3, of proton density weighted image, these are - in the L_1-case: 7.58, 81%, and 59%; in the L_2-case: 9.75, 79%, and 58%; and in the L_∞-case: 37.95, 84%, and 59%. These values are summarized in the following Table 2.10.

	Drop in the L_1-error from the first to the last iterate			Drop in the L_2-error from the first to the last iterate			Drop in the L_∞-error from the first to the last iterate		
	Initial %-Error	First Iterate	Last Iterate	Initial %-Error	First Iterate	Last Iterate	Initial %-Error	First Iterate	Last Iterate
T_2	10.89	87%	69%	15.05	86%	63%	57.44	78%	48%.
T_1	11.82	81%	60%	15.17	77%	50%	39.17	72%	46%
ρ	7.58	81%	59%	9.75	78%	52%	37.95	84%	59%.

Table 2.10: Effectiveness of De-Blurring of T_1, T_2, and Density Weighted Images (p = 2)

For p = 3, Table 2.4 reveals that the %-L_1-errors drop from 13.30 in the case of blurred image to its about 82% value 10.91 in the case of the first iterate. The subsequent decrease of the errors continues to be slow but monotone. The final error 8.58 in the 10th iterate is about 64% of the initial error. The corresponding percentage drops in L_2-errors starting at the value 17.42, are from 79% to 56%, and for the L_∞-error, starting at 45.34, the decrease is from 75% to 51%.

In Table 2.5, of T_2-weighted image, the respective figures in the L_1-case are: 11.87, 88%, and 74%; in the L_2-case: 16.49, 88%, and 70%; and in the L_∞-case: 64.05, 83%, and 56%.

In Table 2.6, of proton density weighted image, these are - in the L_1-case: 8.55, 81%, and 63%; in the L_2-case: 11.18, 79%, and 57%; and in the L_∞-case: 41.88, 85%, and 72%. These values are summarized in the following Table 2.11.

	Drop in the L_1-error from the first to the last iterate			Drop in the L_2-error from the first to the last iterate			Drop in the L_∞-error from the first to the last iterate		
	Initial %-Error	First Iterate	Last Iterate	Initial %-Error	First Iterate	Last Iterate	Initial %-Error	First Iterate	Last Iterate
T_1	13.30	82%	64%	17 42	79%	56%	45.34	75%	51%
T_2	11.87	88%	74%	16 49	88%	70%	64.05	83%	56%.
ρ	8.55	81%	63%	11.18	79%	57%	41.88	85%	72%.

Table 2.11: Effectiveness of De-Blurring of T_1, T_2, and Density Weighted Images (p = 3)

In Table 2.7 the %-L_1-errors drop from 14.35 in the case of blurred image to its about 81% value 11.75 in the case of the first iterate. The subsequent decrease of the errors is slow but monotone. The final error 9.40 in the 10th iterate is about 65% of the initial error. The corresponding percentage drops in L_2-errors starting at the value 19.00, are from 79% to 58%, and for the L_∞ -error, starting at 49.46, the decrease is from 76% to 52%.

In Table 2.8, of T_2-weighted image, the respective figures in the L_1-case are: 12.51, 88%, and 75%; in the L_2-case: 17.40, 88%, and 72%; and in the L_∞-case: 67.95, 85%, and 59%.

In Table 2..9, of proton density weighted image, these are - in the L_1-case: 9.24, 81%, and 64%; in the L_2-case: 12.19, 79%, and 59%; and in the L_∞-case: 44.15, 87%, and 75%. These values are summarized in the following Table 2.12.

	Drop in the L_1-error from the first to the last iterate			Drop in the L_2-error from the first to the last iterate			Drop in the L_∞-error from the first to the last iterate		
	Initial %-Error	First Iterate	Last Iterate	Initial %-Error	First Iterate	Last Iterate	Initial %-Error	First Iterate	Last Iterate
T_1	14.35	81%	65%	19.00	79%	58%	49.46	76%	52%
T_2	12.51	88%	75%	17.40	88%	72%	67.95	85%	59%.
ρ	9.24	81%	64%	12.19	79%	59%	44.15	87%	75%.

Table 2.12: Effectiveness of De-Blurring of T_1, T_2, and Density Weighted Images (p = 4)

2.4.3 SIGNED ERRORS IN THE ITERATIVE DE-BLURRINGS BY $L_{n,p}^{[m]}$

The information on the point-wise behavior of the convergence of the iterative de-blurrings by $L_{n,p}^{[m]}f$ (p = 2, 3, & 4), is given in Graphs. 2.10 (a)-(b)-2.12 (a)-(b), for p = 2, 3, & 4, where the point-wise signed errors $f - L_{n,p}^{[m]}f$ in the reconstructions $L_{n,p}^{[m]}f$ of f are shown in the form of strip-graphs for the first T_1-weighted cross-section. These errors were calculated for the horizontal 128th mid-row and for all the 256- pixels on it, as before. The unit for the graphs is one gray level when the original is assumed to be a 256-gray level image.

These strip-graphs too, show a more or less monotone behavior of the point-wise errors with increasing m. The point-wise errors $f - L_{n,p}^{[m]}f$ (p = 2, 3 & 4) along the mid line, shown blackened, may be observed to be relatively small for the pixels where the cross-section is relatively more smooth and large where the cross sections is less smooth. The error patterns for different m's are more or less similar and the magnitudes of errors keep on reducing as m increases. One may also notice a sudden surge in the errors as the pixels under consideration come near the boundary of an anatomical structure.

A comparison of these strip graphs shows that the maximum error amplitudes occur in the case of p = 4, followed by p = 3 and p = 2. The nature of the oscillations is similar in all of these. The greater oscillations occur near the edges of anatomical structures, as had been the case with the Fejér sum operators in Chapter 1. However, the oscillations for the generalized Jackson operators seem to diminish much more slowly as compared with the Fejér case. This indeed is because of the relatively poor approximation properties of the present operators. For, going by the theoretical error estimates, say e.g., for Lip α functions, the respective errors should be roughly proportional to α[th] powers of 1/35, 1/45, 1/65, and 1/128, in the respective cases of the Jackson operators with p = 4, 3, 2, and the Fejér sums.
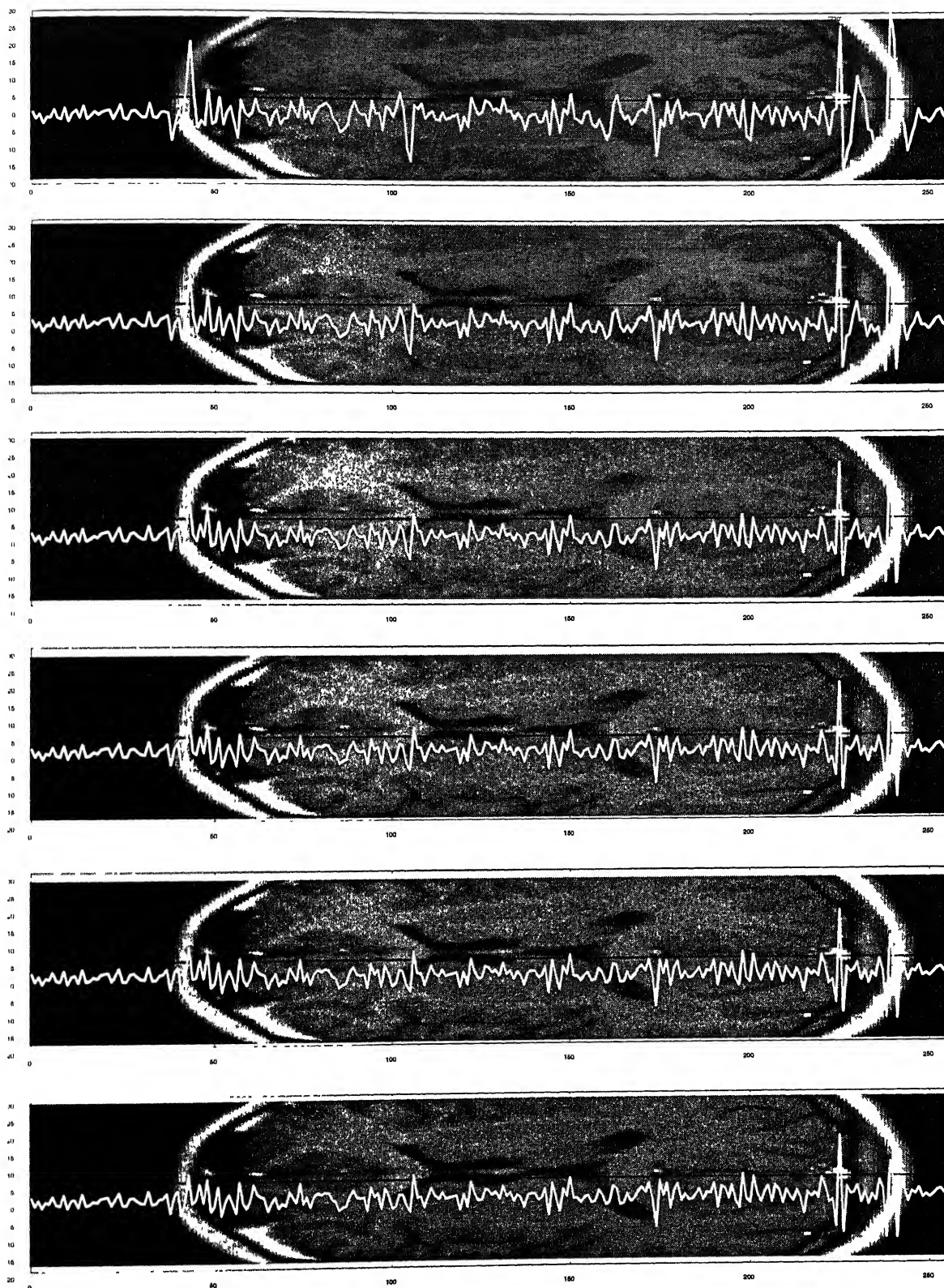
Graph 2.10(a): Signed de-blurring errors ($f - L_{n,2}^{[m]} f$, $m = 1,2,3,4,5,6$)
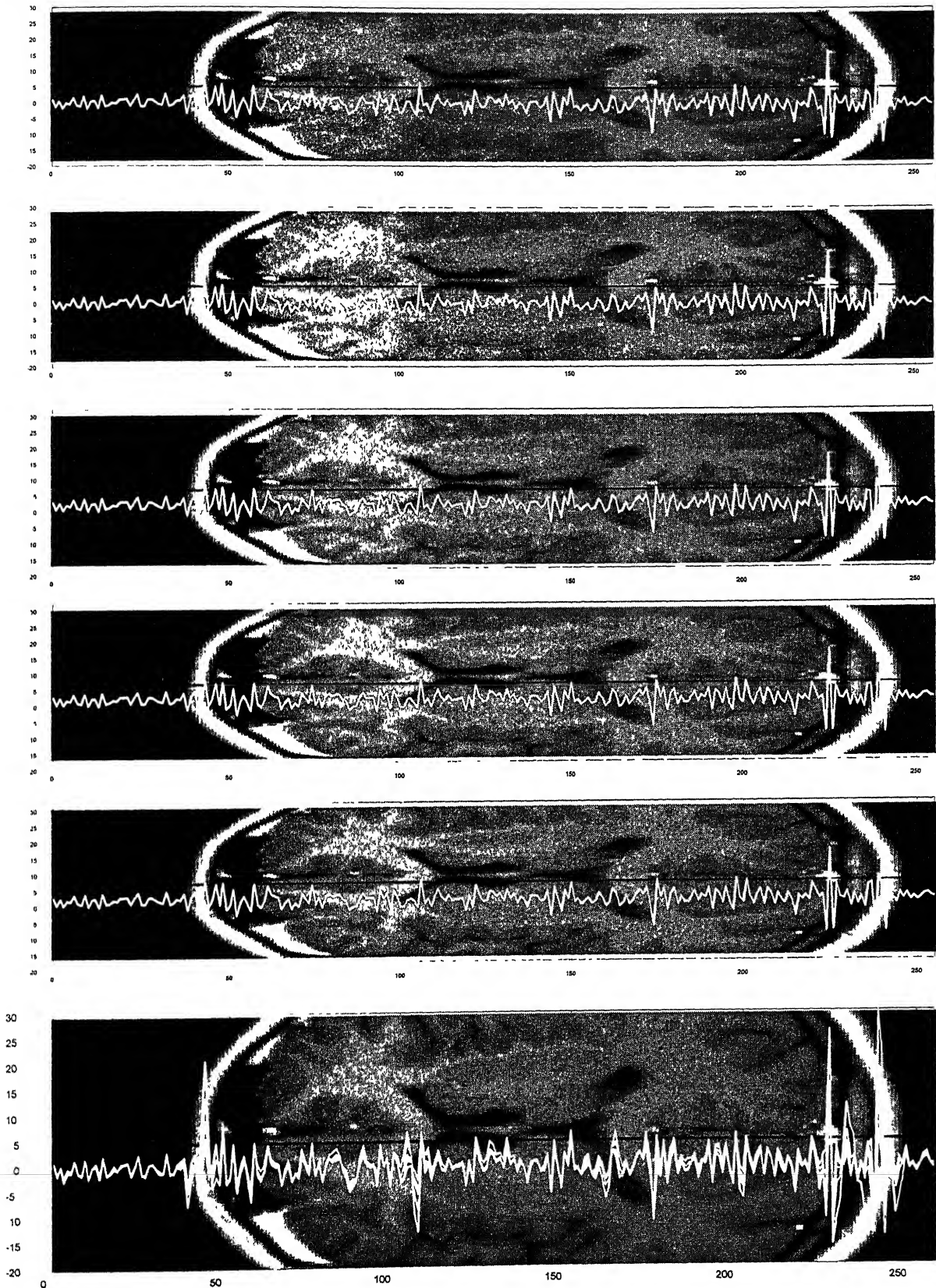
Graph 2.10. (b): Signed de-blurring errors ($f - L_{n,2}^{[m]} f, m = 7,8,9,10,11$) & superposition of all 11
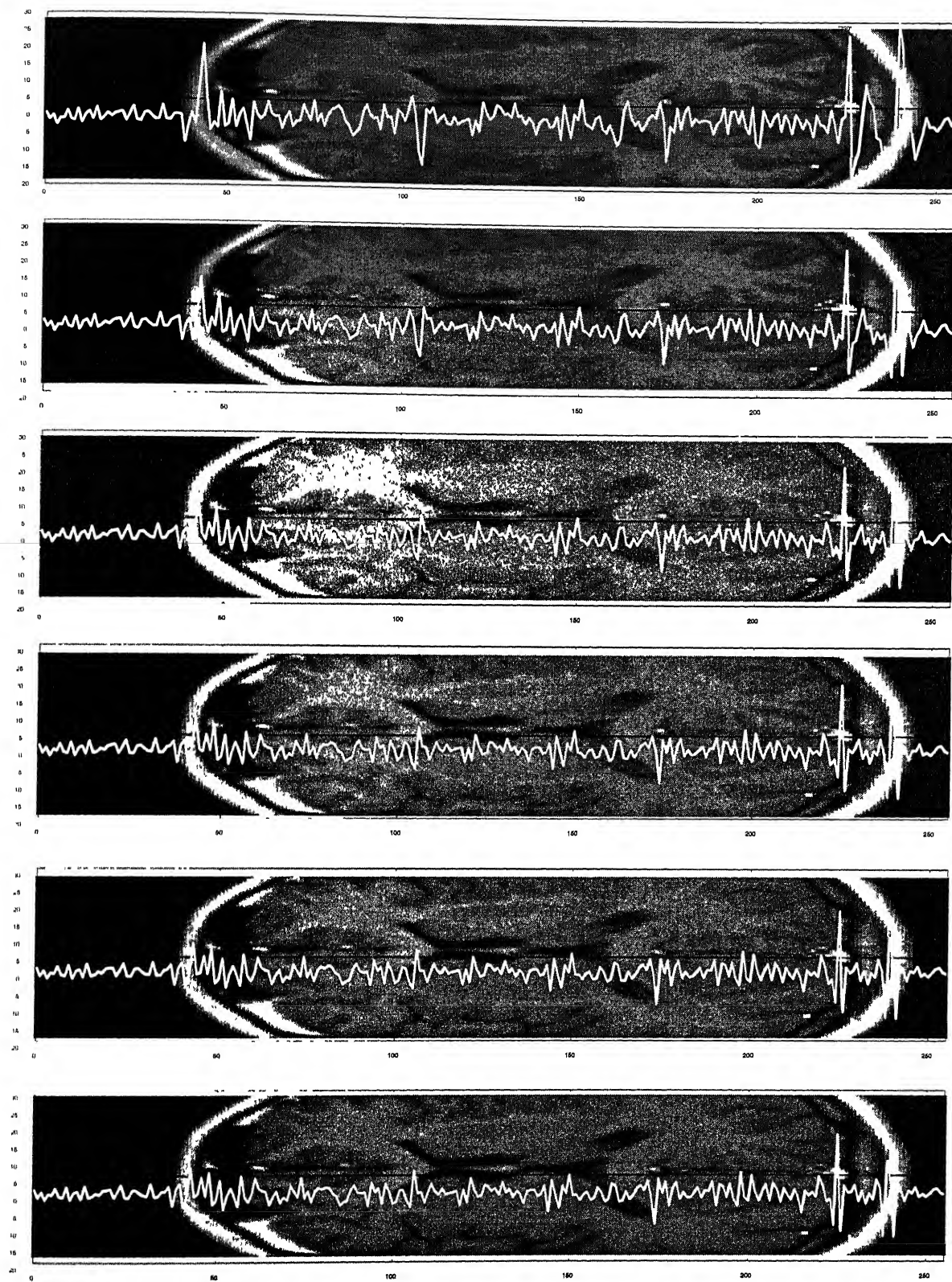
Graph 2.11. (a): Signed de-blurring errors ($f - L_{n,3}^{[m]} f$, $m = 1,2,3,4,5,6$)

84
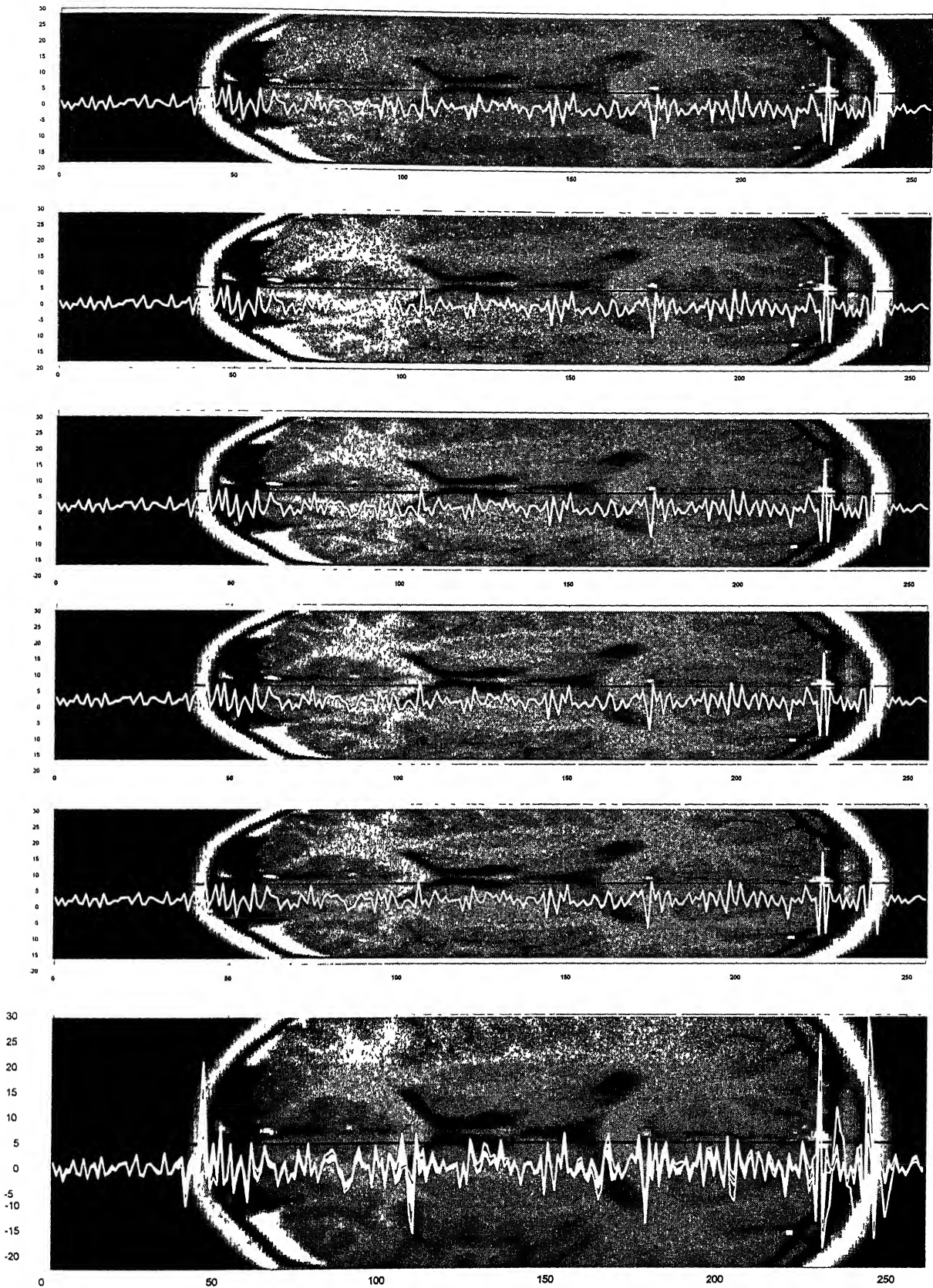
Fig. 2.11.(b) : Signed de-blurring errors ($f - L_{n,3}^{[m]}f$, $m = 7,8,9,10,11$) & superposition of all 11 above
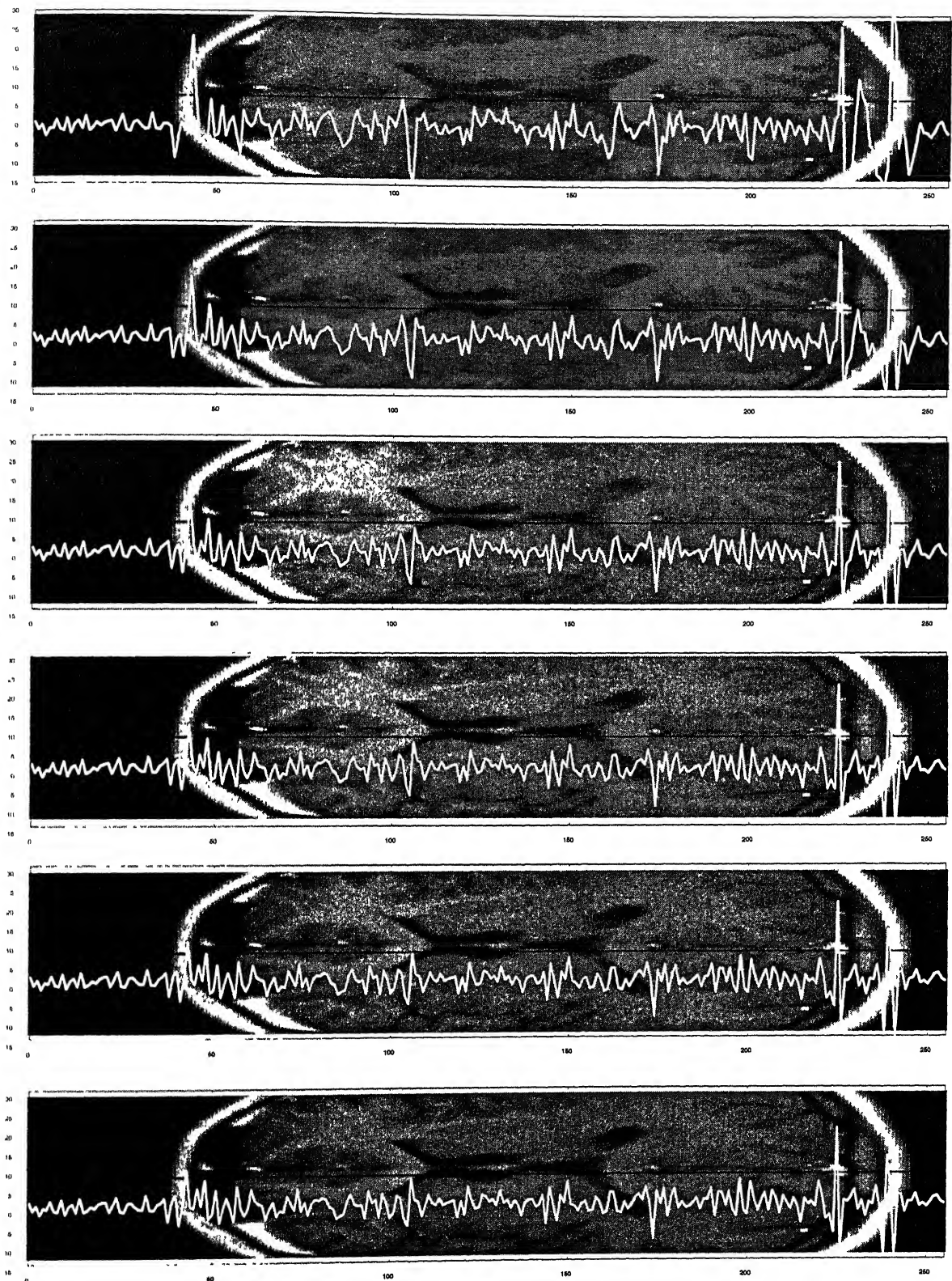
Graph 2.12(a) : Signed de-blurring errors ($f - L_{n,4}^{[m]} f$, $m = 1,2,3,4,5,6$)
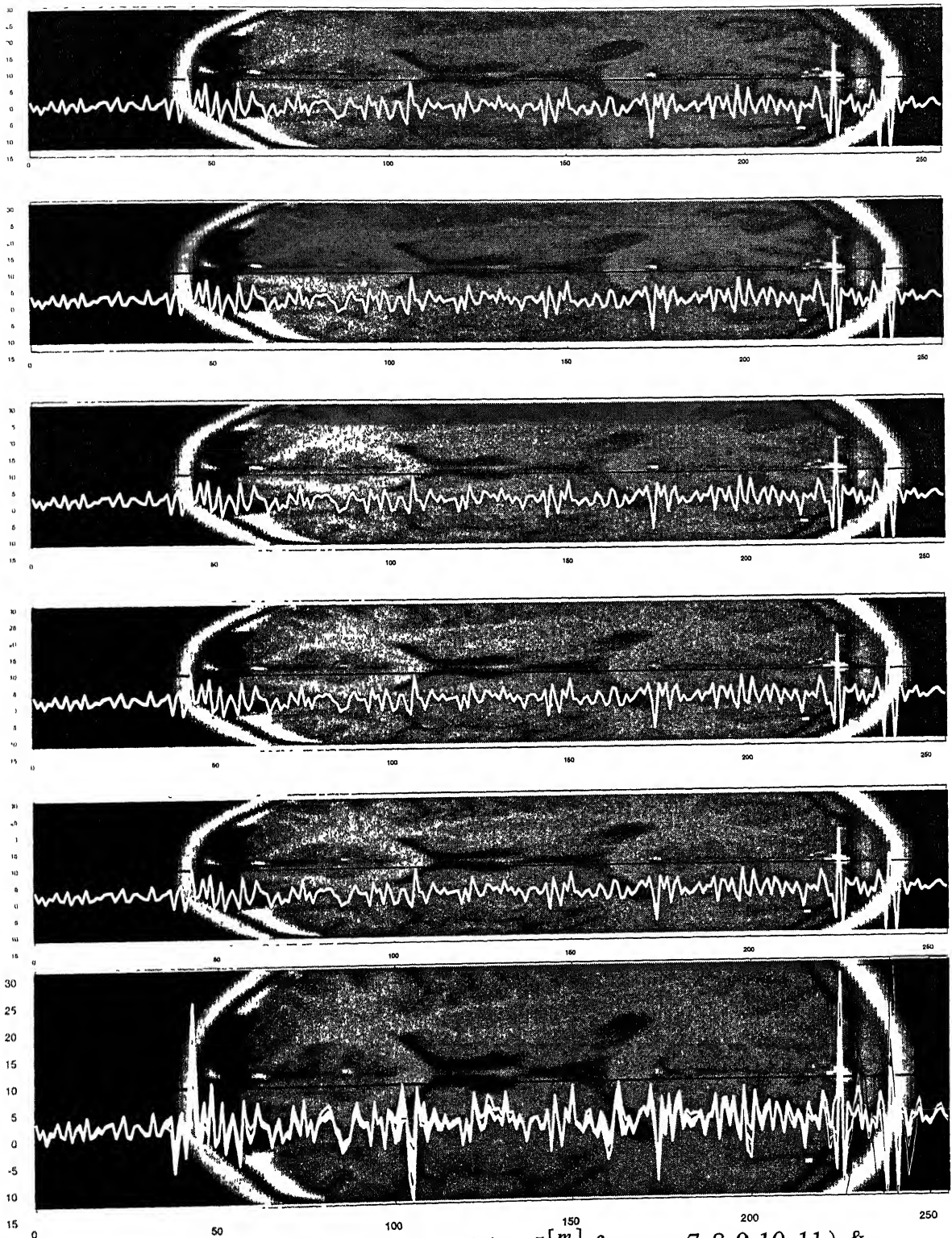
Graph 2.12(b) : Signed de-blurring errors $(f - L_{n,4}^{[m]} f , \ m = 7,8,9,10,11)$ &

superposition of all 11 above.

CHAPTER 3 : DE-BLURRING BY THE DE LA VALLÉE-POUSSIN INTEGRALS

In this chapter we study the degree of approximation in the de-blurring associated with the De la Vallée-Poussin integrals (see I.P. Natanson (1964)):

$$V_n = V_n(f;x) = \frac{(2n)!!}{2\pi(2n-1)!!} \int_{-\pi}^{\pi} f(t) \cos^{2n} \frac{t-x}{2} \, dt.$$

In the first section entitled De la Vallée-Poussin Integrals we collect some material about the operators $\{V_n\}$, the second section contains some basic results needed in the subsequent analysis, and the third section contains our main results on the rate of convergence of the sequence $\{V_n^{[m]}(f;x)\}$ defined as:

$$V_n^{[m]}(f;x) = \sum_{j=1}^{m} (-1)^{j-1} \binom{m}{j} V_n^j(f;x).$$

The final section on the simulation results includes numerical illustrations of the de-blurring achieved on MRI cross-sections.

3.1. DE LA VALLÉE POUSSIN INTEGRALS

These (see J. De la Valée Poussin (1908)) derive the importance from their simplicity, interesting approximation properties and theirs being variation diminishing (a result due to I.J. Schoenberg (1959)). Some well known quantitative results about them are as follows:

3.1.1. THEOREM (I. P. NATANSON (1944))

If a function $f(x) \in C_{2\pi}$ has modulus of continuity $\omega(\delta)$, then the inequality

$$|V_n(x) - f(x)| \leq 3\omega\left(\frac{1}{\sqrt{n}}\right)$$

holds for all values of x.

3.1.2. THEOREM (I.P. NATANSON (1946))

If $U_n(\alpha) = \sup_f \left\{ \max_x |V_n(x) - f(x)| \right\}$, *wherein* $f(x)$ *runs through all functions with*

period 2π *of class* $\text{Lip}_1\alpha$, *then*

$$U_n(\alpha) = \frac{2^\alpha}{\sqrt{\pi n^\alpha}} \Gamma\left(\frac{1+\alpha}{2}\right) + \frac{\rho_n}{\sqrt{n^\alpha}}$$

where $\lim_{n \to \infty} \rho_n = 0$.

3.1.3. THEOREM (I. P. NATANSON (1944))

If the function $f(x) \in C_{2\pi}$ *possesses for a value of* x *a finite second derivative* $f''(x)$,
then the formula

$$V_n(x) = f(x) + \frac{f''(x)}{n} + \frac{\rho_n}{n}$$

with $\lim_{n \to \infty} \rho_n = 0$ *holds true for this* x.

The following theorem concerns the point-wise convergence of the derivative of De
la Vallée-Poussin integrals:

3.1.4. THEOREM (I. P. NATANSON(1964))

If at a point x, $f(x) \in C_{2\pi}$ *has a finite derivative* $f'(x)$, *then the relation*

$$\lim_{n \to \infty} V_n'(x) = f'(x)$$

holds true for this value of x.

3.1.5. THEOREM (P.C. SIKKEMA AND R.K.S. RATHORE (1976))

Let $0 < \alpha \leq 1$, *and* p *be a positive integer. If*

$$E(\alpha, p; V_n, x) = \sup_f \left\{ \left\| V_m\left([f(t) - \sum_{v=0}^{p} \frac{f^{(v)}(x)}{v!} (t-x)^v]; x \right) \right\| \right\}, \quad x \in \mathbb{R},$$

where f runs through all functions with $f^{(p)} \in \text{Lip}_1\alpha$, *then with* $(a)_p = \prod_{i=1}^{p}(a+i-1)$,

$$\frac{2^{p+2\alpha-1}\Gamma(\frac{p+\alpha+1}{2})}{(1+\alpha)_p \sqrt{\pi}} \leq \lim_{n \to \infty} n^{\frac{p+\alpha}{2}} E(\alpha, p; V_n, x) \leq \frac{2^{p+\alpha}\Gamma(\frac{p+\alpha+1}{2})}{(1+\alpha)_p \sqrt{\pi}}.$$

3.1.6. COROLLARY

If p is a positive integer, then

$$\lim_{n \to \infty} n^{(p+1)/2} E(1, p; V_n, x) = \frac{2^{p+1} \Gamma(\frac{p}{2} + 1)}{(p+1)! \sqrt{\pi}}.$$

The following result generalizes the approximation of first derivative result Theorem 3.1.4 of I.P. Natanson (1964) and shows that the De la Valée Poussin integrals, in fact, enjoy the pointwise convergence in simultaneous approximation of derivative of an arbitrary order:

3.1.7. THEOREM (P.C. SIKKEMA AND R.K.S. RATHORE (1976))

Let m be a positive integer. If $f \in C_{2\pi}$ and at a point $x \in \mathbb{R}$, $f^{(m)}(x)$ exists, then

$$\lim_{n \to \infty} \frac{d^m}{dx^m} V_n(f; x) = f^{(m)}(x).$$

3.2. SOME BASIC RESULTS

In this section we derive some results which we use in the proofs of our main results in the next section.

3.2.1. LEMMA

Let for $k \geq 1$, $\lambda_{k,n} = V_n(\sin^{2k} \frac{t}{2}; 0)$. Then: $\lambda_{k,n} \cong \pi^{-1/2} \Gamma(\frac{2k+1}{2}) n^{-k}$, $n \to \infty$.

Proof: Since,

$$\int_{-\pi}^{\pi} \cos^{2n} \frac{t}{2} \sin^{2k} \frac{t}{2} dt = 2 \frac{\Gamma(\frac{2n+1}{2}) \Gamma(\frac{2k+1}{2})}{\Gamma(n+k+1)}$$

$$\cong 2\frac{e^{-\frac{2n+1}{2}}(\frac{2n+1}{2})^n}{e^{-(n+k)}(n+k)^{n+k+\frac{1}{2}}}\Gamma(\frac{2k+1}{2})$$

$$\cong 2n^{-k}\Gamma(\frac{2k+1}{2}),$$

it follows that

$$\lambda_{k,n} \cong \frac{\Gamma(\frac{2k+1}{2})}{\sqrt{\pi}}n^{-k}.$$

3.2.2. LEMMA

If T is a trigonometric polynomial, $\|V_n^{[m]}T - T\| = O(n^{-m}), n \to \infty$.

Proof: It follows along the lines of the corresponding result about the generalized Jackson operators obtained in the previous chapter.

3.2.3. LEMMA

Let $0 \le m \le n$ be integers. Then

$$\frac{\partial^{2m}}{\partial x^{2m}}\cos^{2n}\frac{t-x}{2} = \cos^{2n}\frac{t-x}{2}\sum_{j=0}^{m}g_{m+j}^{[m]}(n)\tan^{2j}\frac{t-x}{2},$$

where $g_j^{[m]}(n)$ is a polynomial in n of degree $\le j$.

Proof: For $m = 0$, the result is trivial. Hence assuming it for m and differentiating twice

$$\frac{\partial^{2m+2}}{\partial x^{2m+2}}\cos^{2n}\frac{t-x}{2}$$

$$= \cos^{2n}\frac{t-x}{2}\sum_{j=0}^{m}g_{m+j}^{[m]}(n)\left[(n-j)(n-j-\tfrac{1}{2})\tan^{2j+2}\frac{t-x}{2}\right.$$

$$\left. -\{(n-j)(j+\tfrac{1}{2})+(n-j+\tfrac{1}{2})j\}\tan^{2j}\frac{t-x}{2} + j(j-\tfrac{1}{2})\tan^{2j-2}\frac{t-x}{2}\right],$$

from which the result is clear, as the coefficients of $\tan^{2j+2}\frac{t-x}{2}$, $\tan^{2j}\frac{t-x}{2}$, and

$\tan^{2j-2}\frac{t-x}{2}$, inside the square brackets are respectively of degree 2, 1, and zero in n.

3.2.4. LEMMA (BERNSTEIN TYPE INEQUALITY)

$$\left\|(V_n^{[m]}f)^{(2m)}\right\| \le D_m n^m \|f\|, \quad f \in C_{2\pi}, \ m,n \ge 1,$$

where the constant D_m does not depend on n or f.

Proof: As we have to show that $\left\|V_n^{(2m)}f\right\| = O(n^m)\|f\|$, in view of the Lemma 3.2.3 we just have to verify that

$$\frac{1}{\pi}\frac{(2n)!!}{(2n-1)!!}\int_0^\pi \cos^{2(n-j)}\frac{x}{2}\sin^{2j}\frac{x}{2}\,dx = O(n^{-j}), \quad 0 \le j \le m,$$

which, however, is a consequence of our Lemma 3.2.1.

The m-th order modulus of smoothness for $f \in C_{2\pi}$, $\delta > 0$, $m \ge 1$, is defined by

$$\omega_m(f;\delta) = \sup_{|h|\le\delta}\left\|\sum_{j=0}^m (-1)^{m-j}\binom{m}{j}f(x+jh)\right\|,$$

and the m-th order Peetre's K-functional for $f \in C_{2\pi}$, $t > 0$, $m \ge 1$, by

$$K_m(f;t) = \inf_{g \in C_{2\pi}^{(m)}}\left\{\|f-g\| + t\left\|g^{(m)}\right\|\right\}.$$

We may recall the following well-known equivalence (see e.g., Z. Ditzian and V. Totik (1987)) between the two:

$$A_m\omega_m(f;\ t) \le K_m(f;t^m) \le B_m\omega_m(f;\ t), \quad f \in C_{2\pi}, t > 0, \ m \ge 1.$$

where A_m and B_m are absolute constants independent of t and f.

In this chapter, we shall take $\phi(t) = t^{2m}$, m a positive integer. For this choice of $\phi(t)$, some examples of appropriate $\varphi(t)$ are t^α, $t^\alpha\log(1/t)$, $t^\alpha/(\log(1/t))^3$, $0 < \alpha < 2m$, any k-th order modulus of smoothness $\omega_k(t)$ ($k < 2m$) of any function in L_q ($1 \le q \le \infty$), $C_{2\pi}$ etc. As before, the statement "$\varphi(t)$ is associated with $\phi(t)$" means that the order function $\varphi(t)$ and the growth function $\phi(t)$ are positive functions on $(0, c]$, for some c such that for all $h \in (0, 1]$: $q(h) = \sup_{t \in (0,c]} (\phi(th)\varphi(t))/(\phi(t)\varphi(th)) < \infty$, $u(h) = \sup_{t \in (0,c]} \varphi(t)/\varphi(th) < \infty$, $w(h) = \sup\{u(t) : t \in [h, 1]\} < \infty$, and $\lim_{t \to 0} q(t) = 0$.

3.3. DEGREE OF DE-BLURRING BY THE DE LA VALLÉE-POUSSIN INTEGRALS $V_n^{[m]}$

Based on the results of the previous section, a direct theorem on the degree of approximation of f by the de-blurring operation $V_n^{[m]}f$ is as follows:

3.3.1. THEOREM (DIRECT)

For all $f \in C_{2\pi}$, there holds the error estimate:

$$\left\| V_n^{[m]}f - f \right\| \le A_m \omega_{2m}(f; n^{-1/2}), \quad 1 \le m, (n \ge 1).$$

where the constant A_m does not depend on n or f.

Proof: Operating on the estimate

$$| f(t) - f(x) - \sum_{k=1}^{2m-1} [f^{(k)}(x)/k!] T_k(t-x) | \le A \left\| f^{(2m)} \right\| \sin^{2m}(t-x)/2,$$

obtained in the Lemma 2.2.4, and using Lemma 3.2.1 and Lemma 3.2.2, we have

$$\left| V_n^{[m]}(f;x) - f(x) \right| \le \sum_{k=1}^{2m-1} \frac{\left\| f^{(k)}(x) \right\|}{k!} B_{k,m} n^{-m} + A(2^m - 1)\left\| f^{(2m)} \right\| O(n^{-m}),$$

From which, in view of the G. Freud's inequalities given in Lemma 2.2.3, as before

$$\left\| V_n^{[m]}f - f \right\| \le B n^{-m} \left\| f^{(2m)} \right\|, \quad 1 \le m, \quad f \in C_{2\pi}^{(2m)},$$

where B is an absolute constant, independent of f and n. Hence, using the result of Lemma 2.2.6. of G.I. Sunouchi (1964), due to $\left\| V_n^j \right\| = 1$, $(j \ge 1)$, we have

$$\left\| V_n^{[m]}f - f \right\| \le K_{2m}\left(\left\| V_n^{[m]} - I \right\| + v^{2m}\left\| (V_n^{[m]} - I)^{(2m)} \right\| \right) \omega_{2m}(f; v^{-1}),$$

$$\le K_{2m}\left(2^m + v^{2m}Bn^{-m} \right)\omega_{2m}(f; v^{-1})$$

from which, taking $v = n^{1/2}$, the result follows.

For the De la Valée Poussin integrals, referring to the Oh-oh-Lemma 1.2.3, below we shall use the order function $\varphi(t)$ associated with the function $\phi(t) = t^{2m}$

3.3.2. THEOREM (INVERSE)

Let $\varphi(t)$ be an order function associated with the growth function $\phi(t) = t^{2m}$. Then, for $f \in C_{2\pi}$:

$$\left\| V_n^{[m]} f - f \right\| = O(\varphi(1/\sqrt{n})) \quad \text{iff} \quad \omega_{2m}(f;\delta) = O(\varphi(\delta)),$$

and

$$\left\| V_n^{[m]} f - f \right\| = o(\varphi(1/\sqrt{n})) \quad \text{iff} \quad \omega_{2m}(f;\delta) = o(\varphi(\delta)).$$

Proof: By the Lemma 3.2.4, there exist constants A and B, independent of $g \in C_{2\pi}^{(2m)}$, and $f \in C_{2\pi}$ such that

$$K_{2m}(f;t^{2m}) \leq K_{2m}(f - V_n^{[m]}f;t^{2m}) + K_{2m}(V_n^{[m]}(f-g);t^{2m}) + K_{2m}(V_n^{[m]}g;t^{2m})$$

$$\leq \left\| V_n^{[m]} f - f \right\| + t^{2m}[An^m \| f - g \| + B \| g^{(2m)} \|].$$

Taking infimum over $g \in C_{2\pi}^{(2m)}$, for a constant M independent of f,

$$K_{2m}(f;t^{2m}) \leq M \, [\left\| V_n^{[m]} f - f \right\| + (t^2 n)^m K_{2m}(f; 1/n^m)].$$

By the Oh-oh-Lemma 1.2.3, therefore, we have

$$\left\| V_n^{[m]} f - f \right\| = O(\varphi(n^{-1/2})) \Rightarrow K_{2m}(f;t^{2m}) = O(\varphi(t)),$$

and

$$\left\| V_n^{[m]} f - f \right\| = o(\varphi(n^{-1/2})) \Rightarrow K_{2m}(f;t^{2m}) = o(\varphi(t)).$$

By the equivalence of K_{2m} and ω_{2m}, and since the direct part of the result is already covered in the Theorem 3.3.1, the proof is complete.

3.3.3. COROLLARY

Let $0 < \alpha < 2m$. Then, for $f \in C_{2\pi}$:

$$\left\| V_n^{[m]} f - f \right\| = O(n^{-\alpha/2}) \quad \text{iff} \quad \omega_{2m}(f;\delta) = O(\delta^\alpha),$$

and

$$\left\| V_n^{[m]} f - f \right\| = o(n^{-\alpha/2}) \quad \text{iff} \quad \omega_{2m}(f;\delta) = o(\delta^\alpha).$$

3.4. SIMULATION RESULTS

This section contains numerical simulations with the de-blurring induced by the De La Vallée-Poussin integral V_n. As in the previous chapters, the blurring, de-blurrings and the direct inversion are done in both phase and frequency encoding directions using the two dimensional Cartesian methodology described in Chapter 0. As before, we: (i) compare the iterative de-blurring with a direct inversion, (ii) compute the reconstructions, error tables, and the error graphs for the supposedly known set of weighted MRI cross-sections, and (iii) obtain graphs of the point-wise signed errors along the straight line through the middle of the cross-section, superimposed on a crop of the cross-section.

3.4.1 ITERATIVE DE-BLURRING COMPARED WITH DIRECT INVERSION

The first experiment verifies the effectiveness of the de-blurring scheme $V_n^{[m]}$ as compared with the de-blurring based on a direct inversion of the De La Vallée-Poussin filter. The same actual machine image output, as taken in the previous two chapters, called "Original" is taken to be the example of the blurred image. The assumed blurring model here is the De La Vallée-Poussin filter V_n corresponding to n = 16×128, out of which only the 128 filter coefficients are utilized in the simulations. The images associated with the original, four of the iterates $V_n^{[m]}$, named "Iteration1", "Iteration 2", "Iteration 3", and "Iteration 4" that correspond to m = 2, 3, 4, and 5 and the result of the inverse filtering, called "Direct filter inversion" have been displayed in Fig. 3.1.

It is clear from the visual comparison of the images in Fig. 3.1 that the inverse De La Vallée-Poussin filter produces severe artifacts, whereas the iterative de-blurrings with $V_n^{[m]}$ produce much sharper images. Their clarity and effectiveness in delineating the fine structure of the entire topography of the regions containing CSF, is amply clear from the figure. Note also a better gray and white matter discrimination as compared with the case *p=3* in iterations *2-4* of chapter *2* (Fig. *2.2*).

Original
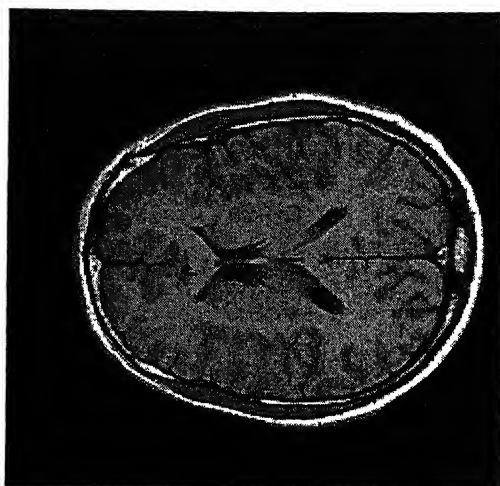
Iteration 1
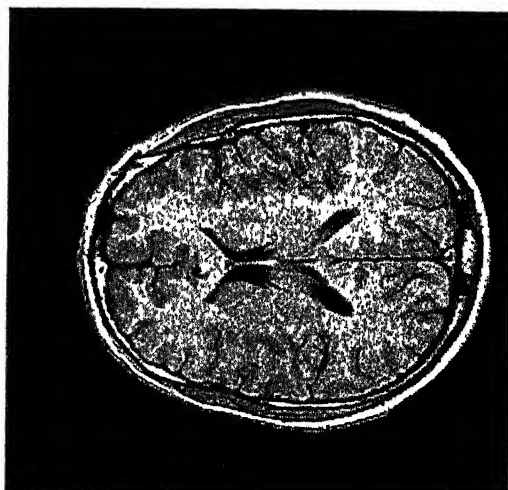
Iteration 2
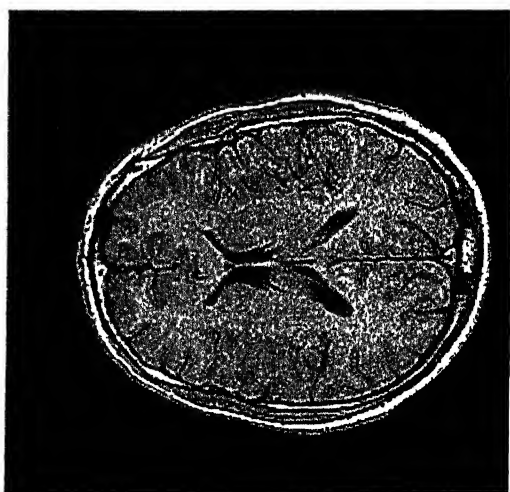
Iteration 3
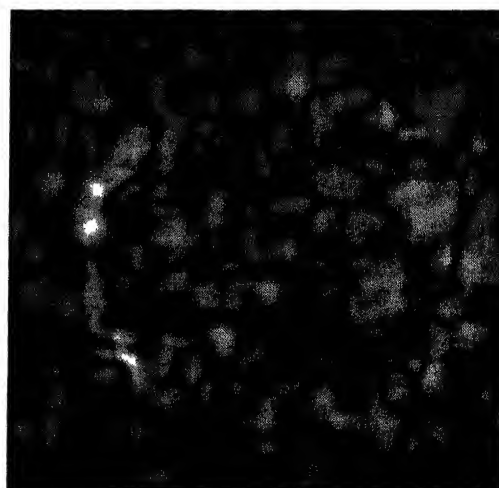
Iteration 4

Direct Filter Inversion

Fig. 3.1. : De-blurring by De La Vallée-Poussin and direct filter inversion
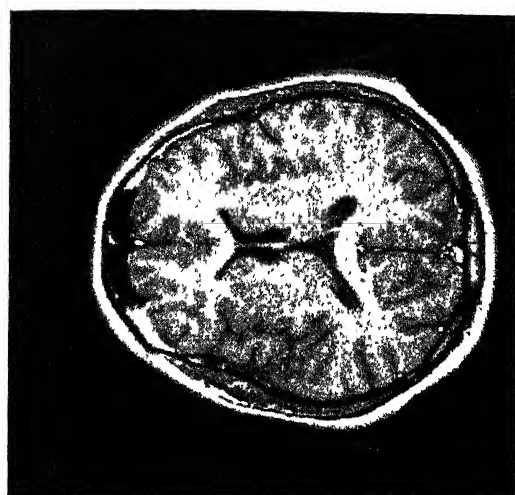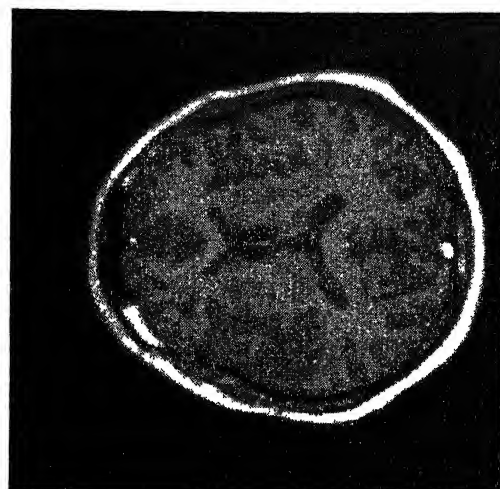
Original

Blurred
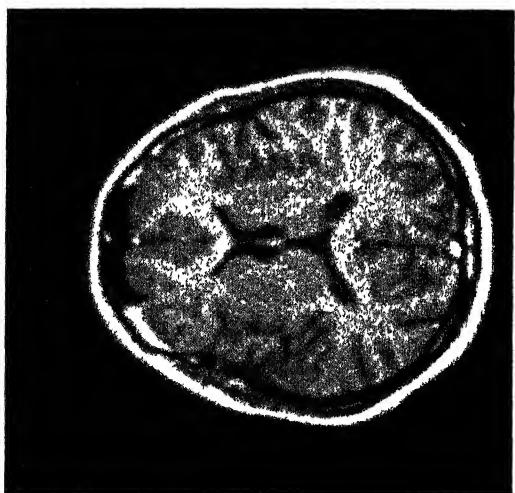
Iteration 1

Iteration 4

Iteration 7

Iteration 10

Fig. 3.2. : De-Blurring by De La Vallée-Poussin integrals (T$_1$ weighted image)
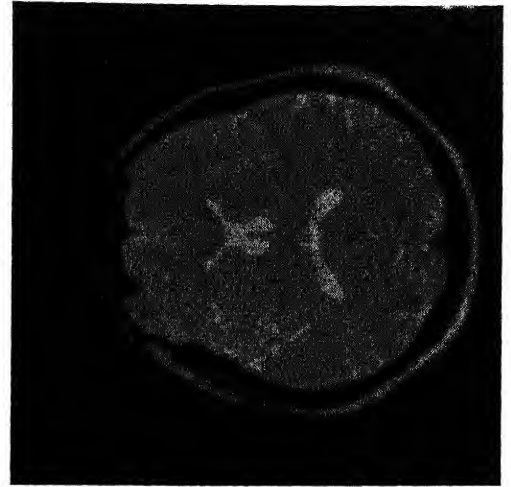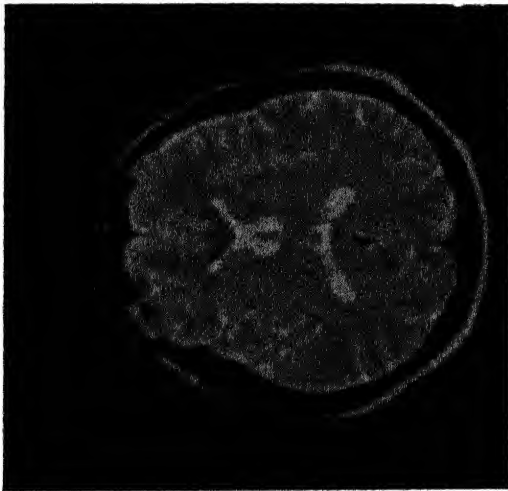
Original

Blurred
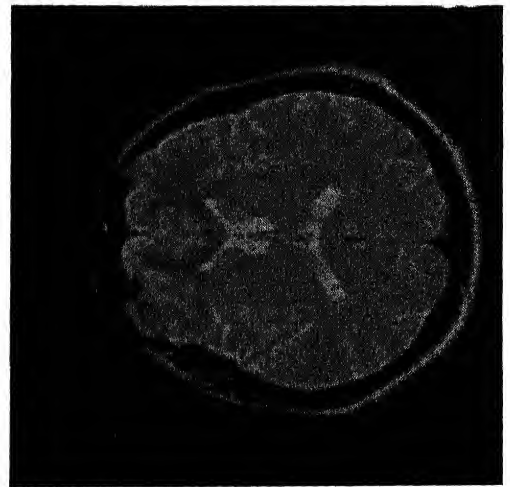
Iteration1

Iteration 4
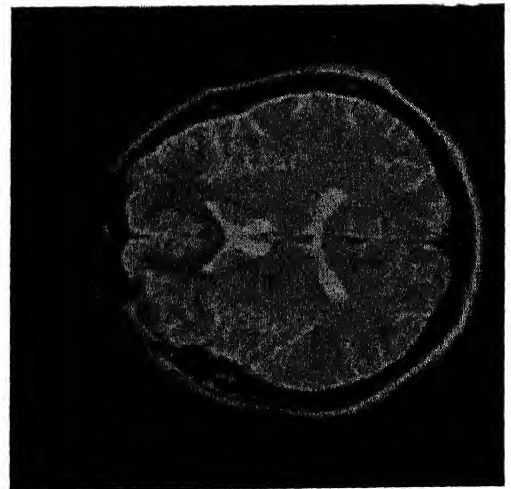
Iteration 7

Iteration 10

Fig. 3.3. : De-Blurring by De La Vallée-Poussin integrals (T_2 weighted image)
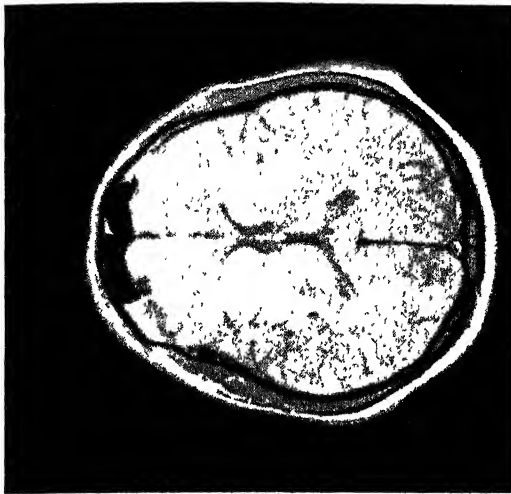
Original
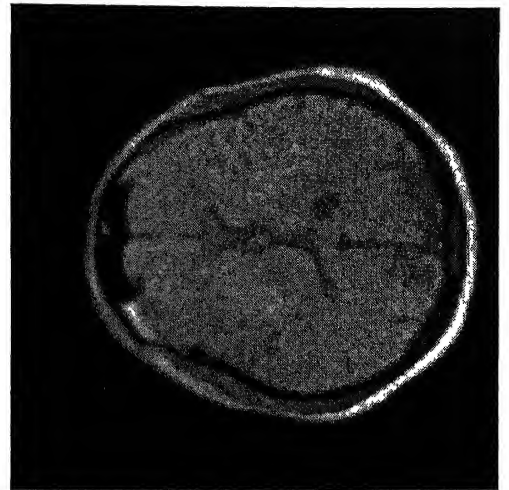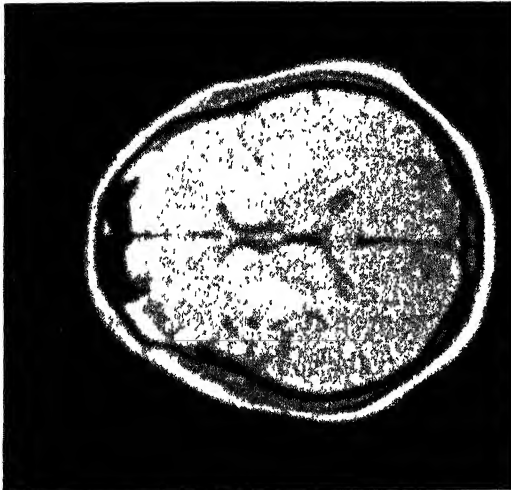
Blurred
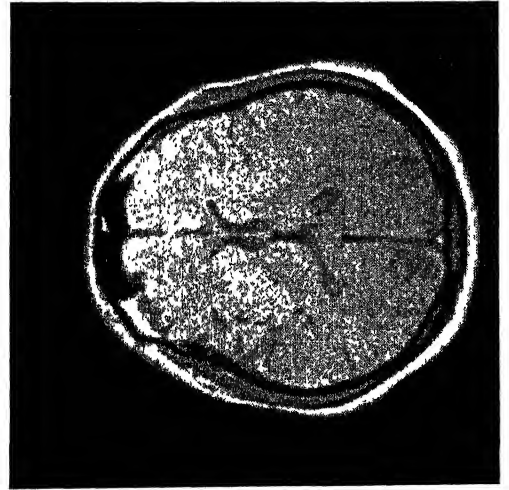
Iteration 1

Iteration 4
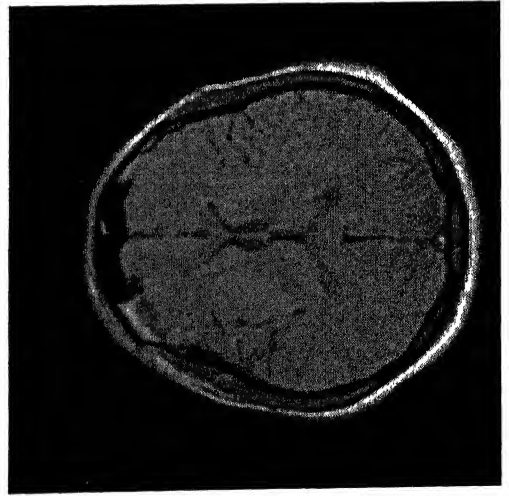
Iteration 7

Iteration 10

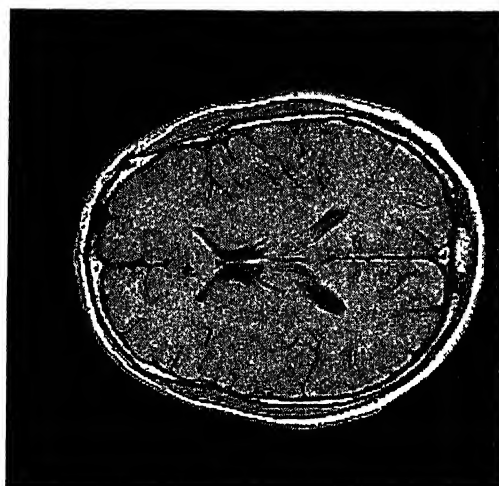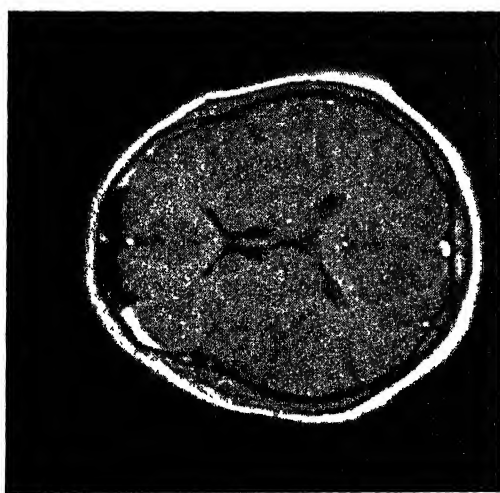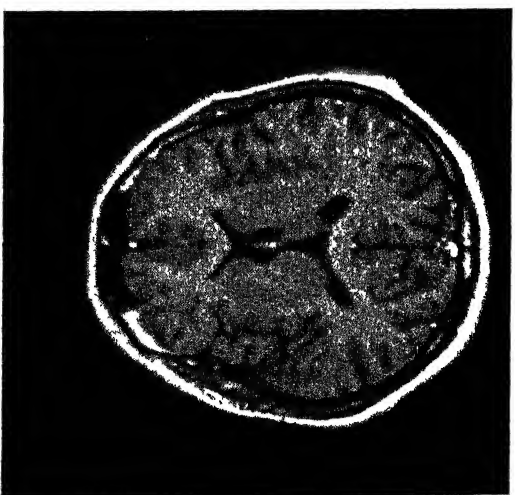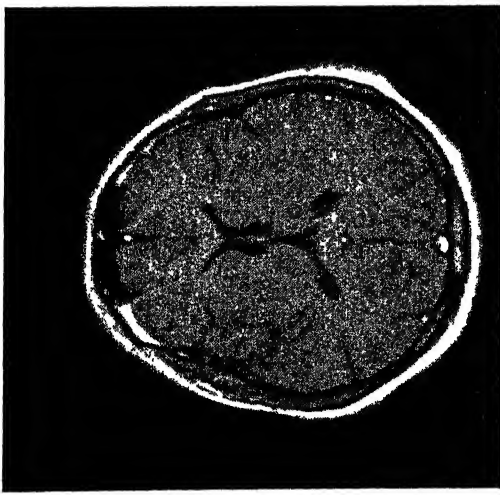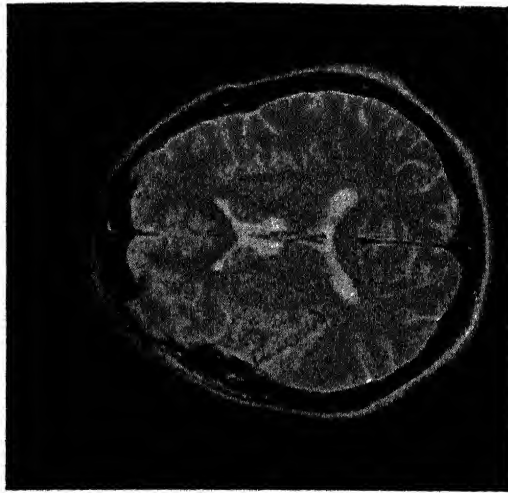**Fig. 3.4.** : De-Blurring by De La Vallée-Poussin integrals (Density weighted image)

	L_1 Error	L_2 Error	L_∞ Error
blurred	13.518874	17.757774	46 268749
A_1	11 067230	14.037602	34 946190
A_2	10.271811	12 694630	30 083900
A_3	9.836020	11.938289	28 262102
A_4	9.533145	11.418419	27 065260
A_5	9 301290	11 022747	26.133268
A_6	9.112067	10 703659	25.376198
A_7	8.951344	10.436556	24.741747
A_8	8 811568	10.207154	24.197197
A_9	8 688163	10 006439	23 720888
A_{10}	8 578032	9.828348	23.297813

Table 3.1. %-Errors in De-Blurring by De La Vallée-Poussin integral
(T₁ weighted image)

	L_1 Error	L_2 Error	L_∞ Error
blurred	12.005098	16 666893	64 805298
A_1	10 635724	14.673879	54.058949
A_2	10.106552	13.794727	48.286686
A_3	9.776073	13.239385	44.509380
A_4	9 541142	12.834176	42 134560
A_5	9 364327	12 516259	40 548008
A_6	9 224312	12 255375	39 251434
A_7	9.107256	12.034124	38.155491
A_8	9 004295	11 841676	37 206196
A_9	8 910651	11.670034	36 368710
A_{10}	8 824517	11.513990	35 619312

Table 3.2 : %-Errors in De-Blurring by De La Vallée-Poussin integrals
(T₂ weighted image)

	L_1 Error	L_2 Error	L_∞ Error
blurred	8.696555	11.395054	42.332867
A_1	7.093175	9.006601	36.220360
A_2	6.567901	8.169998	33.887886
A_3	6.274099	7.707120	33.582581
A_4	6 071949	7.392573	33.156796
A_5	5.918304	7.154491	32.671185
A_6	5.793479	6.962598	32.161728
A_7	5.688051	6.801755	31.648882
A_8	5 597083	6 663292	31.144051
A_9	5.517218	6.541728	30.653318
A_{10}	5.446238	6.433475	30.179653

Table 3.3. : %-Errors in De-Blurring by De La Vallée-Poussin integrals
(Density weighted image)
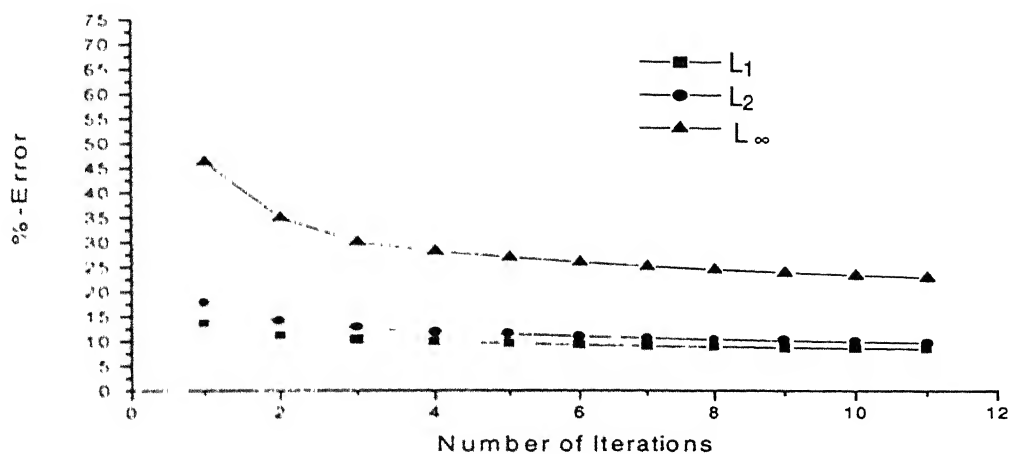
Graph 3.1 : %-Error in De-Blurring by De La Vallée-Poussin integrals (T_1 weighted image)
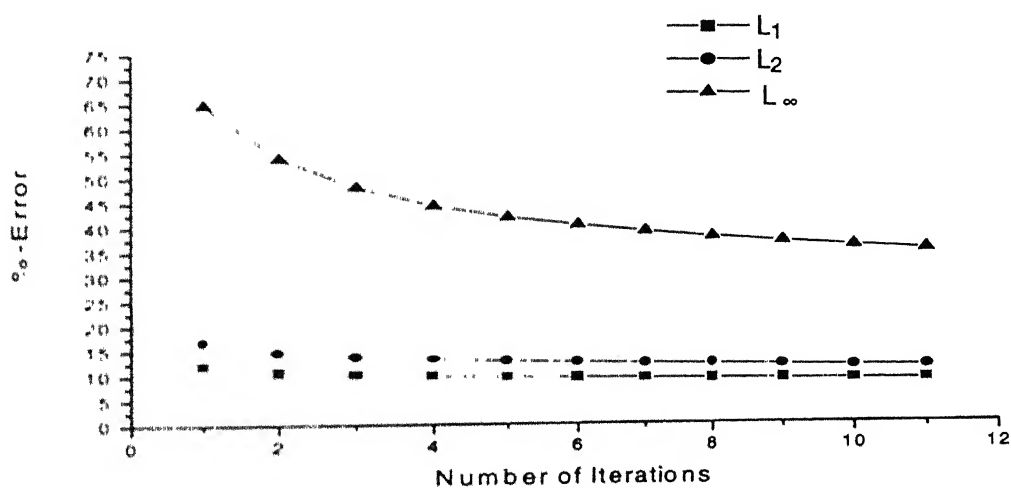
Graph 3.2 : %-Error in De-Blurring by De La Vallée-Poussin integrals (T_2 weighted image)
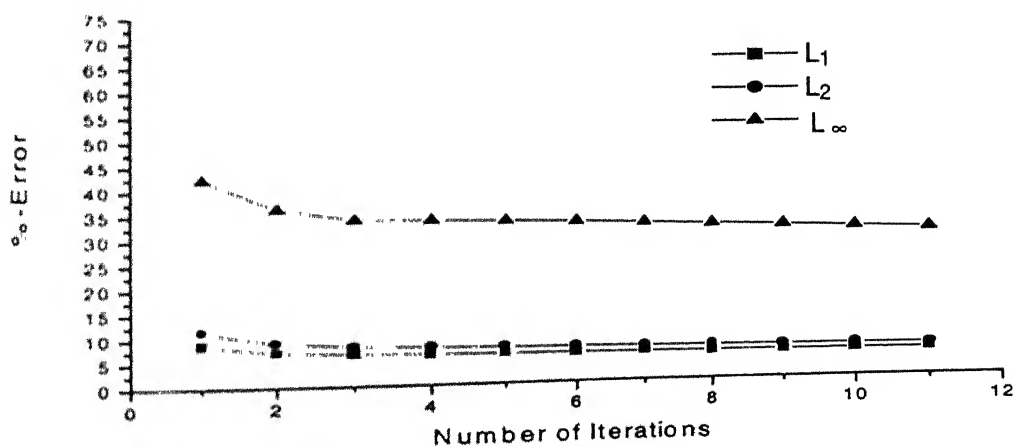
Graph 3.3: %-Error in De-Blurring by De La Vallée-Poussin integrals (Density weighted image)

A look at Table 3.1 reveals that the %-L_1-errors suddenly drop from 13.51 in the case of blurred image to its about 81% value 11.06 right in the case of the first iterate. The subsequent decrease of the errors is rather slow but monotone. The final error 8.57 in the 10th iterate is about 63% of the initial error. The corresponding percentage drops in L_2-errors starting at the value 17.75, are from 79% to 55%, and for the L_∞-error, starting at 46.26, the decrease is from 75% to 50%.

In Table 3.2 corresponding to the T_2-weighted image, the respective figures in the L_1-case are: 12.00, 88%, and 73%; in the L_2-case: 16.66, 88%, and 69%; and for the L_∞-case: 65.80, 83%, and 54%.

In Table 3.3, corresponding to the proton density weighted image, these are - in the L_1-case: 8.69, 81%, and 62%; in the L_2-case: 11.39, 79%, and 56%; and in the L_∞-case: 42.33, 85%, and 71%.

These values are summarized in the following Table 3.4. On the basis of the initial errors it gets reiterated that the density weighted images are the smoothest, followed by the T_2 weighted and the T_1 weighted images, which are approximately of the same smoothness. The exception occurs in the T_2 weighted L_∞-case where the initial error falls out of the line. This, as remarked earlier, is attributable to the generally fluctuating nature of the discretely computed L_∞-errors.

	Drop in the L_1-error from the first to the last iterate			Drop in the L_2-error from the first to the last iterate			Drop in the L_∞-error from the first to the last iterate		
	Initial %-Error	First Iterate	Last Iterate	Initial %-Error	First Iterate	Last Iterate	Initial %-Error	First Iterate	Last Iterate
T_1	13.51	81%	63%	17.75	79%	55%	46.26	75%	50%
T_2	12.00	88%	73%	16.66	88%	69%	64.80	83%	54%.
ρ	8.69	81%	62%	11.39	79%	56%	42.33	85%	71%.

Table 3.4 · Effectiveness of De-Blurring of T_1, T_2, & Density weighted images by Vallée-Poussin integrals

The interesting point to be observed here is that even though the numerical errors for iterates do not reduce very substantially, the visual effect of their de-blurring as well their visual nearness to the original is unmistakable.

3.4.3 SIGNED ERRORS IN THE ITERATIVE DE-BLURRINGS BY $V_n^{[m]}$

The information on the point-wise behavior of the convergence of the iterative de-blurrings by $V_n^{[m]}$ is presented in the following strip-graphs (Graphs 3.4 (a-b)). As in the previous chapters, the signed errors $f - V_n^{[m]}f$ in the reconstructions $V_n^{[m]}f$ of f are shown in the form of the strip-graphs for the first T_1-weighted cross-section. The errors are displayed for the same horizontal 128th mid-row and for all the 256-pixels on it. As in the case of strip-graphs in Chapters 1-2, the unit for these graphs is one gray level when the original is assumed to be a 256-gray level image.

The signed errors for the blurred image $f - V_n f \equiv f - V_n^{[1]}f$ are shown in the first strip graph. These errors for the de-blurred cases of the first ten iterates $f - V_n^{[m]}f$, $(2 \leq m \leq 11)$ occur in the next ten strip-graphs. The last strip-graph is a superposition of all the signed errors in the ten iterates, as well as in the blurred image.

As pointed out earlier in the case of the Fejér sums in Chapter 1, here, too, some of the points where the values undergo an abrupt change have not got depicted in the strip graphs. This is indeed so for the cases m = 1, 2, and 3, where the range exceeds the limit 30 depicted in the graphs.

These strip-graphs show a similar, more or less monotone, behavior of the point-wise errors with increasing m. The errors, along the blackened mid line, may be observed to be relatively small for the pixels where the cross-section is relatively smooth and large where the cross section is less smooth. The error patterns for different m's are similar where the magnitudes of errors keep decreasing as m increases. A surge in the error activity, analogous to that seen with the earlier cases of Fejér and the generalized Jackson operators, for pixels near the boundaries of anatomical structure is observable here too. Similar to what has been the case with the percentage errors presented in the tables before, the signed errors for the De la Vallée-Poussin blurring and de-blurrings closely mimic the case of the generalized Jackson operators $L_{n,p}$ with p = 3, and n = 45.
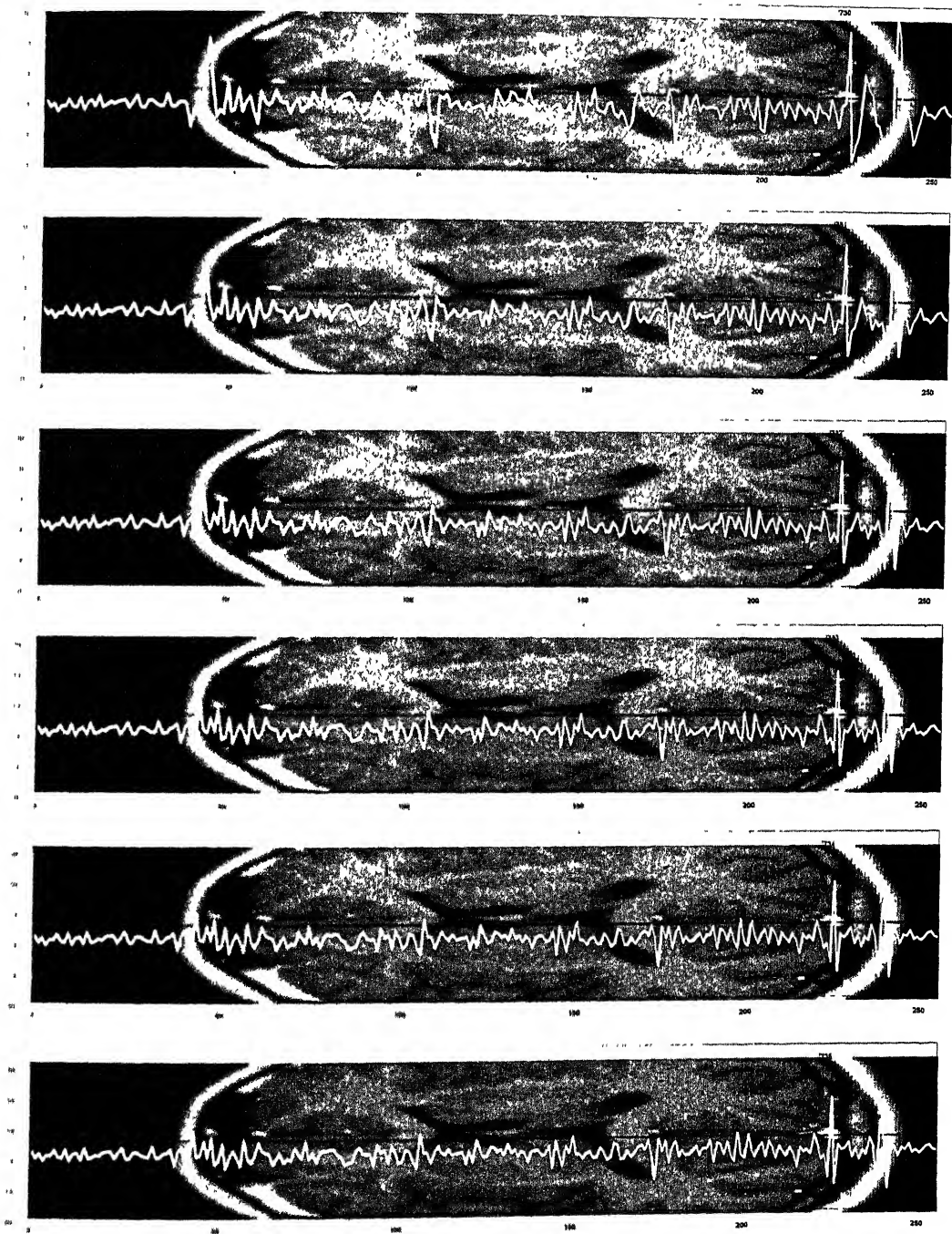
Graph 3.4 (a) : Signed de-blurring errors $\left(f - V_n^{[m]} f,\; m = 1,2,3,4,5,6\right)$
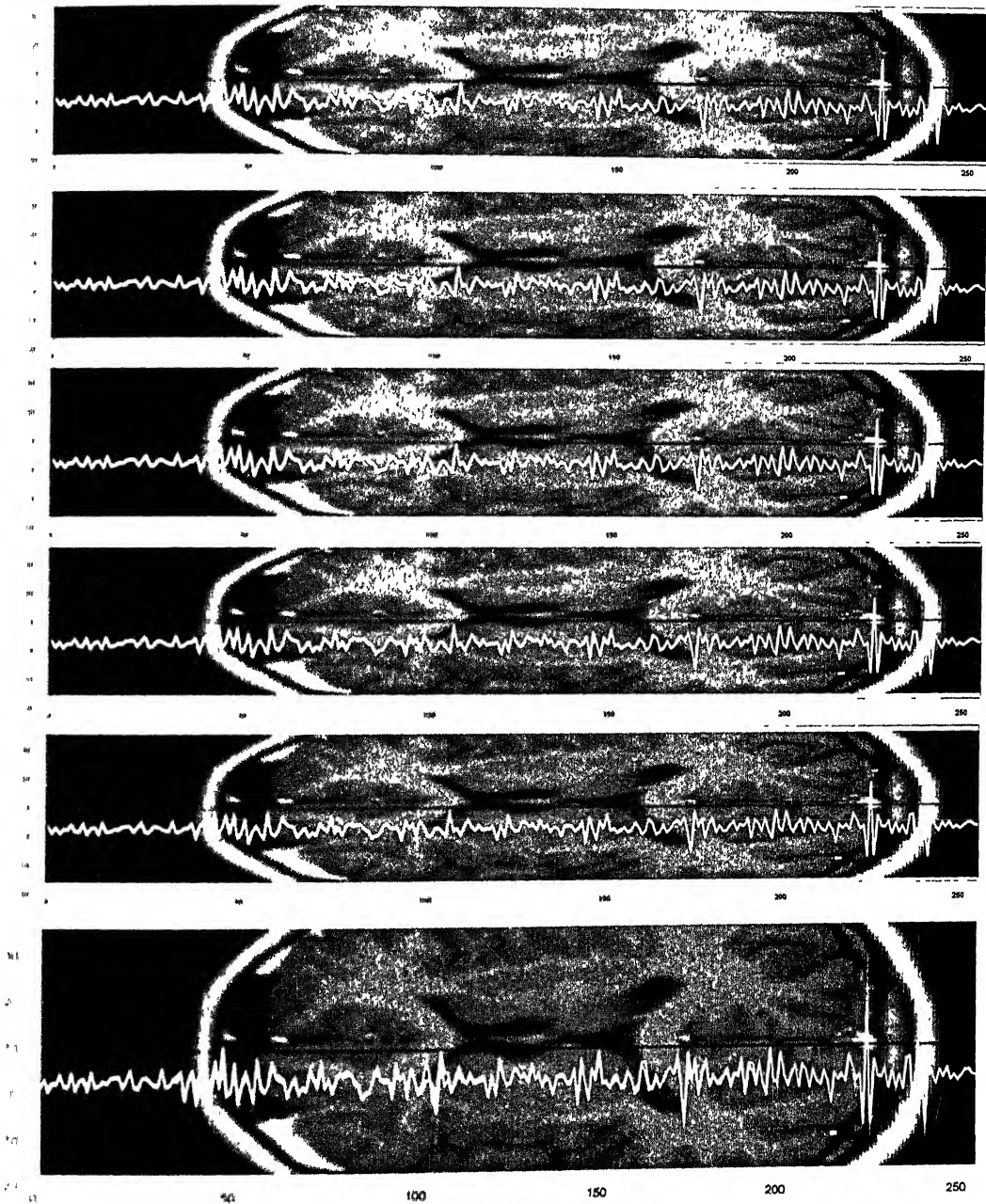
Graph 3.4 (b) : Signed de-blurring errors $\left(f - V_n^{[m]} f, \; m = 7,8,9,10 \right)$ and the superposition of all eleven above

CHAPTER 4: APPLICATIONS TO MRI DIAGNOSIS

In this final chapter we round-up the work of the previous chapters by discussing some aspects of the applicability of the de-blurring scheme of Rathore, with a special emphasis on his choice of Fejér sums as an easy to implement, general purpose blurring model for the routine MRI work. The simulations presented in the previous chapters clearly demonstrated the applicability of the scheme to improved visual diagnosis on actual MRI cross-sections. The de-blurred images, even with only moderately close other choices of blurring models, are relatively sharp, possess improved tissue contrast and boundary delineation, and do not seem to overemphasize the noise.

In the following, we numerically analyze and experiment with some of the questions and issues pertaining to: (i) a practical choice of the system blurring operator, (ii) the behavior of the de-blurring scheme with respect to varying sizes of machine data, (iii) the mechanism of de-blurring, and (iv) an application to improved numerical tissue parameter estimation.

A model of the system blurring is indeed the most crucial and important input to the scheme of de-blurring. The question is whether the scheme is robust with respect to the choice of the blurring model, or does it too critically depend on it. The estimates of Rathore in Chapter 0 asserted that if $\|\Delta\| = \|I\text{-}A\| < 1$,

$$A_m(Uf) - f \rightarrow A^{-1}(U\text{-}A)f,$$

and $$\|A_m N\| \leq [(1\text{-}\|\Delta\|^m)/(1\text{-}\|\Delta\|)]\|N\|.$$

It follows that unless the system blurring operator U is too far away from the identity operator I, any reasonable choice of A lying, so to say, in between the U and the I and more towards U in the sense of $\|U\text{-}I\| < \|A\|\,\|I\text{-}A\|$, are expected to result in a reasonable de-blurring. Moreover, since A_m acts on the diffused noise N, unless both m and $\|\Delta\|$ are large the noise is not expected to reassert itself.

4.1 A COMPARISON OF THE FILTER COEFFICIENTS
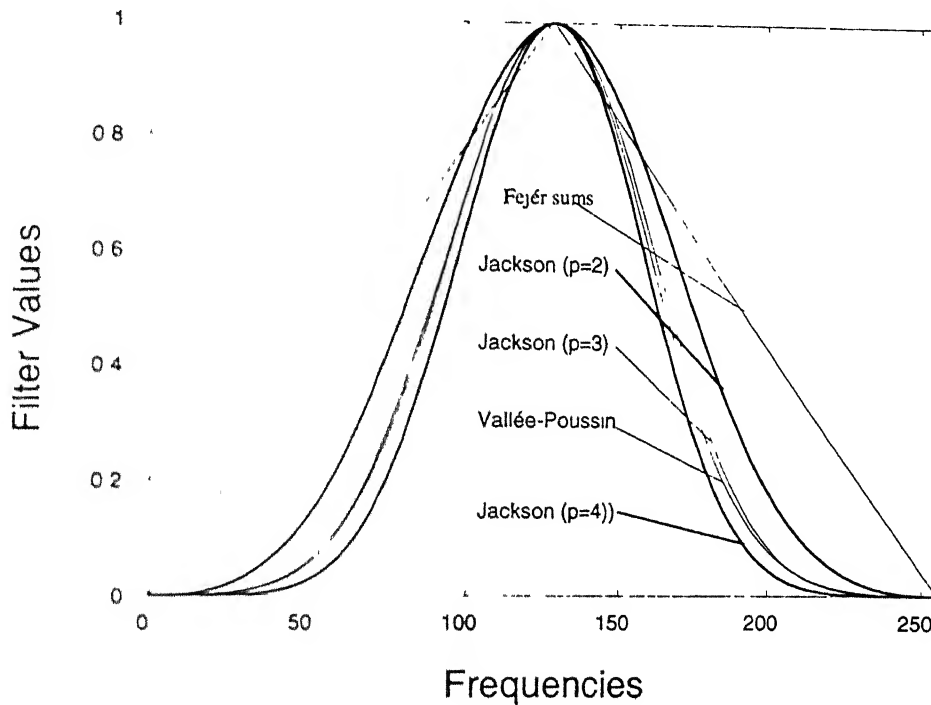
Graph 4.1. Filter Coefficients of Fejér, Jackson (p = 2, 3, 4), and Vallée-Poussin Operators

The blurring operations considered in the Chapters 1-4 have been 2D-convolutions with the 1D-kernels of the type:

$$K_n(t) = 1/2 + \sum_{k=1}^{n} \rho_k^{(n)} \cos kt,$$

where the coefficients of the kernels associated with the Fejér operators, the generalized Jackson operators and the Vallée-Poussin operators are given as:

Fejer operators: $\rho_k^{(n)} = 1 - k/n$,

Jackson operators: $\rho_k^{(n)} = \mu_k^{n,p} / \mu_0^{n,p}$, where $\mu_k^{n,p} = \sum_{j=0}^{p-1} (-1)^j \binom{2p}{j} \binom{np + p - n\,j - k - 1}{2p - 1}$, &

Vallée-Poussin operators: $\rho_k^{(n)} = \dfrac{(n!)^2}{(n-k)!(n+k)!}$.

The graph above (Graph 4.1) shows the filter coefficients, appropriately renumbered and symmetrically folded, for the operators that have been used in Chapters 1-3 for the simulations there. It makes clear that a gradation of these operator, according to an increasing order of the associated blurring, is given by: σ_n, L_{n2}, L_{n3}, V_n, and L_{n4}. The closeness of the graphs of filter values of $L_{n.3}$, and V_n is clearly responsible for the near equal behavior of these operators in all the simulations.

On the basis of the above graph the Fejér sums σ_n are expected to produce the least blurring, and so the associated approximation errors ought to be the smallest for them. Amongst the Jackson operators the errors are expected to be the least for L_{n2}, followed by $L_{n.3}$, and $L_{n.4}$. The Vallée-Poussin operators V_n should fall in between $L_{n.3}$, and $L_{n.4}$. The following error tables, which present the %-L_1, %-L_2, and %-L_∞ errors reassorted from the tables of the previous chapters, readily illustrate this point:

%-L_1 Errors	Fejér sums	Jackson 2	Jackson 3	Vallée-Poussin	Jackson 4
T_1	11.26	10.89	13.30	13.51	14.35
T_2	9.86	11.82	11.87	12.00	12.51
ρ	7.28	7.58	8.55	8.69	9.24

Table 4.1: %-L_1 Errors in the blurring of T_1, T_2 and ρ-images by σ_n, L_{n2}, L_{n3}, V_n, and L_{n4}

%-L_2 Errors	Fejér sums	Jackson 2	Jackson 3	Vallée-Poussin	Jackson 4
T_1	14.12	15.05	17.42	17.75	19.00
T_2	13.04	15.17	16.49	16.66	17.40
ρ	9.15	9.75	11.18	11.39	12.19

Table 4.2 %-L_2 Errors in the blurring of T_1, T_2 and ρ-images by σ_n, L_{n2}, L_{n3}, V_n, and L_{n4}

%-L_∞ Errors	Fejér sums	Jackson 2	Jackson 3	Vallée-Poussin	Jackson 4
T_1	36.46	39.17	45.34	46.26	49.46
T_2	48.78	57.44	64.05	64.80	67.95
ρ	32.42	37.95	41.88	42.33.	44.15

Table 4.3 %-L_∞ Errors in the blurring of T_1, T_2 and ρ-images by σ_n, L_{n2}, L_{n3}, V_n, and L_{n4}

4.2 AN EXPERIMENT WITH THE CROSS-FILTERING

Indeed one of the principal advantages of the iterative de-blurring is its interactive monitoring feature of continuing the iterations only till the noise does not start reasserting itself. Practical experience with the iterates tells that each of these has something useful to tell about the cross-section studied. Quite often the individual iterates suggestively point out to some typical feature of the cross-section which subsequently gets accepted or rejected by a closer look at the original and all the available iterates jointly. The present section consists of simulations done in order to obtain an insight into this applicability of the de-blurring in the actual practice where the knowledge of the system blurring operator could normally be obtained only indirectly. Thus, if nothing better is available, one could start with a reasonable set of empirical filter functions and examine their applicability by obtaining a few trial reconstructions. Reconstructions based on well-calibrated phantoms may also be useful in generating approximations of the system blurring operator.

In the simulations below the T_1, T_2, and ρ-weighted cross-sections in Fig. 0.4 are blurred by each of the three operators σ_n, $L_{n,p}$ ($p = 3$), and V_n. As the generalized Jackson and the De la Vallée-Poussin operators induce similar but a greater blurring than the Fejér sums, the numerical experiment below provides insight into the nature of de-blurring when the assumed blurring model results in a slightly more (or less) smoothing compared to that of the actual system blurring operator. Thus by modeling the system blurring operator after the above mentioned operators σ_n, $L_{n,p}$ ($p = 3$), and V_n, each blurred image is subsequently iteratively de-blurred by the associated de-blurring operators. The resulting images may be readily cross analyzed. The experimental findings point out that the de-blurrings associated with the Fejér operators $\sigma_{n,m}$ result in sharpened images of least error out of all of the operators considered here. This methodology, with appropriate models of the blurring, could be used empirically for estimating system blurring on an MRI machine. The results also indicate that neighboring models perform more or less equally well and thereby point out to the robustness of the de-blurring technique. The images and tables presented in Fig. 4.1-4.3 and Tables 4.4-4.6 correspond to the third (m = 4) iterates, which in actual practice have been found to be quite satisfactory.
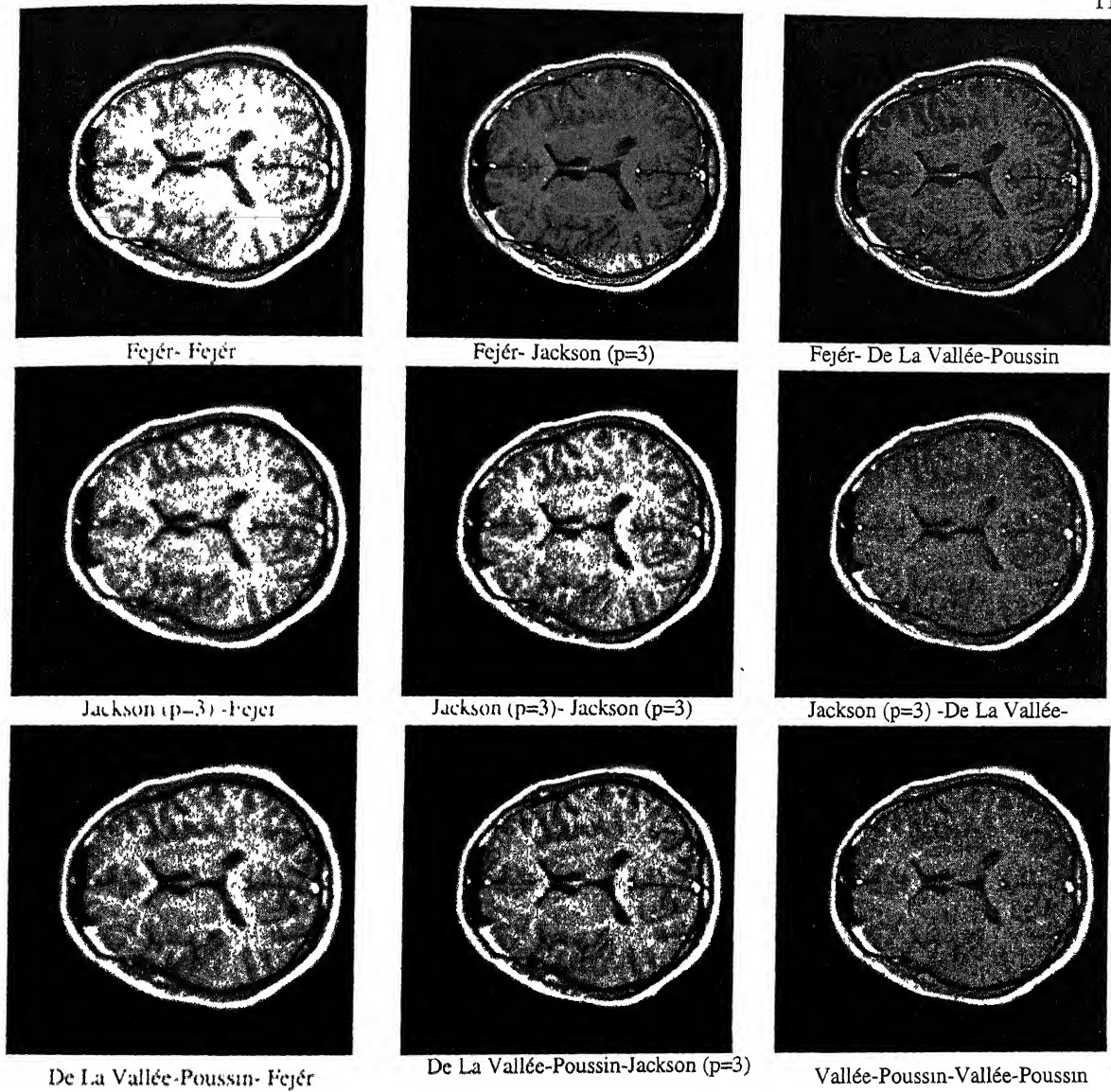
Fejér- Fejér | Fejér- Jackson (p=3) | Fejér- De La Vallée-Poussin

Jackson (p=3) -Fejér | Jackson (p=3)- Jackson (p=3) | Jackson (p=3) -De La Vallée-

De La Vallée-Poussin- Fejér | De La Vallée-Poussin-Jackson (p=3) | Vallée-Poussin-Vallée-Poussin

Fig. 4. 1: Blurring and De-Blurring by Different De-Blurring Operators on a T_1-Weighted Image

	Fejér	Jackson (p=3)	Vallée-Poussin
Fejér	5 501431	6 843048	7.142781
Jackson(p= 3)	10.955830	9.755668	9.755668
Vallée-Poussin	11.143796	9.882319	9.836020

L_1 Error

	Fejér	Jackson (p=3)	Vallée-Poussin
Fejér	5.805688	7.658533	8.092607
Jackson(p=3)	13.614547	11.791772	11.791772
Vallée-Poussin	13.903517	12.052172	11.938289

L_2 Error

	Fejér	Jackson (p=3)	Vallée-Poussin
Fejér	14.031715	16.998110	18.222013
Jackson(p=3)	32.352612	27.978689	27.978689
Vallée-Poussin	33.391159	28.647913	28.262102

L_∞ Error

Table 4. 4: Blurring and De-Blurring by Different De-Blurring Operators on a T_1-Weighted Image

Fejér- Fejér Fejér- Jackson (p=3) Fejér- De La Vallée-Poussin

Jackson (p=3) -Fejér Jackson (p=3)- Jackson (p=3) Jackson (p=3) -De La Vallée-

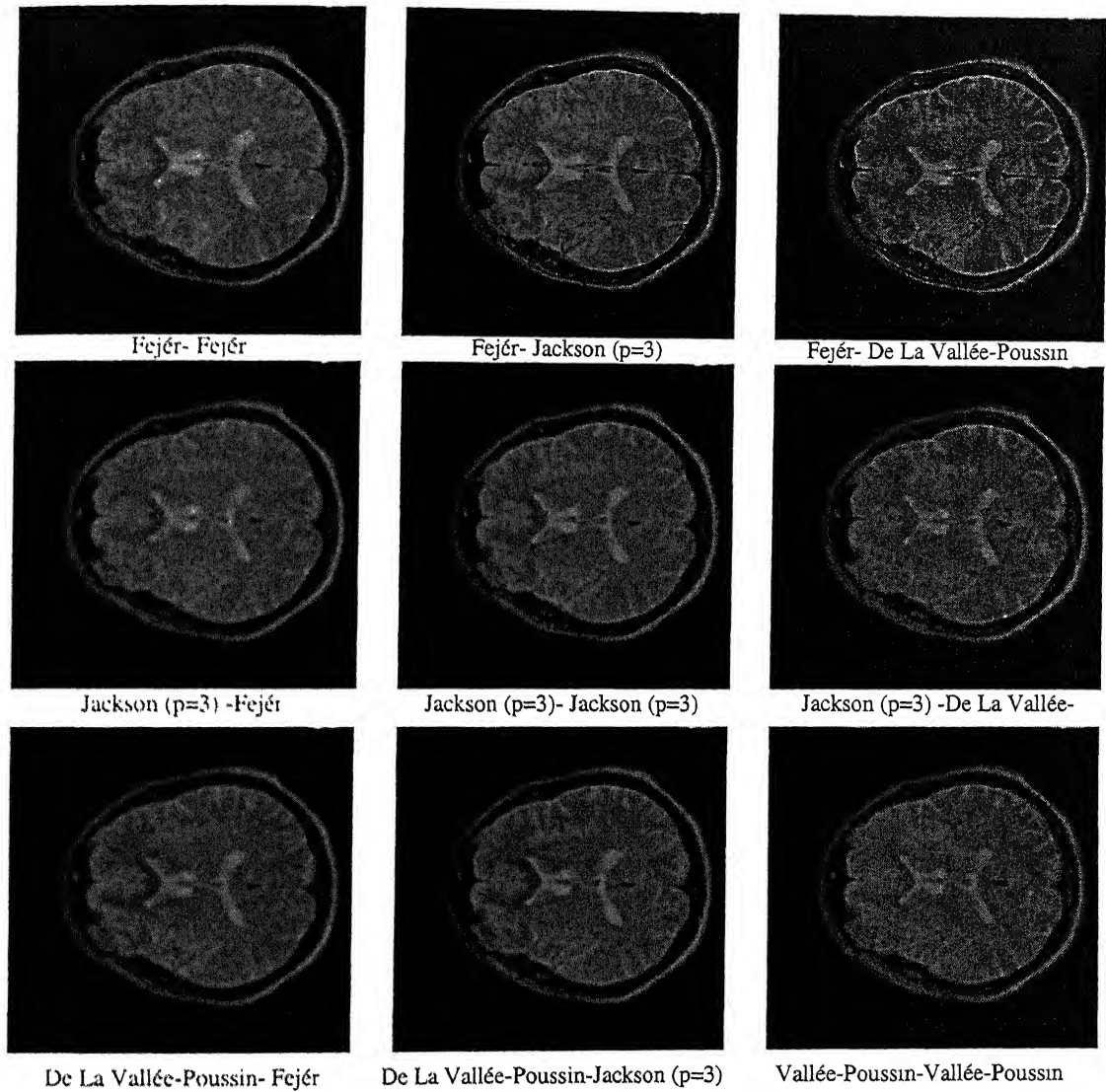De La Vallée-Poussin- Fejér De La Vallée-Poussin-Jackson (p=3) Vallée-Poussin-Vallée-Poussin

Fig. 4. 2: Blurring and De-Blurring by Different De-Blurring Operators on a T_2-Weight Image

	Fejér	Jackson (p=3)	Vallée-Poussin
Fejér	5.909182	6.485254	6.668396
Jackson(p=3)	10.502147	9.730365	9.717400
Vallée-Poussin	10.612084	9.801308	9.776073

L_1-Error

	Fejér	Jackson (p=3)	Vallée-Poussin
Fejér	7.100663	7.104949	7.369535
Jackson(p=3)	14.437531	13.189909	13.139686
Vallée-Poussin	14.586150	13.302277	13.239385

L_2-Error

	Fejér	Jackson (p=3)	Vallée-Poussin
Fejér	19.793056	15.321804	16.175762
Jackson(p=3)	51.579433	43.934147	43 159855
Vallée-Poussin	52.697315	45.431942	44 509380

L_∞-Error

Table. 4.5 : Blurring and De-Blurring by Different De-Blurring Operators on a T_2-Weighted image

Fejér- Fejér   Fejér- Jackson (p=3)   Fejér- De La Vallée-Poussin

Jackson (p=3)- Fejér   Jackson (p=3)- Jackson (p=3)   Jackson (p=3) -De La Vallée-

De La Vallée-Poussin- Fejér   De La Vallée-Poussin-Jackson (p=3)   Vallée-Poussin-Vallée-Poussin

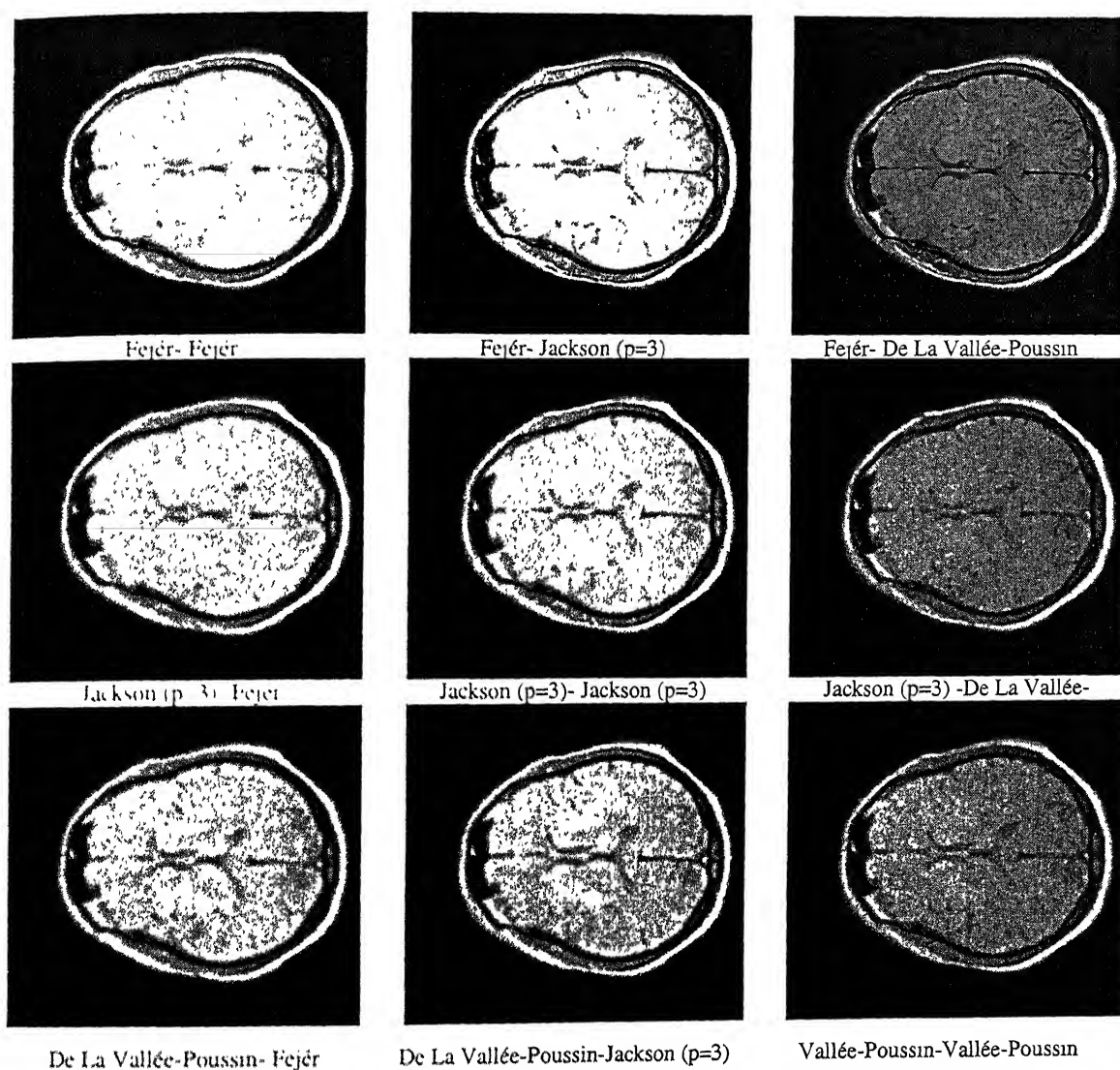**Fig. 4.3:** Blurring and De-Blurring by Different De-Blurring Operators on a Density-Weighted Image

	Fejér	Jackson (p=3)	Vallée-Poussin
Fejér	3.477801	4.455467	4.660405
Jackson(p=3)	7.061089	6.221765	6 206601
Vallée-Poussin	7.187753	6.307024	6 274099

L_1 Error

	Fejér	Jackson (p=3)	Vallée-Poussin
Fejér	3.828713	5.043094	5.337027
Jackson(p=3)	8.760753	7.623755	7.574858
Vallée-Poussin	8.950841	7.778380	7.707120

L_2 Error

	Fejér	Jackson (p=3)	Vallée-Poussin
Fejér	15.780841	14.786440	15.769584
Jackson(p=3)	34.737602	33.660534	33.788979
Vallée-Poussin	35.423737	33.459160	33.582581

L_∞ Error

Table 4.6 : Blurring and De-Blurring by Different De-Blurring Operators on a Density-Weighted Image.

4.3 NUMERICAL RESULTS ON DE-BLURRINGS AT DIFFERENT RESOLUTIONS

The theoretical results in the previous chapters were concerned with the behavior of the de-blurring operators as the parameter n, related with the data size there, approaches infinity. Even though the results predict improvements in the reconstructions with increasing n, in the actual practice we are constrained to work with the moderate values of n such as 256. In this connection, the theoretical results in conjunction with realistic numerical simulations, nevertheless, help us in making projections about the future practice when the larger sizes may become possible due to improvements in the technology. Also, realistic numerical simulations provide an added incentive for the needed technological developments if the results at the larger sizes are expected to be an order of magnitude better, as compared with the present state of the art.

The next experiment in this chapter is intended in the same direction. In it we examine the efficacy of the de-blurring on different sizes of cross-sectional data, or equivalently on the MRI images of different resolutions such as 64×64, 128×128, 256×256, 512×512, etc. Much of the present clinical practice is based on 256×256 machine data. With the discovery of newer and faster pulse sequences and improved machination, it is expected that soon in the future routine MRI diagnosis may switch over to the 512×512 case. Images at the 512×512 resolution would be capable of revealing finer details than is possible with the 256×256 images. Indeed it is possible right now to acquire the 512×512 data. However for it to match the noise characteristics of the 256×256 images the required imaging times are prohibitive at the moment.

To carry out a realistic numerically-simulated error analysis, we used a T_1-weighted 512×512 spin echo image data at TE = 15 ms and TR = 400 ms, to generate the "Original" cross sections of sizes 64×64, 128×128, 256×256, and 512×512, from which the respective blurred images were obtained by using the Fejér filter coefficients for the size 512×512. This is keeping in mind that the basic machine out-put is this data for the image and not the image itself. As an implication, the blurring would be maximal for the image of the size 512×512 and minimal for that of 64×64. The de-blurrings were done by

the corresponding Fejér filters. Two kinds of errors were calculated: (i) on the 512×512 grid of the original, in which the lower size images were extended to the size 512×512 by using zero padding in the frequency domain (the extended images thus representing the values of the same trigonometric polynomial on a larger grid of points), and (ii) the individual errors in reconstructing the images themselves of the respective sizes 64×64, 128×128, 256×256, and 512×512. Thus the percentage errors in (i) are with respect to the "Original" of size 512×512, and in (ii) these are with respect to the "Originals" of the sizes 64×64, 128×128, 256×256, and 512×512. One expects large errors in (i), and much smaller errors in (ii), since the filtering is progressively less for the smaller image sizes. Hence, in the case (i) the errors are not supposed to decrease any significantly, they being predominantly due to the basic errors in the approximation by the partial sums of the Fourier series associated with the image sizes 64×64, 128×128, 256×256, and 512×512. However, these errors for the sizes 64×64, 128×128, and 256×256 in case (i) do give us a rough idea of the actual errors incurred in MRI reconstructions with the respective sizes 64×64, 128×128, and 256×256. The errors in both (i) and (ii) for the size 512×512 are indeed to be the same and they reflect the reduction of the errors in the successive de-blurring iterates, as they do for the remaining sizes in (ii).

The related images are shown in Figs. 4.4-4.7. The numerical errors in the case-(i) are presented in the Tables 4.7-4.9 and the same are also shown in the Graphs 4.2-4.4. The same in the case-(ii) are given in Tables 4.10-4.12 and Graphs 5.5-4.7. As seen from these, the nature of the errors is, indeed, as described in the previous paragraph. The agreement of the order of the errors in Tables 4.10-4.12 for the size 512×512, and in Table 1.1 (for the T_1-weighted cross-section there in Chapter 1) seem to confirm the appropriateness of the model of the filters chosen. On the other hand, the relatively too small errors in Tables 4.10-4.12 for the sizes 64×64, 128×128, and 256×256 indicate a better performance of the de-blurring iterates if $\|\Delta\|$ (as described in Chapter 1) is relatively small.

We also include a repeat of experiment of Fig. 1.1 in Fig. 4.8, where the 512×512 image is regarded as a machine output (with 512×512 Fejér blurring model)and the de-blurring iterates and the result of a direct filter inversion are shown. The improvements are as before and a similarity in the results of direct inversions in the two cases is striking.
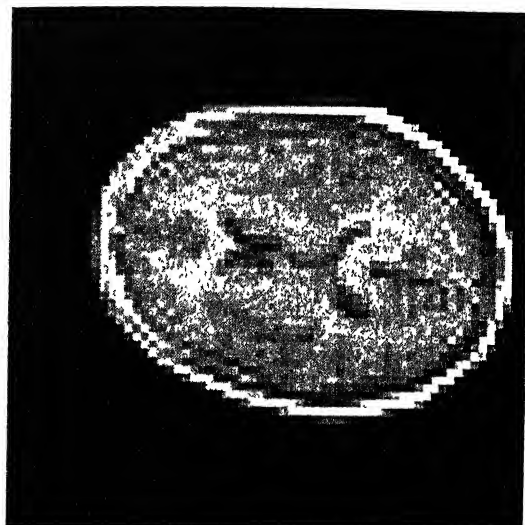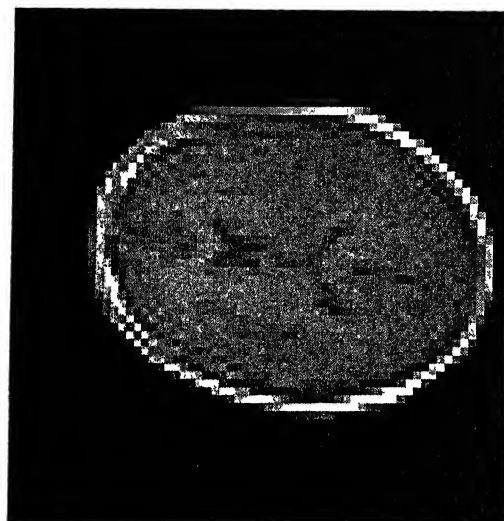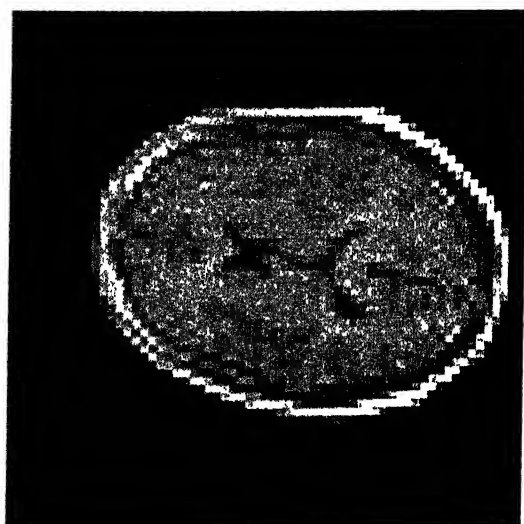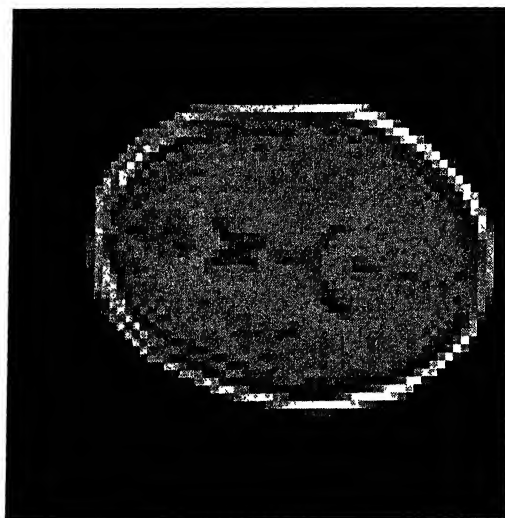
64x64 Reconstruction
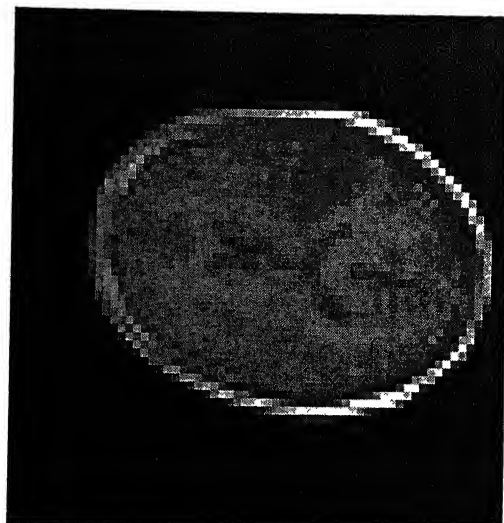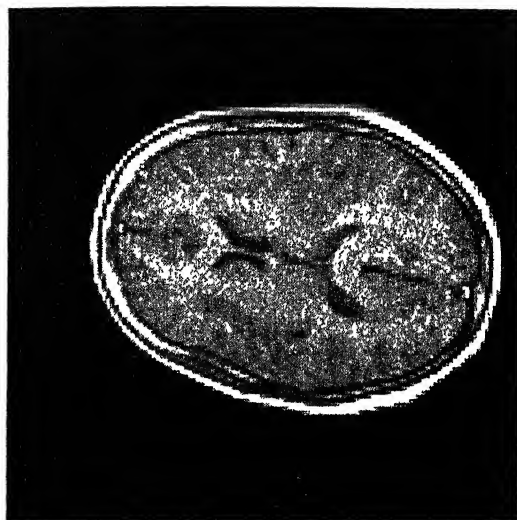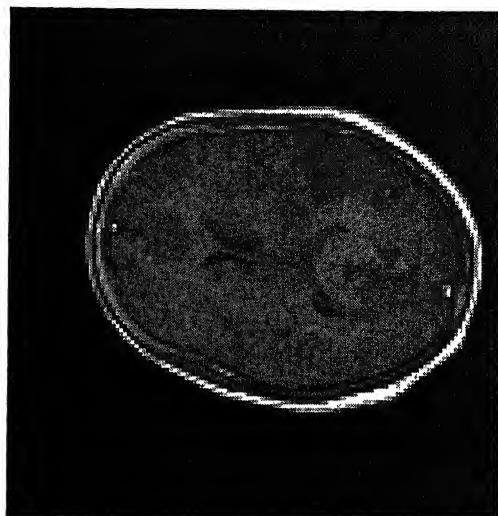
Blurred
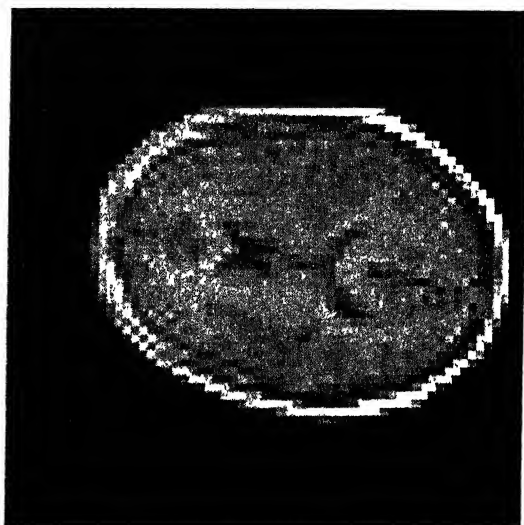
Iteration 1

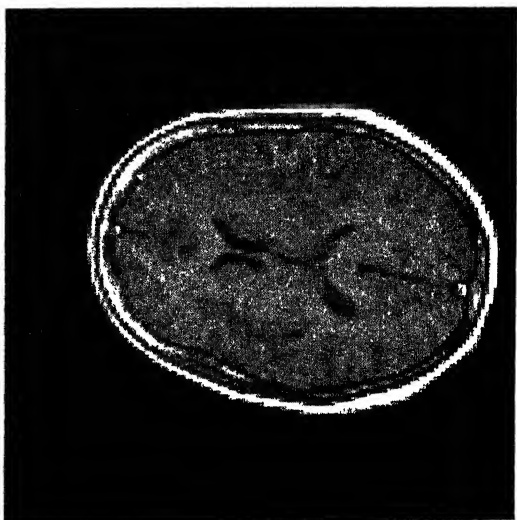Iteration 4

Iteration 7

Iteration 10

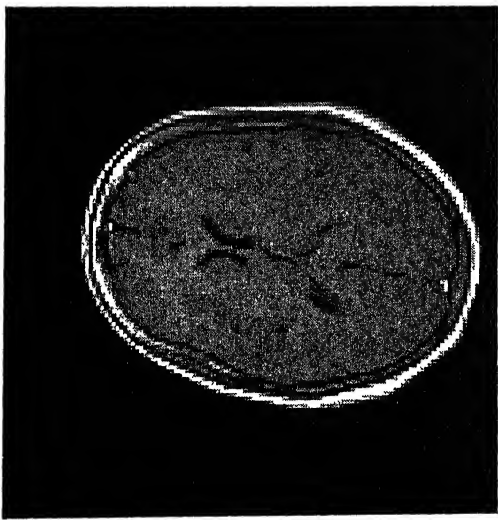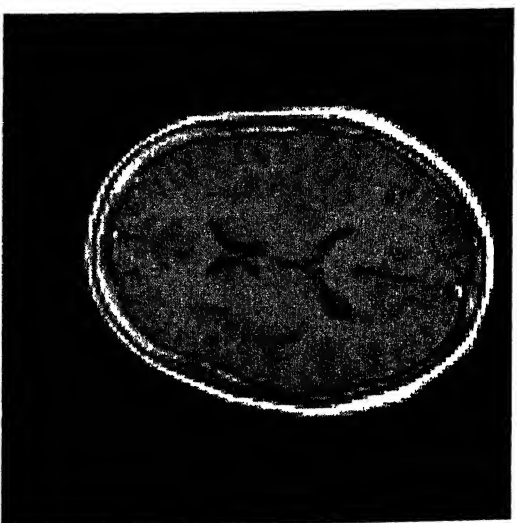**Fig. 4.4 :** De-Blurring by Fejér sums (64x64 T_1-Weighted Image)
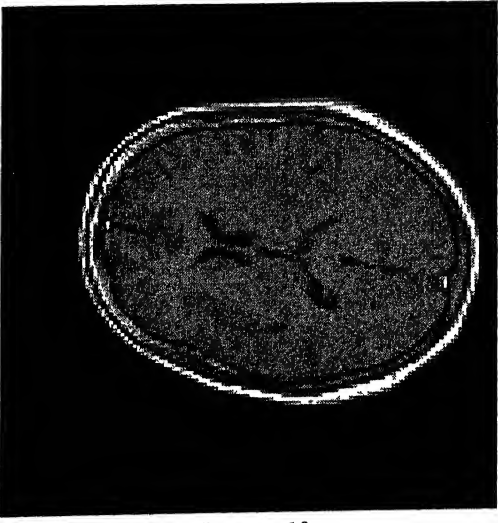
128x128 Reconstitution
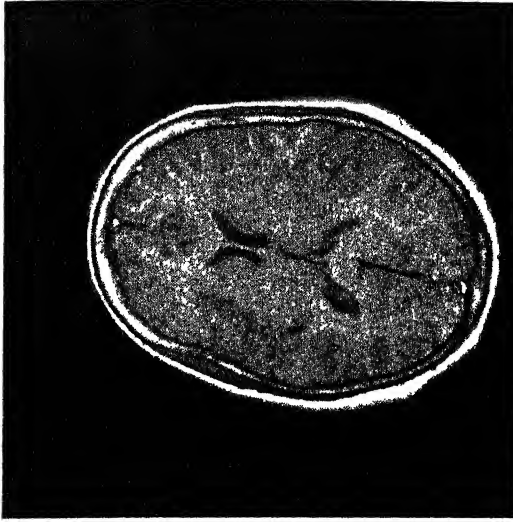
Blurred
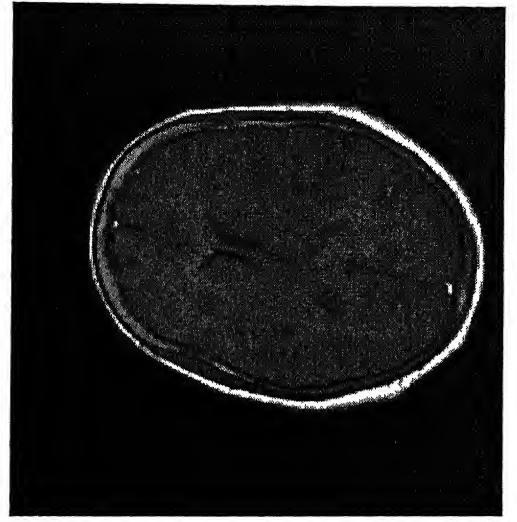
Iteration 1
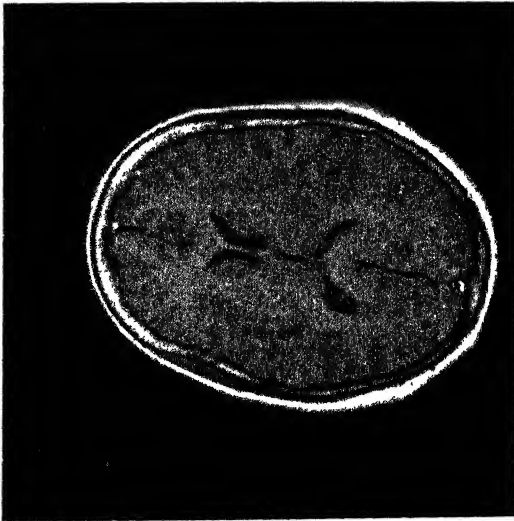
Iteration 4

Iteration 7

Iteration 10

Fig. 4.5 : De-Blurring by Fejér sums (128x128 T_1-Weighted Image)

256x256 Reconstruction

Blurred

Iteration 1

Iteration 4

Iteration 7

Iteration 10

Fig. 4.6 : De-Blurring by Fejér sums (256x256 T_1-Weighted Image)
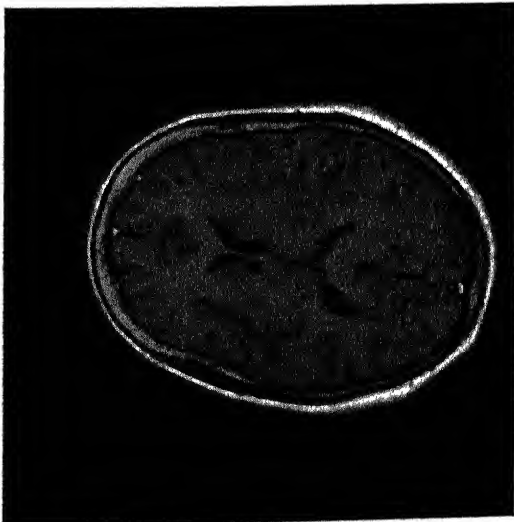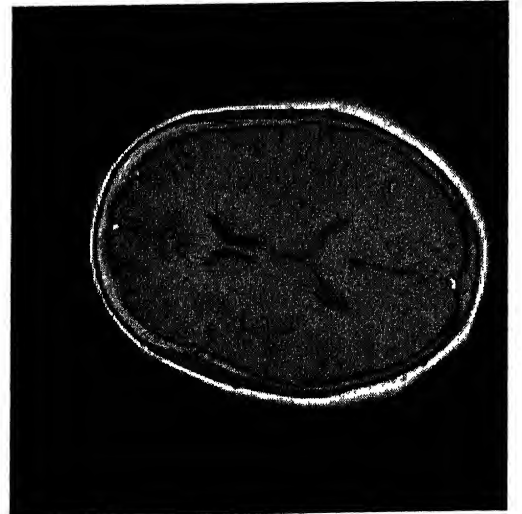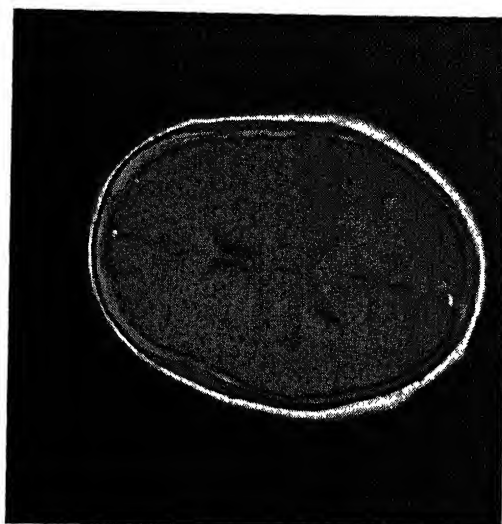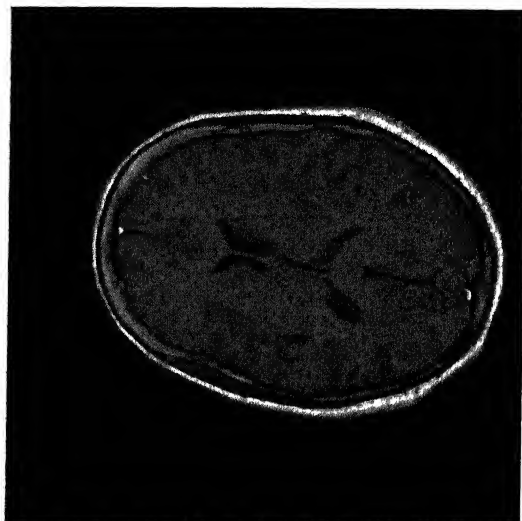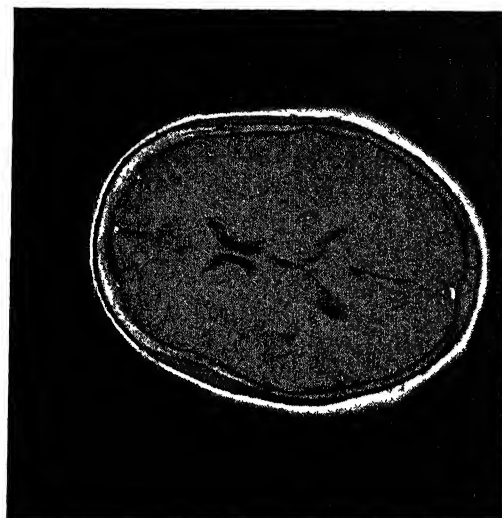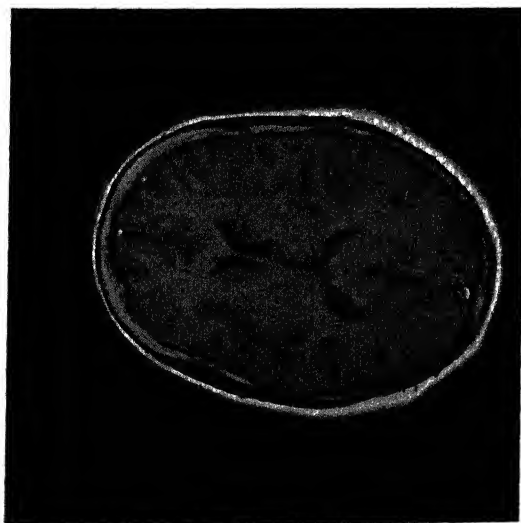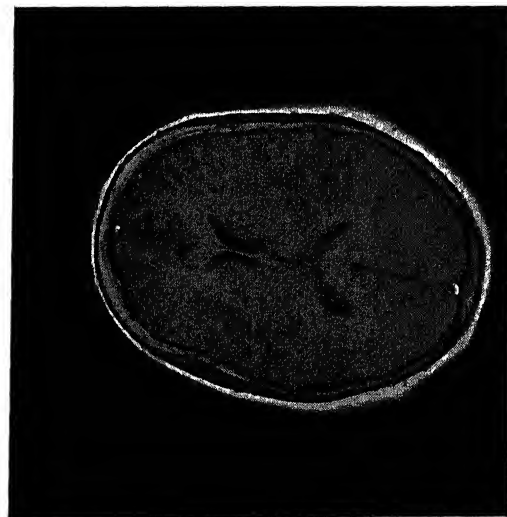
Original
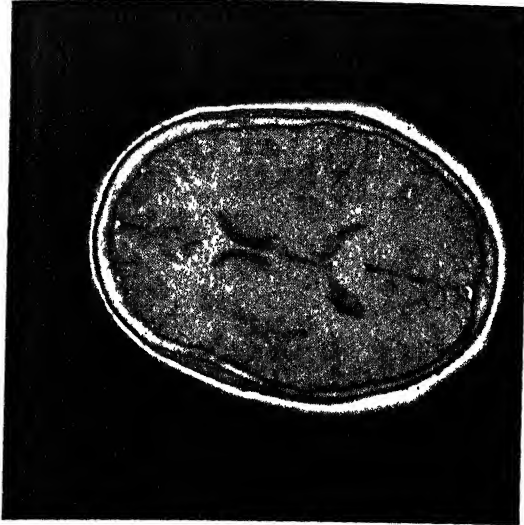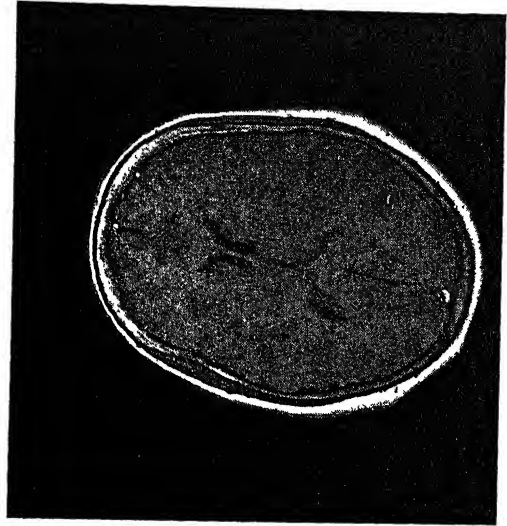
Blurred

Iteration 1

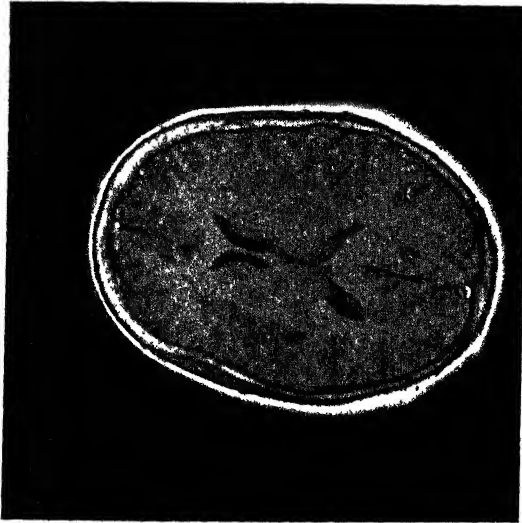Iteration 4

Iteration 7

Iteration 10

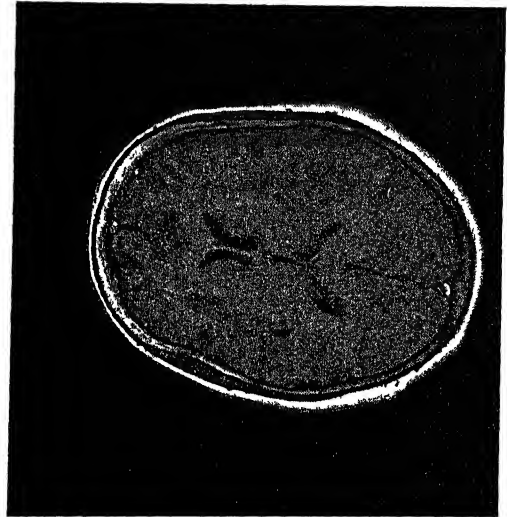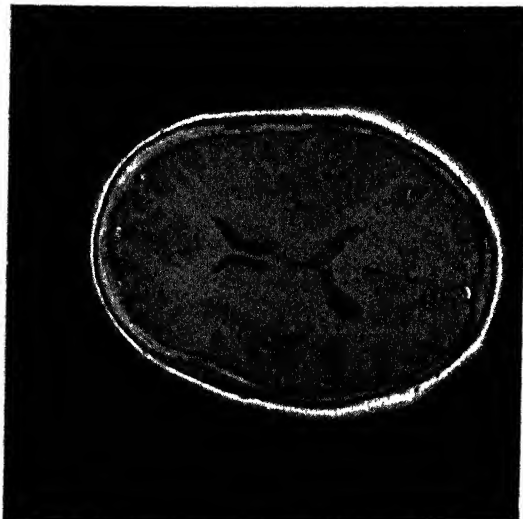**Fig. 4.7** : De-Blurring by Fejér sums (512x512 T_1-Weighted Image)
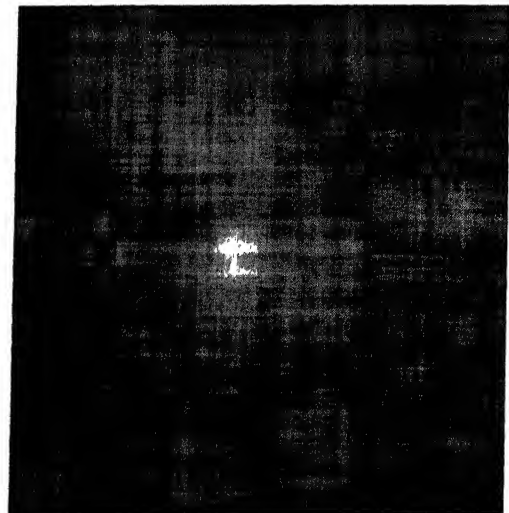
Original

Iteration 1

Iteration 2

Iteration 3

Iteration 4

Direct filter inversion

Fejér sums and direct filter inversion

|	64	128	256	512
blurred	21.898491	15.397139	12.760939	11 232959
A_1	21 971647	14.937742	11.327273	8 407426
A_2	22 010511	14 968604	11.159102	7.322424
A_3	22.017773	14.984726	11 127623	6.648437
A_4	22 019058	14.990157	11 122073	6 161029
A_5	22 019287	14 991931	11.122254	5.782414
A_6	22 019329	14.992516	11.123207	5.475666
A_7	22.019337	14.992712	11 124063	5 219060
A_8	22 019337	14.992780	11 124699	4.999608
A_9	22 019333	14.992803	11.125145	4 808920
A_{10}	22.019327	14.992813	11.125442	4 640935

Table 4.7 : L_1 Errors in reconstructing original 512×512cross-section by image data of different sizes (blurring & de-blurrings associated with Fejér sums for n = 256).

	64	128	256	512
blurred	26 422277	16 756004	12 835905	11.379604
A_1	26 087387	15 765809	10.638448	7.717406
A_2	26 066189	15.709594	10.357162	6 543892
A_3	26 063768	15 703228	10 293384	5 875368
A_4	26 063438	15.702043	10 274142	5.410994
A_5	26 063391	15 701744	10 267305	5 058268
A_6	26 063385	15 701655	10.264592	4.776148
A_7	26 063387	15 701626	10 263425	4 542590
A_8	26.063387	15.701616	10.262887	4 344323
A_9	26.063389	15.701613	10.262620	4.172835
A_{10}	26 063391	15.701612	10.262481	4.022374

Table 4.8 : L_2 -Error Errors in reconstructing original 512×512cross-section by image data of different sizes (blurring & de-blurrings associated with Fejér sums for n = 256).

	64	128	256	512
blurred	69.105209	53.528534	41.391506	37.572300
A_1	68.204979	48.251698	33.933582	26.652369
A_2	68 062378	46.826370	32.256283	21.929525
A_3	68 039215	46.472794	31.923101	18.960024
A_4	68 035393	46.471657	31.895712	16.670185
A_5	68 034737	46.468437	31.924402	14.764875
A_6	68.034622	46.466652	31.952774	13.141476
A_7	68.034599	46.465881	31.971827	11.748270
A_8	68.034599	46.465652	31.983000	10.899012
A_9	68.034607	46.465771	31.989004	10.190278
A_{10}	68.034599	46.466305	31.991884	9 577790

Table 4.9 : L_∞ -Error Errors in reconstructing original 512×512cross-section by image data of different sizes (blurring & de-blurrings associated with Fejér sums for n = 256)
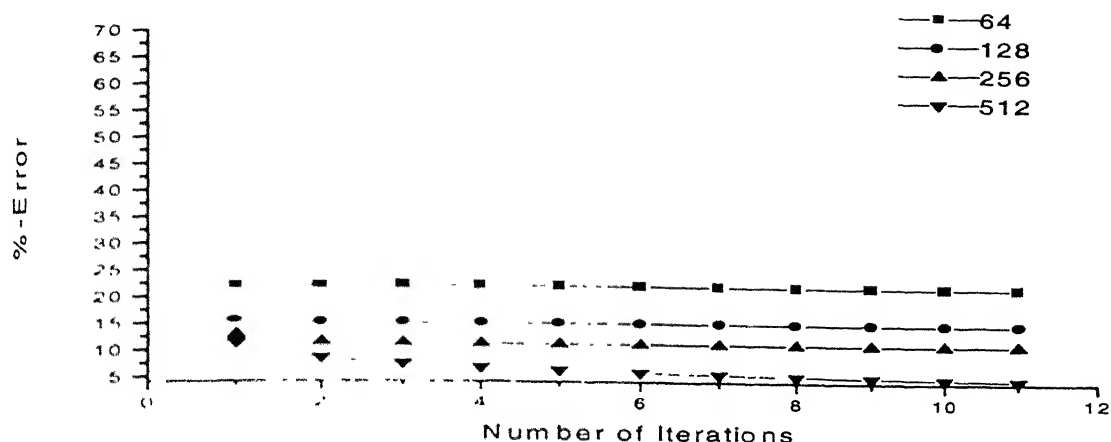
Graph 4.2 : L_ Error Errors in reconstructing original 512×512cross-section by image data of different sizes (blurring & de-blurrings associated with Feiér sums for n = 256).

Graph 4.3 : L_2-Error Errors in reconstructing original 512×512cross-section by image data of different sizes (blurring & de blurrings associated with Feiér sums for n = 256).
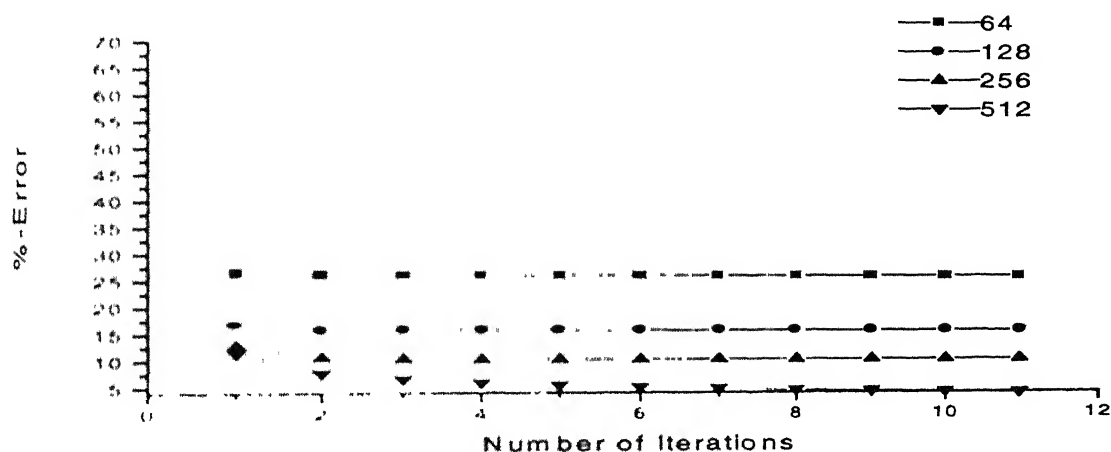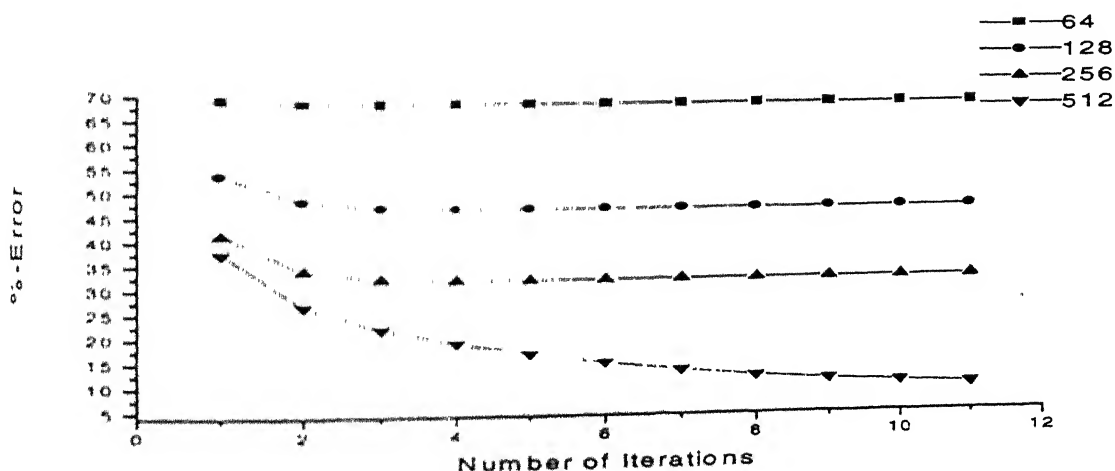

Graph 4.4 : L_ -Error Errors in reconstructing original 512×512cross-section by image data of different sizes (blurring & de-blurrings associated with Feiér sums for n = 256).

	64	128	256	512
blurred	2 418032	3.818776	5 611177	11.232959
A_1	0.324249	0 860875	2 270876	8.407426
A_2	0 051506	0 242072	1 191611	7.322424
A_3	0.009190	0.075348	0 689982	6.648437
A_4	0 002316	0 025235	0 420825	6.161029
A_5	0.001470	0.009099	0.265632	5.782414
A_6	0.001450	0.003753	0.171963	5.475666
A_7	0.001500	0.002055	0 113500	5 219060
A_8	0.001622	0.001666	0 076070	4.999608
A_9	0.001912	0.001839	0 051608	4.808920
A_{10}	0.002547	0 002461	0 035410	4.640935

Table 4.10 : %-L_1 Errors in reconstructing original cross-sections of different sizes (blurring & deblurrings associated with Fejér sums for n = 256).

|	64	128	256	512
blurred	3.420601	5.804968	7.707932	11 379604
A_1	0.432999	1.271163	2.765119	7.717406
A_2	0.067814	0.346227	1 351323	6.543892
A_3	0.012200	0.105967	0 754756	5.875368
A_4	0.003433	0.035028	0.451532	5.410994
A_5	0.002680	0.012368	0.281519	5 058268
A_6	0.002748	0.004987	0.180475	4.776148
A_7	0.002853	0.002930	0.118067	4.542590
A_8	0.002965	0.002584	0.078458	4.344323
A_9	0.003140	0.002669	0.052805	4.172835
A_{10}	0.003559	0.003091	0.035959	4.022374

Table 4.11: %-L_2 Errors in reconstructing original cross-sections of different sizes (blurring & deblurrings associated with Fejér sums for n = 256).

	64	128	256	512
blurred	7.346234	13.665717	24.851616	37.572300
A_1	0.979912	3.829877	10.249213	26.652369
A_2	0.151225	1.180119	5.414123	21.929525
A_3	0.024498	0.382845	3.110082	18.960024
A_4	0.008779	0.128460	1.884815	16.670185
A_5	0.009864	0.043945	1.182202	14.764875
A_6	0.010758	0.015377	0.758503	13.141476
A_7	0.011491	0.009114	0.494281	11.748270
A_8	0.012109	0.009488	0.325697	10.899012
A_9	0.012641	0.009688	0.216301	10.190278
A_{10}	0.013116	0.009726	0.144287	9.577790

Table 4.12 : %-L_∞ Errors in reconstructing original cross-sections of different sizes (blurring & deblurrings associated with Fejér sums for n = 256).
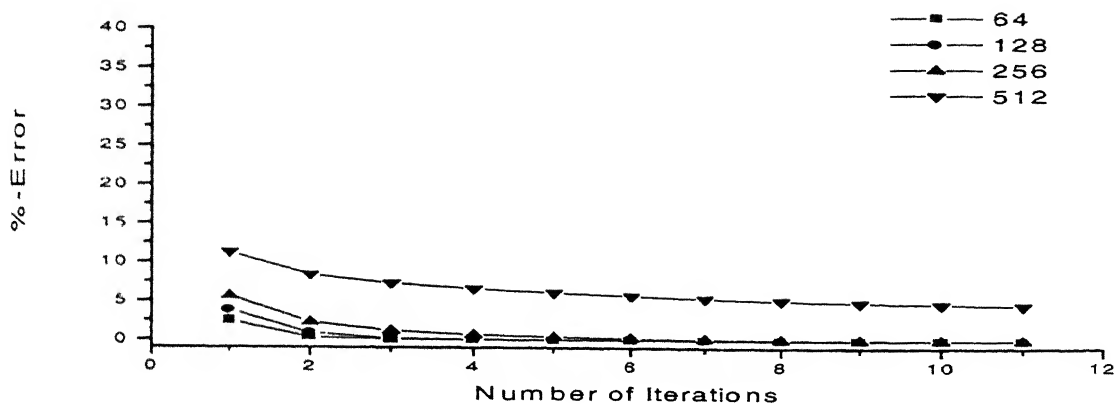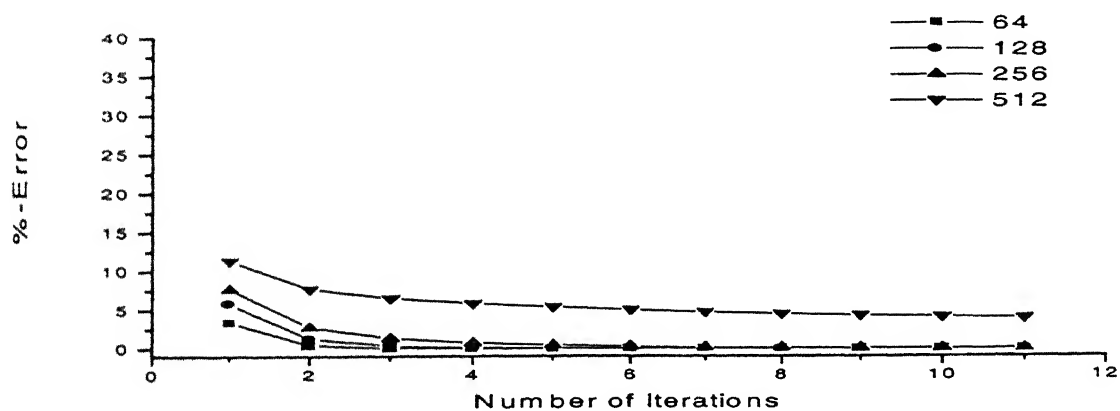
Graph 4.5 : %-L_1 Errors in reconstructing original cross-sections of different sizes (blurring & de-blurrings associated with Fejér sums for n = 256).

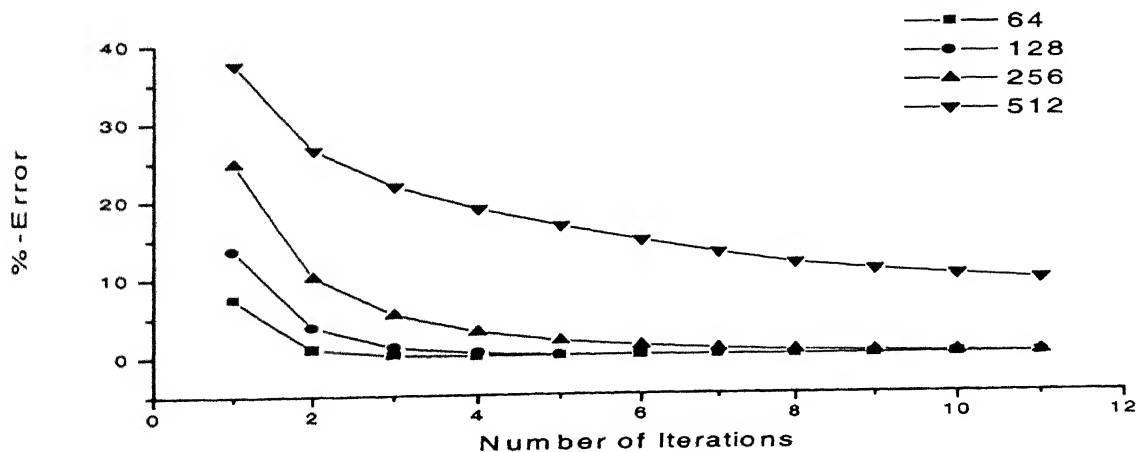**Graph 4.6** : %-L_2 Errors in reconstructing original cross-sections of different sizes (blurring & de-blurr associated with Fejér sums for n = 256).

Graph 4.7 : %-L_∞ Errors in reconstructing original cross-sections of different sizes (blurring & de-blurrings associated with Fejér sums for n = 256).

# 4.4 AN APPLICATION TO IMPROVED TISSUE PARAMETERS ESTIMATION

The next numerical experiment in this chapter explores the use of iterative de-blurring in obtaining a relatively more accurate set of T_1, T_2 and Proton density (ρ) weighted images from the corresponding blurred images, a use of which in the calculation of the corresponding T_1, T_2 and Proton density maps may reasonably be expected to give better results.

A calculation of T_1, T_2 and Proton density (ρ) values indeed involves the solutions of the Bloch equations for the various imaging protocols associated with different pulse sequences. For the SE images, e.g., one uses the equation

$$f(T_1, T_2, \rho; TE, TR) = M(1 - 2e^{-(TR-TE/2)/T_1} + e^{-TR/T_1})e^{-TE/T_2},$$

where the function f denotes the image intensity and the rest magnetization M is proportional to the proton density ρ. Thus, given a set of independent cross-sectional data using three appropriate sets of TE's and TR's, the tissue parameters T_1, T_2 and proton density (ρ) could be obtained by solving the related system of equations for each pixel, where in principle any convergent numerical solution procedure is supposed to give the same values (we have used an in house method developed by S.B. Rao et al.(2000)).

We utilized the T_1, T_2 and Proton density weighted images of Fig.0.4 and tissue parameters were calculated from these as described before. These were taken as the reference T_1, T_2 and proton density maps of the cross-section, using which, T_1, T_2 and density weighted spin echo images at the same pulse sequence parameters of the original images (i.e., TE/TR = 15/300, 20/2000, 80/2000 ms) were synthesized. These image sets were blurred and iteratively de-blurred by the Fejér sums, and the tissue parameter values were computed from each of the reconstructed image sets. . The resulting T_1, T_2 and ρ maps are shown in Figs. 4.9-4.11. From these the associated percentage L_1-errors (with respect to the original reference maps) have been computed and are presented in Tables 4.13 and depicted in the Graphs 4.8. The resulting improvements in the tissue parameter calculations with the successive de-blurrings are obvious from these.
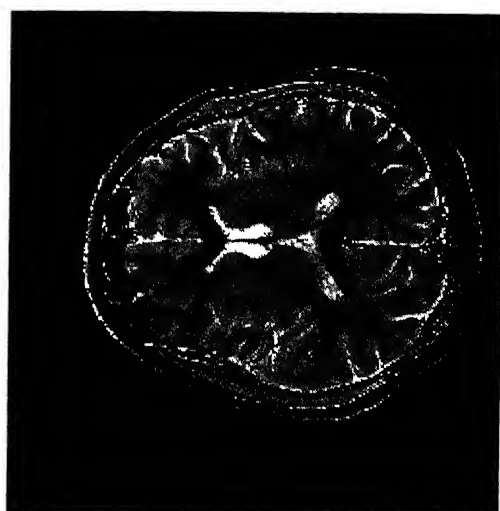
Original
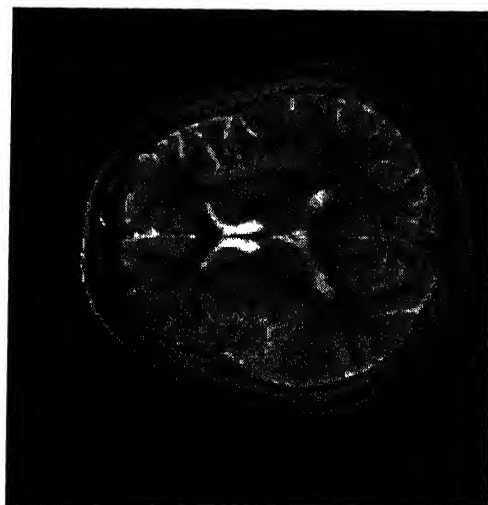
Blurred
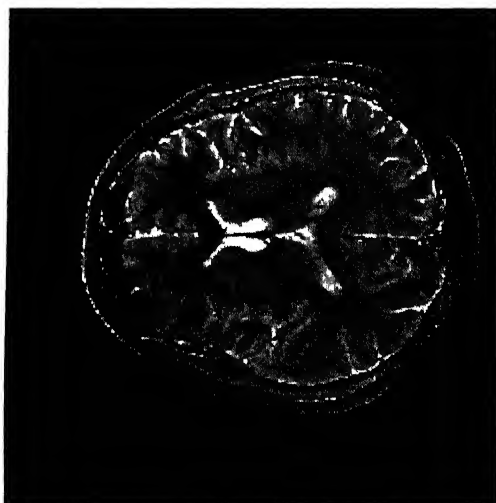
Iteration1

Iteration 4

Iteration 7

Iteration 10

Fig. 4.9 : T_1 maps calculated from synthesized images blurred and iteratively De-Blurred by Fejér sum

Original

Blurred
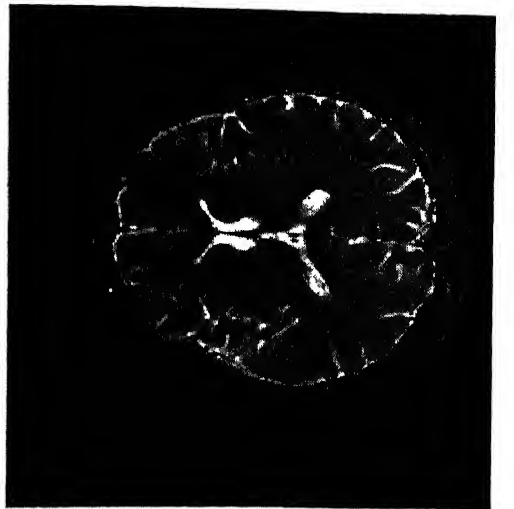
Iteration 1
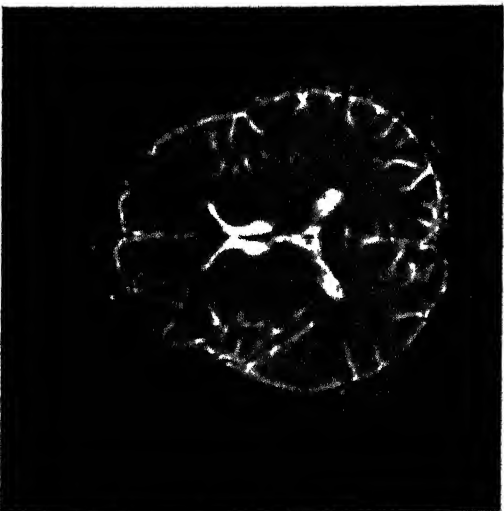
Iteration 4
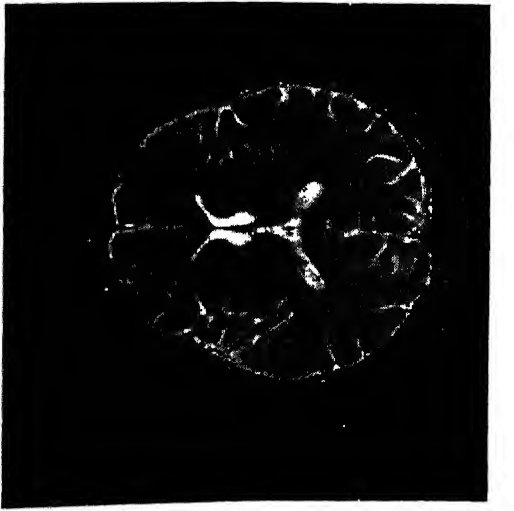
Iteration 7

Iteration 10

Fig. 4.10 : T_2 maps calculated from synthesized images blurred and iteratively De-Blurred by Fejér sums
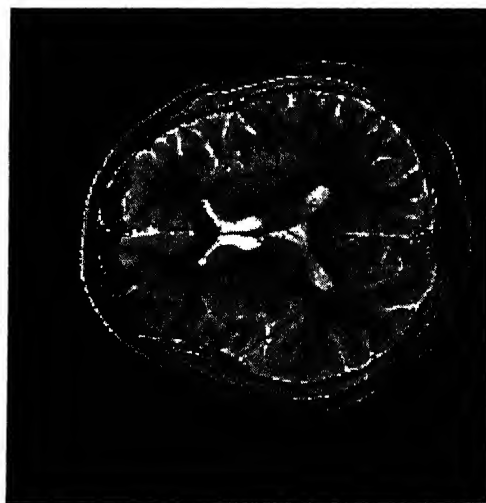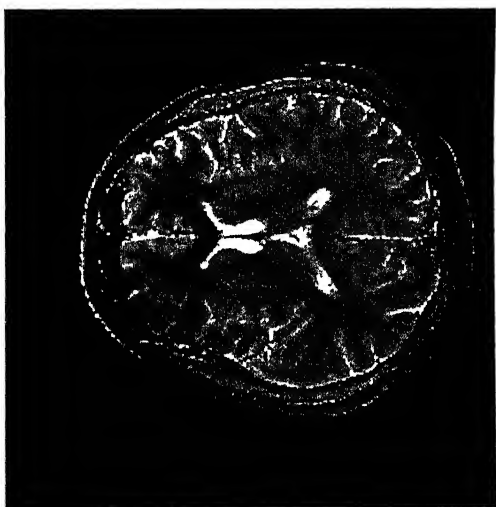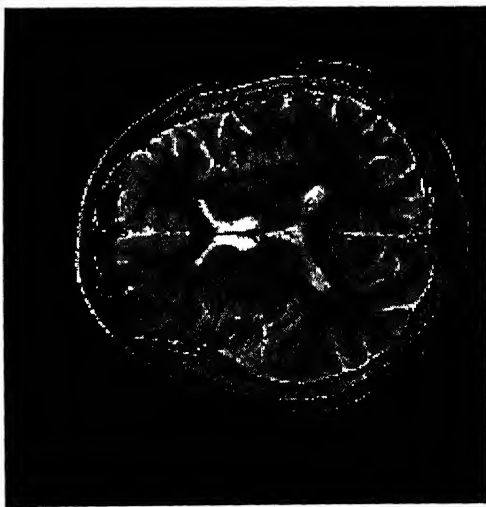
Original

Blurred
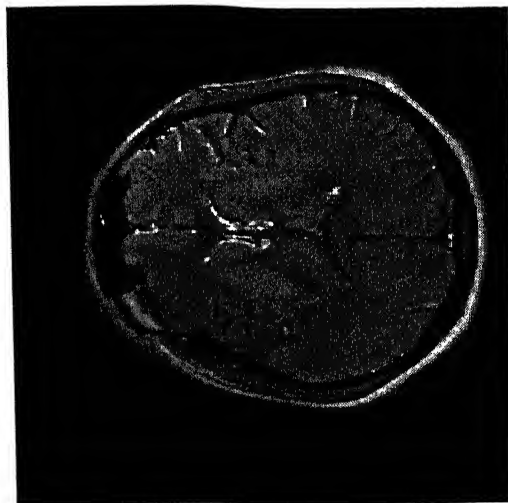
Iteration 1
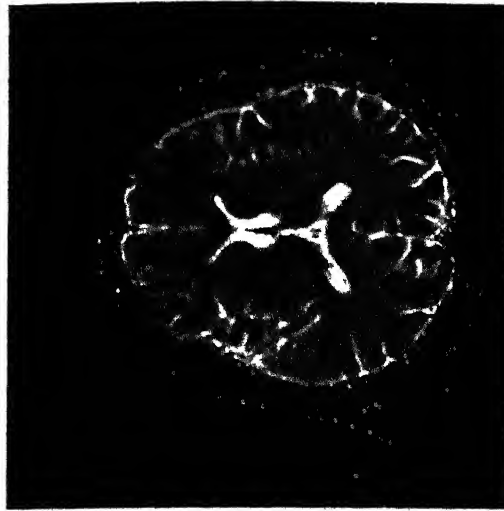
Iteration 4

Iteration 7
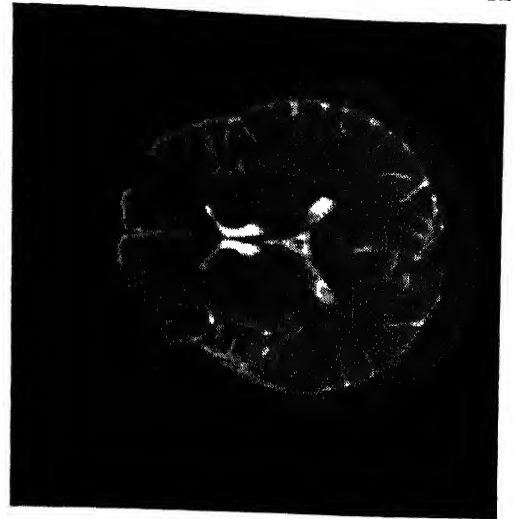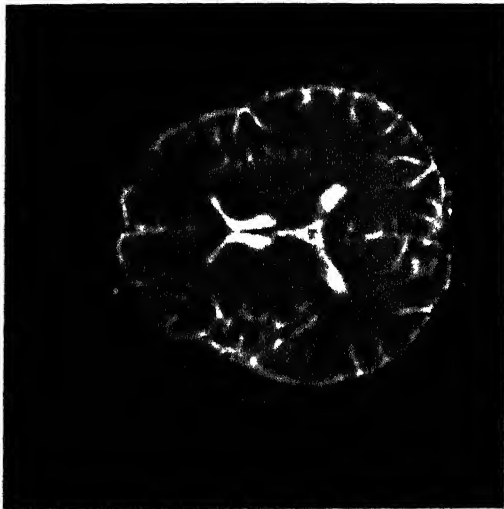
Iteration 10

Fig. 4.11 : ρ maps calculated from synthesized images blurred and iteratively De-Blurred by Fejér sums

	T_1	T_2	ρ
blurred	32.963605	64.191503	13.256375
A_1	12.744166	28.951161	4.795761
A_2	7 609981	18.757510	2 792503
A_3	5.305053	13.854168	1.912086
A_4	4 047702	10.957348	1 438919
A_5	3.272199	9.011048	1 147793
A_6	2 750937	7.295271	0 955418
A_7	2.262199	2.333124	0 788742
A_8	1.972128	2.034584	0.682532
A_9	1.754901	1.798596	0.599979
A_{10}	1.551487	1.675068	0.529480

Table 4.13 : %-L$_1$ Errors in T1, T_2 and ρ maps calculated from synthesized images blurred and iteratively De-Blurred by Fejér sums
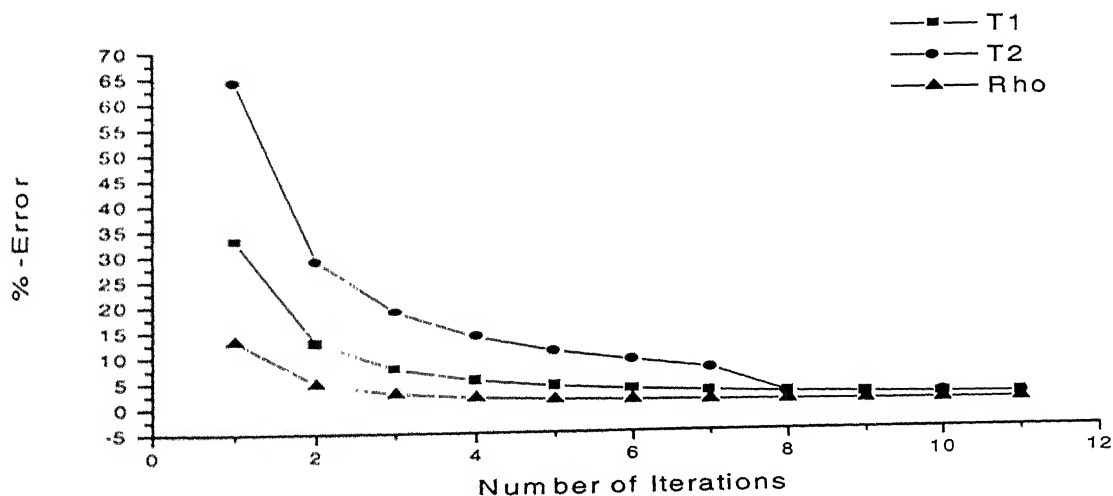
Graph 4.8 : %-L$_1$ Errors in T_1, T_2 and ρ maps calculated from synthesized images blurred and iteratively De-Blurred by Fejér sums.

Finally, we conclude the work by appending: (i) the graphical output for the discrete point spread functions associated with the blurring and de-blurring operators considered in the previous chapters, and (ii) the error maps (considerably brightened to show the pattern of the errors) associated with the de-blurred reconstructions of the T_1-weighted image (Fig. 0.4) for all the operators considered previously. These, so to say, provide the information on "de-blurring in action" and pictorially illustrate the working of the de-blurring scheme.

The first graph below shows the psf's of the Fejér sum and the related de-blurring operators. We note that whereas the central output of the Fejér sum lies between 0.4- 0.6, the out put of the 10th de-blurring operator is near 0.9. Moreover, the psf of the Fejér sum contributes only positively (leading to blurring), the negative contributions of the de-blurring operators are responsible for the de-blurring by them. The behavior of the 1st to the 9th de-blurring operators is in between that of the Fejér sum and the 10th de-blurring operator. The psf's of the generalized Jackson and the De la Vallée-Poussin operators follow next.
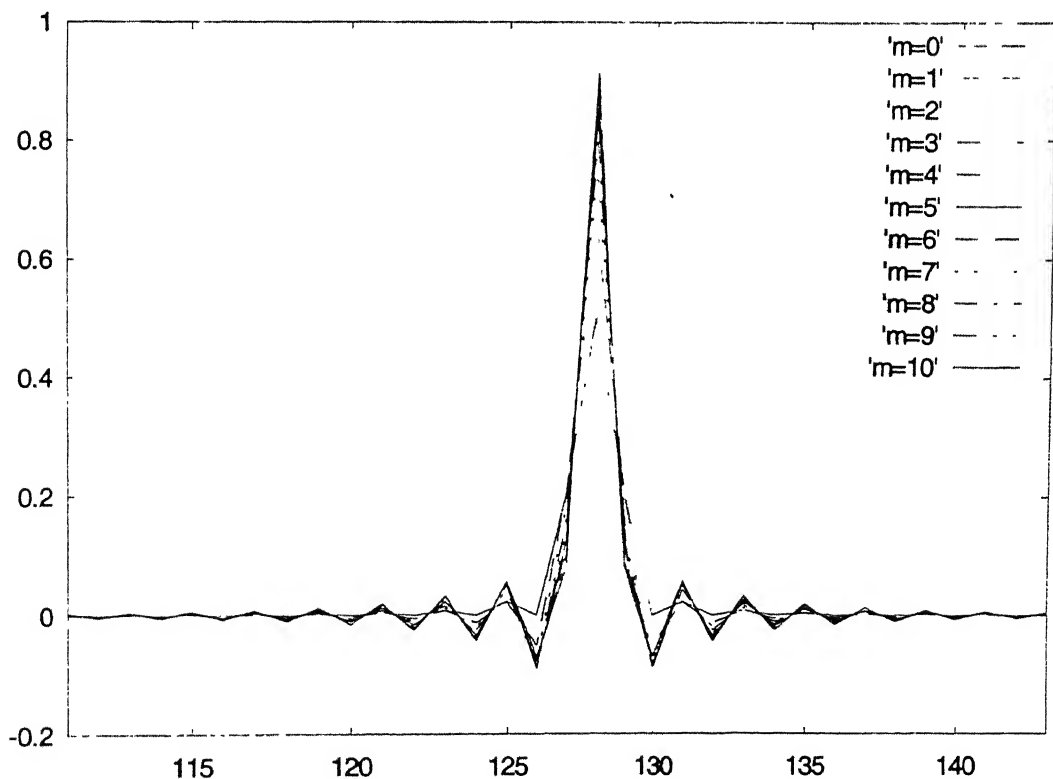
Graph 4.9 . PSF's of De-Blurs (by Fejér sums)
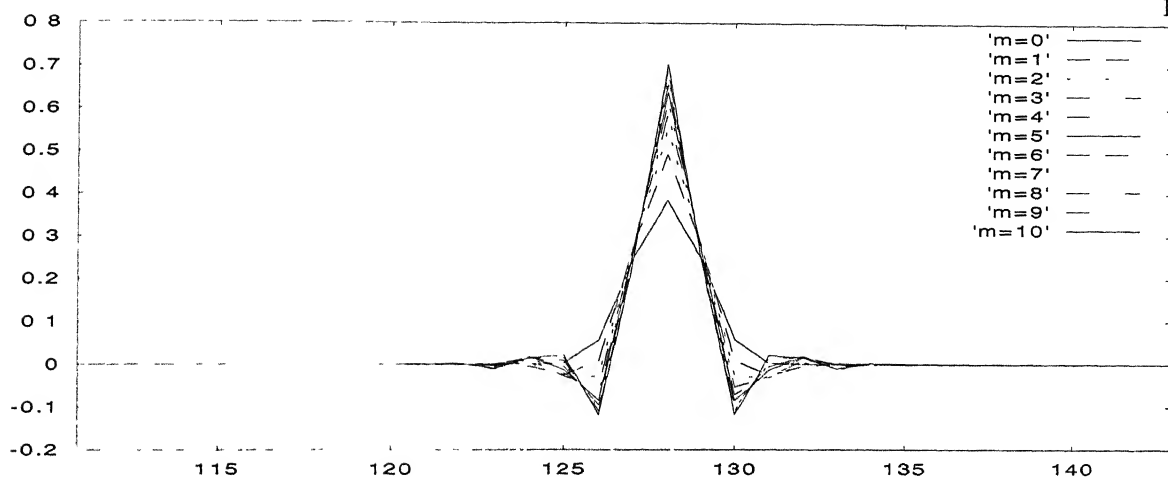
Graph 4.10 · PSF's of the De-blurs (Generalized Jackson operator (p=2))
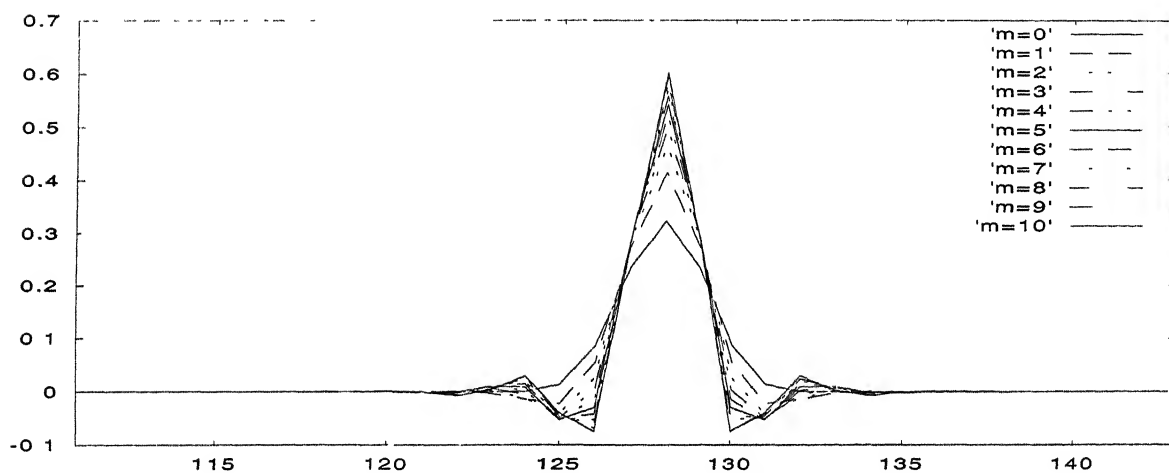
Graph 4.11 : PSF's of the De-blurs (Generalized Jackson operator (p=3))
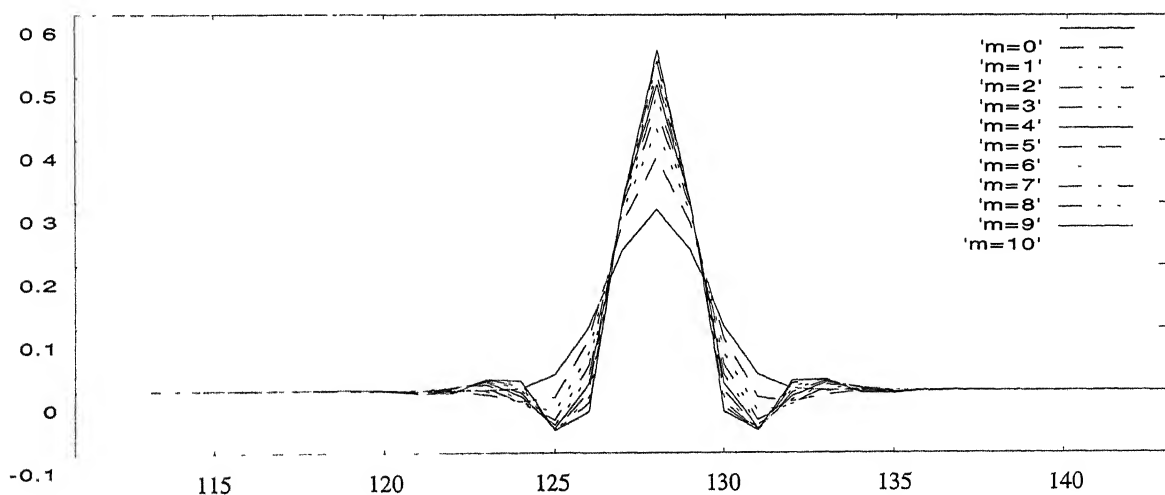
Graph 4.12 : PSF's of the De-blurs (Generalized Jackson operator (p=4))
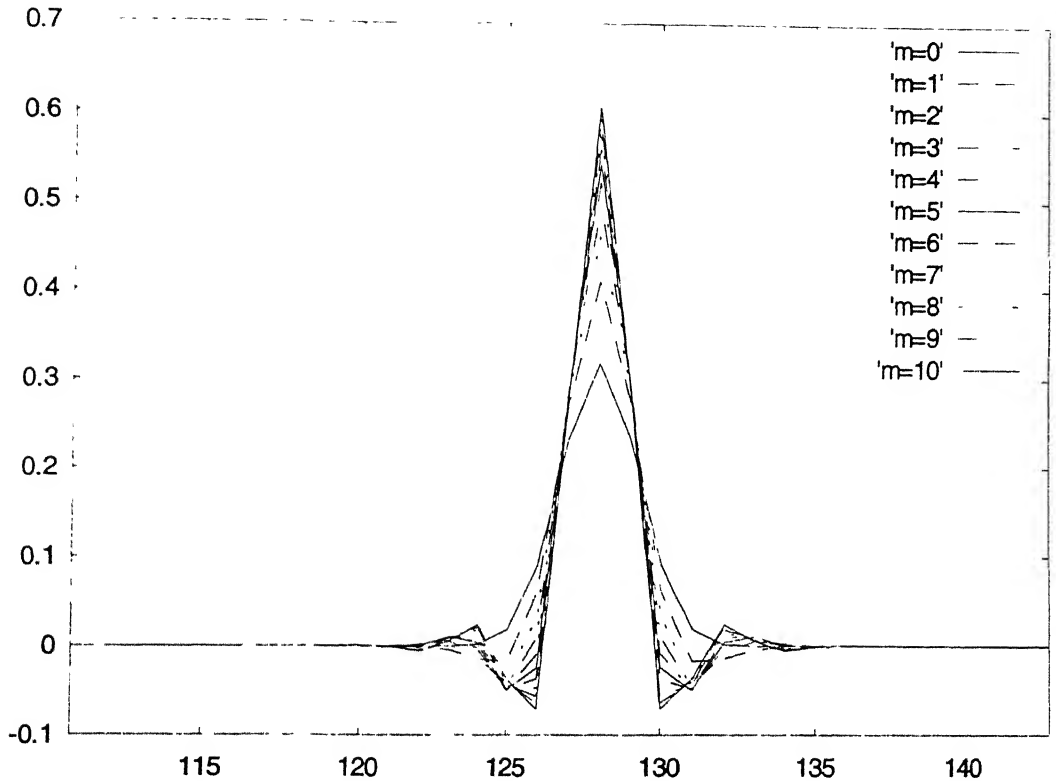
Graph 4.13 : PSF's of the De-blurs (Dé La Vallée-Poussin)

We note, from the Graph 4.10-12 of the psf's related with the generalized Jackson operators, that in the respective cases of p = 2, 3, and 4, the central outputs of the basic operators and the last of the de-blurring operators are respectively between 0.3-0.4, and near 0.7 for p = 2; near 0.3, and near 0.6 for p = 3; between 0..2-0.3 and between 0.5-0.6 for p = 4; and the same for the De la Vallée-Poussin are near 0.3, and near 0.6). The positive and negative output character of all these cases is similar to the case of the Fejér sum. The central outputs in all the cases increase monotonically in value. These graphs at once corroborate the earlier observed approximation and the blurring and the de-blurring properties.

Thus, the peaks near .5, .4,.3, below .3 and near .3 of the basic operators grade their blurring properties, whereas those near .9, .7, .6, below .6, and near .6 of the last iterates grade the corresponding order of approximation properties of the associated de-blurring operators. Finally the sign changes observed for all the de-blurring operators assert their de-blurring attribute.

Original

Original - Blurred

Original-Iteration 1

Original-Iteration 2

Original-Iteration 3

Original-Iteration 4

Original-Iteration 5

Original-Iteration 6

Original-Iteration 7

Original-Iteration 8

Original-Iteration 9

Original-Iteration 10
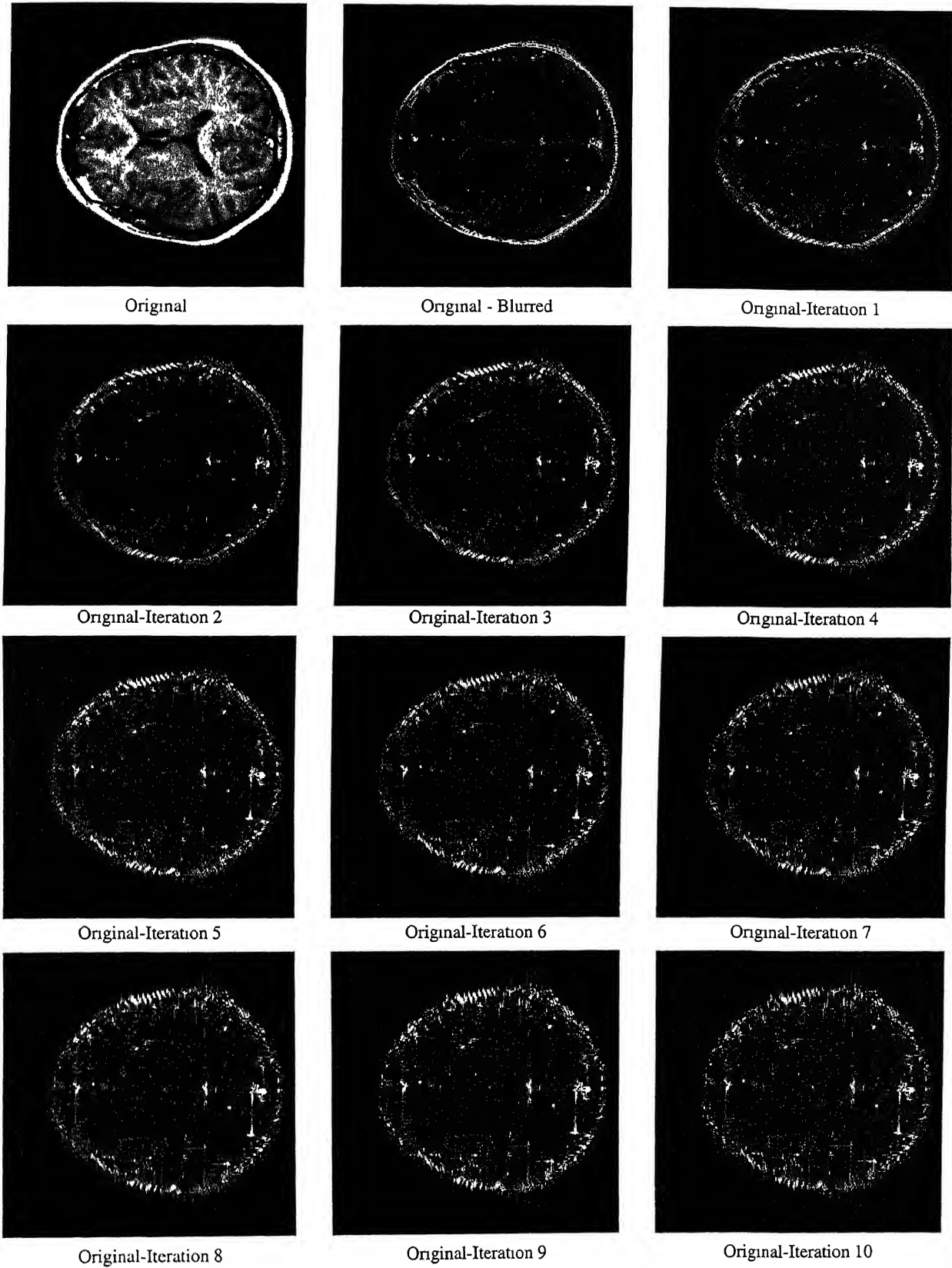
Fig. 4.12: Magnitudes of Difference Images in De-Blurring by Fejér sum

Original

Original - Blurred

Original-Iteration 1

Original-Iteration 2

Original-Iteration 3

Original-Iteration 4

Original-Iteration 5

Original-Iteration 6

Original-Iteration 7

Original-Iteration 8

Original-Iteration 9

Original-Iteration 10
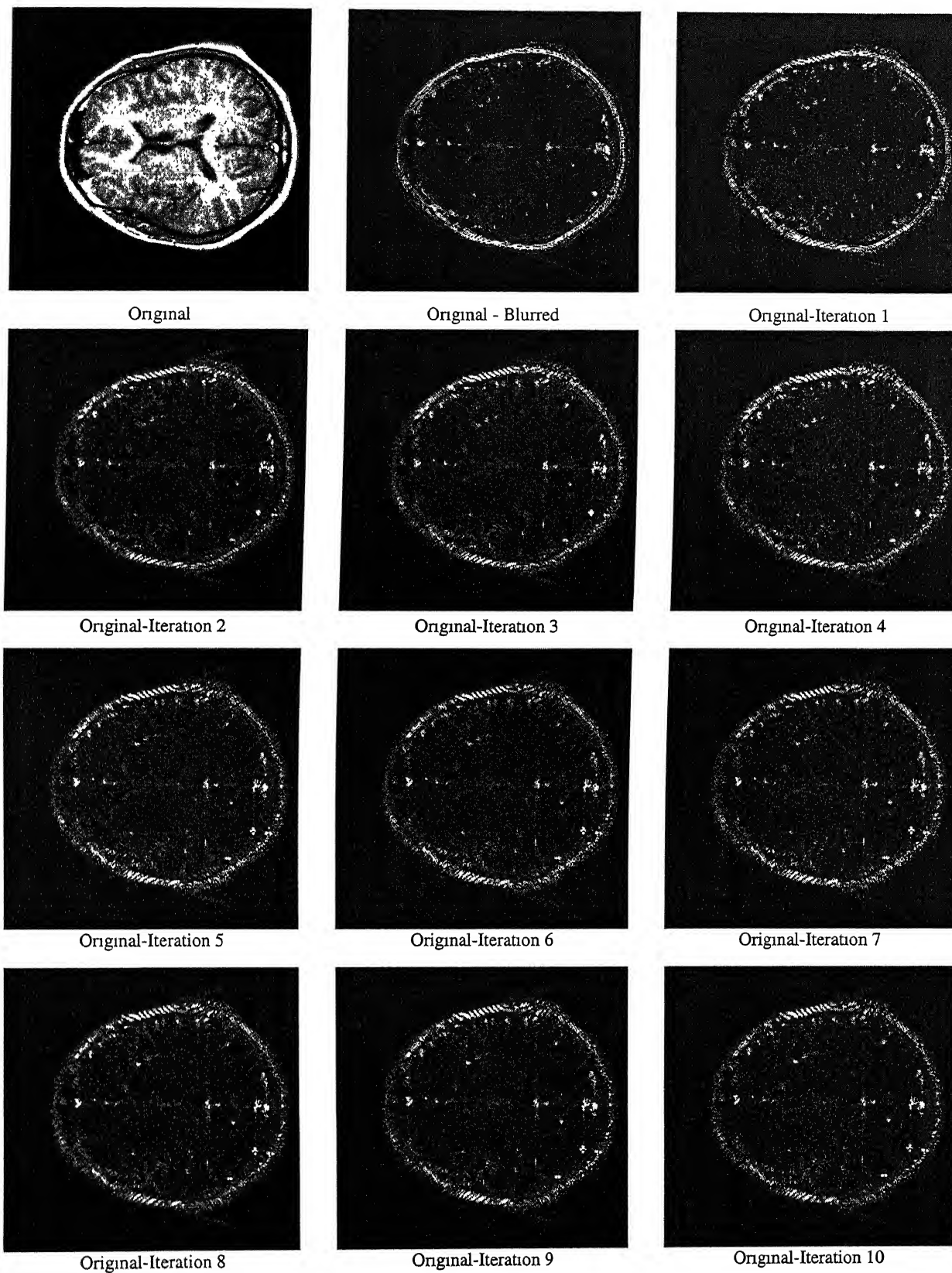
Fig. 4.13 : Magnitudes of Difference Images in De-Blurring by Generalized Jackson Operator (p=2)

Original	Original - Blurred	Original-Iteration 1
Original-Iteration 2	Original-Iteration 3	Original-Iteration 4
Original-Iteration 5	Original-Iteration 6	Original-Iteration 7
Original-Iteration 8	Original-Iteration 9	Original-Iteration 10
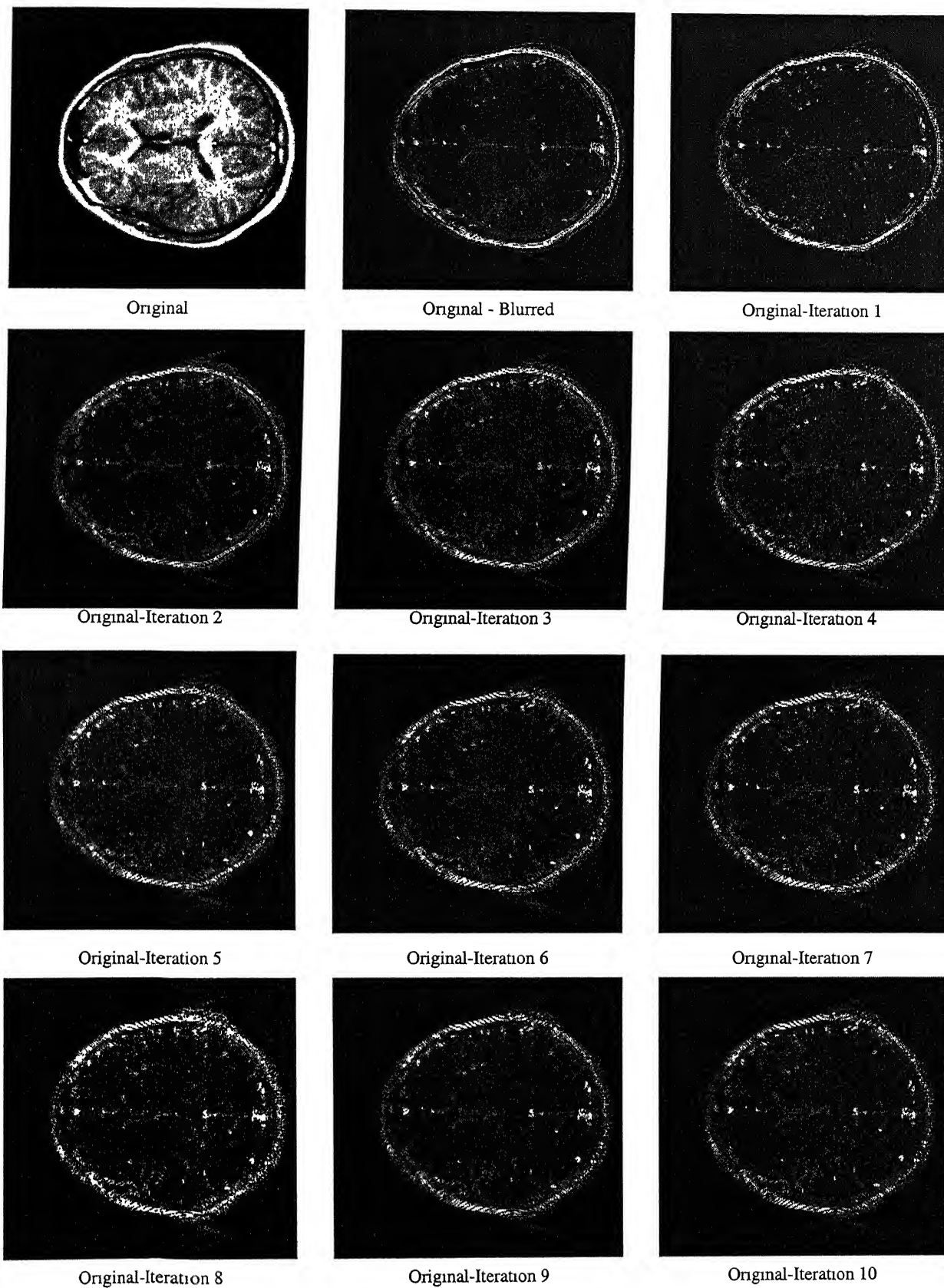
Fig. 4.15 : Magnitudes of difference Images in De-Blurring by Generalized Jackson Operator (p=4).

Original

Original - Blurred

Original-Iteration 1

Original-Iteration 2

Original-Iteration 3

Original-Iteration 4

Original-Iteration 5

Original-Iteration 6

Original-Iteration 7

Original-Iteration 8

Original-Iteration 9

Original-Iteration 10

Fig. 4.16 : Magnitude of Difference Images in De-Blurring by De La Vallée-Poussin Operator

The intensified images of the errors presented in Figs. 4.11-4.16 reiterate the qualitative behavior suggested by the graphs of the discrete psf's, discussed before. From these we also observe the progressive increase in the error of approximation by the de-blurring iterates for the Fejér sums (n =128), the generalized Jackson operators (with p = 2, n = 65; p = 3, n = 45; and p = 4, n = 35), respectively, and the near similarity of the error images for the case of the generalized Jackson operators (with p = 3, n = 45) and the De la Vallée-Poussin operators (n = 128). The interesting common feature, however, has been the visually unmistakable de-blurring property (in all the reconstructions presented in Chapters 1-3, including in the case of generalized Jackson operators for p = 4, in spite of their poor approximation property) observed for all the operators subjected to de-blurring scheme of Rathore.
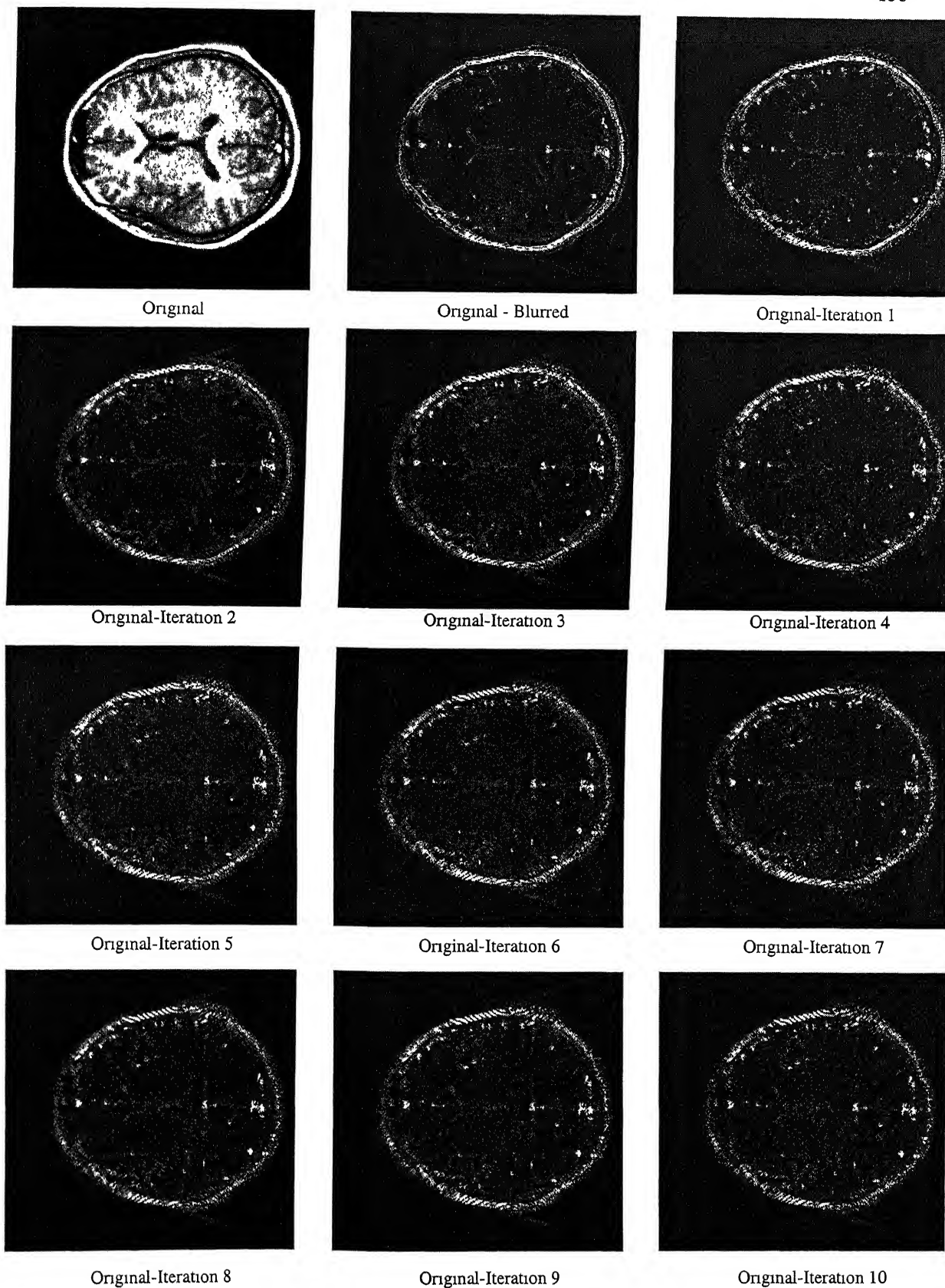
In conclusion, the approximation and the de-blurring properties are two distinct aspects of the same de-blurring operators

$$A_m = \sum\nolimits_{j=1}^{m} (-1)^{j-1} \, ^{m}C_j A^{j-1}, m = 1, 2, 3, 4, \ldots$$

which the theoretical and the simulation results of the thesis have tried to clarify and illustrate with the operators σ_n, $L_{n,p}$, and V_n, considered for the purposes of application in the field of MRI diagnosis.

REFERENCES

[01]   Abragam, A., (1961) The Principles of Nuclear Magnetism, Oxford University Press, New York.

[02]   Alexits, G., (1941) Sur l'ordre de grandeur de l'approximation d'une fonction par les moyennes de sa serie Fourier, (Hungar.) Mat. Fizikai Lapok, 48, 410-422.

[03]   Aljancic, S., (1961) Approximation of continuous functions by typical means of their Fourier series, Proc. A.M.S., 12, 681-688.

[04]   Bernstein, S.N., (1912) Sur l'ordre de la meilleure approximation des fonctions continues par polynômes de degré donné, Mém. Acad. de Belgique.

[05]   Bloch, F., (1946) Nuclear induction, Phys. Rev., 70, 460-474.

[06]   Butzer, P.L., and Berens, H., (1967) Semi-groups of operators and approximation, Grundlehren der Math. Wiss., 145, Springer, New York.

[07]   Callaghan, P.T., (1991) Principles of Nuclear Magnetic Resonance Microscopy, Clarendon Press, Oxford.

[08]   Carslaw, H.S., (1930) Introduction to the theory of Fourier's series and integrals, Dover Publications, Inc., USA.

[09]   De La Vallée-Poussin, J., (1908) Sur l'approximation des fonctions d'une variable réelle et de leurs dérivées par des polynómes et des suites de Fourier, Bull. Acad. De Belgique.

[10]   DeVore, R. A., (1972) The Approximation of Continuous Functions by Positive Linear Operators, Lecture Notes, Springer Verlag, Berlin-New York.

[11]   Ditzian, Z., and Totik, V., (1987) Moduli of Smoothness, Springer Verlag, New York.

[12]   Farrar, T., and Becker, E., (1971) Pulse and Fourier Transform NMR, Academic Press, New York.

[13]   Fejér, L., (1904) Untersuchungen über Fouriersche Reihen, Math. Ann.

[14]   Hinshaw, W.S., and Lent, A.H., (1983) An introduction to NMR imaging : From the Bloch equation to the imaging equation, Proc IEEE, 71, 338-350.

[15]   Jackson, D., (1912) On approximation by trigonometric sums and polynomials, TAMS, 13, 491-515.

[16]   Korovkin, P.P., (1960) Linear operators and approximation theory, Hindustan Publishing Corp., India.

[17]   Lauterbur, P.C., (1973) Image formation by induced local interactions: Examples employing NMR, Nature, 242, 190-191.

[18]   Lorentz, G.G., (1966) Approximation of Functions, Holt, Rinehart and Winston, New York.

[19]   Mansfield, P., and Morris, P., (1982) NMR Imaging in Biomedicine, Supl. 2, Advances in Magnetic Resonance, Academic Press, New York.

[20]   Natanson, I.P., (1944) *Nekotorye otsenki, svyazannye s singulyarnym integralom Valle-Pussena* (Some estimates connected with the singular intergal of De la Vallée-Poussin). DAN.

[21]   Natanson, I.P., (1964) Constructive Function Theory, I, Federick Ungar Publishing Co., New York.

[22]   Niekerk, F.D. van, (1965) The exact constant of approximation of continuous periodic functions by singular integrals of the Jackson type. Math. Institute of the Technological University Delft, report.

[23]   Nikolskiy, S.M., (1940) Ob asimptoticheskom povedenii ostatka pri priblizhenii funktsiy, udovletvoryayushchikh usloviyu Lipshitsa, summami Feyera, IAN, Math. Series.

[24]   Partain, C.L., Price, R.R., Patton, J.A., Kulkarni, M.V., and James Jr. A.E., (1988) Magnetic Resonance Imaging, II, W.B. Saunders Company, Philadelphia.

[25]   Petrov, I.M., (1958) On the order of approximation of functions $\in$ Z by some polynomial operators, Uspehi Mat. Nauk, 13, 6 (84), 127-131, (in Russian).

[26]   Price, R.R., Stephens, W.H., and Partain, C.L., (1988) NMR Physical Principles, In: Magnetic Resonance Imaging, II (eds,) Partain C.L., Price R.R., Patton J.A., Kulkarni M.V., and James Jr. A.E., W.B. Saunders Company, Philadelphia.

[27]   Rao, S.B., Gupta, R.K., Kaliprasad, V.S.N., Sushmita Datta, Rathore, R.K.S., (2000) A robust method for tissue parameters estimation in MR imaging, paper presented at the 6th National Symposium on Magnetic Resonance, January 17-20, TIFR, Mumbai.

[28]   Rathore, R.K.S., (1974) On a sequence of linear trigonometric polynomial operators, SIAM J. Math. Anal., 5, 908-917.

[29]   Rathore, R.K.S., (1994) Optimal inputs for approximate linear systems in Hilbert spaces, JMAA, Academic Press, New York and London, 188, 398-409.

[30]   Rathore, R.K.S., (1994) The problem of Timan on the precise order of decrease of the best approximations, Journal of Approx. Th., Academic Press, New York and London, 77, 153-166.

[31]   Rathore, R.K.S., (1994) Total Error in the discrete convolution back projection algorithm in computerized tomography, J. Comp. and Appl. Math. 54, 79-97.

[32]   Rathore, R.K.S., (2000) A generalized frame-work for inverse and equivalence results in approximation theory, (to appear in: Mathematical Analysis and Applications, ed. Dwivedi, A.P.), Narosa Publishing House, New Delhi, 20-35.

[33]   Schoenberg, I.J., (1959) On variation diminishing approximation methods, 249-274, (Rudolph E. Langer (ed.), On Numerical Approximation, The University of Wisconsin Press, Madison).

[34]   Schurer, F., and Steutel, F.W., (1967) On linear positive operators of the Jackson type, Mathematica, 9, 155-184.

[35]   Sebastiani, G., and Barone, P., (1991) Mathematical principles of basic magnetic resonance imaging in medicine, Signal Processing, 25, 227-250.

[36]   Shapiro, H.S., (1969) Smoothing and approximation of functions, Van Nostrand Reinhold Company, New York.

[37]   Sikkema, P.C., and Rathore, R.K.S., (1976) Convolutions with powers of bell-shaped functions, (report), Onderafdeling der Wiskunde Technische Hogeschool Delft.

[38] Sunouchi, G., and Watari, C., (1959) On determination of the class of saturation in the theory of approximation I – Proc. Jap. Acad. 34(1958), 477-481; II – Tohoku Math. J. 11, 480-488.

[39] Timan, A.F., (1966) Theory of approximation of functions of a real variable, Hindustan Publishing Corp., India.

[40] Wiener, N., (1932) The Fourier integral, Cambridge.

[41] Zamansky, M., (1949) Classes de saturation de certaines procédés d'approximation des series de Fourier des fonctions continues et applications a quelques problems d'approximation, Ann. Sci. Ecole Norm Sup. 66, 19-93.

[42] Zygmund, A., (1959) Trigonometric Series, second ed., Cambridge.